UNIVERSIDADE ESTADUAL DE CAMPINAS
Faculdade de Engenharia Química

JULIA RESENDE DE ANDRADE

REMOÇÃO DO CONTAMINANTE FARMACÊUTICO LOSARTANA POTÁSSICA DE SOLUÇÃO AQUOSA POR PROCESSOS AVANÇADOS: ADSORÇÃO COM ARGILA ORGANOFÍLICA E OXIDAÇÃO CATALÍTICA COM CARBONO POROSO E PEROXIMONOSULFATO

REMOVAL OF THE PHARMACEUTICAL CONTAMINANT LOSARTAN POTASSIUM FROM AQUEOUS SOLUTION BY ADVANCED PROCESSES: ADSORPTION WITH ORGANOPHILIC CLAY AND CATALYTIC OXIDATION WITH POROUS CARBON AND PEROXYMONOSULFATE

Campinas
2020

JULIA RESENDE DE ANDRADE

REMOÇÃO DO CONTAMINANTE FARMACÊUTICO LOSARTANA POTÁSSICA DE SOLUÇÃO AQUOSA POR PROCESSOS AVANÇADOS: ADSORÇÃO COM ARGILA ORGANOFÍLICA E OXIDAÇÃO CATALÍTICA COM CARBONO POROSO E PEROXIMONOSULFATO

REMOVAL OF THE PHARMACEUTICAL CONTAMINANT LOSARTAN POTASSIUM FROM AQUEOUS SOLUTION BY ADVANCED PROCESSES: ADSORPTION WITH ORGANOPHILIC CLAY AND CATALYTIC OXIDATION WITH POROUS CARBON AND PEROXYMONOSULFATE

Tese de Doutorado apresentada à Faculdade de Engenharia Química da Universidade Estadual de Campinas como parte dos requisitos para a obtenção do título de Doutora em Engenharia Química.

Orientadora: Prof.ª Dr.ª Melissa Gurgel Adeodato Vieira

ESTE TRABALHO CORRESPONDE À VERSÃO FINAL DA TESE DEFENDIDA PELA ALUNA JULIA RESENDE DE ANDRADE, E ORIENTADA PELA PROF.A DR.A MELISSA GURGEL ADEODATO VIEIRA

Campinas

2020

FICHA CATALOGRÁFICA

Ficha catalográfica
Universidade Estadual de Campinas
Biblioteca da Área de Engenharia e Arquitetura
Rose Meire da Silva - CRB 8/5974

An24r

Andrade, Julia Resende de, 1989-
Remoção do contaminante farmacêutico losartana potássica de solução aquosa por processos avançados : adsorção com argila organofílica e oxidação catalítica com carbono poroso e peroximonosulfato / Julia Resende de Andrade. – Campinas, SP : [s.n.], 2020.

Orientador: Melissa Gurgel Adeodato Vieira.
Tese (doutorado) – Universidade Estadual de Campinas, Faculdade de Engenharia Química.

1. Adsorção. 2. Processo oxidativo avançado. 3. Argila organofílica. 4. Catalisadores. 5. Fármacos. I. Vieira, Melissa Gurgel Adeodato, 1979-. II. Universidade Estadual de Campinas. Faculdade de Engenharia Química. III. Título.

Informações para Biblioteca Digital

Título em outro idioma: Removal of the pharmaceutical contaminant losartan potassium from aqueous solution by advanced processes : adsorption with organophilic clay and catalytic oxidation with porous carbon and peroxymonosulfate
Palavras-chave em inglês:
Adsorption
Advanced oxidative process
Organophilic clay
Catalysts
Pharmaceutical
Área de concentração: Engenharia Química
Titulação: Doutora em Engenharia Química
Banca examinadora:
Melissa Gurgel Adeodato Vieira [Orientador]
Adriano Luiz Tonetti
Marcus Bruno Soares Forte
João Jorge Ribeiro Damasceno
Guilherme Luiz Dotto
Data de defesa: 17-07-2020
Programa de Pós-Graduação: Engenharia Química

Identificação e informações acadêmicas do(a) aluno(a)
- ORCID do autor: https://orcid.org/0000-0001-5505-9112
- Currículo Lattes do autor: http://lattes.cnpq.br/7262558680520693

FOLHA DE APROVAÇÃO

Tese de Doutorado defendida por Julia Resende de Andrade e aprovada em 17 de julho de 2020 pela banca examinadora constituída pelos professores doutores:

Prof.ª Dr.ª Melissa Gurgel Adeodato Vieira

Presidente e orientadora
Faculdade de Engenharia Química – FEQ/UNICAMP

Prof. Dr. Adriano Luiz Tonetti

Faculdade de Engenharia Civil, Arquitetura e Urbanismo – FEC/UNICAMP
Videoconferência

Prof. Dr. Marcus Bruno Soares Forte

Faculdade de Engenharia de Alimentos – FEA/UNICAMP
Videoconferência

Prof. Dr. João Jorge Ribeiro Damasceno

Universidade Federal de Uberlândia – UFU
Videoconferência

Prof. Dr. Guilherme Luiz Dotto

Universidade Federal de Santa Maria – UFSM
Videoconferência

A Ata da Defesa, assinada pelos membros da Comissão Examinadora, consta no SIGA/Sistema de Fluxo de Dissertação/Tese e na Secretaria do Programa da Unidade.

AGRADECIMENTOS

Agradeço a Deus de infinita bondade por guiar minha vida, proteger meu caminho e preencher meu coração com a certeza de que nunca estou sozinha.

Agradeço à minha querida família, meus pais, Alessandra e Valério, e minhas irmãs, Vanessa e Isadora, pelo amor incondicional e apoio em todos os momentos.

Agradeço ao Fernando por todo zelo, amor, carinho e paciência independente da distância. Nosso encontro foi o melhor presente que a Unicamp me proporcionou.

Agradeço à professora Melissa Vieira pela oportunidade de desenvolver este trabalho, orientação e suporte ao longo desses quatro anos.

Agradeço ao professor Shaobin Wang por me receber na *Curtin University* durante o doutorado sanduíche na Austrália, e ao seu grupo de pesquisa pelas contribuições essenciais.

Agradeço à professora Meuris Gurgel pela colaboração, e ao professor Marcelino Gimenes pelo apoio e incentivo nesta jornada. Aos profissionais do Laboratório de Recursos Analíticos e de Calibração (LRAC) e ao professor Richard Landers por contribuírem com as análises de caracterização.

Agradeço ao programa de pós-graduação em Engenharia Química da Unicamp pela infraestrutura e equipe excepcionais.

Agradeço aos professores que aceitaram compor as bancas avaliadoras pelas valiosas contribuições à minha tese.

Agradeço aos colegas e amigos do LEA/LEPA pela troca de conhecimentos e de experiências, pela ajuda, pelas risadas e pelo companheirismo no dia-a-dia. Aos alunos de Iniciação Científica, em especial Franco Sbragia, pelo auxílio na realização de experimentos.

Agradeço aos meus grandes amigos que são fonte inesgotável de carinho e que estão sempre nas minhas melhores lembranças. Agradeço também aos meus familiares pelas boas vibrações.

O presente trabalho foi realizado com apoio da Coordenação de Aperfeiçoamento de Pessoal de Nível Superior – Brasil (CAPES) - Código de Financiamento 001 [Proc. 88882.329686/2018-01; 88881.188856/2018-01, 88881.310551/2018-01], Conselho Nacional de Desenvolvimento Científico e Tecnológico (CNPq) [Proc. 406193/2018-5] e Fundação de Amparo à Pesquisa do Estado de São Paulo – Brasil (FAPESP) [Proc. 2016/05007-1]. Pesquisa desenvolvida com o auxílio do CENAPAD SP. Agradeço à SpectroChem por fornecer gentilmente a argila Spectrogel e à Purifarma pelo fármaco para realização do estudo.

RESUMO

Fármacos são contaminantes emergentes continuamente inseridos no meio ambiente e frequentemente detectados em efluentes e matrizes aquáticas. Assim, tem-se buscado métodos avançados para a remoção eficaz de fármacos de meios aquosos. Esta tese de doutorado objetivou avaliar duas tecnologias preeminentes, adsorção e processo oxidativo avançado (POA), para tratamento de soluções contendo o contaminante farmacêutico losartana potássica, que é um dos anti-hipertensivos mais consumidos no mundo. Com relação à adsorção, a argila do tipo bentonita organofílica, Spectrogel-Tipo C, foi selecionada como material adsorvente. Ensaios descontínuos demonstraram que o tempo de equilíbrio de adsorção a 25 °C é de 36,7 horas e que o perfil cinético segue o modelo de pseudossegunda ordem. A resistência à transferência de massa em filme externo foi identificada como etapa limitante predominante. Isotermas de adsorção de losartana em Spectrogel apresentaram máximas capacidades de adsorção pelo modelo de Langmuir de 0,082 mmol/g a 25 °C e 0,099 mmol/g a 40 °C. O estudo termodinâmico revelou que o processo é espontâneo e endotérmico. O metanol forneceu eficiência de dessorção de 65%. Comparativamente à argila Spectrogel, o carvão ativado de casca de coco apresentou cinética mais lenta (40 horas) e menor capacidade adsortiva a 25 °C (0,044 mmol/g). Análises de caracterização mostraram que a química de superfície é mais relevante do que propriedades morfológicas na captação do fármaco. A adsorção contínua de losartana foi examinada em leito fixo empacotado com Spectrogel e comparada à adsorção do fármaco anti-inflamatório diclofenaco de sódio nas mesmas condições experimentais. Em vazão volumétrica de 0,4 mL/min e concentração de alimentação de 0,15 mmol/L, obteve-se capacidades de adsorção no ponto de saturação de 0,020 mmol/g para losartana e 0,032 mmol/g para diclofenaco. Resultados teóricos baseados na teoria DFT corroboraram a maior reatividade química molecular do diclofenaco em relação à losartana. O modelo fenomenológico proposto, *Dual Site Diffusion*, descreveu as curvas de ruptura com elevada precisão. Alternativamente à adsorção, avaliou-se a oxidação catalítica de losartana via ativação de peroximonossulfato (PMS) usando carbono poroso dopado com nitrogênio (N-PC). A remoção de losartana foi atribuída a efeitos sinérgicos de adsorção e reações de oxidação. A condição de pH inicial próximo à neutralidade beneficiou a atividade catalítica, enquanto que a variação da temperatura de reação pouco impactou o processo. A presença de ácido húmico, íon bicarbonato e íon cloreto em solução prejudicaram a eficiência de decomposição de losartana. A taxa de mineralização de 70% indicou que o fármaco e seus intermediários foram em sua maioria efetivamente degradados no sistema N-PC/PMS. A atividade catalítica do N-PC reduziu expressivamente após três ciclos consecutivos, o que pôde ser relacionado às modificações de porosidade, composição elementar, grau de grafitização e grupos funcionais causadas pelo processo. Testes evidenciaram que o N-PC ativa o PMS por múltiplas vias, mas com predominância do mecanismo oxidativo sem radicais, que envolve a formação de complexo reativo ou oxigênio singlete. Em suma, o estudo demonstrou que ambos processos de adsorção e de oxidação são atraentes para tratar losartana, mas que ainda oferecem desafios, tais como eficiência, custo-benefício e sustentabilidade.

Palavras-chave: adsorção; processo oxidativo avançado; contaminante farmacêutico; losartana potássica; argila organofílica; carbono poroso.

ABSTRACT

Pharmaceuticals are emerging contaminants that have been continuously released into the environment and that have been frequently detected in effluents and aquatic matrices. Hence, advanced methods have been pursued for the effective removal of pharmaceuticals from aqueous media. This thesis aimed at evaluating two preeminent technologies, adsorption and advanced oxidation process (AOP), to treat solutions containing the pharmaceutical contaminant losartan potassium, which is a most globally consumed anti-hypertensive. Regarding adsorption, the organophilic clay of bentonite type, Spectrogel-Type C, was selected as adsorbent material. Discontinuous assays showed that the equilibration time of adsorption at 25 °C is 36.7 hours and that the kinetic profile follows the pseudo-second order model. The mass transfer resistance in external film was identified as the dominant rate-limiting step. Adsorption isotherms of losartan on Spectrogel exhibited maximum adsorption capacity from Langmuir model as 0.082 mmol/g at 25 °C and 0.099 mmol/g at 40 °C. The thermodynamic study revealed that the process is spontaneous and endothermic. Methanol provided 65% desorption efficiency. Compared to Spectrogel organoclay, coconut shell-based activated carbon showed slower kinetics (40 hours) and lower losartan adsorption capacity at 25 °C (0.044 mmol/g). Characterization analyzes showed that surface chemistry is more relevant than morphological properties in the pharmaceutical uptake. Continuous adsorption of losartan was examined in fixed-bed packed with Spectrogel and compared to the adsorption of the anti-inflammatory pharmaceutical diclofenac sodium under the same experimental conditions. At flow rate of 0.4 mL/min and inlet concentration of 0.15 mmol/L, it was obtained exhaustion adsorption capacities as 0.020 mol/g for losartan and 0.032 mmol/g for diclofenac. Theoretical results based on DFT theory corroborated the higher molecular reactivity of diclofenac in relation to losartan. The proposed phenomenological model, Dual Site Diffusion, described the breakthrough curves with high precision. Alternatively to adsorption, it was evaluated the catalytic oxidation of losartan via peroxymonosulfate (PMS) activation using nitrogen-doped porous carbon (N-PC). Losartan removal was attributed to synergistic effects of adsorption and oxidation reactions. The condition of initial pH close to neutrality enhanced catalytic activity, whereas the variation of reaction temperature had minor impact on the process. The presence of humic acid, bicarbonate ion and chloride ion in solution impaired the degradation efficiency of losartan. The mineralization rate of 70% indicated that the pharmaceutical and its intermediates were mostly effectively degraded in the N-PC/PMS system. The catalytic activity of N-PC expressively reduced after three consecutive cycles, which could be linked to changes in porosity, elemental composition, graphitization degree and functional groups caused by the process. Tests evidenced that N-PC activates PMS by multiple pathways, but with a predominance of the non-radical oxidative mechanism, which involves the formation of a reactive complex or singlet oxygen. In summary, the study demonstrated that both adsorption and oxidation processes are attractive to treat losartan, but still offer challenges such as efficiency, cost-effectiveness and sustainability.

Keywords: adsorption; advanced oxidative process; pharmaceutical contaminant; losartan potassium; organophilic clay; porous carbon.

LISTA DE ILUSTRAÇÕES

LISTA DE TABELAS

SUMÁRIO

CAPÍTULO 1. Introdução e Objetivos

1.1 Motivação à pesquisa

A contaminação da água se destaca como um dos desafios mais críticos do mundo. Conforme as Nações Unidas (UNESCO), a demanda mundial por água vem crescendo em cerca de 1% ao ano desde os anos 1980 e estima-se que quase um terço da população global já não tenha acesso à água potável de qualidade (UNESCO/WWAP 2019). Há grande atenção voltada para os chamados "contaminantes emergentes", que são compostos naturais ou antropogênicos que não são tradicionalmente monitorados, mas que têm sido verificados no meio ambiente e que podem causar efeitos adversos conhecidos ou suspeitos. Os contaminantes emergentes incluem fármacos, produtos de cuidado pessoal, pesticidas, hormônios, drogas ilícitas, microplásticos, dentre outros (MONTAGNER et al., 2019). Tais contaminantes oferecem problemas como persistência ambiental, bioacumulação e toxicidade (EBELE; ABOU-ELWAFA ABDALLAH e HARRAD, 2017). Em relação aos fármacos, estes são compostos biologicamente ativos que em baixas concentrações individuais na ordem de nanogramas por litro podem ter efeitos ecotoxicológicos inexistentes ou insignificantes. Contudo, a contínua inserção de diversos fármacos nos meios aquáticos cria uma mistura complexa com potenciais efeitos sinérgicos como ameaça ambiental (FENT; WESTON e CAMINADA, 2006; VASQUEZ et al., 2014).

Uma pesquisa recente sobre a qualidade das águas na América Latina revelou a disseminação de fármacos, dentre outros contaminantes emergentes, em águas superficiais, subterrâneas, potáveis e residuais, bem como em influentes e afluentes de estações de tratamento de água (PEÑA-GUZMÁN et al., 2019). No Brasil, a presença de fármacos em rios e em esgoto tratado e não tratado foi primeiramente reportada por STUMPF et al. (1999) e TERNES et al. (1999). Mais recentemente, a ocorrência de fármacos em matrizes aquáticas brasileiras tem sido tema de diversos estudos (CAMPANHA et al., 2015; MACHADO et al., 2016; SPOSITO et al., 2018; FRANCISCO et al., 2019; MONTAGNER et al., 2019). Apesar destes esforços, as legislações vigentes no Brasil ainda são deficitárias em seus critérios de qualidade de água, e contemplam somente cerca de trinta tipos de pesticidas dentre as centenas de substâncias de preocupação emergente (MONTAGNER; VIDAL e ACAYABA, 2017).

O despejo de efluentes é fonte primordial de contaminação, haja vista que cerca de 80% das águas residuais geradas no mundo são descartadas no meio ambiente sem tratamento satisfatório (UNESCO/WWAP 2017). Neste contexto, a situação do Brasil é alarmante, pois os últimos levantamentos oficiais mostram que somente a metade das águas residuais foram

tratadas de forma segura em 2016 e que o índice médio de tratamento de esgoto sanitário gerado não ultrapassou 46,3% em 2018. Consequentemente, há grande aporte de poluentes sendo introduzidos diretamente nos corpos hídricos brasileiros, cuja proporção com boa qualidade da água ficou menor que 70% em 2015 (AGÊNCIA NACIONAL DE ÁGUAS, 2019; BRASIL, 2019a).

Dessa forma, apesar de escassas as informações sobre os potenciais efeitos de fármacos à saúde humana e ao meio ambiente, há um consenso sobre a necessidade de melhorias nas condições de saneamento básico no Brasil, bem como implementação de métodos avançados de tratamento de água e efluentes. Este último ponto acompanha um esforço em nível mundial de busca por tecnologias efetivas para mitigação de contaminantes emergentes, dentre as quais os processos de adsorção e os processos de oxidação são apontados como promissores. Por exemplo, a Suíça conjectura implantar até 2040 técnicas avançadas de ozonização e/ou adsorção em carvão ativado em cerca de 100 das suas 700 estações municipais de tratamento de esgoto, visando diminuir em mais de dois terços a carga de micropoluentes orgânicos, como fármacos (BOURGIN et al., 2018).

No que se refere à operação de adsorção, esta se baseia na transferência de moléculas adsortivas da fase fluida para a superfície de material sólido adsorvente (SING et al., 1985). O processo oferece flexibilidade e simplicidade de projeto, fácil operação e alta eficiência, além de não introduzir subprodutos ao sistema e propiciar o uso de diferentes sólidos adsorventes (SEO et al., 2016). O carvão ativado é o adsorvente prevalecente no uso comercial, sendo altamente eficiente na remoção de uma vasta gama de contaminantes orgânicos em baixas concentrações. Contudo, o carvão ativado comercial apresenta a desvantagem de custo relativamente alto, o que encarece sua aplicação em larga escala (PUTRA et al., 2009; AHMED et al., 2015). Assim, adsorventes alternativos e de baixo custo têm sido investigados, com destaque para materiais argilosos, que apresentam estabilidade química e mecânica, capacidade de troca iônica e abundância na natureza (BABEL e KURNIAWAN, 2003). Apesar de vantajoso e econômico, o processo de adsorção pode ser limitado nos casos de concentrações ultrabaixas de poluentes e oferece desafios relacionados à regeneração e disposição do adsorvente saturado.

Como alternativa à técnica de adsorção, os processos oxidativos avançados (POAs) visam à completa degradação e mineralização de contaminantes emergentes a partir de geração de espécies altamente reativas, tais como radicais hidroxila (•OH) e sulfato ($SO_4^{\bullet -}$). Entretanto, a formação de intermediários de reação desconhecidos é fator limitante desta tecnologia (ZHANG et al., 2016). A maioria dos POAs, destacadamente o processo Fenton, vale-se

exclusivamente de radicais •OH. Contudo, há grande interesse na aplicação de $SO_4^{\bullet-}$, que tem maior potencial de oxidação em ampla faixa de pH e vida útil mais longa. Radicais •OH e $SO_4^{\bullet-}$ podem ser gerados simultaneamente a partir persulfatos, cuja ativação por catálise heterogênea se caracteriza por elevada produtividade de $SO_4^{\bullet-}$, condições brandas de operação, baixo consumo de energia e menor risco de lixiviação metálica em comparação à catálise homogênea (TIAN et al., 2018a; KANG et al., 2019). No que tange aos catalisadores, materiais a base de carbono, tais como óxido de grafeno, carbonos porosos e nanotubos de carbono, sobressaem pela benignidade ambiental, elevada área específica e propriedades físico-químicas ímpares. Entretanto, como os carbonos puros em geral sofrem de baixa estabilidade e desempenho catalítico limitado, tem-se buscado sintetizar catalisadores funcionalizados com propriedades aprimoradas. O método de dopagem com átomo de nitrogênio, por exemplo, pode ser adotado para induzir propriedades eletrônicas ao material a base de carbono (PENG et al., 2018; AHAMAD et al., 2019; WANG et al., 2019).

Considerando a onipresença de contaminantes farmacêuticos emergentes no meio ambiente e a dificuldade para a sua completa remediação, com o presente trabalho pretende-se contribuir na área de Engenharia Ambiental, mais especificamente para a melhoria da qualidade geral de matrizes aquáticas, com pesquisa em adsorção e POA como tecnologias avançadas de tratamento terciário (ou de polimento) para remoção de um fármaco de interesse acadêmico e ambiental, a losartana potássica. Enquanto que o processo de adsorção proposto oferece como diferencial a aplicação de argila organofílica como material adsorvente não convencional, de baixo custo e alternativo ao carvão ativado, o POA se distingue pelo emprego de catalisador ambientalmente benigno a base de carbono e sem metal. A losartana potássica foi escolhida como o contaminante farmacêutico a ser estudado por ser um dos anti-hipertensivos mais consumidos globalmente. No Brasil, a hipertensão afeta pelo menos 24% da população das capitais conforme levantamento do Ministério da Saúde em 2018 (BRASIL, 2019b), e a losartana é o segundo fármaco específico mais utilizado no país para o seu tratamento (MENGUE et al., 2016). O uso massivo de losartana leva à sua crescente introdução no meio ambiente, com consequente ocorrência em águas e efluentes, e à necessidade de estudos aprofundados em métodos para sua remoção. Para completar o quadro, comparativamente a outros fármacos, tais como propranolol, metformina e amoxicilina, a losartana potássica apresentou maior potencial de adsorção por argila organofílica em testes preliminares.

Ponderando todo o exposto, fica clara a relevância deste trabalho, na medida em que se propõe avaliar a remoção do contaminante emergente losartana potássica de solução por duas técnicas avançadas diferentes, mas ao mesmo tempo promissoras, e que têm vantagens e

limitações inerentes. Além de trazer novas contribuições à área ambiental, este projeto também poderá atrair setores industriais, sobretudo o farmacêutico, que se beneficiariam com o desenvolvimento de métodos avançados para o tratamento de efluentes contendo fármacos.

1.2 Objetivos

O objetivo principal da tese de doutorado foi avaliar a remoção do fármaco anti-hipertensivo losartana potássica por dois métodos avançados de tratamento: i) processo de adsorção usando argila comercial do tipo bentonita organofílica, Spectrogel-Tipo C, como adsorvente não convencional e de baixo custo, ii) processo oxidativo avançado usando carbono poroso dopado com nitrogênio para ativação de peroximonosulfato.

Para atender ao propósito do trabalho, os seguintes objetivos específicos foram desenvolvidos:

- Avaliar a afinidade de diferentes fármacos com materiais argilosos para seleção do sistema com maior potencial de remoção;
- Avaliar a influência individual do pH inicial da solução e da quantidade de adsorvente na eficiência de remoção de losartana potássica pela argila organofílica comercial Spectrogel-Tipo C;
- Estudar a cinética e o equilíbrio de adsorção de losartana em banho finito usando Spectrogel, aplicar modelos matemáticos aos resultados experimentais, e determinar grandezas termodinâmicas;
- Realizar testes comparativos de cinética e equilíbrio de adsorção de losartana em banho finito usando um carvão ativado comercial;
- Caracterizar a argila Spectrogel antes e após aplicação como adsorvente, e o carvão ativado *in natura* para elucidação dos mecanismos de remoção de losartana;
- Realizar testes em banho finito para dessorção de losartana de Spectrogel usando diferentes eluentes;
- Estudar a adsorção de losartana em sistema contínuo de leito fixo empacotado com Spectrogel e aplicar modelos matemáticos às curvas de ruptura da coluna;
- Caracterizar a superfície da Spectrogel antes e após adsorção de losartana por espectroscopia de fotoelétrons excitados por raios X (XPS);
- Realizar testes comparativos de adsorção do fármaco diclofenaco de sódio em sistema de leito fixo com Spectrogel;
- Realizar cálculos baseados na teoria DFT para obtenção de descritores químicos moleculares dos fármacos losartana potássica e diclofenaco de sódio;

- Fabricar o catalisador de carbono poroso dopado com nitrogênio N-PC, utilizando farinha de trigo, bicarbonato de sódio, hidróxido de potássio, e diciandiamida;
- Caracterizar do catalisador N-PC antes e após a degradação oxidativa de losartana potássica por diferentes técnicas;
- Avaliar o custo de produção do catalisador N-PC;
- Avaliar a remoção de losartana potássica por adsorção em N-PC, por oxidação utilizando somente peroximonosulfato (PMS) e por oxidação catalítica utilizando N-PC juntamente com PMS;
- Avaliar o efeito de diferentes parâmetros na ativação catalítica de PMS, incluindo dosagem de PMS, temperatura de reação, pH inicial da solução, e presença de íons e matéria orgânica em solução;
- Avaliar a taxa de mineralização por medida de Carbono Orgânico Total;
- Avaliar a estabilidade e reuso do catalisador N-PC em três ciclos consecutivos;
- Estudar os mecanismos de reação por meio de testes de ressonância paramagnética eletrônica (EPR) e testes de inibição.

1.3 Apresentação da Tese em capítulos

A execução do projeto de doutorado em sua totalidade deu-se como conjunto de cinco blocos principais, conforme esquematizado na Figura 1.1.

Figura 1.1. Principais blocos de execução do projeto de Doutorado.

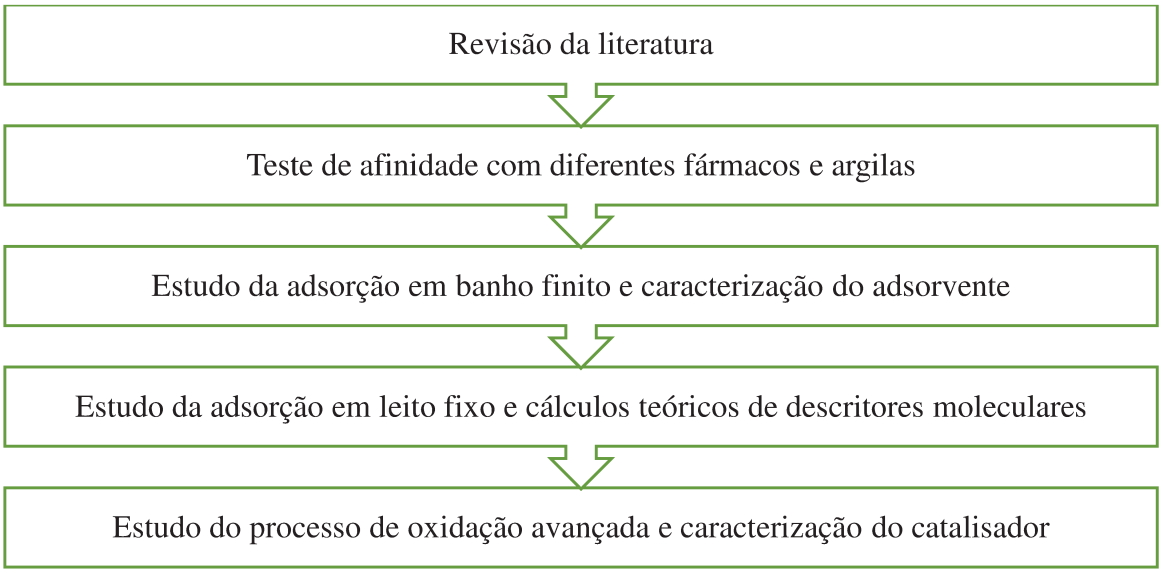

O presente trabalho foi estruturado na forma de capítulos, os quais apresentam os resultados de cada uma das etapas de pesquisa propostas. Os avanços na área de tratamento avançado de contaminantes farmacêuticos são aqui discutidos usando os artigos científicos oriundos da tese. Tais artigos são apresentados no formato dos periódicos internacionais nos quais foram publicados. Além do artigo de revisão propriamente dito para considerações abrangentes sobre o Estado da Arte, os três artigos originais desenvolvidos trazem revisões sucintas, mas específicas e relevantes, para contextualização e embasamento nos tópicos aos quais se propõem.

O **Capítulo 2** apresenta o artigo de revisão publicado na revista *Industrial & Engineering Chemistry Research* e intitulado *"Adsorption of Pharmaceuticals from Water and Wastewater Using Non-Conventional Low-Cost Materials: a Review"*, que traz discussão sobre a problemática de contaminação por compostos farmacêuticos, com relação à ocorrência, principais fontes, implicações ambientais e tecnologias disponíveis para remediação. Ademais, apresenta fundamentos teóricos sobre a tecnologia de adsorção e compila artigos disponíveis na literatura nos quais materiais adsorventes alternativos ao carvão ativado são empregados para remoção de contaminantes farmacêuticos.

O **Capítulo 3** contém o teste de afinidade, o qual é fundamental como etapa preliminar para definição do fármaco a ser estudado como adsorbato e o material argiloso a ser empregado como adsorvente não convencional. Para isto, avaliou-se a remoção de quatro fármacos de interesse acadêmico e ambiental, *i.e.*, cloridrato de propranolol, cloridrato de metformina, losartana potássica e amoxicilina trihidratada, e três argilas do tipo bentonita, *i.e.*, Verde-lodo calcinada, Fluidgel calcinada e Spectrogel – Tipo C. Considerando eficiência e capacidade de adsorção, selecionou-se o sistema losartana potássica e argila organofílica comercial, Spectrogel – Tipo C, para o estudo aprofundado de adsorção. Os resultados foram apresentados no 12º Encontro Brasileiro sobre Adsorção (EBA 12) no trabalho intitulado "Adsorção do Fármaco Losartana Potássica em Argila Organofílica Comercial: Teste de Afinidade e Planejamento Experimental".

No **Capítulo 4** é apresentado o artigo publicado na revista *Journal of Environmental Chemical Engineering* e intitulado *"Performance of organoclay in adsorptive uptake of antihypertensive losartan potassium: A comparative batch study using micro-grain activated carbon"*. Este artigo teve como objetivo principal investigar detalhadamente a adsorção descontínua de losartana potássica usando a argila organofílica Spectrogel. O processo foi avaliado em termos de cinética e equilíbrio de adsorção, além de termodinâmica. Testes de dessorção foram realizados e os possíveis mecanismos de remoção foram discutidos. O

desempenho da argila Spectrogel foi comparado àquele obtido usando um carvão ativado comercial. Tanto a argila Spectrogel pré- e pós-processo, quanto o carvão ativado fresco tiveram propriedades físico-quimicas e texturais caracterizadas por diferentes técnicas.

O **Capítulo 5** apresenta o trabalho *"Comparative adsorption of diclofenac sodium and losartan potassium in organophilic clay-packed fixed-bed: X-ray photoelectron spectroscopy characterization, experimental tests and theoretical study on DFT-based chemical descriptors"*, que foi publicado na revista *Journal of Molecular Liquids*. Este artigo discorre sobre a adsorção monocomponente dos fármacos diclofenaco de sódio e losartana potássica em sistema de leito fixo empacotado com argila Spectrogel. Os efeitos de vazão volumétrica e concentração de entrada de cada fármaco foram inspecionados. Os testes com diclofenaco de sódio foram incluídos no artigo visando a uma maior relevância e abrangência na área, já que este fármaco teve adsorção descontínua anteriormente avaliada pelo grupo de pesquisa, no âmbito da dissertação de mestrado de Gabriella Simon Maia, com resultados promissores apresentados no artigo "*Adsorption of diclofenac sodium onto commercial organoclay: Kinetic, equilibrium and thermodynamic study"* da revista *Powder Technology*. O **Capítulo 5** traz não somente testes experimentais de adsorção dos dois fármacos, mas também desenvolvimento e aplicação de modelos matemáticos às curvas de ruptura, caracterização da superfície externa da argila Spectrogel por espectroscopia de fotoelétrons excitados por raios X (XPS), e estudo teórico da reatividade química molecular da losartana potássica e do diclofenaco de sódio.

O **Capítulo 6** contém o artigo publicado na revista *Chemical Engineering Journal* com o título *Oxidative degradation of pharmaceutical losartan potassium with N-doped hierarchical porous carbon and peroxymonosulfate*. Neste trabalho, avaliou-se a oxidação catalítica de losartana potássica via ativação de peroximonossulfato (PMS) usando um carbono com estrutura hierarquicamente porosa dopado com nitrogênio (N-PC). Os ensaios de oxidação foram conduzidos durante o período de Doutorado Sanduíche da autora desta tese no Departamento de Engenharia Química da *Curtin University* (Perth, Austrália) entre Novembro/2018 e Abril/2019. O catalisador foi sintetizado seguindo um método simples e disponível na literatura e teve seu custo de produção em escala laboratorial estimado. A remoção de losartana potássica foi avaliada usando somente N-PC como adsorvente, usando somente PMS e usando a combinação de N-PC e PMS. A taxa de mineralização de losartana no sistema N-PC/PMS foi aferida por medida de Carbono Orgânico Total. A estabilidade e reutilização do catalisador N-PC foi avaliada em três ciclos. Os mecanismos de reação foram estudados por meio de testes de ressonância paramagnética eletrônica e testes de inibição. O sólido N-PC foi caracterizado por diferentes técnicas.

O **Capítulo 7** oferece uma discussão geral sobre os principais resultados obtidos neste Tese de Doutorado.

Por fim, no **Capítulo 8**, são relatadas as conclusões gerais desta pesquisa bem como as sugestões para trabalhos futuros usando adsorção ou processo oxidativo avançado para a remoção de contaminantes emergentes.

CAPÍTULO 2. Revisão Bibliográfica

Adsorption of Pharmaceuticals from Water and Wastewater Using Non-Conventional Low-Cost Materials: A Review[§]

Julia Resende de Andrade, Maria Fernanda Oliveira, Meuris Gurgel Carlos da Silva, Melissa Gurgel Adeodato Vieira

Department of Processes and Products Design, School of Chemical Engineering – University of Campinas, Albert Einstein Avenue, 500, 13083-852, Campinas – São Paulo – Brazil.

Abstract

Pharmaceuticals are environmental contaminants that have been widely detected in aquatic media. In this review, the occurrence of pharmaceuticals in the environment, its major causes, and implications along with effective procedures for their removal from contaminated water have been studied. Adsorption stands out as a promising treatment method, since it offers advantages such as lower energy consumption and simpler operation conditions in comparison to other tertiary treatments. Although commercial activated carbon is extensively studied as an adsorbent of pharmaceuticals, its large-scale application is limited by the high costs. Therefore, different non-conventional low-cost materials have been investigated and adsorbents based on clays, biochars, chitosan, agricultural and industrial wastes, and metal-organic frameworks have been addressed in many studies for pharmaceuticals uptake from water and wastewater. This article reviews key publications on this subject, discussing adsorption performance in terms of kinetics, equilibrium, thermodynamics, continuous fixed-bed process, regeneration capability, and historical, economical, and practical aspects.

Keywords: Review; Water Treatment; Adsorption; Low-Cost Adsorbents; Emerging Contaminants; Pharmaceuticals Removal.

[§] Manuscript published in *Industrial & Engineering Chemistry Research* 57 (2018) 3103-3127. DOI: 10.1021/acs.iecr.7b05137. Reprinted with permission from *Industrial & Engineering Chemistry Research*. Copyright 2018 American Chemical Society (*Anexo A*).

2.1 Introduction

Pharmaceutical compounds belong to the class of emerging contaminants that have been identified in low concentrations in the environment and that can negatively affect human health and/or ecosystems. In the literature, there are several studies on the discharge, incidence, and implications of pharmaceuticals in the environment, besides studies on analytical methods for their detection in water.[1-3]

The widespread occurrence of pharmaceuticals in water brings into light the inefficacy of conventional methods of water and wastewater treatment and there is a growing consensus that alternative technologies must be implemented for the optimized uptake of emerging contaminants.[4]

Since adsorption offers simple design and operation and does not add unwelcome byproducts to the system, this method has been considered promising for pharmaceutical removal from water and effluents in the field of pollution control and waste management.[5, 6] Activated carbon (AC) is the most widely employed and studied adsorbent for organic compounds; nevertheless, the high cost of the material and its difficult regeneration can make the adsorption process unfeasible.[7-9] Hence, alternative adsorbent materials have been investigated, such as clays, biochar, chitosan, and other low-cost materials, including agro-industrial wastes and metal-organic frameworks (MOFs).[5, 10]

The use of activated carbon as adsorbent for pharmaceuticals uptake from water and wastewater, especially antibiotics, has been widely reviewed in recent years.[11-14] Nevertheless, to the extent of authors' knowledge, no other review of literature concerns the adsorption of pharmaceuticals specifically by alternative materials. Therefore, the present work aims to summarize the major studies on nonconventional low-cost adsorbents for pharmaceutical removal from water and wastewater. This review will discuss: (i) brief background of the occurrence in the environment, potential risks, sources, and treatment options for pharmaceuticals; (ii) adsorption historical and technical aspects; (iii) kinetics, equilibrium thermodynamics, and continuous fixed-bed adsorption; (iv) pharmaceutical removal by adsorption process using nonconventional low-cost materials; (v) economical and practical aspects, progress, and future perspectives for pharmaceutical adsorption from water and wastewater.

2.2 Methodology

Initially, a comprehensive literature search was performed using selected keywords, such as adsorption, water treatment, emerging contaminants, pharmaceutical contamination,

alternative adsorbents, clay adsorbents, biochar adsorbents, chitosan adsorbents, agricultural adsorbents, industrial adsorbents, and metal−organic framework adsorbents. Several search engines were employed, including Scopus, ScienceDirect, American Chemical Society, and Royal Society of Chemistry. The literature search encompassed papers from the entire world and preferably published in the last 15 years, except for the cases of areas with limited research available or highly cited papers. Literature was selected based on the relevance to the subject and their references were also accessed for significant information. Special attention was given to those studies concerning pharmaceutical compounds that are most frequently detected in the environment. In comparison with other microcontaminants, such as toxic metal ions and dyes, the literature on pharmaceutical adsorption is relatively scarce and developments are still under progression, especially for adsorbents other than activated carbon. It is important to emphasize that the present review has a narrowed down scope, focusing on specific materials that have been used as pharmaceutical adsorbents (clays, chitosan, biochar, agro-industrial wastes, and MOFs). In the end, a total of 212 references were used, mostly papers of journals on engineering, chemistry, and environmental science. In addition, a few books and reports were selected.

2.3 **Background**

2.3.1 *Occurrence in the environment*

For at least 80 years, it has been reported that natural and synthetic compounds are able to affect hormonal activity in animals.[15-17] In the 1960s, discussions began in the Unites States on water contamination by complex chemicals synthesized for industrial, agricultural, and personal use. In the 1990s, reproductive anomalies were reported in fish from downstream of wastewater treatment plants (WWTPs), including feminization.[18-20] In the 1970s, the administration of synthetic estrogen diethylstilbestrol (DES) by pregnant women for miscarriage prevention evidenced the effects of compounds with estrogenic activity in human health: vaginal carcinoma and uterine abnormalities were detected in daughters of mothers treated with DES.[21]

Although the potential of pharmaceuticals as endocrine disruptors is obvious, it dates back to 1965 the first survey that specifically addressed the detection of these compounds in water and wastewater.[22] Later in the 1990s, pharmaceuticals were acknowledged as environmental contaminants at trace concentrations.[23-25] A variety of studies have reported their incidence in wastewater, surface water, and less commonly, in drinking and groundwater all

over the world: USA,[26, 27] Germany,[28, 29] Italy,[30] Australia,[31] China,[3] South Africa [32] and Brazil.[33-36]

Regardless of being widely identified in water bodies, the majority of the emerging contaminants is not included in legislations related to water quality. Pioneering actions have been taken by the U.S. Environmental Protection Agency [37] and by European Union [38] with lists of priority contaminants.*

**Notas da autora sobre avanços nas legislações ambientais:*

Nos Estados Unidos, está em elaboração pela U.S. EPA a quinta atualização da lista de candidatos a contaminantes (CCL5, do inglês Contaminant Candidate List) com compostos que atualmente não estão sujeitos a nenhuma regulamentação americana de água potável, mas que são conhecidos ou previstos para ocorrer em sistemas públicos de água. A quarta atualização da lista data de 2016 e conta com 97 substâncias ou grupos de substâncias químicas e 12 contaminantes microbianos, incluindo patógenos aquáticos, produtos farmacêuticos e químicos, pesticidas, toxinas biológicas e subprodutos de desinfecção. Tais contaminantes podem exigir regulamentação futura dentro da legislação americana, Safe Drinking Water Act (U.S. EPA, 2016).

Na União Europeia, a legislação prevê medidas contra a poluição das águas superficiais, incluindo a seleção e a regulamentação de substâncias ditas prioritárias dentro da Water Framework Directive (2000/60/EC) e Priority Substances Directive Directive (2008/105/EC) (alterado por Directive 2013/39/EU) (UNIÃO EUROPEIA, 2008; 2013; 2014). Atualmente, a lista de substâncias prioritárias com padrões de qualidade ambiental estabelecidos contém 33 substâncias ou grupos de substâncias, incluindo o pesticida atrazina e o detergente nonifenol, mas nenhum composto farmacêutico. Em março de 2019, a Comissão Europeia passou a adotar uma abordagem estratégica para fármacos no ambiente. Foram identificadas seis áreas de atuação, abrangendo todas as etapas do ciclo de vida de produtos farmacêuticos, desde o design e produção até o descarte e o gerenciamento de resíduos (UNIÃO EUROPEIA, 2019). Em 2005, a Comissão Europeia iniciou o projeto NORMAN, que constitui uma rede independente de laboratórios de referência, centros de pesquisa e organizações para o monitoramento de contaminantes de interesse emergente (NORMAN Network, 2016).

A nível internacional, a Agenda 2030 para o Desenvolvimento Sustentável estabelecida pela Assembleia Geral das Nações Unidas (2015) tem como Objetivo Global 6 assegurar a disponibilidade e gestão sustentável da água e saneamento para todos. Planos de ação voltados especificamente para a problemática de resistência antimicrobiana têm sido abordados pela Organização Mundial da Saúde e G7/G20.

No Brasil, a problemática dos contaminantes emergentes vem sendo amplamente debatida e foco de crescentes pesquisas, o que tem atraído a atenção de órgãos governamentais, agências reguladoras e companhias de saneamento brasileiras. Contudo, as legislações vigentes no Brasil ainda carecem de novos critérios de qualidade de água. Dentre as centenas de substâncias de preocupação emergente, somente cerca de trinta tipos de pesticidas são contemplados nas legislações vigentes no Brasil relacionadas à qualidade da água, sendo estas a Portaria do Ministério da Saúde 2914/2011 (BRASIL, 2011) que dispõe de padrões de potabilidade da água, e as Resoluções do Conselho Nacional do Meio Ambiente, CONAMA 430/2011 que tratam das condições e padrões de lançamento de efluentes, e 396/2008 e 357/2005 sobre qualidade de águas subterrâneas e superficiais, respectivamente (CONAMA, 2005; 2008; 2011).

2.3.2 *Environmental concentrations*

Advances on analytical techniques for the detection of pharmaceuticals, even at low concentrations (ng/L−μg/L), have allowed more extensive and in-depth evaluations on their occurrence in the environment. Recently, a wide survey showed the occurrence of 631 different drugs and their metabolites in 71 countries of all the five United Nations regional groups of the world. In common, all the regions presented residues of 16 pharmaceutical substances in surface, drinking, and groundwater: diclofenac, carbamazepine, ibuprofen, sulfamethoxazole, naproxen, estrone, estradiol, ethinylestradiol, trimethoprim, paracetamol, clofibric acid, ciprofloxacin, ofloxacin, estriol, norfloxacin, and acetylsalicylic acid. The reported global average concentrations ranged from 0.003 μg/L (estradiol) to 18.99 μg/L (ciprofloxacin).[39] In emerging countries such as Brazil, the reported average concentrations of pharmaceuticals in waters may be even higher.[40-43]

2.3.3 *Sources in the environment*

Several are the paths and sources for the incidence of pharmaceuticals in water media and the major ones are discussed here. WWTPs receive pharmaceuticals that are consumed in health care facilities and in households that were metabolized to a certain degree in human body and excreted in feces and urine. Before reaching WWTPs, hospital wastewater can be separately treated. Owing to inappropriate disposal, unused drugs (expired, rejected) can also reach WWTPs, where some of the pharmaceuticals and their metabolites are complete or partially degraded, resulting in a combination of microbial metabolites and parent compounds that enter surface and groundwater through effluent discharge.[44]

During the treatment in WWTPs, a sorption process may occur and some pharmaceutical pollutants may be transferred to sewage sludge, which can be incinerated, landfilled, or applied to agricultural lands. In the last two cases, the remaining compounds in the sludge may be introduced to the aquatic environment. In addition, contamination can be caused by the agricultural use of pharmaceuticals as livestock therapeutics, growth promoters, or feed additives for fish.[44]

Drugs are also uninterruptedly inserted into the environment by the input of highly polluted effluents from pharmaceutical industries. For instance, Dolar, et al.[45] reported concentrations of 27.68 and 17.48 mg/L for trimethoprim and ciprofloxacin, respectively, in wastewater effluent originating from the pharmaceutical industry in Croatia*. It is important to mention that wastewater in industrial facilities should be treated in the source, since the

treatment is more effective when the contaminated effluent is still not mixed with wastewater from other sources. After dilution, the treatment becomes more difficult and expensive.[46]

Moreover, it is important to list the direct release of *in natura* sewage as a source of drugs in the environment. For example, in Brazil, only about 42.7% of the generated sewage is treated and the deficiencies in sanitation system are evidenced by the concentrations of cocaine and its metabolite benzoylecgonine in surface waters, which were found to be up to 100 times higher than those of European countries.[36, 47]

Despite the variety of possible routes of contamination of aquatic media by drugs, the release of both *in natura* and treated effluents is considered as the main source. For that reason, advanced treatment methods need to be implemented to ensure greater removal of these contaminants in WWTPs and in drinking water treatment plants (DWTPs).[48]

2.3.4 *Environmental impacts*

In general, pharmaceuticals are biologic active, persistent, and bioaccumulative. Although being detected in low concentrations (ng/L to µg/L range), the incidence of a variety of contaminants in the environment sharing the same mechanism of action may cause pronounced effects through additive exposures, including endocrine disruption, genotoxicity, aquatic toxicity, and development resistant pathogenic bacteria.[25, 49]

Drugs are inserted in the environment in their essentially unaltered free form or as their transformation products (metabolites and conjugates), which can also offer adverse effects, since their physiologic activities can be greater than the parent compound. Once in the aquatic realm, most drugs are prevented of escaping due to their nonvolatile and polar nature, and even drugs with relatively short half-lives are treated as highly persistent pollutants in aqueous media because of continuous infusion of effluents from WWTPs and DWTPs.[25]

Information is scarce and imprecise about the ecological impacts of drugs and their transformation products in the environment, as well as about the long-term effects to human wellbeing by the ingestion of these compounds present in potable water. This is because tests for toxicological effects are extremely complex and, in general, only provide rough indications of directly measurable acute effects.[25] Another challenge is the choice of the pharmaceutical contaminant to be investigated, since there are more than 3000 different compounds that are used as medicines.[3]

2.3.5 *Removal efficiency from water and wastewater*

WWTPs are designed to handle macropollutants that are received on a regular basis and in great amounts (mainly nutrients, such as phosphorus and potassium, and organic matter).

This condition is opposite to that of pharmaceuticals, which are individual compounds with unique behavior that, in very low concentrations, represent a minimal portion of the organic load of the effluent to be treated.[4]

The uptake of trace contaminants in conventional WWTPs relies primarily upon the biological treatment step, especially the sorption process onto suspended solids and subsequent removal by decantation.[50] The organic micropollutants sorption onto sewage sludge depends on two mechanisms: absorption (hydrophobic interactions) and adsorption (electrostatic interactions). The adsorption mechanism is predominant at neutral pH; however, in this condition, several acidic drugs present negative charge due to deprotonated carboxyl radicals, which impairs the adsorption process, making negligible their sorption into sewage sludge. That is what happens with the polar drugs acetylsalicylic acid, ibuprofen, clofibric acid and bezafibrate.[50] In contrast, sorption through specific interactions is reported for the removal of basic and amphoteric drugs, such as the antibiotics ciprofloxacin and norfloxacin of the fluoroquinolones group.[51] Since sorption processes involve the phase transfer of pollutants from liquid effluent to sewage sludge, it can be said that the drugs are actually removed from the environment only if the sludge is incinerated. As previously mentioned, land applications or landfilling deposition of the sludge may lead to subsequent pollution of water.[44]

In addition to sorption onto sewage sludge, the process of biological degradation in WWTPs can lead to complete or partial removal of pharmaceuticals that are present in low concentrations. The affinity of pharmaceuticals and metabolites for bacterial sludge enzymes influences whether the compound is readily biodegradable (*e.g.*, as ibuprofen, bezafibrate, and caffeine) or not or very little. This is the case of clofibric acid, carbamazepine, and diclofenac that were not removed (or not significantly) in WWTPs of Berlin.[29]

Table 2.1 depicts the removal efficiency for different pharmaceuticals in WWTPs that have tertiary treatment with activated sludge. It can be noticed that removal percentages greatly vary with values ranging from 7% (diclofenac) to 98% (ibuprofen). Removal varies even for the same compound in different WWTPs.

Table 2.1. Pharmaceutical concentrations in influent and effluent and removal efficiency, REM (%), of wastewater treatment plants that have tertiary treatment with activated sludge.

Pharmaceutical	$C_{influent}$ (ng/L)	$C_{effluent}$ (ng/L)	REM (%)	Country	Reference
Diclofenac	1400	1300	7	Austria	Clara, et al.[52]
	905	780	14	Austria	Clara, et al.[52]
Ibuprofen	1200	24	98	Austria	Clara, et al.[52]
	2640-5700	910-2100	64 [a]	Spain	Carballa, et al.[53]
Bezafibrate	7600	4800	37	Austria	Clara, et al.[52]
	1550	715	54	Austria	Clara, et al.[52]
Sulfamethoxazole	75	51	32	Austria	Clara, et al.[52]
	1786	304	83 [a]	USA	Kwon and Rodriguez[54]
Naproxen	1790-4600	800-2600	48 [a]	Spain	Carballa, et al.[53]
Genfibrozil	934	41	96 [a]	USA	Kwon and Rodriguez[54]
Losartan	500	60	88 [a]	Netherlands	Oosterhuis, et al.[55]
Metformin	73730	1820	98 [a]	Netherlands	Oosterhuis, et al.[55]

[a] Average value

2.3.6 *Technologies for pharmaceutical removal*

Several techniques of water treatment, conventional or not, have been studied for greater pharmaceuticals uptake from wastewater. Simple physicochemical treatments, such as coagulation, flotation, lime softening, sedimentation, and filtration, are commonly applied at different stages of water treatment and are economically viable.[56-58] However, these treatments do not effectively remove most of pharmaceuticals and personal care products (PPCPs).[5, 57, 59] Although some of these compounds may be reactive with common disinfectant agents, such as chlorine or ozone, the possibility of forming toxic oxidative byproducts is of great concern.

Westerhoff, et al.[59] performed bench-scale experimentation to simulate individual treatment processes in a DWTP for the removal of PPCPs and endocrine-disrupting compounds. While coagulation and lime softening treatments decreased the initial concentration of these compounds by no more than 25%, separate chlorination or ozonation provided removal percentages from <10% to >90%. However, the oxidative processes produced byproducts that can pose greater risks than the parent compounds. Moreover, ozonation is particularly expensive due to high energy consumption, being estimated that this process, with about 0.1 kWh/m³, can increase by 40–50% the energy required in conventional treatment plants.[4]

In view of the present-day low quality of wastewater inputs to water bodies, existing treatment plants have to be upgraded with novel end-of-pipe methods that offer higher removal percentages than conventional treatments. In this context, advanced technologies have been studied, including membrane filtration, activated carbon adsorption, and advanced oxidation processes (AOPs).[44]

Membrane separation systems, for example micro- and nanofiltration, ultrafiltration, reverse osmosis, and electrodialysis, can be used to remove high molecular weight compounds, but they are difficult to apply due to high operation pressure requirements and they cannot treat large volumes.[60] In the case of micro- and ultrafiltration, pharmaceuticals are solely removed when associated with colloidal organic matter or particles, since most of the compounds have a molecular size between 150 and 500 kDa. Although tight nanofiltration (NF) and reverse osmosis (RO) methods can be employed to remove most of the pharmaceuticals, the processes are influenced by polarity, charge, and hydrophobicity of the compounds, and also by competition with cations and natural organic matter in solution.[2] Dolar, et al.[45] employed RO and NF as the final step of wastewater treatment for a real effluent from the pharmaceutical industry, pretreated by coagulation and microfiltration, and reported removal percentages ranging from 94 to 100% for veterinary drugs. Nevertheless, considering the high consumption of energy and of materials, reverse osmosis and nanofiltration have been more discussed for the case of the reuse of wastewater.[4]

It is well established that AOPs (*e.g.*, H_2O_2/UV, Fe^{2+}/H_2O_2, Fe^{2+}/H_2O_2/UV, O_3/ H_2O_2, O_3/UV) are effective for PPCPs removal and have a low demand of additional chemicals.[5, 61, 62] As disadvantages, they can form oxidation intermediates (byproducts), the toxicity of which can be higher than that of the original pollutant, and the processes are operationally complex and expensive, especially considering energy consumption.[5, 63]

Adsorption offers several advantages, such as low energy consumption, mild operation conditions, and lack of byproducts added to the system; therefore, this technology can be potentially used for pharmaceutical removal.[64]

2.4 Adsorptive process for pharmaceutical removal

2.4.1 *Definition*

Adsorptive processes are known to humans since antiquity. Ancient Egyptians, Greeks, Sumerians, Phoenicians, and Romans used to apply adsorbent materials such as clay, sand, and wood charcoal for desalination of water, clarification of fat and oil, as well as purification of water for medicinal purposes.[65, 66] The XVIII century marks the beginning of quantitative studies about adsorption, the first industrial applications of this technology, and the liquid phase adsorption studies. At this time, charcoal was used for gas adsorption and decolorization of tartaric acid and sugar syrup.[65, 67] In the 20th century, during the two World Wars, adsorption began to be used to remove and control water's taste and odor. Later, there was an increase in

detection in water of organic compounds harmful to health, including pharmaceuticals, which increased the interest in using adsorption in water and wastewater treatment.[68, 69]

Adsorption implies the transference and accumulation of adsorptive molecules from the fluid phase to the interfacial layer and can involve physical and/or chemical interactions.[70] While physical adsorption originates from intermolecular forces, such as van der Waals, chemisorption implies chemical interactions with concomitant transfer of electrons between the adsorbent and the adsorbate.[71]

Several factors determine the process efficiency, including the properties of adsorbent, absorptive, and solvent, as well as pH, temperature, and agitation speed operational conditions.[72] The chemical properties, superficial net charge (also dependent from solute), and porous structure of the adsorbent material affect the adsorption equilibrium. To be effective in separation processes, the material must present accessible internal volume to the compounds to be removed and satisfactory mechanical properties. Most applications also require the adsorbent to be regenerated in an efficient way and without further damages to mechanical and adsorptive properties.[73] For the adsorptive and solvent, adsorption depends on their structure, interactions (mutual and with the solid surface), and differences between physicochemical properties, such as solubility, molecular weight, and hydrophobicity.[72]

2.4.2 *Adsorption kinetics*

Kinetic study evaluates the adsorption rate, which can be limited by different mass transfer resistances depending on temperature and pressure conditions and on adsorbent and adsorbate nature. Two main resistances characterize the solid material: resistance to external diffusion (interparticle), related to mass transfer from bulk fluid to external surface, and intraparticle diffusion, related to mass transfer from an external surface to internal porous structure.[73] Several models have been proposed to examine mechanisms and the potential rate-determining steps. The adsorption kinetics of pharmaceuticals has been mostly represented by the models of pseudo-first-order (Eq. 2.1) [74] and pseudo-second order (Eq. 2.2):[75]

$$q(t) = q_e(1 - e^{-K_1 t}) \tag{2.1}$$

$$q(t) = \frac{K_2 q_e{}^2 \mathrm{t}}{1 + K_2 q_e \mathrm{t}} \tag{2.2}$$

where $q(t)$ is the amount of sorbent adsorbed onto the adsorbent at any time t (mg/g); q_e is the amount of solute adsorbed onto the adsorbent at equilibrium (mg/g); K_1 is the rate constant of pseudo-first-order model (min^{-1}); t is the time (min); K_2 is the rate constant of the pseudo-second-order model (g/mg/min).

Table 2.2 exhibits the adjustments of pseudo-first-order and pseudo-second-order equations to kinetic experimental data of pharmaceuticals adsorption onto different nonconventional materials.

2.4.3 *Adsorption equilibrium*

Dynamic adsorption equilibrium is established when adsorption and desorption rates are equivalent. In this condition, the global mass transfer of solute is zero since chemical potential is the same in both phases. For a given temperature and pressure, adsorption isotherms relate the amount of solute adsorbed in the solid phase and its equilibrium concentration in the liquid phase.[90] The modeling of isotherms is indispensable to properly evaluate and design adsorption systems. The most used parameters are generally obtained from the isotherm models of Langmuir (Eq. 2.3),[91] Freundlich (Eq. 2.4),[92] and Dubinin–Radushkevich (Eq. 2.5):[93]

$$q_e = \frac{q_{max} K_L C_e}{(1+K_L C_e)} \quad (2.3)$$

$$q_e = K_F {C_e}^{1/n} \quad (2.4)$$

$$q_e = X_m \exp\left(-K_{DR}\varepsilon^2\right) \quad (2.5)$$

where q_e is the concentration in the solid phase at equilibrium (mg/g); q_{max} is the Langmuir maximum adsorption capacity (mg/g); K_L is the Langmuir isotherm constant (L/mg); C_e is concentration of solute in solution at equilibrium (mg/L); C_0 is the initial solute concentration (mg/L); K_F is the Freundlich constant associated with adsorption capacity of the adsorbent [(mg/g).(L/mg)$^{1/n}$]; n is the Freundlich heterogeneity factor (-); X_m is the adsorption capacity of D-R isotherm (mg/g); ε is the Polanyi potential calculated by $\varepsilon = -RT\ln\left(C_e/C_S\right)$, in which R is the universal gas constant (J/mol/K), T is the temperature, and C_s is the water solubility of the adsorbate.[94]

Values of maximum adsorption capacity from the Langmuir model are exhibited in Tables 2.3, 2.4, 2.5 and 2.6 for the equilibrium of adsorption of several pharmaceuticals onto clay materials, biochar, chitosan, adsorbents based on agro-industrial wastes, and MOFs, respectively.

Table 2.2. Parameters of pseudo-first-order and pseudo-second-order models adjusted to kinetic adsorption data obtained under experimental conditions of initial concentration of pharmaceutical, temperature, pH, agitation speed, maximum contact time and concentration of adsorbent material (clay, agro-industrial wastes, modified chitosan, biochar, or MOFs).

Adsorbent	Experimental conditions	Pharmaceutical	Initial concentration (mg/L)	Pseudo-first order			Pseudo-second order			Reference
				Q_e (mg/g)	k_1 (min^{-1})	R^2	Q_e (mg/g)	k_2 (g/(mg.min))	R^2	
Bentonite (Clay)	22 ºC, pH not adjusted, 150 rpm, 60 min, 0.25 g/L	Ciprofloxacin	20	4.78	0.0387	0.4928	73.53	0.0183	0.9989	Genç and Dogan[77]
			25	9.38	0.0434	0.8541	91.74	0.0138	0.9998	
			30	17.35	0.0460	0.7787	107.53	0.00733	0.9981	
			40	28.4	0.0658	0.8178	138.89	0.00518	0.9999	
				2.29	0.0098	0.1099	14.53	0.08638	0.9771	
Natural clay (mixture smectite and kaolinite)	25 °C, 250 rpm, 6 h, 1 g/L	Ibuprofen	50	1.0030	0.0360	0.242	37	0.0018	0.999	Khazri, et al.[78]
		Naproxen		1	0.0060	0.171	37	0.0008	0.997	
		Carbamazepine		1	0.0030	0.050	40	0.0012	0.999	
Tetrabutylammonium - montmorillonite (Clay)	25 °C, 160 rpm, 16 h, 4 g/L	Flurbiprofen	245 [a]	1.77336	610.6625	0.976	2.34421	0.054449	0.999	Akçay, et al.[76]
Tetrabutylammonium - montmorillonite (Clay)	40 °C, 160 rpm, 16 h, 4 g/L	Flurbiprofen	245 [a]	0.73524	3492.9895	0.873	1.67199	0.1277301	0.998	Akçay, et al.[76]
Grape stalk	20 °C, pH=6.0, 30 rpm, 6.66 g/L	Paracetamol	20	0.00409	1.692	---	---	---	---	Villaescusa, et al.[79]
Acid activated red mud	28 °C, pH=7, 200 rpm, 75 min, 50 g/L	Ciprofloxacin	50	19.25	0.125	0.941	20.14	0.748	0.997	Balarak, et al.[80]
Magnetic-molecularly imprinted polymer based on chitosan/Fe_3O_4	200 rpm, 2 h, 2 g adsorbent/L	Carbamazepine	100	46.0725	0.4979	0.9802	50.2544	0.00635	0.9908	Zhang, et al.[81]
Cross-linked chitosan-zinc microparticles	37 °C, pH=6.5, 300 min, 1 g adsorbent/L	Ciprofloxacin	25	0.07	6,220	0.9940	15.64	660	0.7373	Reynaud, et al.[82]
			50	0.01	920	0.1068	30.30	2070	0.9883	
			100	0.14	4,370	0.6522	78.74	1470	0.9891	
			200	0.17	1,150	0.1009	153.84	4440	0.9903	
			300	0.33	3,220	0.7236	222.23	350	0.9669	
			400	0.44	12,200	0.8153	326.31	10	0.9620	

cont. **Table 2.2**

Biochar derived from rice straw (Biochar-500)	Room temperature, 100 min, 0.5 g adsorbent/L	Ibuprofen	---	98	0.00000542	0.92	165	230	0.99	Salem and Yakoot[83]
Commercial bone char	30 ºC, pH=7.0,	Naproxen	50 100 200	1.120 2.769 2.979	0.0179 0.0072 0.0109	0.94 0.99 0.96	1.037 0.129 0.198	0.0173 0.0022 0.0033	0.913 0.990 0.980	Reynel-Avila, et al.[84]
Primary paper mill sludge (PS800-150-HCl)	18 °C, pH=7–7.5, 90 rpm, 500 min, 2 g adsorbent/L	Methanesulfonate	250	83	0.28	0.9635	0.006	87	0.9862	Ferreira, et al.[85]
Cr-based MOF (MIL-101)	25 °C, pH=4.5, 10 min-12 h, 100 g adsorbent/L	Naproxen	10 13 15	-- -- --	-- -- --	-- -- --	94.7 113.3 121.8	0.00145 0.00147 0.00155	0.984 0.985 09996	Hasan, et al.[86]
Al-based MOF [MIL-53(Al)]	29.85 °C, pH=6.4, 48 h, 1 g adsorbent/L	Dimetridazole	40	2.54	0.0079	0.58	38.402	0.0302	0.999	Peng, et al.[87]
Methanol activated Cu-based MOF (HKUST-1)	25 °C, pH=7.5, 10 min-2 h, 0.1 g adsorbent/L	Sulfachloropyridazine	20 40	-- --	-- --	-- --	160 286	0.0062 0.0022	1 0.999	Azhar, et al.[88]
Chloroform activated Zr-based MOF (UiO-66)	25 °C, pH=5.5, 250 rpm, 5 min-2 h, 0.1 g adsorbent/L	Sulfachloropyridazine	5 25 45	-- -- --	-- -- --	-- -- --	50 220 404	0.088 0.061 0.022	1.00 0.998 0.999	Azhar, et al.[89]

[a] Solution of water and methanol

Table 2.3. Langmuir isotherm parameters for pharmaceuticals adsorption onto clay materials at certain experimental conditions of temperature, pH, agitation speed, contact time, initial concentration of adsorbate solution, and concentration of clay material.

Clay	Modification	S (m^2/g)	Operating conditions	Pharmaceutical	K_L ($L.mg^{-1}$)	Q_m ($mg.g^{-1}$)	Reference
Commercial montmorillonite KSF	Acid treatment	---	30 °C, initial pH=3.0, 7 h, 4 g adsorbent/L	Trimethoprim	0.00017	129.51	Bekçi, et al.[95]
Commercial montmorillonite K10	Acid treatment	---	25 °C, 150 rpm, 6 h, C_0=116.13-377.42 mg/L, 4 g adsorbent/L	Trimethoprim	0.00004	75.66	Bekçi, et al.[96]
Natural mixture of smectite and kaolinite	Purified with NaCl solution	69.5	25 ºC, pH=6, 250 rpm, 6 h, 1 g adsorbent/L	Ibuprofen Naproxen Carbamazepine	0.72993 2.32558 0.68493	3.52 2.87 3.40	Khazri, et al.[78]
Bentonite	---	91.627	30 °C, pH=2.31, 200 rpm, 8 h, C_0=300 mg/L, 2-30 g adsorbent/L	Amoxicillin	0.0074	53.9315	Putra, et al. [122]
Bentonite	---	23	24.85 °C, 17-24 h, C_0=10-100 mg/L, 0.5 g adsorbent/L	Promethazine Triflupromazine Trimethoprim Carbamazepine Ibuprofen	0.00061 0.00094 0.00034 0.00003 0.00003	151.98 145.56 100.00 92.08 16.41	Salihi and Mahramanlıoğlu[98]
Bentonite	---	---	Initial pH=4.5, 150 rpm, 30 min, C_0=50-500 mg/L, 2.5 g adsorbent/L	Ciprofloxacin	0.27	147.06	Genç, et al.[99]
Bentonite	---	67	20 °C, pH=6, 4 h, C_0=18-110 mg/L, 0.25 g adsorbent/L	Ciprofloxacin	0.24	337.55	Roca Jalil, et al.[100]
Reactorite	---	10	pH=4-5, 150 rpm, 24 h, C_0=50-1000 mg/L, 5 g adsorbent/L	Tetracycline	Not informed	140	Chang, et al.[101]
Exfoliated vermiculite	Thermal treatment	---	20 °C, pH=7, no agitation, 72 h, C_0=1-30 mg/L, 130 g/L	Gemfibrozil Mefenamic acid Naproxen	0.00471 0.00232 0.2054	1.0509 2.0202 0.06566	Dordio, et al.[102]
Lightweight expanded clay aggregates (LECA)	Thermal treatment	---	20 °C, pH=7, no agitation, 144 h, C_0=1-30 mg/L, 130 g adsorbent/L	Gemfibrozil Mefenamic acid Naproxen	0.6489 0.421 0.5738	0.01991 0.02368 0.01553	Dordio, et al.[102]
Na- montmorillonite organoclay	*Non-modified* Cation TMA[a] Cation DDTMA[b] Cation HDTMA[c]	84 73 6 9	25 °C, pH=5.5, 24 h, C_0=0-644.43 mg/L, 0.133 g adsorbent/L	Tetracycline	0.00731 0.00601 0.00187 0.00338	341.77 554.54 888.87 740.43	Liu, et al.[103]

cont. **Table 2.3**

Bentonite organoclay	Cation HDTMA[c]	3.79	30 °C; 250 rpm; 60 min; C_0=10-500 mg/L, 4 g adsorbent/L	Amoxicillin	3.701	27.85	Zha, et al.[104]
Illite organoclay	Cation CTA[d]	51	24 h, C_0=159.07-636.28 mg/L, 20 g adsorbent/L	Diclofenac	0.12573	15.91	Sun, et al.[105]
Montmorillonite organoclay	Cation CTA[d]	65	24 h, C_0=159.07-1590.7 mg/L, 3.5 g adsorbent/L	Diclofenac	0.10058	318.14	Sun, et al.[105]
Montmorillonite organoclay	Cation BDTMA[e] Cation HDTMA[c]	---	25 °C, pH=6.5, 50 rpm, 24 h, C_0=10-2000 mg/L	Diclofenac	0.0078 0.0049	55.67 50.64	De Oliveira, et al.[106]
Bentonite organoclay	Cation DMA[f]	0.31	30 °C, 250 rpm, 24 h, C_0=31.813-954.39 mg/L, 10 g adsorbent/L	Diclofenac	0.1927	36.58	Maia, et al.[107]
Aluminum pillared sericite organoclay	Cation HDTMA[c] Cation AMBA[g]	0.93 1.71	25 °C, pH=7.1, 24 h, C_0=1-20 mg/L, 0.2 g adsorbent/L	Diclofenac	0.003724 0.001954	0.845 2.295	Tiwari, et al. [123]

[a]TMA: tetramethylammonium; [b]DDTMA: dodecyltrimethylammonium; [c]HDTMA: hexadecyltrimethylammonium; [d]CTA: cetyltrimethylammoium; [e]BDTMA: benzyl decyltrimethylamcmonium; [f]DMA: dialkyl dimethylammonium; AMBA: alkyldimethylbenzyl ammonium chloride

Table 2.4. Langmuir isotherm parameters for pharmaceuticals adsorption onto biochars at certain experimental conditions of temperature, pH, agitation speed, contact time, initial concentration of adsorbate solution, and concentration of biochar material.

Biochar source	**Pyrolysis conditions (temperature, time and atmosphere) and posterior modifications**	***S*** **(m²/g)**	**Operating conditions**	**Pharmaceutical**	K_L **(L/mg)**	Q_m **(mg/g)**	**Reference**
Torrefied loblolly pine chip	300 °C 15 min Pure nitrogen gas Activated by NaOH	1360	Room temperature, pH=7, 500 rpm, 7 d, C_0=20 µmol/L, 0.005-0.04 g adsorbent/L	Diclofenac Naproxen Ibuprofen	5.89 8.9 8.2	372 290 311	Jung, et al.[108]
Torrefied loblolly pine chip	300 °C 15 min 7% oxygen and 93% nitrogen gas Activated by NaOH	1151	Room temperature, pH=7, 500 rpm, 7 d, C_0=20 µmol/L, 0.005-0.04 g adsorbent/L	Diclofenac Naproxen Ibuprofen	3.19 10.9 6.81	214 228 286	Jung, et al.[108]
Rice straw	600 °C 6 h Oxygen-limited conditions -	29.6	25 °C, pH=6, 150 rpm, 24 h, C_0=0-200 mg/L, 2.5 g adsorbent/L	Sulphamethoxazole	0.016	1.963	Li, et al.[109]
Alligator flag	600 °C 6h Oxygen-limited conditions -	7.1	25 °C, pH=6, 150 rpm, 24 h, C_0=0-200 mg/L, 2.5 g adsorbent/L	Sulphamethoxazole	0.024	3.650	Li, et al.[109]
Sludge from sludge concentration tank at a sewage treatment plant (FN)	550 °C 1h Nitrogen atmosphere Rinsed with HCl	217.1	25 °C, 170 rpm, 96 h, C_0=10-100 mg/L, 6 g adsorbent/L	Gatifloxacin	0.49	20.6	Yao, et al.[110]
Dehydration sludge from dairy wastewater plant (MT)	550 °C 1h Nitrogen atmosphere Rinsed with HCl	248.6	25 °C, 170 rpm, 96 h, C_0=10-100 mg/L, 6 g adsorbent/L	Gatifloxacin	0.48	20.3	Yao, et al.[110]
Bone char	Commercial bone char produced from bovine bones	74	30 ºC, pH=7, 24 h, C_0=20-250 mg/L, 10 g adsorbent/L	Naproxen	0.053	3.351	Reynel-Avila, et al.[84]

Table 2.5. Langmuir isotherm parameters for pharmaceuticals adsorption onto chitosan at certain experimental conditions of temperature, pH, agitation speed, contact time, initial concentration of adsorbate solution and concentration of chitosan material.

Chitosan	**Characteristics**	S **(m²/g)**	**Operating conditions**	**Pharmaceutical**	K_L **(L/mg)**	Q_m **(mg/g)**	**Reference**
>85% degree of deacetylation	Particle size <100 μm Particle size >350 μm	4.56 0.74	26 °C, pH=7, 15 rpm, 24 h, 2.22 g adsorbent/L	Ketotifen Fumarate	0 0.1	6629 3236	Alkhamis, et al.[111]
>85% degree of deacetylation	Particle size <100 μm Particle size >350 μm	4.56 0.74	26 °C, pH=10, 15 rpm, 24 h, 2.22 g adsorbent/L	Ketotifen Fumarate	147.3 79.3	5 14	Alkhamis, et al.[111]
Magnetic-molecularly imprinted polymer based on chitosan/Fe_3O_4	---	98.5	25 °C, 200 rpm, 2 h, C_0=10-200 mg/L, 2 g adsorbent/L	Carbamazepine	0.0715	88.294	Zhang, et al.[81]
Magnetic chitosan/Fe_3O_4 composite particles	---	3-50	pH uncontrolled, 2h, C_0=10-200 mg/L, 2 g adsorbent/L	Diclofenac	0.08078	31.47145	Zhang, et al.[112]
Magnetic chitosan/Fe_3O_4 composite particles with core-brush topology (CD-MCP)	Reacted with monomer 2-methyl acryloyloxyethyl trimethyl ammonium chloride	8.48	25 °C, 140 rpm, 12 h, C_0=20-200 mg/L	Diclofenac Sodium Tetracycline Hydrochloride	0.107 0.045	196 50.1	Zhang, et al.[113]
Graphite oxide/poly(acrylic acid) grafted chitosan	---	< 3	25 °C, pH=3, 160 rpm, 24 h, C_0=0-500 mg/L, 1 g adsorbent/L	Dorzolamide	0.119	233	Kyzas, et al.[114]

Table 2.6. Langmuir isotherm parameters for pharmaceuticals adsorption onto agro-industrial based materials at certain experimental conditions of temperature, pH, agitation speed, contact time, initial concentration of adsorbate solution and concentration of adsorbent.

Residue	Modification	S (m^2/g)	Operating conditions	Pharmaceutical	K_L (L/mg)	Q_m (mg/g)	Reference
Isabel grape bagasse	---	2	22 °C, natural pH=5, 50 rpm, 72 h, C_0=5-30 mg/L, 0.2 g adsorbent/L	Diclofenac sodium	0.02	76.98	Antunes, et al.[115]
Carbon black (BP-1300)	---	511	20 °C, 40 rpm, 10 days, C_0=50 mg/L, 0.044-1.111 g adsorbent/L	Naproxen Ketoprofen	1.17 1.34	90.51 82.17	Cuerda-Correa, et al.[116]
Grape stalk	---	---	20 °C, pH=6, 30 rpm, 48 h, C_0=20 mg/L, 3.33-33.33 g adsorbent/L	Paracetamol	1.3	2.18	Villaescusa, et al.[79]
Grape stalk	*In natura* Modified by phosphoric acid action	6.23 4.21	Room temperature, pH=2.0, 60 min, C_0=20-5000 mg/L, 25 g adsorbent/L (*in natura*), 15 g adsorbent/L (modified)	Caffeine	0.001 0.007	68.633 96.401	Portinho, et al.[117]
Red mud	Acid activation	28.7	28±2 °C, pH=6.5 ± 0.2, 200 rpm, 75 min, 50 g adsorbent/L	Ciprofloxacin	0.038	19.12	Balarak, et al.[80]
Coal fly ash	Treated with 6 M NaOH	17.5	30 °C, pH not adjusted, 100 min, C_0=40-140 mg/L, 40 g adsorbent/L	Ciprofloxacin	0.1226	1.443	Zhang, et al.[118]
Primary paper mill sludge (PS800-150)	Pyrolyzed at 800 °C for 150 min.	209.12	25°C, 50 rpm , C_0=5 mg/L, 0.1-2.5 g adsorbent/L	Citalopram	2.9	19.6	Calisto, et al.[119]
Primary paper mill sludge (PS800-150)	Pyrolyzed at 800 °C for 150 min.	209.12	25.0 ± 0.1 °C, 80 rpm, C_0=5 mg/L, 0.15-4.0 g adsorbent/L	Carbamazepine Oxazepam Sulfamethoxazole Piroxicam Cetirizine Venlafaxine Paroxetine	2.7 34 2.9 30 11 3.3 0.7	12.6 7.8 1.69 5.82 8.2 8.5 38	Calisto, et al.[120]
Primary paper mill sludge (PS800-150-HCl)	Pyrolyzed at 800 °C for 150 min and washed with 1.2 M HCl	414	25 ± 1 °C, 50 rpm, 0.1-0.5 g adsorbent/L	Carbamazepine Paroxetine Oxazepam	14.41 26.68 26.96	17.48 23.99 20.07	Calisto, et al.[121]
Primary paper mill sludge (PS800-150-HCl)	Pyrolyzed at 800 °C for 150 min and washed with 1.2 M HCl	414	18 °C, 90 rpm, C_0=100-500 mg/L, 2 g adsorbent/L	Methanesulfonate	0.4	93Ferreira, et al.[124]Ferreira, et al.[124]	

Table 2.7. Langmuir isotherm parameters for pharmaceuticals adsorption onto metal-organic frameworks (MOFs) at certain experimental conditions of temperature, pH, agitation speed, contact time, initial concentration of adsorbate solution, and concentration of adsorbent.

MOF	S (m^2/g)	Operating conditions	Pharmaceutical	K_L (L/mg)	Q_m (mg/g)	Reference
Cr-based MOF (MIL-101)	3014	25 °C, pH=4.5, 12 h, C_0=10-15 mg/L, 100 g adsorbent/L	Naproxen Clofibric acid	2.92 0.029	132 244	Hasan, et al.[86]
Acidic Cr-based MOF (AMSA-MIL-101)	2322	25 °C, 12 h, C_0=10-15 mg/L, 100 g adsorbent/L	Naproxen Clofibric acid	1.60 0.018	93 105	Hasan, et al.[125]
Basic Cr-based MOF (ED-MIL-101)	2555	25 °C, 12 h, C_0=50-150 mg/L, 100 g adsorbent/L	Naproxen Clofibric acid	3.25 0.024	154 347	Hasan, et al.[125]
Al-based MOF [MIL-53(Al)]	1401	29.85 °C, pH=6.4, 48 h, 1 g adsorbent/L	Dimetridazole	0.0512	467.3	Peng, et al.[87]
Methanol activated Cu-based MOF (HKUST-1)	1700	25 °C, pH=7.5, 2 h, C_0=20-100 mg/L, 0.1 g adsorbent/L	Sulfachloropyridazine	0.40	348	Azhar, et al.[88]
Chloroform activated Zr-based MOF (UiO-66)	1155	25 °C, pH=5.5, 250 rpm, 2 h, C_0=5-100 mg/L, 0.1 g adsorbent/L	Sulfachloropyridazine	0.75	417	Azhar, et al.[89]

2.4.4 *Adsorption thermodynamics*

Together with kinetic and equilibrium studies, thermodynamic study is essential to determine the nature of the adsorption process. From equilibrium results gathered at distinct temperatures, the thermodynamic parameters Gibb's energy (ΔG, kJ/mol), enthalpy (ΔH, kJ/mol) and entropy (ΔS, J/(mol.K)) can be calculated using the following equations (Eq. 2.6 and 2.7):

$$\ln K_C = \frac{-\Delta G}{RT} \quad (2.6)$$

$$\Delta G = \Delta H - T\Delta S \quad (2.7)$$

Adsorption is favorable and spontaneous at a certain temperature in the case that $\Delta G < 0$. Negative ΔH values indicate that the process is exothermic and involves physical adsorption, chemical adsorption, or a combination of both. In contrast, endothermic process ($\Delta H > 0$) suggests the occurrence of chemisorption.[71, 126] Positive ΔS values imply that the solid/solution interface has further randomness, which can be associated with the fact that the translational energy that is gained by the displaced solvent molecules (*e.g.*, water) is greater than that lost by the adsorbate molecules.[127]

Thermodynamic parameters reported in literature for the process of pharmaceuticals adsorption onto several non-conventional materials are listed in Table 2.8.*

*Notas da autora sobre as estimativas de constante de equilíbrio termodinâmico (K_C):

A estimativa dos parâmetros termodinâmicos é diretamente afetada pela constante de equilíbrio termodinâmico (K_C). Na termodinâmica de adsorção, K_C deve ser adimensional e pode derivar das constantes de isotermas de adsorção (e.g., Langmuir, Freundlich, Henry) ou do coeficiente de partição. As diferentes abordagens de estimativa de K_C podem levar a variações nos parâmetros termodinâmicos (TRAN; YOU e CHAO, 2016).

Na Table 2.8, "Thermodynamic parameters for adsorption of different pharmaceuticals by non-conventional low-cost adsorbents (clay, biochar, chitosan, agro-industrial wastes and MOFs)", os trabalhos listados usam abordagens diversas para as estimativas de K_C, sendo que alguns deles até mesmo não respeitam o critério de adimensionalidade de K_C. A autora recomenda consultar os trabalhos originais para maiores detalhes.

Table 2.8. Thermodynamic parameters for adsorption of different pharmaceuticals by non-conventional low-cost adsorbents (clay, biochar, chitosan, agro-industrial wastes and MOFs).

Adsorbent	**Pharmaceutical**	***T* (°C)**	**K_C (-)**	**ΔG (kJ/mol)**	**ΔH (kJ/mol)**	**ΔS (J/(mol.K))**	**Reference**
Bentonite organoclay	Amoxicillin	20	–	2.83	2.28	-1.868	Zha, et al.[104]
		30	–	2.85			
		40	–	2.86			
Montmorillonite KSF	Trimethoprim	23	2.338	-2.087	-14.233	-41.145	Bekçi, et al.[95]
		38	1.739	-1.428			
		50	1.430	-0.960			
Natural clay (mixture smectite and kaolinite)	Ibuprofen	20	1	-0.00729	10.50	30	Khazri, et al.[78]
		40	1.14	-0.34079			
		60	1.67	-1.43395			
Natural clay (mixture smectite and kaolinite)	Naproxen	20	1.00	-0.01214	11.05	30	Khazri, et al.[78]
		40	1.30	-0.69273			
		60	2.22	-2.21293			
Natural clay (mixture smectite and kaolinite)	Carbamazepine	20	1	-0.0092	8.01	20	Khazri, et al.[78]
		40	1	-0.28326			
		60	1.48	-1.10217			
Isabel grape bagasse	Diclofenac sodium	22	0.30	2.99	-36.86	-135.85	Antunes, et al.[115]
		30	0.16	4.57			
		42	0.10	6.10			
		50	0.08	6.81			
Sericin	Ibuprofen	27	25100[a]	-133.342	19.312	151,232	Verma and Subbiah[128]
Chitosan-based magnetic composite particles	Diclofenac sodium	15	22400[b]	-24.0	-16.6	-183	Zhang, et al.[113]
		25	34000 [b]	-25.9			
		35	14500 [b]	-24.5			
Chitosan-based magnetic composite particles	Tetracycline hydrochloride	15	12900 [b]	-22.7	32.5	192	Zhang, et al.[113]
		25	20100 [b]	-24.6			
		35	31000 [b]	-26.5			
Graphite oxide/poly(acrylic acid) grafted chitosan	Dorzolamide	25	99.02	–11.39	48.54	0.201	Kyzas, et al.[114]
		45	399.01	–15.84			
		65	999.04	–19.41			
Biochar derived from rice straw	Sulphamethoxazole	15		-11.28	5.3	57.58	Li, et al.[109]
		25	---	-11.86			
		35		-12.43			

cont. **Table 2.8**

Biochar derived from alligator flag	Sulphamethoxazole	15 25 35	– – –	-9.75 -10.24 -10.74	4.37	49.05	Li, et al.[109]
Commercial bone char	Naproxen	20 30 40	– – –	-0.33 -0.72 -1.22	75.11	230.0	Reynel-Avila, et al.[84]
Fe_3O_4/coffee composite	Tetracycline	25 55 85	1.36 1.21 1.09	-0.7661 -0.5093 -0.2522	-3.317	-8.56	Oladipo, et al.[129]
Methanol activated Cu-based MOF (HKUST-1)	Sulfachloropyridazine	25 35 45	0.40 0.41 0.61	-28.8 -29.8 -40.9	4.0	110.3	Azhar, et al.[88]
Chloroform activated Zr-based MOF (UiO-66)	Sulfachloropyridazine	25 35 45	0.75 0.41 0.16	-30.4 -29.8 -28.3	-60.6	-100.9	Azhar, et al.[89]

a: mol^{-1}, b: L/mol

2.4.5 *Continuous fixed-bed adsorption*

For an engineered adsorption process, fixed-bed reactors are usually preferred for large-scale wastewater treatment due to simplicity and high removal efficiency.[130] In a fixed-bed adsorption, the adsorbent is packed in a column and the fluid at certain concentration passes through it for mass transference of the adsorbate.[131] From laboratory column experiments, breakthrough curves (BTCs) can be determined. BTCs relate the outlet-to-inlet concentration ratio versus time (or effluent volume) and are essential for the design of full-size fixed-bed adsorption processes.[132]

Experimental BTC data can be analyzed by mathematical models and the most common ones are those of Bohart and Adams[133] (Eq. 2.8), Thomas[134] (Eq. 2.9), Yoon and Nelson[135] (Eq. 2.10), Clark[136] (Eq. 2.11), and Yan, et al.[137] (Eq. 2.12):

$$\frac{C(t)}{C_0} = \frac{e^{\tau}}{e^{\tau} + e^{\xi} - 1} \tag{2.8}$$

$$\frac{C(t)}{C_0} = \frac{1}{1 + e^{\frac{K_{Th}}{F}(q_{Th}m - C_0 Ft)}} \tag{2.9}$$

$$\frac{C(t)}{C_0 - C(t)} = e^{K_{YN}(t - t^*)} \tag{2.10}$$

$$\frac{C(t)}{C_0} = \left(\frac{1}{1 + A_C e^{-r_c t}}\right)^{1/(n-1)} \tag{2.11}$$

$$\frac{C(t)}{C_0} = 1 - \frac{1}{1 + [Ft/(q_Y m/C_0)]^a} \tag{2.12}$$

where: $C(t)$ is the adsorbate concentration at time t (mg/L); C_0 is the adsorbate initial concentration (mg/L); t is the time (min); τ is the equation parameter calculated by $\tau = K_{BA}.C_0(t - z/v)$;[138] ξ is the equation parameter calculated by $\xi = [K_{BA}.q_s.z/v][(1 - \varepsilon_b)/\varepsilon_b]$,[138] in which K_{BA} is the kinetic Bohart-Adams constant (L/(mg.min)), z is the bed height (cm), v is the linear velocity (cm/min), ε_b is the voidage of adsorbent bed, q_s is the saturation concentration (mg/L); K_{Th} is the rate constant of adsorption for the Thomas model (mL/(mg·min)); F is the flow rate (L/min); q_{Th} is the maximum solid-phase solute concentration estimated by Thomas model (mg/g); m is the adsorbent mass (g); A_C is the equation parameter calculated by $A_C = \left[\left({C_0}^{n-1}/{C_b}^{n-1}\right) - 1\right]e^{r_c t_b}$;[136] r_c is the Clark model constant (min^{-1}); t_b is the breakthrough time (min); n is the Freundlich's isotherm parameter (-); K_{YN} is the rate velocity constant (min^{-1}); t^* is the time in required for 50% adsorbate breakthrough (min); a is the constant of Yan et al. model; q_Y is the maximum adsorption capacity estimated by Yan et al. model (mg/g).

The characteristics of BTCs are expressed by several parameters, such as: breakthrough time (t_b, min); volume of treated effluent until t_b (V_b, L); breakthrough adsorption capacity; (q_u, mg/g); saturation/exhaustion time (t_s, min); volume of treated effluent until t_s (V_{ef}, L); saturation adsorption capacity (q_s, mg/g); and length of mass transfer zone (z_{MTZ}, cm). The breakthrough point is generally settled according to the target quality of the final effluent, hence it varies from one paper to another. This is also true for saturation point, the settlement of which may fluctuate from C/C_0=0.9 to C/C_0=1.

Table 2.9 exhibits experimental breakthrough data for continuous adsorption of pharmaceuticals onto different nonconventional materials, as well as the parameters reported for the Thomas model adjustment.

Table 2.9. Parameters of fixed bed adsorption of pharmaceuticals onto non-conventional low-cost adsorbents under certain operational conditions (length-inner diameter ratio (L/D_i), pH, temperature, bed height (z), adsorbent weight (m), flow rate (F), superficial velocity (u)) and the parameters from Thomas model.

Adsorbent	Pharmaceutical	Operational parameters	C_0 (mg/L)	t_b (min)	V_b (mL)	q_u (mg/g)	t_s (min)	V_{ef} (mL)	q_s (mg/g)	z_M (cm)	K_{Th} (mL/mg/min)	q_{Th} (mg/g)	R^2	Reference
Pyrolyzed paper mill sludge	Methanesulfonate	L/D_i=13/1; pH=7-7.5; 18 °C; z=4.5 cm; F=56 mL/(min.m²) upwards; u=5.5×10^{-5} m/min	100 250 400	170[a] 80[a] 57[a]	748 352 251	– – –	310[d] 155[d] 93[d]	– – –	87 102 125	– – –	0.49 0.4 0.4	85.6 107.5 124	0.99 1 0.99	Ferreira, et al.[85]
Fe_3O_4/Coffee composite	Tetracycline	L/D_i=40/2; pH=5; 25 °C; z=8 cm; F=3.3 mL/min; u=0.01 m/min	50 100 200	140.5 126.8 87.3	– – –	– – –	231.9[e] 205.4[e] 140.8[e]	770 610 460	33.5* 50.5* 70.7*	3.15 3.06 3.00	0.042 – –	298.3 – –	0.991 – –	Oladipo, et al.[129]
Biochar derived from mung bean husk	Ranitidine hydrochloride	L/D_i=35/1; pH=2; 28 °C; z=3 cm; F=2 mL/min downwards; u=0.03 m/min	100 150 200	110[b] 80[b] 63[b]	– – –	– – –	– – –	– – –	10.476[f] 11.429[f] 12[f]	1.308 1.4 1.424	– – –	– – –	– – –	Mondal, et al.[139]
Sepiolite clay	Caffeine	L/D_i=30/0.6; 25 °C; m=1.6 g; F=0.6 mL/min downwards; u=0.02 m/min	0.84 1.77 2.9	17982[c] 13158[c] 12036[c]	– – –	4.99 8.67 14.09	40200[g] 36090[g] 27666[g]	– – –	6.21 13.11 18.99	2.16 3.72 2.84	– – –	– – –	– – –	Sotelo, et al.[9]
Aluminum pillared AMBA modified sericite	Diclofenac	D_i=1 cm; pH=7.1; m=0.5 g; F=1 mL/min upwards; u=0.01 m/min	5	–	110	–	–	–	–	–	0.00648	1.056	–	Tiwari, et al.[123]
Aluminum pillared HDTMA modified sericite				–	170	–	–	–	–	–	0.0125	0.561	–	

[a] C/C_0=0.1; [b] C/C_0=0.50; [c] C/C_0=0.10; [d] C/C_0=0.95; [e] C/C_0=0.949; [f] C/C_0=0.90; [g] C/C_0=1; * q_s given in mg.

2.4.6 *Regeneration capability of non-conventional low-cost adsorbents*

The adsorbent capacity dictates the operating time of a fixed-bed adsorption unit, because, once the exhaustion is reached, the adsorbent has to be replaced by new or regenerated. Therefore, for continuous treatment of water and wastewater, the application of multiple adsorption systems is more adequate. Two or more fixed-bed columns can be connected in series and, when a column reaches a predetermined saturation level, the incoming fluid begins to flow in the next column, with the same characteristics of the first one, while the previous has its adsorbent replaced by new or regenerated material.[132, 140]

The term regeneration implies the desorption of the adsorbates from the adsorbent surface. Different regeneration techniques may be used, including desorption by steam, thermal swing, solvent extraction, pH shift, microbiological, electrochemical, and ultrasonic. The selection of the most adequate method is dependent on the type of the adsorbent, quality of the water/effluent, further treatment goals, and regeneration costs. This last factor is crucial for economic efficiency of an industrial adsorption process.[14, 132] Besides minimizing the need for fresh adsorbents, regeneration can reduce the issues related to disposal of used adsorbents.[141]

2.4.7 *Adsorbent materials*

Among adsorbent materials, activated carbons offer a well developed surface area, high microporosity, and great adsorption capacity, and have proven efficiency to remove organic contaminants in low concentrations (less than 1 mg/L).[142] Zhang, et al.[143] obtained substantial removal efficiencies as high as 99.6% for 28 antibiotics present in superficial water employing powdered activated carbon (PAC). Sotelo, et al.[144] investigated fixed bed adsorption with activated carbon and reported removal efficiencies up to 95% and 98% for diclofenac and caffeine, correspondingly. Notwithstanding the high capacity to remove organic contaminants, the widespread use of activated carbons is restricted by the high prices of those conventional and commercial materials, as well as by the high regeneration costs.[14, 97]

Lately, attempts have been made to substitute activated carbon for low-cost adsorbents.[5, 10] Nonconventional low-cost adsorbents have to be inexpensive and efficient for contaminant removal, with high adsorption capacity and high selectivity for different contaminant concentrations.[7] In the literature a wide variety of low-cost materials has been investigated, and this review discusses developments reported for the use of clays, chitosan, biochar, agro-industrial residues, and MOFs as adsorbents of pharmaceuticals from contaminated water.

2.5 Non-conventional low-cost adsorbents for pharmaceutical compounds

2.5.1 *Clays*

Clays are naturally occurring phyllosilicates with layer structure composed by tetrahedral and octahedral sheets in 1:1 or 2:1 proportions. While kaolinite and serpentine groups are 1:1 type clay minerals, groups such as pyrophyllite, talc, smectite, vermiculite, mica, chlorite, sepiolite, palygorskite, and loughlinite are 2:1 type.[145, 146] The interest in the use of clays as adsorbents is due to their high specific area, great mechanical and chemical stability, and ion exchange capacity. The adsorption capacity of a clay material depends on its chemical nature and pore structure.[6, 10]

Low-cost is another merit of clays as adsorbents; for example, the cost of montmorillonite (Mt), which is from the smectite group, can be up to 20 times cheaper than activated carbon.[10] In addition, pharmaceuticals removal efficiencies by clays can be comparable or even higher than by activated carbons. For instance, Genç and Dogan[77] tested bentonite, activated carbon, zeolite, and pumice as adsorbents of ciprofloxacin, and the highest removal efficiency (91%) was obtained for bentonite, which is a clay material especially rich in Mt. According to Table 2.2, the pseudo-second-order model well represented the kinetic experimental results with great values of the linear regression correlation coefficient, and bentonite presented the highest amount adsorbed at equilibrium.

Studies on the use of nonmodified bentonites have been conducted for the adsorption of a variety of pharmaceutical compounds, such as the antibiotics amoxicillin [97] and ciprofloxacin.[99, 100] For comparative purposes, Table 2.3 summarizes the reported values of maximum adsorption capacity from Langmuir model for the aforementioned systems, as well as for others involving pharmaceutical adsorption by clays (modified or not). Salihi and Mahramanlıoğlu[98] analyzed the adsorption of five pharmaceuticals onto bentonite and obtained the highest values of adsorption capacity, at a certain temperature, for promethazine, followed by triflupromazine, trimethoprim, carbamazepine, and ibuprofen (Table 2.3). All drugs had kinetic data well described by the pseudo-second-order equation, except for ibuprofen (pseudo-first-order), and the presence of surfactants in solution was shown to highly influence adsorption capacities, but not the equilibrium time of the process.

Chang, et al.[101] used rectorite, a clay mineral made of 1:1 ratio of illite and Mt, and obtained a sorption maximum of 140 mg/g for tetracycline uptake from aqueous solution (Table 2.3). Recently, a natural clay mixture of smectite–kaolinite and quartz, purified with NaCl, was tested for adsorption of ibuprofen, naproxen, and carbamazepine by Khazri, et al.[78].

The authors verified the lowest amount adsorbed for carbamazepine (32 mg/g), possibly because this drug was in its neutral form, while ibuprofen and naproxen were both protonated. Kinetics study showed that experimental data followed the pseudo-second-order model (Table 2.2) and thermodynamic evaluation indicated that the process was spontaneous and endothermic in nature (Table 2.8).

Na-rich Mt was tested as an adsorbent of sulfonamide and tetracycline antibiotics from synthetic effluent and field wastewater effluent. Under environmental pH conditions, adsorption capacity was negligible for sulfonamides, but high for tetracyclines.[147] Sotelo, et al.[9] and Álvarez, et al.[148] studied fixed-bed adsorption of caffeine using natural sepiolite clay (Minclear SG36). The system performance evaluation indicated that breakthrough time (C/C_0=0.1) decreased with decreasing mass of adsorbent, increasing volumetric flow rate and increasing inlet caffeine concentration (Table 2.9). Moreover, the process was found to be intraparticle mass transfer controlled. From the Bohart and Adams model, the adsorption capacity was of 3.98 mg/g, which is considerably inferior to that informed for the granular activated carbon-caffeine system, 155.6 mg/g.[144]

Aiming at increased removal efficiencies of negatively charged organic contaminants and/or nonpolar and hydrophobic persistent contaminants, clays have been chemically and physically modified to synthesize different adsorbents.[10, 149] When submitted to thermal treatment, clay minerals may be dehydrated and dihydroxylated. As a result of partial loss of adsorbed and hydration water, the material becomes more hydrophilic and has a higher surface acidity and may also have altered plasticity and macro- and microporosity.[150] Recently, Dordio, et al.[102] conducted studies about gemfibrozil, mefenamic acid, and naproxen adsorption onto lightweight clay materials, namely lightweight expanded clay aggregates (LECA) and exfoliated vermiculite. From Table 2.3, vermiculite exhibited higher maximum adsorption capacities; nevertheless, considering that LECA provided superior absolute removals, the authors concluded that a combination of the two materials would be promising. Maia, et al.[151] used Verde-lodo bentonite calcined at 500 °C and obtained a caffeine removal percentage of approximately 90%. Recent studies report the use of this same calcined clay to successfully remove metallic ions (silver and copper) from single and binary aqueous solution.[152, 153]

Clays may also be modified by acid activation using a mineral acid solution, commonly HCl or H_2SO_4. Although the obtained material is in part dissolved, it presents an enhanced porous structure, and higher specific surface area, and surface acidity.[154] Bekçi, et al.[95,96] examined trimethoprim uptake using two different acidic commercial clays: KSF and K10, respectively. KSF presented higher adsorption capacity (Table 2.3) and the estimated

thermodynamic parameters (ΔG, ΔH and ΔS) (Table 2.8) revealed that trimethoprim sorption onto this clay is spontaneous, exothermic and favorable. Moreover, the process might involve physical adsorption, since the calculated ΔG values varied between -20 and 0 kJ/mol. Besides thermal and acid washing, smectite clays, especially Mt, have been modified by organic molecules that are introduced to the interlayer space or adsorbed onto the surface to synthesize organoclays.[155]

Organoclays have higher affinity for organic compounds and can be prepared using small organic cations (*e.g.*, benzyltriethylammonium (BTEA), tetramethylammonium (TMA), or trimethylphenylammonium (TMPA)); organic cations with long alkyl chain (*e.g.*, hexadecyltrimethylammonium (HDTMA)); and singular organic modifiers (*e.g.*, chelating reagents, cationic polymers, and nonionic surfactants, ionic liquids, or more than one type of organic modifier).[149, 156]

The ionic liquid 1-hexadecyl-3-methylimidazolium chloride was recently employed by Sun, et al.[157] to modify the clays Mt and illite for chloramphenicol antibiotic uptake. The sorption followed a linear isotherm for both modified illitte and Mt, with distribution coefficients up to 14 L/kg and 179 L/kg, respectively. The same research group[105] prepared modified Mt and illite using cationic surfactant cetyltrimethylammoium bromide (CTAB) for diclofenac uptake. Modified Mt showed higher diclofenac adsorption capacity than modified illite, as illustrated in Table 2.3 for the surfactant loading level of 2.0 of cation exchange capacity.

Diclofenac adsorption was also studied by De Oliveira, et al.[106] using Mt modified with two different cationic surfactants and Table 2.3 reveals that the values obtained for maximum adsorption capacity were lower than those reported for CTAB-modified Mt. In common, both Sun, et al.[105] and De Oliveira, et al.[106] verified that pseudo-second-order model satisfactorily correlated kinetic data of diclofenac adsorption. Conversely, Maia, et al.[107] obtained better fittings for the pseudo-first-order model when using, as adsorbent, commercial organoclay (Spectrogel), which is functionalized by dialkyl dimethylammonium (DMA) surfactant. From Table 2.3, the value of maximum adsorption capacity of diclofenac from the Langmuir model obtained at 30 °C was approximately 36.58 mg/L.

Batch and column reactor operations studies on diclofenac adsorption were conducted by Tiwari, et al.[123] using aluminum pillared sericite modified with HDTMA (Al-AMBA-sericite) or AMBA (alkyldimethylbenzyl ammonium chloride) (Al-HDTMA-sericite). Equilibrium data were well fitted by the Langmuir isotherm model, for which the monolayer adsorption capacity was estimated as 0.845 mg/g and 2.295 mg/g for Al-AMBA-sericite and

Al-HDTMA-sericite, respectively (Table 2.3). The removal capacities obtained in column experiments were lower in comparison to those from batch experiments, probably due to insufficient contact time. From Table 2.9, the loading capacities of the Thomas equation were 0.561 mg/g (Al-AMBA-sericite) and 1.056 mg/g (Al-HDTMA-sericite).

In addition to diclofenac, bentonite organoclays modified with cationic surfactants have been successfully used as adsorbents of amoxicillin and propranolol,[151] and also of nicotine.[158] The study of Zha, et al.[104] indicated that the organoclay synthesized with long alkyl chain (HDTMA) was efficacious for amoxicillin uptake with a maximum adsorption capacity from the Langmuir model of 27.85 mg/g (Table 2.3). Table 2.8 shows the thermodynamic parameters of amoxicillin adsorption onto the organobentonite. The process was found to present endothermic and physisorptive character (ΔH=2.28 kJ/mol), decreasing randomness at the solid/solution interface (ΔS=-1.868 J/k mol) and to be favored at higher temperatures (increasing temperatures lead to increasing positive values of ΔG).

Akçay, et al.[76] examined the adsorption of the pharmaceutical flurbiprofen onto Mt modified with tetrabutylammonium and found out that pseudo-second-order model, rather than pseudo-first-order, better described kinetic data (Table 2.2).

2.5.2 *Biochar*

Biochar is a carbon-rich material that is prepared from the pyrolysis of organic matter, and that offers high affinity and sorption capacity toward organic contaminants, including pharmaceuticals.[159] Pyrolysis consists of the thermal degradation of biomass under relative low temperatures and in the absence of oxygen.[160] The process poses simplicity, affordability, and robustness for converting organic matter into bio-oil, biochar, and syngas.[161]

As stated in , Lehmann and Joseph,[159] biochar is formed at temperatures ranging from 300 to 700 °C, and the pyrolysis has residence time and heating rates as important operating parameters. Laird, et al.[161] classify the thermochemical technology in four categories: slow pyrolysis, flash pyrolysis, fast pyrolysis, and gasification. The last two are designed for maximum production of syngas and bio-oil, respectively, whereas slow pyrolysis offers biochar yields of approximately 35%, and flash pyrolysis offers the maximum production of biochar, yielding typically 60% biochar.

Biochar production technologies have as environmental advantages the reduced CO_2 emission and the possibility of using byproducts as feedstock. In this last case, the pyrolysis of residues may reduce the risks and costs associated with the disposal of waste materials and produce electricity.[162] Biochar can be a low-cost alternative to relatively more expensive

traditional adsorbents, such as activated carbon. The main difference between these materials is that while biochar is produced by heating biomass under a restricted supply of oxygen and at temperatures usually bellow 700 °C, activated carbon is "activated" by steam or chemicals at higher temperatures (superior to 700 °C).[159] Given the substantially lower costs of biochar, the traditional adsorbent granular activated carbon could be replaced by or augmented with biochar, aiming for the reduction of water treatment costs.[163]

Different materials can be pyrolyzed to produce biochar, including agricultural wastes and nonconventional materials such as waste tires, plants and algae, municipal and industrial solid waste, bones, bioenergy residues, and food waste.[164] To exemplify, Yao, et al.[110] prepared biochars with sludge from sewage and industrial wastewater treatment plants. The authors verified that they are efficient adsorbents of gatifloxacin, considering that more than 96% of the pharmaceutical was removed from the aqueous phase using most of the prepared biochars. Although the Freundlich model best fitted all experimental results, Table 2.4 presents values of highest maximum adsorption capacities from the Langmuir model (> 20 mg/g) obtained for two sludge-derived biochars.

Jung, et al.[108,165] used biochars derived from torrefied loblolly pine chip for the single- and multisolute adsorption of different pharmaceuticals. From single adsorption data, the maximum adsorption capacities followed the order diclofenac > naproxen > ibuprofen for biochar pyrolyzed with pure nitrogen (N-biochar). The opposite order was reported for biochar pyrolyzed with 7% oxygen with 93% nitrogen gas (O-biochar). Salem and Yakoot[83] conducted a study using biochars from rice straw pyrolyzed at distinct temperatures (400, 500 and 600 °C) and noticed that the one pyrolyzed at 500 °C (Biochar-500) yielded the highest ibuprofen removal. Regarding kinetic modelling, pseudo-second order was considered the best fitting model since it had calculated Q_e values similar to experimental data and an R^2 value (0.99) higher than pseudo-first-order (0.92). Twenty-seven different biochars, prepared from pine bark, fiber, bamboo, peanut hull, Brazilian pepper, and various woods, were tested as adsorbents by Mitchell, et al.[166] Six of the biochars well removed florfenicol, while ceftiofur was adsorbed by 15 of them.

Recently, Mondal, et al.[139] prepared stem activated biochar derived from mung bean husks for ranitidine hydrochloride removal in fixed-bed columns. The influence of operation parameters on breakthrough curves were analyzed and the highest adsorption capacity of 12.38 mg/g was obtained at 2 mL/min flow rate, 200 mg/L inlet concentration, and 3 cm bed depth (Table 2.9). The dynamic behavior of the column was better described by the Yoon-Nelson model than by the Bohart-Adams or Thomas models.

Several studies from the literature report the use of biochars for sorption of sulfonamides, such as sulfamethoxazole, sulfamethazine, and sulfapyridine. Yao, et al.[167] showed that biochars derived from bamboo and sugar cane bagasse have relatively high sorption ability for antibiotic sulfamethoxazole. These biochars were amended in sand soil, and column assays revealed that 2–14% of sulfamethoxazole in reclaimed water was transported through biochar-amended soils, while 60% was found in the leachate of unamended soils. Li, et al.[109] used two rice straw and alligator flag-based biochars to adsorb sulfamethoxazole and the first was shown to provide higher maximum adsorption capacity (Table 2.4). Equilibrium experiments were conducted at 15, 25, and 35 °C, and the adsorption capacity was found to be not influenced by temperature. This was evidenced by the very small oscillation on the calculated values of Gibbs free energy, as can been seen on Table 2.8. The authors verified that the adsorption processes are spontaneous (negative ΔG values) and identified that the physical mechanism of sorption is predominant, since ΔG values are less than 40 kJ/mol.

Lian, et al.[168] also studied the adsorption of sulfamethoxazole, but used pyrolyzed herb residue of Danshen, a Chinese medicine, as adsorbent. Sulfamethazine adsorption was investigated by Teixidó, et al.[169] employing a biochar prepared from the slow pyrolysis of hardwood litter. Xie, et al.[170] scrutinized the adsorption of sulfamethoxazole and sulfapyridine onto three pine-wood biochars prepared under different thermochemical conditions. The underlying mechanisms of sulfamethoxazole sorption by biochars were investigated by Zheng, et al.[171] and it was found that adsorption prevailed over partitioning and that both concentration and pH influenced the process. Recently, Lin, et al.[163] investigated three biochars for the adsorption of sulfamethoxazole, as well as of anti-inflammatory ibuprofen, using both reclaimed water reverse osmosis concentrate and synthetic solutions. In comparison to granular activated carbon (GAC), one of the tested biochar offered 10% lower removal for ibuprofen, but 20% higher removal for sulfamethoxazole, indicating that the biochar is a promising adsorbent.

2.5.3 *Chitosan*

Among the most plentiful natural biopolymers are cellulose followed by chitin, which is encountered in the exoskeleton of shellfish and crustaceans.[10] Several million tons of seafood crustaceans are consumed annually and about 50% of this amount is discarded as shell waste. Considering that the composition of prawn, lobster, and crab shells is approximately 15–20% of chitin, the availability of this residue becomes very large in the environment, which justifies the increase of interest for developing new applications for it.[172] The alkaline N-deacetylation

of chitin produces chitosan, which is considered a promising environment-friendly adsorbent material, since it presents adsorption properties, nontoxicity, high biodegradability, biocompatibility, and large availability, representing a low-cost alternative to activated carbon.[173] The molecular structure of chitosan is rich in amino and hydroxyl functional groups, which are capable of adsorbing a variety of molecules, from organics to metal ions, contaminants commonly found in wastewater. Besides being highly selective toward pollutants, chitosan is chemically stable, highly reactive, and has exceptional chelation behavior.[7] However, the development of chitosan-based materials as adsorbents at the industrial-scale is challenging, because the origin of the polysaccharide and the degree of deacetylation influence adsorption properties. Moreover, the characteristics of the materials can lead to column fouling and hydrodynamic restrictions, preventing large-scale columns operation.[7]

Chitosan particles were employed by Alkhamis, et al.[111] for the sorption of ketotifen fumarate. According to Table 2.5, sorption capacity was higher at pH 7 than 10, due to the swelling ability of chitosan. Regarding uptake mechanisms, ketotifen fumarate might have been absorbed both into the bulk structure of the material and on its surface. On one hand, the inherent attractive physicochemical characteristics of chitosan enable its use as adsorbent in raw form, but on the other hand, chitosan has modifiable positions in its chemical structure and can be grafted or cross-linked to form materials with better properties, including resistance to extreme conditions and enhanced adsorption capacity.[174]

Aiming at improved water treatment efficiency, magnetic carrier technology has been applied, such as by the introduction of Fe3O4 into chitosan biopolymer gel particles.[113] Zhang, et al.[81] synthesized a magnetic molecularly imprinted polymer based on chitosan- Fe_3O_4 composite and applied it for carbamazepine removal from Millipore water. Kinetic data were better fitted to the pseudo-second-order equation than to the pseudo-first-order equation (Table 2.2), indicating that carbamazepine adsorption was predominantly chemical. Assays carried out using real water samples (tap water, river water, and final sewage effluent water) revealed the feasibility of selective sorption of carbamazepine by the prepared adsorbent.

Later, Zhang, et al.[112] used magnetic chitosan derivatives to investigate the effects of ionic strength and natural organic matters on pharmaceuticals adsorption (diclofenac, clofibric acid, and carbamazepine) from aqueous media. There was no sorption reported for carbamazepine, due to the amide group and higher pK_a value, and high sorption affinity for diclofenac and clofibric acid. The isotherm curve of the latter was better fitted by the Freundlich equation, while the Langmuir equation better described diclofenac data with an estimated maximum adsorption capacity of approximately 31.47 mg/g (Table 2.5).

Zhang, et al.[113] synthesized several chitosan-based magnetic composite particles with a core-brush structure by grafting different polymeric branches onto chitosan-Fe_3O_4. The adsorption behavior of the materials was examined for the uptake of diclofenac sodium and tetracycline hydrochloride from single and binary solute solutions. Particles prepared by the reaction with the monomer 2-methyl acryloyloxyethyl trimethylammonium chloride (CD-MCP) were selected as the best adsorbent and experimental isothermal equilibrium data of the pharmaceuticals was best represented by the Langmuir model (Table 2.5). Thermodynamic analysis (Table 2.8) revealed that both adsorption processes were spontaneous (($\Delta G < 0$ and driven by entropy increase (($\Delta S > 0$), but diclofenac adsorption was exothermic and of tetracycline hydrochloride endothermic.

Reynaud, et al.[82] prepared cross-linked chitosan-metal microparticles using iron or zinc ions and showed that these materials are promising adsorbents for hospital wastewater containing ciprofloxacin. The authors observed that the presence of metal strongly enhances antibiotic uptake and higher adsorption capacities were provided by chitosan–Fe(III) and chitosan–Zn(II) microparticles. Kinetic data were better modeled by the pseudo-second-order equation than by pseudo-first-order equation, as evidenced in Table 2.2, which presents kinetic parameters obtained for ciprofloxacin adsorption onto chitosan–Zn(II) microparticles.

Kyzas, et al.[173] investigated pramipexole dihydrochloride adsorption using chitosan cross-linked with glutaraldehyde (Cs) and two further modified chitosan derivatives: grafted with N-(2-carboxybenzyl) groups (CsNCB) and grafted with sulfonate groups (CsSLF). The best adsorption behavior was verified for CsSLF, followed by CsNCB and Cs, and the optimum pH value was 10. More complex modifications in chitosan were performed by Kyzas, et al.[114]: chitosan cross-linked with glutaraldehyde and grafted with poly(acrylic acid) was further functionalized with graphite oxide (GO/CSA). The final nanocomposite material was used for the adsorption of dorzolamide from biomedical synthetic wastewaters and a removal capability of 92% was obtained at pH 3 (optimum value). Experimentally, higher temperatures enhanced pharmaceutical adsorption. This behavior was corroborated by thermodynamic analysis: increasing absolute values of ΔG with increasing temperature and positive values of ΔH. Table 2.8 presents thermodynamic parameters reported for the initial concentration of 20 g/L. ΔG values were negative, indicating that the process is spontaneous, while ΔS values were positive, reflecting the affinity of the adsorbent toward dorzolamide, conjointly with greater degree of freedom of the adsorbed species.

Recently, Kyzas, et al.[175] used chitosan derivative grafted with sulfonic groups and cross-linked with glutaraldehyde for the adsorption of pramipexole dihydrochloride. The

authors found out that the presence of humic acids in adsorbate solution negatively influences the adsorption capacity of the pharmaceutical.

2.5.4 *Agro-industrial wastes*

Large quantities of agro-industrial waste are generated because of industrial development. A novel attribution of greater added value is given by the application of the residues as adsorbents. Although their removal capacities are usually lower than those of activated carbon, their use in industrial scale is more economically attractive.[176] Besides low-cost, higher abundance, and availability, the agro-industrial waste adsorbents offer environmental advantages in comparison with conventional adsorbents, including renewable nature and the possibility of partial reduction of the waste.[5, 57, 115] Cellulose is the main contaminant of agro-industrial wastes and the one that contributes most to their adsorption properties. Other important components are hemicellulose, lignin, lipids, proteins, simple sugars, water, hydrocarbons, and starch.[177, 178]

Even though agricultural and industrial wastes may be employed to produce activated carbons and biochars,[10] there are several studies involving their direct employment as adsorbents of contaminants, including pharmaceutical compounds. The materials can be used *in natura* or physically or chemically modified.[5] For example, besides in the form of activated carbon, Portinho, et al.[117] used grape stalk from *Vitis vinifera* species in the raw form and modified by phosphoric acid action. The latter form presented higher caffeine adsorption capacities than the unmodified form, thanks to the greater availability of oxygenated surface functional groups. Table 2.6 shows the maximum adsorption capacities from the Langmuir isotherm model for these materials, as well as for other agro-industrial-based adsorbents that have been studied for pharmaceutical removal.

Antunes, et al.[115] studied the potential of Isabel grape bagasse, a residue generated from wine production, for diclofenac sodium adsorption from water. Langmuir maximum adsorption capacity obtained for the bagasse is presented in Table 2.6; nevertheless, it is noteworthy to mention this value is not relevant, since the correlation coefficient of the Langmuir isotherm was not satisfactory (about 0.5). The equilibrium data were best fitted by the Freundlich model, suggesting a multilayer adsorption of diclofenac sodium onto Isabel grape bagasse, and thermodynamic evaluation revealed the process was of an exothermic nature and accompanied by a decreasing randomness at the solid/solution interface (Table 2.8). Villaescusa, et al.[79] also investigated a waste generated after wine production (grape stalk), as well as after yohimbe extraction (yohimbine bark) and after taps manufacturing (cork bark), for the adsorption of

paracetamol. Grape stalk was shown to be the most effective adsorbent and the pseudo-first-order model (Table 2.2) and Langmuir isotherm (Table 2.6) were applied to model adsorption kinetic and equilibrium data, respectively.

Oladipo, et al.[129] verified that coating waste coffee residue with Fe_3O_4 confers magnetic separability, improved surface area, and consequent enhanced the adsorption capacity of tetracycline (up to 285.6 mg/g). While the Langmuir model better described the isotherms, the pseudo-second order model better fitted the kinetic data, suggesting the chemical nature of tetracycline adsorption onto the Fe_3O_4/coffee composite. According to Table 2.8, the process is exothermic (ΔH<0), spontaneous (ΔG<0), and accompanied by decreased randomness at the solid–liquid interface (ΔS<0). Dynamic studies of tetracycline adsorption revealed that breakthrough time increased with increasing bed height, decreasing flow rate, and decreasing influent concentration. The Thomas model was shown to suitably describe the process with R2 values higher than 0.99 for all the evaluated conditions (Table 2.9).

Industrial wastes that have been investigated as pharmaceutical adsorbents include fly ash and those from the aluminum industry and paper industry, as well as other materials. Fly ash is a waste byproduct material originated from coal combustion in thermal power plants. It finds applications on road construction and bricks and cements manufacturing, but it can also be employed as efficient adsorbent of organic pollutants, due to the high percentage of silica and alumina.[141, 177]

Zhang, et al.[118] presented modified coal fly ash as a promising adsorbent of ciprofloxacin, claiming that the material is cheaper than other alternative adsorbents, such as clay minerals, and can offer relatively larger adsorption capacities. Swarcewicz, et al.[179] inspected a mixture of soil and coal fly ash for carbamazepine adsorption from water–ethanol solution. Batch assays showed that when the content of coal fly ash in the soil was beyond 30% the mean removed amounts of the pharmaceutical were higher than 92.8%.

Among wastes from the aluminum industry, there is red mud, which is generated from bauxite processing for the production of alumina. Although red mud is a serious pollutant, after some treatment, it can be used for water treatment. Recently, an acid activated red mud was used by Balarak, et al.[80] for ciprofloxacin removal from synthetic wastewater and a removal efficiency as high as 96.5% was reached. By comparison with the pseudo-first-order, the pseudo-second-order kinetic model represented experimental results more satisfactorily with correlation coefficients up to 0.997 (Table 2.2)

Regarding paper industry waste, Calisto, et al.[119] prepared different alternative adsorbents based on pyrolyzed primary and biological paper mill sludge. The derivatives from

primary paper mill sludge were most effective for antidepressant citalopram uptake and the material pyrolyzed at 800 °C for 150 min (PS800–150) presented the highest Langmuir maximum adsorption capacity of 19.6 mg/g (Table 2.6). It is worth highlighting that this was a promising result, since obtaining effective, cheap, and environmentally friendly carbon adsorbents without employing chemical or physical activation is a feasible way of valorizing subproducts, such as those from the paper industry. Posterior studies report the use of the same pyrolyzed primary pulp mill sludge, PS800-150, for the adsorption of several pharmaceuticals from single solutions.[120, 180]

Recently, Calisto, et al.[121] employed PS800-150 washed with 1.2 M HCl (PS800-150-HCl) for single, binary, and ternary adsorption of carbamazepine, oxazepam, and paroxetine from ultrapure water. Concerning the single component system, the obtained values of Langmuir maximum adsorption capacity are displayed in Table 2.6. In the mixtures, individual reduced maximum adsorption capacities were obtained for most of the pharmaceuticals, which could be related with competitive effects. Acid-washed pyrolyzed primary and biological paper mill sludge were employed by Ferreira, et al.[124] for comparison with powdered activated carbon (PAC) in methanesulfonate removal (fish anesthetics). Although PAC displayed higher adsorption capacities, the authors posit that the alternative adsorbents offer advantages, such as production without activating chemicals, null costs of the precursors, and possible elimination of managing costs of residues (sludge) from the paper industry.

Later, Ferreira, et al.[85] performed studies in continuous mode using the same acid washed pyrolyzed biological paper mill sludge for methanesulfonate removal. It was shown that decreasing concentration and influent flux lead to greater volumes of treated effluent at breakthrough time, and the values obtained for total adsorption of the bed were high as 125 mg/g (Table 2.9). The models of Thomas, Yoon–Nelson, Clark, and Yan were applied to describe the breakthrough curves, and the latter was found to be the most adequate.

Carbon blacks are small particle size carbon pigments made of the thermal decomposition of hydrocarbons recovered from waste tires. Although carbon blacks have less developed porous texture than other carbon adsorbents, which could cause reduced adsorption capacities, these materials have mostly macro- and mesoporous textures, which makes them suitable for organic pollutant adsorption. For instance, Cuerda-Correa, et al.[116] used carbon blacks for the adsorption of naproxen and ketoprofen, the first being better removed from Milli-Q water than the latter (Table 2.6). The same behavior was noticed when using river water as the aqueous matrix; however, in this case larger adsorption capacities were obtained, possibly because of the presence of solid matter in suspension that may act as coadsorbent.

Other nonconventional adsorbents that have been analyzed are derivatives of sewage sludge and fish waste that were carbonized at different temperatures and used for the adsorption of carbamazepine,[181] and sulfamethoxazole and trimethoprim.[182] Silk manufacturing generates large amounts of sericin, a natural globular protein of silkworm cocoons that, due to its attractive properties, has been evaluated as a potential adsorbent of different contaminants, such as metal ions[183] and pharmaceuticals. Verma and Subbiah[128] used an integrated adsorbent-membrane process to remove ibuprofen from aqueous solution. The material used as adsorbent was sericin, a globular protein obtained from silkworm cocoons, which showed potential to enhance the adsorption capacity of ibuprofen from aqueous solution. Table 2.8 shows that the ibuprofen adsorption process was spontaneous (ΔG=-133.42 kJ/mol) and endothermic in nature (ΔH=19.312 kJ/mol).

2.5.5 *Metal-organic frameworks*

MOFs represent an innovative class of functional hybrid materials that are made by linking metal-containing units and organic units through strong bonds (reticular synthesis). The flexibility in varying size, functionality, and geometry of the constituents has enabled the development of thousands of different MOFs. Fundamentally, a MOF consists of a crystalline framework with permanent porosity, which is typically more than 50% of its crystal volume. Moreover, the usual values of surface area of MOFs (1000–10,000 m^2/g) are superior to those of zeolites and carbons.[184] In addition to superhigh pore volume and surface area, MOFs also have physicochemical properties easily tuned. Therefore, MOFs have been used as promising materials in different applications, including hydrogen storage, CO_2 capture, CH_4 storage, catalysis, and drug delivery systems, sensors, and separations.[88, 185] The first studies on the application of MOFs in WWTPs date back to 2010, but research on pharmaceuticals removal is still scarce.[88] Among the major challenges for using MOFs as adsorbents, one may cite large-scale production, water stability, and reusability. Since the majority of MOFs are not stable in contact with water, low recoveries and even second pollution of metal leaching may occur.[186]

Among the various MOFs developed so far, MIL-101 (chromium-benzenedicarboxylate, $Cr_3O(F/OH)(H_2O)_2[C_6H_4(CO_2)_2]$), has been widely studied for potential applications, because of its huge porosity (1.9 cm^3/g). MIL-101, in which MIL stands for Material of Institute Lavoisier, was pioneered for use by Hasan, et al.[86] as an adsorbent of pharmaceuticals. The authors proved that MIL-101, as well the MOF iron-benzenetricarboxylate (MIL-100-Fe), can be potentially used for naproxen and clofibric acid removal. Adsorption kinetics was found to follow the pseudo-second-order model (Table 2.2)

and equilibrium data was well represented by the Langmuir isotherm (Table 2.7). Adsorption performance of the MOFs was compared to that of AC, and the decreasing removal efficiency followed the order MIL-101 > MIL-101-Fe > activated carbon.

Later, Hasan, et al.[125] functionalized MIL-101 with an acidic group (AMSA-MIL-101) and basic group (ED-MIL-101) and tested the adsorption efficiency for naproxen and clofibric acid removal in batch tests. The MOF ED-MIL-101 offered the highest removal efficiency in terms of adsorption rate and adsorption capacity (Table 2.2 and Table 2.7). Acid–base interactions between adsorbent and adsorbates were suggested to explain the adsorption mechanism. Seo, et al.[64] also employed MIL-101 for naproxen adsorption. However, the authors functionalized MIL-101 with H-donor functional groups such as −OH and $-NH_2$. The importance of H-bonding mechanism was verified, and the highest adsorption capacity was obtained for MIL-101-OH (185 mg/g at 25 °C).

Seo, et al.[187] further modified MIL-101(Cr) by grafting urea or melamine on its open metal sites and tested the adsorption of three nitroimidazole antibiotics (dimetridazole, metronidazole, or menidazole). Although presenting lower specific surface area in comparison to pristine MIL-101, urea-MIL-101 and melamine-MIL-101 offered the highest adsorbed quantities of nitroimidazoles. The H-bonding between $-NH_2$ of the modified MOFs and $-NO_2$ of the antibiotics was indicated as the main adsorption mechanism. Dimetridazole removal was also investigated by Peng, et al.[87], but using a highly flexible Al-based MOF [MIL-53(Al)]. The obtained saturated adsorption capacity from the Langmuir model was of 467.3 mg/g (Table 2.7), which was associated with the reinforced van der Waals interaction between dimetridazole and the framework of MIL-53(Al). It was reported a fast kinetics, being that 90% of dimetridazole was removed within the first 10 min of contact.

Hasan, et al.[188] investigated Zr-based MOFs as adsorbents of diclofenac sodium. The authors used virgin MOF, UiO-66 (UiO stands for University of Oslo), and modified MOFs, SO_3H-UiO-66, and NH_2–UiO-66. Experiments were also carried out with activated carbon for comparison purposes. The best adsorption performance was given by SO_3H-UiO-66, the adsorption capacity of which was up to 13-times higher than that of AC.

Azhar, et al.[88] carried out batch studies on adsorptive removal of sulfachloropyridazine antibiotic from wastewater using a Cu-based MOF that was activated with methanol (HKUST-1). While adsorption kinetics data were best represented by the pseudo-second-order model, the Langmuir isotherm best fitted equilibrium data with a maximum adsorption capacity of 384 mg/g at 25 °C (Table 2.7). According to Table 2.8, the process was found to be thermodynamically spontaneous and endothermic. It was also noticed that some interactions,

such as electrostatic and π–π stacking, play important roles in the high obtained adsorption capacity. Those interactions, along with hydrophobicity, were also found to mainly contribute to elevate adsorption capacity of sulfachloropyridazine by chloroform activated Zr-based MOF (UiO-66).[89] From Table 2.7, this material, in comparison to HKUST-1, presents higher Langmuir adsorption capacity (417 mg/g). Thermodynamic study indicated that the adsorption process is spontaneous and exothermic in nature (Table 2.8).

2.6 Adsorbent regeneration

Considering how sophisticated and expensive an adsorbent is, its recovery after use is an important factor for economic efficiency of the industrial adsorption process. In the case of weak interactions between the adsorbent and the adsorbate, such as dispersion-van der Waals, the organic contaminant can be easily desorbed to obtain a regenerated adsorbent. In the literature, one may find several studies on regeneration of spent ACs after pharmaceutical uptake using different approaches, such as thermal regeneration,[189] chemical desorption,[190] and catalytic ozonation.[191] Because of the relatively low costs of PAC as compared to GAC, PACs are generally employed in batch adsorption as one-way adsorbents and are disposed of by landfill or incineration. On the other hand, GACs in fixed-bed systems have adsorption capacities typically restored by reactivation. However, reactivation is a thermal process with hard-to-find optimum conditions and that may unavoidably lead to weight losses and changes in a porous structure, impacting adsorption capacity.[132] As a result, several papers report that reactivated ACs may not be as efficient as new ones. The hard regeneration makes adsorption using ACs costly and limits the application in a large scale.[192]

A restricted number of publications examines regeneration and reutilization of spent nonconventional low-cost adsorbents after pharmaceuticals removal. Similarly to PACs, these materials are also not typically regenerated but disposed of by incineration or landfill. Considering economic efficiency of the whole adsorption process, obtaining fresh low-cost adsorbents, such as those from waste products, can be more profitable than regenerating the spent ones.[132] In the present work, we attempt to present recent data on regeneration and reusability of nonconventional adsorbents after pharmaceutical adsorption, using different approaches.

Recently, Ferreira, et al.[85] investigated thermal regeneration of pyrolyzed paper mill sludge after adsorption of methanesulfonate in continuous mode (Table 2.9). The authors performed three consecutive cycles of adsorption–desorption and concluded that regeneration and reusability of the adsorbent could be considered for one cycle only, due to remarkable

decrease in adsorption performance. The authors highlight that economic efficiency has to be addressed in this case, since pyrolyzed paper mill sludge derives from a waste product and its preparation costs can be lower than the regeneration costs.

Shan, et al.[193] employed the technique of ball milling not only to prepare ultrafine magnetic biochar (biochar/Fe_3O_4), which effectively adsorbed carbamazepine and tetracycline, but also to degrade the adsorbed pollutants on the spent adsorbent. The degradation efficiency was up to 99% for tetracycline adsorbed on spent biochar/Fe_3O_4 (3 h ball-milling), and up to 98.4% for carbamazepine (6 h of ball-milling with quartz sand addition). Although the authors did not study adsorbent regeneration, their results show that ball milling can be an effective technique to degrade adsorbed pollutants, aimed at reducing environmental risk related to disposal of spent adsorbents.

Reguyal, et al.[194] prepared magnetic biochar from pine sawdust for sulfamethoxazole removal and tested adsorbent regeneration using water (<4% desorption) and eight organic solvents (~45–67% desorption). Hence, solvent polarity was found to play an important role in the regeneration process, and the authors suggest that thermal or chemical regeneration could be more suitable for desorbing sulfamethoxazole from spent magnetic biochar.

In addition to the continuous mode, studies on the regeneration of spent low-cost nonconventional adsorbents have also been carried out in batch mode. Zhang, et al.[81] showed that magnetic molecularly imprinted polymers based on chitosan–Fe_3O_4 can be effectively regenerated by methanol/acetic acid and used at least in 10 cycles for carbamazepine adsorption without prejudices in adsorption capacity. Regeneration studies with similar magnetic chitosan adsorbent was also performed by Zhang, et al.[112] However, these authors employed a thermal process and found out that nanopowder Fe_3O_4 can be recovered to be reused in the synthesis again. In the work of Zhang, et al.[113] after diclofenac and tetracycline adsorption, chitosan-based magnetic composite particles with core-brush topology were separated under magnetic field and a solution of ethanol and water with NaOH was used for the desorption of the pharmaceuticals. Five adsorption–desorption cycles were performed and decreasing adsorption efficiencies were obtained in the first cycles.

Kyzas, et al.[173] and Kyzas, et al.[114] examined reuse ability of different grafted chitosan adsorbents for pharmaceuticals removal. Desorption tests were performed in batch mode with deionized water with pH-adjusted values. At optimum desorption pH, sequential cycles of adsorption–desorption were performed and both studies report reduction of adsorption efficiencies, which was attributed to several reasons, such as adsorbent degradation, gradual saturation of active sites/groups and gradual blocking of active sites by impurities.

Aiming at reduced costs for commercial applications, regeneration studies have also been reported for MOFs after pharmaceutical adsorption. Hasan, et al.[125] evaluated reuse ability of Cr-based MOF MIL-101 functionalized with an basic group (ED-MIL-101) for naproxen adsorption in batch mode. Ethanol was better for regeneration than water, and recycle tests revealed that up to three runs could be carried out with prejudice to the adsorption performance of naproxen. Similarly, Seo, et al.[64] also found out that functionalized MIL-101 with −OH group (MIL-101-OH) can be regenerated several times with ethanol, offering high adsorption efficiencies for naproxen removal. In the work of Seo, et al.[187] acetone was used as desorption agent to test reusability of MIL-101 modified with urea (urea-MIL-101) for dimetridazole adsorption in four-run cycles. The authors noticed that the performance of the material slightly decreased with consecutive use; however, urea-MIL-101 adsorbent, even after four runs, presented higher adsorbed quantities of dimetridazole than fresh activated carbon. Acetone was also employed by Peng, et al.[87] in regeneration studies of an Al-based MOF [MIL-53(Al)]. They revealed that adsorption capacity of dimetridazole removal onto MIL-53(Al) after the fourth run was almost the same than that obtained with fresh adsorbent.

2.7 Cost estimation

Adsorption processes can be efficient for the removal of pharmaceuticals from contaminated water. The ACs, especially in the granular form, are the most employed adsorbent materials with a great number of studies on its applicability available in the literature.[63] Despite that, ACs are expensive and, if used to remove polar organic contaminants, demand high usage rates, due to reduced lifetime and low regeneration capacity, what increases the costs of the adsorption process.[65, 195, 196] Depending on the type of adsorbent, the cost of water treatment using adsorption processes is estimated to be in the range from US $10 to US $200 per million liters, while when using technologies like reverse osmosis, ion exchange, electrodialysis, and electrolysis, the cost can reach US $450 per million liters.[197]

To reduce the costs of adsorption technology, the scientific community has been looking for alternative low-cost adsorbents. The present work summarizes the main findings on the applicability of some nonconventional low-cost adsorbents in batch and continuous processes for the removal of pharmaceuticals. The comparison of efficacy of different adsorbents is challenging, since the materials have distinct adsorption capacities, dependent on experimental conditions, as well as distinct properties. In this context, cost estimates for the adsorbents may be helpful for comparison purposes.[5]

According to Ahmed, et al.[14] the total cost of adsorbent materials can be estimated by the sum of production cost, regeneration costs, and process loss cost. Table 2.10 exhibits the costs of some alternative adsorbents along with activated carbons and ion exchange resins.

Table 2.10. Cost estimates of some adsorbents as reported in the literature.

Adsorbent	Costs	Reference
Bagasse fly ash	US $0.02/kg	Gupta and Ali[198]
Bentonite	US $0.072/kg	U.S. Geological Survey USGS[199]
Biochar	US $2.65/kg	Ahmed, et al.[200]
Chitosan	US $16/kg	Babel and Kurniawan[10]
Chitosan based bioadsorbents	US $8-10/kg	Gandhi and Meenakshi[201]
Commercial activated carbons	US $20-22/kg	Babel and Kurniawan[10]
Ion exchange resins	US $150/kg	Ahmed, et al.[14]
Red mud	US $0.025/kg	Lin and Juang[202]
MOF HKUST-1	US $20/kg	Thallapally and Strachan[203]
MOF MIL-101	US $5/kg	Thallapally and Strachan[203]

However, these estimates are suggestive, since studies on alternative adsorbents seldom report costs as they depend on several factors, including the source of the adsorbent material (natural, wastes, byproducts, or synthesized), local availability, treatment conditions, regeneration and disposal issues.[5] Moreover, the performance of adsorptive processes highly depends on the properties of the adsorbent material; hence, different experimental conditions must be investigated to assess whether alternative adsorbents are effective for pharmaceuticals removal.[63] Environmental significance and economic efficiency also have to be examined, because, although adsorption technology employing wastes and low-cost materials has beneficial environmental effects, such as waste minimization and reuse of waste to mitigate contaminants, it is challenging in terms of regeneration of spent adsorbent and scale-up to make the process viable at commercial level.[194]

2.8 Practical applications of adsorption processes

Literature survey reveals that, to date, most papers available on adsorption of pharmaceuticals using alternative low-cost adsorbents are restricted to batch (kinetics and equilibrium) investigations. Little attention has been given to regeneration studies and fixed-bed studies that are essential for simulation or prediction of dynamic performance. In addition, the great majority of the studies are limited to the laboratory scale for examining adsorptive capacity and uptake mechanisms. There is a lack of knowledge on practical applications, particularly industrial, of adsorptive processes for pharmaceuticals removal. It depends on transferring laboratory adsorption column conditions to pilot plant experiments in small

diameter fixed-beds, aiming full scale design. The scale-up studies can be done through different approaches, including computer simulation,[204, 205] rapid-small scale column tests, and response surface methodology.[206] Pratt, et al.[207] defend the idea that the best way to predict long-term performance of adsorption systems is by full-scale field tests under specific continuous-flow conditions.

Adsorption columns should provide maximum separation of the solute and the fluid phase of which the solute is initially part. Important operational parameters, such as breakthrough curves behavior and mass transfer zones, are optimized in pilot scale column studies, which link laboratory and practical adsorption applications. In column scale-up, adsorbent properties, such as shape, size, and density, must be taken into account in order to avoid operational problems, including hydrodynamic limitations or column fouling. The position of solution feeding is another operational aspect to be considered in column design. Although downward flows are usually adopted, upward flows offer more uniform pollutant distribution and minimize pressure gradients and potential of fouling adsorbent. In addition, when the solution is fed in the bottom of the column, smaller adsorbent particle sizes can be used, reduced volumes of adsorbent are necessary and increased adsorption rates can be obtained.[197, 208]

To the best of the authors' knowledge, no study in the literature evaluates the removal of pharmaceuticals at pilot column using nonconventional low-cost adsorbents. The pilot scale studies available are restricted to evaluate the performance of PACs[209, 210] or GACs[211] for adsorption of several pharmaceuticals. Researches on full-scale pharmaceutical adsorption are even scarcer than pilot scale studies. Until the moment of this review, the studies are restricted to evaluate full-scale adsorption by GAC.[212] The greatest difficulty on changing the scale of an adsorption system is because it is an unsteady-state process.[204]

Therefore, the use of adsorbents other than ACs for pharmaceuticals removal in practical adsorption systems for water purification, or even in pilot scale studies is still not common. Nevertheless, the increasing number of laboratory-scale studies on this subject only in the last five years indicates that it is a matter of time before nonconventional low-cost adsorbents start to be tested in large scale applications.

The transference of adsorption processes using nonconventional low-cost adsorbents from lab-scale to industrial applications is difficult for several reasons: (i) the sorption properties of low-cost adsorbents highly depend on their origin; (ii) the demand at commercial level controls the availability of the resource for industrial users; (iii) physical and chemical pretreatment methods that improve sorption capacity of the materials may not be cost-effective at large-scale nor ecofriendly; (iv) effectiveness of the treatment depends on the type of the

low-cost adsorbent, because each has different properties (*e.g.*, porosity, surface area, surface charge/groups, molecular structure, physical strength; (v) adsorption performance relates to process variables (*e.g.*, temperature, pH, concentration of adsorbate and adsorbent, ionic strength, contact time, particle size of adsorbent, etc.); (vi) inconsistencies in data presentation (experimental conditions, batch, or continuous systems) prevent comparison of different materials for adsorption; (vii) little information is available on adsorption of pollutants from mixtures and real industrial effluents; (viii) the feasibility of low-cost adsorbents on the commercial scale have to be further examined in pilot-plant studies.[7]

2.9 Conclusion and future perspectives

Initially, this review article briefly examined pharmaceutical contamination of the environment and showed that, although it is a certainty that is a result of human and industrial activities, the possible long-term effects to human health and ecological impacts caused by pharmaceuticals in water are not completely comprehended. Apart from conventional methods (*e.g.*, coagulation, flotation, lime softening) and other advanced technologies (*e.g.*, membrane filtration, ozonation, advanced oxidation processes), this review focuses on adsorption technology for the uptake of pharmaceuticals from water and wastewaters.

An attempt has been made to present recent developments related to the employment of nonconventional low-cost adsorbents instead of commercial activated carbons. Adsorption characteristics of clays, biochars, chitosans, agro-industrial wastes, and metal–organic frameworks (MOFs) to several pharmaceuticals have been discussed in depth, considering efficiency parameters of kinetics, equilibrium, thermodynamics, and breakthrough curves. Moreover, regeneration and costing issues of these adsorbent materials have also been reviewed. On the basis of the maximum adsorption capacities reported, this literature survey clearly demonstrated that these nonconventional low-cost materials could be used as adsorbents, but the effectiveness for each type of pharmaceutical pollutants depends on several factors, such as pH, temperature, and affinity between adsorbent and contaminant. Generally, most of the studied adsorption processes present spontaneous nature and kinetics data well described by the pseudo-second-order model, which confirm the existence of chemisorption.

Although laboratory column experiments are essential for designing full-scale fixed-bed processes and evaluating their practical applicability, the majority of the studies on pharmaceutical adsorption are limited to batch investigations. In the case of nonconventional low-cost adsorbents, continuous adsorption is seldom evaluated and, to date, there are no studies on pilot-scale or full-scale pharmaceutical adsorption using such materials. Furthermore, the

cost and reuse ability of adsorbents such as clays, biochars, chitosans, agro-industrial wastes, and MOFs have been rarely reported, being that it is practically impossible to perform a comprehensive comparison among these materials. An analysis of regeneration capability and cost benefit is essential for assessing environmental and economic significance of adsorption processes.

Concluding, despite an increasing number of studies published on nonconventional low-cost adsorbents for pharmaceutical removal, there is still lack of knowledge on their practical application. In addition to further studies on fixed-bed adsorption, adsorbent regeneration, and cost assessment, publications that reflect real systems are also necessary, since the majority of the current studies employ synthetic solutions or monocomponent solutions, at concentrations higher than that usually detected in the environment. Hence, several points still need to be explored for industrial application. Future studies should examine multicomponent adsorption, treatment of real wastewaters, continuous adsorption, and adsorption regeneration.

Acknowledgements

This work was supported by CAPES, CNPq and FAPESP [Proc. 2016/05007-1].

References

(1) Sodré, F. F.; Locatelli, M. A. F.; Jardim, W. F., Occurrence of Emerging Contaminants in Brazilian Drinking Waters: A Sewage-To-Tap Issue. *Water, Air, Soil Pollut.* **2010**, *206*, 57-67.

(2) Snyder, S. A.; Westerhoff, P.; Yoon, Y.; Sedlak, D., Pharmaceuticals, Personal Care Products, and Endocrine Disruptors in Water: Implications for the Water Industry. *Environ. Eng. Sci.* **2003**, *20*.

(3) Richardson, B. J.; Lam, P. K. S.; Martin, M., Emerging chemicals of concern: Pharmaceuticals and personal care products (PPCPs) in Asia, with particular reference to Southern China. *Mar. Pollut. Bull.* **2005**, *50*, 913-920.

(4) Larsen, T. A.; Lienert, J.; Joss, A.; Siegrist, H., How to avoid pharmaceuticals in the aquatic environment. *J. Biotechnol.* **2004**, *113*, 295-304.

(5) Grassi, M.; Kaykioglu, G.; Belgiorno, V.; Lofrano, G., Removal of Emerging Contaminants from Water and Wastewater by Adsorption Process. In *Emerging Compounds Removal from Wastewater*, Lofrano, G., Ed.; Springer Netherlands, 2012; pp 15-37.

(6) Tong, D. S.; Zhou, C. H.; Lu, Y.; Yu, H.; Zhang, G. F.; Yu, W. H., Adsorption of Acid Red G dye on octadecyl trimethylammonium montmorillonite. *Appl. Clay Sci.* **2010**, *50*, 427-431.

(7) Crini, G., Non-conventional low-cost adsorbents for dye removal: A review. *Bioresour. Technol.* **2006**, *97*, 1061-1085.

(8) Derbyshire, F.; Jagtoyen, M.; Andrews, R.; Rao, A.; Martin-Gullón, I.; Grulke, E. A., Carbon Materials in Environmental Applications. *Chem. Phys. Carbon* **2001**, *27*, 1-66.

(9) Sotelo, J. L.; Ovejero, G.; Rodríguez, A.; Álvarez, S.; García, J., Study of Natural Clay Adsorbent Sepiolite for the Removal of Caffeine from Aqueous Solutions: Batch and Fixed-Bed Column Operation. *Water, Air, Soil Pollut.* **2013**, *224*, 1466.

(10) Babel, S.; Kurniawan, T. A., Low-cost adsorbents for heavy metals uptake from contaminated water: a review. *J. Hazard. Mater.* **2003**, *97*, 219-243.

(11) Homem, V.; Santos, L., Degradation and removal methods of antibiotics from aqueous matrices – A review. *J. Environ. Manage.* **2011**, *92*, 2304-2347.

(12) Ahmed, M. J., Adsorption of non-steroidal anti-inflammatory drugs from aqueous solution using activated carbons: Review. *J. Environ. Manage.* **2017**, *190*, 274-282.

(13) Ahmed, M. J., Adsorption of quinolone, tetracycline, and penicillin antibiotics from aqueous solution using activated carbons: Review. *Environ. Toxicol. Pharmacol.* **2017**, *50*, 1-10.

(14) Ahmed, M. B.; Zhou, J. L.; Ngo, H. H.; Guo, W., Adsorptive removal of antibiotics from water and wastewater: Progress and challenges. *Sci Total Environ* **2015**, *532*, 112-26.

(15) Cook, J. W.; Dodds, E. C.; Greenwood, A. W., Sex Change in the Plumage of Brown Leghorn Capons Following the Injection of Certain Synthetic Oestrus-Producing Compounds. *Proc. R. Soc. London, Ser. B* **1934**, *114*, 286-290.

(16) Cook, J. W.; Dodds, E. C.; Hewett, C. L.; Lawson, W., The estrogenic Activity of some Condensed-Ring Compounds in Relation to their other Biological Activities. *Proc. R. Soc. London, Ser. B* **1934**, *114*, 272-286.

(17) Emge, L. A.; Murphy, K. M., The influence of long-continued injections of estrogen on mammary tissue. *Am. J. Obstet. Gynecol.* **1938**, *36*, 750-768.

(18) Sumpter, J. P., Feminized responses in fish to environmental estrogens. *Toxicol. Lett.* **1995**, *82*, 737-742.

(19) Folmar, L. C.; Denslow, N. D.; Rao, V.; Chow, M.; Crain, D. A.; Enblom, J.; Marcino, J.; Guillette, L. J., Vitellogenin induction and reduced serum testosterone concentrations in feral male carp (Cyprinus carpio) captured near a major metropolitan sewage treatment plant. *Environ. Health Perspect.* **1996**, *104*, 1096-1101.

(20) Larsson, D. G. J.; Adolfsson-Erici, M.; Parkkonen, J.; Pettersson, M.; Berg, A. H.; Olsson, P. E.; Förlin, L., Ethinyloestradiol — an undesired fish contraceptive? *Aquat. Toxicol.* **1999**, *45*, 91-97.

(21) Suzuki, A.; Sugihara, A.; Uchida, K.; Sato, T.; Ohta, Y.; Katsu, Y.; Watanabe, H.; Iguchi, T., Developmental effects of perinatal exposure to bisphenol-A and diethylstilbestrol on reproductive organs in female mice. *Reprod. Toxicol.* **2002**, *16*, 107-116.

(22) Stumm-Zollinger, E.; Fair, G. M., Biodegradation of Steroid Hormones. *Journal (Water Pollution Control Federation)* **1965**, *37*, 1506-1510.

(23) Halling-Sørensen, B.; Nors Nielsen, S.; Lanzky, P. F.; Ingerslev, F.; Holten Lützhøft, H. C.; Jørgensen, S. E., Occurrence, fate and effects of pharmaceutical substances in the environment- A review. *Chemosphere* **1998**, *36*, 357-393.

(24) Raloff, J., Drugged waters: Does it matter that pharmaceuticals are turning up in water supplies? *Sci. News* **1998**, *153*, 187-189.

(25) Daughton, C. G.; Ternes, T. A., Pharmaceuticals and personal care products in the environment: agents of subtle change? *Environ. Health Perspect*. **1999**, *107*, 907-938.

(26) Kolpin, D. W.; Furlong, E. T.; Meyer, M. T.; Thurman, E. M.; Zaugg, S. D.; Barber, L. B.; Buxton, H. T., Pharmaceuticals, Hormones, and Other Organic Wastewater Contaminants in U.S. Streams, 1999−2000: A National Reconnaissance. *Environ. Sci. Technol.* **2002**, *36*, 1202-1211.

(27) Benotti, M. J.; Trenholm, R. A.; Vanderford, B. J.; Holady, J. C.; Stanford, B. D.; Snyder, S. A., Pharmaceuticals and Endocrine Disrupting Compounds in U.S. Drinking Water. *Environ. Sci. Technol.* **2009**, *43*, 597-603.

(28) Heberer, T.; Stan, H. J., Determination of Clofibric Acid and N-(Phenylsulfonyl)-Sarcosine in Sewage, River and Drinking Water. *Int. J. Environ. Anal. Chem.* **1997**, *67*, 113-124.

(29) Heberer, T.; Reddersen, K.; Mechlinski, A., From municipal sewage to drinking water: fate and removal of pharmaceutical residues in the aquatic environment in urban areas. *Water Sci. Technol.* **2002**, *46*, 81-88.

(30) Meffe, R.; de Bustamante, I., Emerging organic contaminants in surface water and groundwater: A first overview of the situation in Italy. *Sci. Total Environ.* **2014**, *481*, 280-295.

(31) Watkinson, A. J.; Murby, E. J.; Kolpin, D. W.; Costanzo, S. D., The occurrence of antibiotics in an urban watershed: From wastewater to drinking water. *Sci. Total Environ.* **2009**, *407*, 2711-2723.

(32) De Jager, C.; Aneck-Hahn, N. H.; Barnhoorn, I. E. J.; S., B. M.; Van Vuren, J. H. J.; Burger, A. E. C.; Swemmer, A.; Van Zijl, C.; Van Wyk, S.; Jonker, M. *Endocrine Disrupting*

Chemical (EDC) Activity and Health Effects of Identified Veterinary Growth Stimulants in Surface and Ground Water; South African Water Research Commission: Pretoria, 2011.

(33) Stumpf, M.; Ternes, T. A.; Wilken, R.-D.; Silvana Vianna, R.; Baumann, W., Polar drug residues in sewage and natural waters in the state of Rio de Janeiro, Brazil. *Sci. Total Environ.* **1999**, *225*, 135-141.

(34) Ternes, T. A.; Stumpf, M.; Mueller, J.; Haberer, K.; Wilken, R. D.; Servos, M., Behavior and occurrence of estrogens in municipal sewage treatment plants — I. Investigations in Germany, Canada and Brazil. *Sci. Total Environ.* **1999**, *225*, 81-90.

(35) de Almeida, C. A. A.; Brenner, C. G. B.; Minetto, L.; Mallmann, C. A.; Martins, A. F., Determination of anti-anxiety and anti-epileptic drugs in hospital effluent and a preliminary risk assessment. *Chemosphere* **2013**, *93*, 2349-2355.

(36) Campestrini, I.; Jardim, W. F., Occurrence of cocaine and benzoylecgonine in drinking and source water in the São Paulo State region, Brazil. *Sci. Total Environ.* **2017**, *576*, 374-380.

(37) Contaminant Candidate List 4; 81 FR 81099; U. S. Environmental Protection Agency: Washington, DC, 2016; pp 81099−81114.

(38) *European Union, Directive 2008/105/EC of the European Parliament and of the Council of 16 December 2008*; Official Journal of the European Union: [S.l.], 2008; pp 84-97.

(39) aus der Beek, T.; Weber, F.-A.; Bergmann, A.; Hickmann, S.; Ebert, I.; Hein, A.; Küster, A., Pharmaceuticals in the environment—Global occurrences and perspectives. *Environ. Toxicol. Chem.* **2016**, *35*, 823-835.

(40) Thomas, K. V.; da Silva, F. M. A.; Langford, K. H.; de Souza, A. D. L.; Nizzeto, L.; Waichman, A. V., Screening for Selected Human Pharmaceuticals and Cocaine in the Urban Streams of Manaus, Amazonas, Brazil. *J. Am. Water Resour. Assoc.* **2014**, *50*, 302-308.

(41) Campanha, M. B.; Awan, A. T.; de Sousa, D. N. R.; Grosseli, G. M.; Mozeto, A. A.; Fadini, P. S., A 3-year study on occurrence of emerging contaminants in an urban stream of São Paulo State of Southeast Brazil. *Environ. Sci. Pollut. Res.* **2015**, *22*, 7936-7947.

(42) Locatelli, M. A. F.; Sodré, F. F.; Jardim, W. F., Determination of Antibiotics in Brazilian Surface Waters Using Liquid Chromatography–Electrospray Tandem Mass Spectrometry. *Arch. Environ. Contam. Toxicol.* **2011**, *60*, 385-393.

(43) Sodré, F. F.; Montagner, C. C.; Locatelli, M. A. F.; Jardim, W. F., Ocorrência de Interferentes Endócrinos e Produtos Farmacêuticos em Águas Superficiais da Região de Campinas (SP, Brasil). *J. Braz. Soc. Ecotoxicol.* **2007**, *2*, 187-196.

(44) Ikehata, K.; Naghashkar, N. J.; El-Din, M. G., Degradation of Aqueous Pharmaceuticals by Ozonation and Advanced Oxidation Processes: A Review. *Ozone: Sci. Eng.* **2006**, *28*, 353-414.

(45) Dolar, D.; Zokić, T. I.; Košutić, K.; Ašperger, D.; Pavlović, D. M., RO/NF membrane treatment of veterinary pharmaceutical wastewater: comparison of results obtained on a laboratory and a pilot scale. *Environ. Sci. Pollut. Res.* **2012**, *19*, 1033-1042.

(46) Martz, M., Effective wastewater treatment in the pharmaceutical industry. *Pharmaceutical Engineering* **2012**, *32*, 48-62.

(47) *Brazil, Sistema Nacional de Informações sobre Saneamento: Diagnóstico dos Serviços de Água e Esgotos – 2015*; SNSA: Brasília, 2017; p 212.

(48) Machado, K. C.; Grassi, M. T.; Vidal, C.; Pescara, I. C.; Jardim, W. F.; Fernandes, A. N.; Sodré, F. F.; Almeida, F. V.; Santana, J. S.; Canela, M. C.; Nunes, C. R. O.; Bichinho, K. M.; Severo, F. J. R., A preliminary nationwide survey of the presence of emerging contaminants in drinking and source waters in Brazil. *Sci. Total Environ.* **2016**, *572*, 138-146.

(49) Tambosi, J. L.; Yamanaka, L. Y.; José, H. J.; Moreira, R. d. F. P. M.; Schröder, H. F., Recent research data on the removal of pharmaceuticals from sewage treatment plants (STP). *Quim. Nova* **2010**, *33*, 411-420.

(50) Ternes, T. A.; Joss, A.; Siegrist, H., Peer Reviewed: Scrutinizing Pharmaceuticals and Personal Care Products in Wastewater Treatment. *Environ. Sci. Technol.* **2004**, *38*, 392A-399A.

(51) Golet, E. M.; Alder, A. C.; Giger, W., Environmental Exposure and Risk Assessment of Fluoroquinolone Antibacterial Agents in Wastewater and River Water of the Glatt Valley Watershed, Switzerland. *Environ. Sci. Technol.* **2002**, *36*, 3645-3651.

(52) Clara, M.; Strenn, B.; Gans, O.; Martinez, E.; Kreuzinger, N.; Kroiss, H., Removal of selected pharmaceuticals, fragrances and endocrine disrupting compounds in a membrane bioreactor and conventional wastewater treatment plants. *Water Res.* **2005**, *39*, 4797-4807.

(53) Carballa, M.; Omil, F.; Lema, J. M.; Llompart, M. a.; García-Jares, C.; Rodríguez, I.; Gómez, M.; Ternes, T., Behavior of pharmaceuticals, cosmetics and hormones in a sewage treatment plant. *Water Res.* **2004**, *38*, 2918-2926.

(54) Kwon, J.-W.; Rodriguez, J. M., Occurrence and Removal of Selected Pharmaceuticals and Personal Care Products in Three Wastewater-Treatment Plants. *Arch. Environ. Contam. Toxicol.* **2014**, *66*, 538-548.

(55) Oosterhuis, M.; Sacher, F.; ter Laak, T. L., Prediction of concentration levels of metformin and other high consumption pharmaceuticals in wastewater and regional surface water based on sales data. *Sci. Total Environ.* **2013**, *442*, 380-388.

(56) Binnie, C.; Kimber, M.; Smethurst, G., Basic Water Treatment. *Thomas Telford* **2002**, 291.

(57) Crini, G.; Badot, P., *Sorption Processes and Pollution: Conventional and Non-conventional Sorbents for Pollutant Removal from Wastewaters*. Presses Univ. Franche-Comté: 2010; p 489.

(58) Suarez, S.; Lema, J. M.; Omil, F., Pre-treatment of hospital wastewater by coagulation–flocculation and flotation. *Bioresour. Technol.* **2009**, *100*, 2138-2146.

(59) Westerhoff, P.; Yoon, Y.; Snyder, S.; Wert, E., Fate of Endocrine-Disruptor, Pharmaceutical, and Personal Care Product Chemicals during Simulated Drinking Water Treatment Processes. *Environ. Sci. Technol.* **2005**, *39*, 6649-6663.

(60) Hartig, C.; Ernst, M.; Jekel, M., Membrane filtration of two sulphonamides in tertiary effluents and subsequent adsorption on activated carbon. *Water Res.* **2001**, *35*, 3998-4003.

(61) Broséus, R.; Vincent, S.; Aboulfadl, K.; Daneshvar, A.; Sauvé, S.; Barbeau, B.; Prévost, M., Ozone oxidation of pharmaceuticals, endocrine disruptors and pesticides during drinking water treatment. *Water Res.* **2009**, *43*, 4707-4717.

(62) Sui, Q.; Huang, J.; Deng, S.; Yu, G.; Fan, Q., Occurrence and removal of pharmaceuticals, caffeine and DEET in wastewater treatment plants of Beijing, China. *Water Res.* **2010**, *44*, 417-426.

(63) Kyzas, G. Z.; Fu, J.; Lazaridis, N. K.; Bikiaris, D. N.; Matis, K. A., New approaches on the removal of pharmaceuticals from wastewaters with adsorbent materials. *J. Mol. Liq.* **2015**, *209*, 87-93.

(64) Seo, P. W.; Bhadra, B. N.; Ahmed, I.; Khan, N. A.; Jhung, S. H., Adsorptive Removal of Pharmaceuticals and Personal Care Products from Water with Functionalized Metal-organic Frameworks: Remarkable Adsorbents with Hydrogen-bonding Abilities. *Sci. Rep.* **2016**, *6*.

(65) Dąbrowski, A., Adsorption — from theory to practice. *Adv. Colloid Interface Sci.* **2001**, *93*, 135-224.

(66) Rouquerol, F.; Rouquerol, J.; Sing, K., *Adsorption by Powders and Porous Solids*; Academic Press: London, 1999; Chapter 1, pp 1-26.

(67) Dabrowski, A., *Applications in Industry*; Elsevier Science, 1998.

(68) Le Cloirec, P. *Adsorption in Water and Wastewater Treatments. In Handbook of Porous Solids*; Wiley-VCH Verlag GmbH, 2008; pp 2746-2803.

(69) Gogoi, A.; Mazumder, P.; Tyagi, V. K.; Tushara Chaminda, G. G.; An, A. K.; Kumar, M., Occurrence and fate of emerging contaminants in water environment: A review. *Groundwater for Sustainable Development* **2018**, *6*, 169-180.

(70) Sing, K. S. W.; Everett, D. H.; Haul, R. A. W.; Moscou, L.; Pierotti, R. A.; Rouquérol, J.; Siemieniewska, T., Reporting physisorption data for gas/solid systems with special reference to the determination of surface area and porosity (Recommendations 1984). *Pure Appl. Chem.* **1985**, *57*, 603-619.

(71) Hill, C. G., *An introduction to chemical engineering kinetics and reactor design*. 1st ed.; John Wiley & Sons: USA, 1977.

(72) Deryło-Marczewska, A.; Marczewski, A. W., Effect of adsorbate structure on adsorption from solutions. *Appl. Surf. Sci.* **2002**, *196*, 264-272.

(73) Thomas, W. J.; Crittenden, B. D., *Adsorption Technology and Design*. Butterworth-Heinemann: Lymington, 1998.

(74) Lagergren, S., Zur theorie der sogenannten adsorption gelöster stoffe, Kungliga Svenska Vetenskapsakademiens. *Handlingar* **1898**, *24*, 1-39.

(75) Ho, Y. S.; McKay, G., A comparison of chemisorption kinetic models applied to pollutant removal on various sorbents. *Process Saf. Environ. Prot.* **1998**, *76*, 332-340.

(76) Akçay, G.; Kılınç, E.; Akçay, M., The equilibrium and kinetics studies of flurbiprofen adsorption onto tetrabutylammonium montmorillonite (TBAM). *Colloids Surf., A* **2009**, *335*, 189-193.

(77) Genç, N.; Dogan, E. C., Adsorption kinetics of the antibiotic ciprofloxacin on bentonite, activated carbon, zeolite, and pumice. *Desalin. Water Treat.* **2015**, *53*, 785-793.

(78) Khazri, H.; Ghorbel-Abid, I.; Kalfat, R.; Trabelsi-Ayadi, M., Removal of ibuprofen, naproxen and carbamazepine in aqueous solution onto natural clay: equilibrium, kinetics, and thermodynamic study. *Appl. Water Sci.* **2017**, *7*, 3031-3040.

(79) Villaescusa, I.; Fiol, N.; Poch, J.; Bianchi, A.; Bazzicalupi, C., Mechanism of paracetamol removal by vegetable wastes: The contribution of π–π interactions, hydrogen bonding and hydrophobic effect. *Desalination* **2011**, *270*, 135-142.

(80) Balarak, D.; Mostafapour, F. K.; Joghataei, A., Kinetics and mechanism of red mud in adsorption of ciprofloxacin in aqueous solution. *Biosci. Biotechnol. Res. Commun.* **2017**, *10*, 241-248.

(81) Zhang, Y.-L.; Zhang, J.; Dai, C.-M.; Zhou, X.-F.; Liu, S.-G., Sorption of carbamazepine from water by magnetic molecularly imprinted polymers based on chitosan-Fe3O4. *Carbohydr. Polym.* **2013**, *97*, 809-816.

(82) Reynaud, F.; Tsapis, N.; Deyme, M.; Vasconcelos, T. G.; Gueutin, C.; Guterres, S. S.; Pohlmann, A. R.; Fattal, E., Spray-dried chitosan-metal microparticles for ciprofloxacin adsorption: Kinetic and equilibrium studies. *Soft Matter* **2011**, *7*, 7304-7312.

(83) Salem, N. A.; Yakoot, S. M., Non-steroidal Anti-inflammatory Drug, Ibuprofen Adsorption Using Rice Straw Based Biochar. *Int. J. Pharmacol.* **2016**, *12*, 729-736.

(84) Reynel-Avila, H. E.; Mendoza-Castillo, D. I.; Bonilla-Petriciolet, A.; Silvestre-Albero, J., Assessment of naproxen adsorption on bone char in aqueous solutions using batch and fixed-bed processes. *J. Mol. Liq.* **2015**, *209*, 187-195.

(85) Ferreira, C. I. A.; Calisto, V.; Otero, M.; Nadais, H.; Esteves, V. I., Fixed-bed adsorption of Tricaine Methanesulfonate onto pyrolysed paper mill sludge. *Aquacult. Eng.* **2017**, *77*, 53-60.

(86) Hasan, Z.; Jeon, J.; Jhung, S. H., Adsorptive removal of naproxen and clofibric acid from water using metal-organic frameworks. *J. Hazard. Mater.* **2012**, *209-210*, 151-157.

(87) Peng, Y.; Zhang, Y.; Huang, H.; Zhong, C., Flexibility induced high-performance MOF-based adsorbent for nitroimidazole antibiotics capture. *Chem. Eng. J.* **2018**, *333*, 678-685.

(88) Azhar, M. R.; Abid, H. R.; Sun, H.; Periasamy, V.; Tadé, M. O.; Wang, S., Excellent performance of copper based metal organic framework in adsorptive removal of toxic sulfonamide antibiotics from wastewater. *J. Colloid Interface Sci.* **2016**, *478*, 344-352.

(89) Azhar, M. R.; Abid, H. R.; Periasamy, V.; Sun, H.; Tade, M. O.; Wang, S., Adsorptive removal of antibiotic sulfonamide by UiO-66 and ZIF-67 for wastewater treatment. *J. Colloid Interface Sci.* **2017**, *500*, 88-95.

(90) Treybal, R. E., *Mass-Transfer Operations*; McGraw-Hill: Singapore, 1981.

(91) Langmuir, I., The adsorption of gases on plane surfaces of glass, mica and platinum. *J. Am. Chem. Soc.* **1918**, *40*, 1361-1403.

(92) Freundlich, H. M. F., Over the adsorption in solution. *J. Phys. Chem.* **1906**, *57*, 385–470.

(93) Dubinin, M. M.; Radushkevich, L. V., Equation of the characteristic curve of activated charcoal. *Proc. Acad. Sci., Phys. Chem. Sect.* **1947**, *331-333*, 875-890.

(94) Yang, K.; Xing, B., Adsorption of organic compounds by carbon nanomaterials in aqueous phase: Polanyi theory and its application. *Chem. Rev.* **2010**, *110*, 5989-6008.

(95) Bekçi, Z.; Seki, Y.; Yurdakoç, M. K., Equilibrium studies for trimethoprim adsorption on montmorillonite KSF. *J. Hazard. Mater.* **2006**, *133*, 233-242.

(96) Bekçi, Z.; Seki, Y.; Kadir Yurdakoç, M., A study of equilibrium and FTIR, SEM/EDS analysis of trimethoprim adsorption onto K10. *J. Mol. Struct.* **2007**, *827*, 67-74.

(97) Putra, E. K.; Pranowo, R.; Sunarso, J.; Indraswati, N.; Ismadji, S., Performance of activated carbon and bentonite for adsorption of amoxicillin from wastewater: mechanisms, isotherms and kinetics. *Water Res.* **2009**, *43*, 2419-2430.

(98) Salihi, E. Ç.; Mahramanlıoğlu, M., Equilibrium and kinetic adsorption of drugs on bentonite: Presence of surface active agents effect. *Appl. Clay Sci.* **2014**, *101*, 381-389.

(99) Genç, N.; Can Dogan, E.; Yurtsever, M., Bentonite for ciprofloxacin removal from aqueous solution. *Water Sci. Technol.* **2013**, *68*, 848-855.

(100) Roca Jalil, M. E.; Baschini, M.; Sapag, K., Influence of pH and antibiotic solubility on the removal of ciprofloxacin from aqueous media using montmorillonite. *Appl. Clay Sci.* **2015**, *114*, 69-76.

(101) Chang, P.-H.; Jean, J.-S.; Jiang, W.-T.; Li, Z., Mechanism of tetracycline sorption on rectorite. *Colloids Surf., A* **2009**, *339*, 94-99.

(102) Dordio, A. V.; Miranda, S.; Prates Ramalho, J. P.; Carvalho, A. J. P., Mechanisms of removal of three widespread pharmaceuticals by two clay materials. *J. Hazard. Mater.* **2017**, *323*, 575-583.

(103) Liu, N.; Wang, M.-x.; Liu, M.-m.; Liu, F.; Weng, L.; Koopal, L. K.; Tan, W.-f., Sorption of tetracycline on organo-montmorillonites. *J. Hazard. Mater.* **2012**, *225–226*, 28-35.

(104) Zha, S. x.; Zhou, Y.; Jin, X.; Chen, Z., The removal of amoxicillin from wastewater using organobentonite. *J. Environ. Manage.* **2013**, *129*, 569-576.

(105) Sun, K.; Shi, Y.; Chen, H.; Wang, X.; Li, Z., Extending surfactant-modified 2:1 clay minerals for the uptake and removal of diclofenac from water. *J. Hazard. Mater.* **2017**, *323*, 567-574.

(106) De Oliveira, T.; Guégan, R.; Thiebault, T.; Milbeau, C. L.; Muller, F.; Teixeira, V.; Giovanela, M.; Boussafir, M., Adsorption of diclofenac onto organoclays: Effects of surfactant and environmental (pH and temperature) conditions. *J. Hazard. Mater.* **2017**, *323, Part A*, 558-566.

(107) Maia, G. S. Adsorção de Diclofenaco de Sódio em Material Argiloso. Master's thesis, University of Campinas, Campinas, Brazil, 2017.

(108) Jung, C.; Boateng, L. K.; Flora, J. R. V.; Oh, J.; Braswell, M. C.; Son, A.; Yoon, Y., Competitive adsorption of selected non-steroidal anti-inflammatory drugs on activated biochars: Experimental and molecular modeling study. *Chem. Eng. J.* **2015**, *264*, 1-9.

(109) Li, T.; Han, X.; Liang, C.; Shohag, M. J. I.; Yang, X., Sorption of sulphamethoxazole by the biochars derived from rice straw and alligator flag. *Environ. Technol.* **2015**, *36*, 245-253.

(110) Yao, H.; Lu, J.; Wu, J.; Lu, Z.; Wilson, P. C.; Shen, Y., Adsorption of Fluoroquinolone Antibiotics by Wastewater Sludge Biochar: Role of the Sludge Source. *Water, Air, Soil Pollut.* **2013**, *224*, 1370.

(111) Alkhamis, K. A.; Salem, M. S.; Khanfar, M. S., The Sorption of Ketotifen Fumarate by Chitosan. *AAPS PharmSciTech* **2008**, *9*, 866-869.

(112) Zhang, Y.; Shen, Z.; Dai, C.; Zhou, X., Removal of selected pharmaceuticals from aqueous solution using magnetic chitosan: sorption behavior and mechanism. *Environ. Sci. Pollut. Res.* **2014**, *21*, 12780-12789.

(113) Zhang, S.; Dong, Y.; Yang, Z.; Yang, W.; Wu, J.; Dong, C., Adsorption of pharmaceuticals on chitosan-based magnetic composite particles with core-brush topology. *Chem. Eng. J.* **2016**, *304*, 325-334.

(114) Kyzas, G. Z.; Bikiaris, D. N.; Seredych, M.; Bandosz, T. J.; Deliyanni, E. A., Removal of dorzolamide from biomedical wastewaters with adsorption onto graphite oxide/poly(acrylic acid) grafted chitosan nanocomposite. *Bioresour. Technol.* **2014**, *152*, 399-406.

(115) Antunes, M.; Esteves, V. I.; Guégan, R.; Crespo, J. S.; Fernandes, A. N.; Giovanela, M., Removal of diclofenac sodium from aqueous solution by Isabel grape bagasse. *Chem. Eng. J.* **2012**, *192*, 114-121.

(116) Cuerda-Correa, E. M.; Domínguez-Vargas, J. R.; Olivares-Marín, F. J.; de Heredia, J. B., On the use of carbon blacks as potential low-cost adsorbents for the removal of non-steroidal anti-inflammatory drugs from river water. *J. Hazard. Mater.* **2010**, *177*, 1046-1053.

(117) Portinho, R.; Zanella, O.; Féris, L. A., Grape stalk application for caffeine removal through adsorption. *J. Environ. Manage.* **2017**, *202*, 178-187.

(118) Zhang, C.-L.; Qiao, G.-L.; Zhao, F.; Wang, Y., Thermodynamic and kinetic parameters of ciprofloxacin adsorption onto modified coal fly ash from aqueous solution. *J. Mol. Liq.* **2011**, *163*, 53-56.

(119) Calisto, V.; Ferreira, C. I. A.; Santos, S. M.; Gil, M. V.; Otero, M.; Esteves, V. I., Production of adsorbents by pyrolysis of paper mill sludge and application on the removal of citalopram from water. *Bioresour. Technol.* **2014**, *166*, 335-344.

(120) Calisto, V.; Ferreira, C. I. A.; Oliveira, J. A. B. P.; Otero, M.; Esteves, V. I., Adsorptive removal of pharmaceuticals from water by commercial and waste-based carbons. *J. Environ. Manage.* **2015**, *152*, 83-90.

(121) Calisto, V.; Jaria, G.; Silva, C. P.; Ferreira, C. I. A.; Otero, M.; Esteves, V. I., Single and multi-component adsorption of psychiatric pharmaceuticals onto alternative and commercial carbons. *J. Environ. Manage.* **2017**, *192*, 15-24.

(122) Putra, E. K.; Pranowo, R.; Sunarso, J.; Indraswati, N.; Ismadji, S., Performance of activated carbon and bentonite for adsorption of amoxicillin from wastewater: mechanisms, isotherms and kinetics. *Water Res.* **2009**, *43*, 2419-30.

(123) Tiwari, D.; Lalhriatpuia, C.; Lee, S.-M., Hybrid materials in the removal of diclofenac sodium from aqueous solutions: Batch and column studies. *J. Ind. Eng. Chem.* **2015**, *30*, 167-173.

(124) Ferreira, C. I. A.; Calisto, V.; Otero, M.; Nadais, H.; Esteves, V. I., Comparative adsorption evaluation of biochars from paper mill sludge with commercial activated carbon for the removal of fish anaesthetics from water in Recirculating Aquaculture Systems. *Aquacult. Eng.* **2016**, *74*, 76-83.

(125) Hasan, Z.; Choi, E.-J.; Jhung, S. H., Adsorption of naproxen and clofibric acid over a metal–organic framework MIL-101 functionalized with acidic and basic groups. *Chem. Eng. J.* **2013**, *219*, 537-544.

(126) Tran, H. N.; You, S.-J.; Chao, H.-P., Thermodynamic parameters of cadmium adsorption onto orange peel calculated from various methods: A comparison study. *J. Environ. Chem. Eng.* **2016**, *4*, 2671-2682.

(127) Namasivayam, C.; Yamuna, R. T., Adsorption of chromium (VI) by a low-cost adsorbent: Biogas residual slurry. *Chemosphere* **1995**, *30*, 561-578.

(128) Verma, V. K.; Subbiah, S., Prospects of Silk Sericin as an Adsorbent for Removal of Ibuprofen from Aqueous Solution. *Ind. Eng. Chem. Res.* **2017**, *56*, 10142-10154.

(129) Oladipo, A. A.; Abureesh, M. A.; Gazi, M., Bifunctional composite from spent "Cyprus coffee" for tetracycline removal and phenol degradation: Solar-Fenton process and artificial neural network. *Int. J. Biol. Macromol.* **2016**, *90*, 89-99.

(130) Rosales, E.; Meijide, J.; Pazos, M.; Sanromán, M. A., Challenges and recent advances in biochar as low-cost biosorbent: From batch assays to continuous-flow systems. *Bioresour. Technol.* **2017**, *246*, 176-192.

(131) Ruthven, D. M., *Principles of Adsorption and Adsorption Processes*; John Wiley & Sons: New York, 1984.

(132) Worch, E., *Adsorption Technology in Water Treatment: Fundamentals, Processes, and Modeling;* De Gruyter: Berlim, 2012.

(133) Bohart, G. S.; Adams, E. Q., Some aspects of the behavior of charcoal with respect to chlorine. *J. Am. Chem. Soc.* **1920**, *42*, 523-544.

(134) Thomas, H. C., Chromatography: a problem in kinetics. *Ann. N. Y. Acad. Sci.* **1948**, *49*, 161-182.

(135) Yoon, Y. H.; Nelson, J. H., Application of Gas Adsorption Kinetics I. A Theoretical Model for Respirator Cartridge Service Life. *Am. Ind. Hyg. Assoc. J.* **1984**, *45*, 509-516.

(136) Clark, R. M., Evaluating the cost and performance of field-scale granular activated carbon systems. *Environ. Sci. Technol.* **1987**, *21*, 573-580.

(137) Yan, G.; Viraraghavan, T.; Chen, M., A New Model for Heavy Metal Removal in a Biosorption Column. *Adsorpt. Sci. Technol.* **2001**, *19*, 25-43.

(138) Cooney, D. O., *Adsorption Design for Wastewater Treatment*; Taylor & Francis: 1998.

(139) Mondal, S.; Aikat, K.; Halder, G., Ranitidine hydrochloride sorption onto superheated steam activated biochar derived from mung bean husk in fixed bed column. *J. Environ. Chem. Eng.* **2016**, *4*, 488-497.

(140) McCabe, W.; Smith, J.; Harriott, P., *Unit Operations of Chemical Engineering*; 7th ed.; McGraw-Hill: New York, 2005; p 1152.

(141) Adegoke, K. A.; Oyewole, R. O.; Lasisi, B. M.; Bello, O. S., Abatement of organic pollutants using fly ash based adsorbents. *Water Sci. Technol.* **2017**.

(142) Snyder, S. A.; Adham, S.; Redding, A. M.; Cannon, F. S.; DeCarolis, J.; Oppenheimer, J.; Wert, E. C.; Yoon, Y., Role of membranes and activated carbon in the removal of endocrine disruptors and pharmaceuticals. *Desalination* **2007**, *202*, 156-181.

(143) Zhang, X.; Guo, W.; Ngo, H. H.; Wen, H.; Li, N.; Wu, W., Performance evaluation of powdered activated carbon for removing 28 types of antibiotics from water. *J. Environ. Manage.* **2016**, *172*, 193-200.

(144) Sotelo, J. L.; Rodríguez, A.; Álvarez, S.; García, J., Removal of caffeine and diclofenac on activated carbon in fixed bed column. *Chem. Eng. Res. Des.* **2012**, *90*, 967-974.

(145) Brigatti, M. F.; Galan, E.; Theng, B. K. G., Structures and Mineralogy of Clay Minerals. *Developments in Clay Science*, Bergaya, F.; Theng, B. K. G.; Lagaly, G., Eds.; Elsevier: 2006; Vol. *1*, pp 19-86.

(146) Guggenheim, S.; Martin, R. T., Definition of Clay and Clay Mineral: Joint Report of the Aipea and CMS Nomenclature Committees. *Clay Miner.* **1995**, *30*, 257-259.

(147) Avisar, D.; Primor, O.; Gozlan, I.; Mamane, H., Sorption of Sulfonamides and Tetracyclines to Montmorillonite Clay. *Water, Air, Soil Pollut.* **2010**, *209*, 439-450.

(148) Álvarez, S.; Sotelo, J. L.; Ovejero, G.; Rodríguez, A.; García, J., Low-Cost Adsorbent for Emerging Contaminant Removal in Fixed-Bed Columns. *Chem. Eng. Trans.* **2013**, *32*, 61-66.

(149) Zhu, R.; Chen, Q.; Zhou, Q.; Xi, Y.; Zhu, J.; He, H., Adsorbents based on montmorillonite for contaminant removal from water: A review. *Appl. Clay Sci.* **2016**, *123*, 239-258.

(150) Heller-Kallai, L., Chapter 7.2 Thermally Modified Clay Minerals. *Dev. Clay Sci.* **2006**, *1*, 289-308.

(151) Maia, G. S.; Andrade, J. R.; Oliveira, M. F.; Vieira, M. G. A.; Silva, M. G. C., Affinity studies between drugs and clays as adsorbent material. *Chem. Eng. Trans.* **2017**, *57*, 583 - 588.

(152) de Freitas, E. D.; de Almeida, H. J.; de Almeida Neto, A. F.; Vieira, M. G. A., Continuous adsorption of silver and copper by Verde-lodo bentonite in a fixed bed flow-through column. *J. Cleaner Prod.* **2018**, *171*, 613-621.

(153) Freitas, E. D.; Carmo, A. C. R.; Almeida Neto, A. F.; Vieira, M. G. A., Binary adsorption of silver and copper on Verde-lodo bentonite: Kinetic and equilibrium study. *Appl. Clay Sci. (Print)* **2017**, *137*, 69 - 76.

(154) Komadel, P.; Madejová, J., Chapter 7.1 Acid Activation of Clay Minerals. *Dev. Clay Sci.* **2006**, *1*, 263-287.

(155) Paiva, L. B.; Morales, A. R., Organophilic bentonites based on argentinean and Brazilian bentonites: Part 1: influence of intrinsic properties of sodium bentonites on the final properties of organophilic bentonites prepared by solid-liquid and semisolid reactions. *Braz. J. Chem. Eng.* **2012**, *29*, 525-536.

(156) Park, Y.; Ayoko, G. A.; Frost, R. L., Application of organoclays for the adsorption of recalcitrant organic molecules from aqueous media. *J. Colloid Interface Sci.* **2011**, *354*, 292-305.

(157) Sun, K.; Shi, Y.; Xu, W.; Potter, N.; Li, Z.; Zhu, J., Modification of clays and zeolites by ionic liquids for the uptake of chloramphenicol from water. *Chem. Eng. J.* **2017**, *313*, 336-344.

(158) Akçay, G.; Yurdakoç, K., Removal of nicotine and its pharmaceutical derivatives from aqueous solution by raw bentonite and dodecylammonium-bentonite. *J. Sci. Ind. Res.* **2008**, *67*, 451-454.

(159) Lehmann, J.; Joseph, S., *Biochar for environmental management: Science, Technology and Implementation*. 2 ed.; Earthscan from Routledge: London, UK, 2015; p 944.

(160) Demirbaş, E.; Kobya, M.; Öncel, S.; Şencan, S., Removal of Ni(II) from aqueous solution by adsorption onto hazelnut shell activated carbon: equilibrium studies. *Bioresour. Technol.* **2002**, *84*, 291-293.

(161) Laird, D. A.; Brown, R. C.; Amonette, J. E.; Lehmann, J., Review of the pyrolysis platform for coproducing bio-oil and biochar. *Biofuels, Bioprod. Biorefin.* **2009**, *3*, 547-562.

(162) Meyer, S.; Glaser, B.; Quicker, P., Technical, Economical, and Climate-Related Aspects of Biochar Production Technologies: A Literature Review. *Environ. Sci. Technol.* **2011**, *45*, 9473-9483.

(163) Lin, L.; Jiang, W.; Xu, P., Comparative study on pharmaceuticals adsorption in reclaimed water desalination concentrate using biochar: Impact of salts and organic matter. *Sci. Total Environ.* **2017**, *601*, 857-864.

(164) Inyang, M. I.; Gao, B.; Yao, Y.; Xue, Y.; Zimmerman, A.; Mosa, A.; Pullammanappallil, P.; Ok, Y. S.; Cao, X., A review of biochar as a low-cost adsorbent for aqueous heavy metal removal. *Crit. Rev. Environ. Sci. Technol.* **2016**, *46*, 406-433.

(165) Jung, C.; Park, J.; Lim, K. H.; Park, S.; Heo, J.; Her, N.; Oh, J.; Yun, S.; Yoon, Y., Adsorption of selected endocrine disrupting compounds and pharmaceuticals on activated biochars. *J. Hazard. Mater.* **2013**, *263*, 702-710.

(166) Mitchell, S. M.; Subbiah, M.; Ullman, J. L.; Frear, C.; Call, D. R., Evaluation of 27 different biochars for potential sequestration of antibiotic residues in food animal production environments. *J. Environ. Chem. Eng.* **2015**, *3*, 162-169.

(167) Yao, Y.; Gao, B.; Chen, H.; Jiang, L.; Inyang, M.; Zimmerman, A. R.; Cao, X.; Yang, L.; Xue, Y.; Li, H., Adsorption of sulfamethoxazole on biochar and its impact on reclaimed water irrigation. *J. Hazard. Mater.* **2012**, *209*, 408-413.

(168) Lian, F.; Sun, B.; Song, Z.; Zhu, L.; Qi, X.; Xing, B., Physicochemical properties of herb-residue biochar and its sorption to ionizable antibiotic sulfamethoxazole. *Chem. Eng. J.* **2014**, *248*, 128-134.

(169) Teixidó, M.; Pignatello, J. J.; Beltrán, J. L.; Granados, M.; Peccia, J., Speciation of the Ionizable Antibiotic Sulfamethazine on Black Carbon (Biochar). *Environ. Sci. Technol.* **2011**, *45*, 10020-10027.

(170) Xie, M.; Chen, W.; Xu, Z.; Zheng, S.; Zhu, D., Adsorption of sulfonamides to demineralized pine wood biochars prepared under different thermochemical conditions. *Environ. Pollut.* **2014**, *186*, 187-194.

(171) Zheng, H.; Wang, Z.; Zhao, J.; Herbert, S.; Xing, B., Sorption of antibiotic sulfamethoxazole varies with biochars produced at different temperatures. *Environ. Pollut.* **2013**, *181*, 60-67.

(172) Gerente, C.; Lee, V. K. C.; Cloirec, P. L.; McKay, G., Application of Chitosan for the Removal of Metals From Wastewaters by Adsorption—Mechanisms and Models Review. *Crit. Rev. Environ. Sci. Technol.* **2007**, *37*, 41-127.

(173) Kyzas, G. Z.; Kostoglou, M.; Lazaridis, N. K.; Lambropoulou, D. A.; Bikiaris, D. N., Environmental friendly technology for the removal of pharmaceutical contaminants from wastewaters using modified chitosan adsorbents. *Chem. Eng. J.* **2013**, *222*, 248-258.

(174) Kyzas, G.; Bikiaris, D., Recent Modifications of Chitosan for Adsorption Applications: A Critical and Systematic Review. *Mar. Drugs* **2015**, *13*, 312.

(175) Kyzas, G. Z.; Bikiaris, D. N.; Lambropoulou, D. A., Effect of humic acid on pharmaceuticals adsorption using sulfonic acid grafted chitosan. *J. Mol. Liq.* **2017**, *230*, 1-5.

(176) Contreras, E.; Sepúlveda, L.; Palma, C., Valorization of Agroindustrial Wastes as Biosorbent for the Removal of Textile Dyes from Aqueous Solutions. *Int. J. Chem. Eng.* **2012**, *2012*, 9.

(177) Bhatnagar, A.; Sillanpää, M., Utilization of agro-industrial and municipal waste materials as potential adsorbents for water treatment—A review. *Chem. Eng. J.* **2010**, *157*, 277-296.

(178) De Gisi, S.; Lofrano, G.; Grassi, M.; Notarnicola, M., Characteristics and adsorption capacities of low-cost sorbents for wastewater treatment: A review. *Sustainable Materials and Technologies* **2016**, *9*, 10-40.

(179) Swarcewicz, M. K.; Sobczak, J.; Październioch, W., Removal of carbamazepine from aqueous solution by adsorption on fly ash-amended soil. *Water Sci. Technol.* **2013**, *67*, 1396-1402.

(180) Coimbra, R. N.; Calisto, V.; Ferreira, C. I. A.; Esteves, V. I.; Otero, M., Removal of pharmaceuticals from municipal wastewater by adsorption onto pyrolyzed pulp mill sludge. *Arabian J. Chem.* **2015**, x DOI: 10.1016/j.arabjc.2015.12.001.

(181) Nielsen, L.; Zhang, P.; Bandosz, T. J., Adsorption of carbamazepine on sludge/fish waste derived adsorbents: Effect of surface chemistry and texture. *Chem. Eng. J.* **2015**, *267*, 170-181.

(182) Nielsen, L.; Bandosz, T. J., Analysis of sulfamethoxazole and trimethoprim adsorption on sewage sludge and fish waste derived adsorbents. *Microporous Mesoporous Mater.* **2016**, *220*, 58-72.

(183) da Silva, T. L.; da Silva, A. C.; Vieira, M. G. A.; Gimenes, M. L.; da Silva, M. G. C., Biosorption study of copper and zinc by particles produced from silk sericin – alginate blend: evaluation of blend proportion and thermal cross-linking process in particles production. *J. Cleaner Prod.* **2016**, *137*, 1470-1478.

(184) Furukawa, H.; Cordova, K. E.; O'Keeffe, M.; Yaghi, O. M., The Chemistry and Applications of Metal-Organic Frameworks. *Science* **2013**, *341*.

(185) Kumar, P.; Bansal, V.; Kim, K.-H.; Kwon, E. E., Metal-organic frameworks (MOFs) as futuristic options for wastewater treatment. *J. Ind. Eng. Chem.* **2018**. 10.1016/j.jiec.2017.12.051.

(186) Pi, Y.; Li, X.; Xia, Q.; Wu, J.; Li, Y.; Xiao, J.; Li, Z., Adsorptive and photocatalytic removal of Persistent Organic Pollutants (POPs) in water by metal-organic frameworks (MOFs). *Chem. Eng. J.* **2017**. 10.1016/j.cej.2017.12.092

(187) Seo, P. W.; Khan, N. A.; Jhung, S. H., Removal of nitroimidazole antibiotics from water by adsorption over metal–organic frameworks modified with urea or melamine. *Chem. Eng. J.* **2017**, *315*, 92-100.

(188) Hasan, Z.; Khan, N. A.; Jhung, S. H., Adsorptive removal of diclofenac sodium from water with Zr-based metal–organic frameworks. *Chem. Eng. J.* **2016**, *284*, 1406-1413.

(189) Marques, S. C. R.; Marcuzzo, J. M.; Baldan, M. R.; Mestre, A. S.; Carvalho, A. P., Pharmaceuticals removal by activated carbons: Role of morphology on cyclic thermal regeneration. *Chem. Eng. J.* **2017**, *321*, 233-244.

(190) Pouretedal, H. R.; Sadegh, N., Effective removal of Amoxicillin, Cephalexin, Tetracycline and Penicillin G from aqueous solutions using activated carbon nanoparticles prepared from vine wood. *Journal of Water Process Engineering* **2014**, *1*, 64-73.

(191) Yaghmaeian, K.; Moussavi, G.; Alahabadi, A., Removal of amoxicillin from contaminated water using NH4Cl-activated carbon: Continuous flow fixed-bed adsorption and catalytic ozonation regeneration. *Chem. Eng. J.* **2014**, *236*, 538-544.

(192) Sophia A, C.; Lima, E. C., Removal of emerging contaminants from the environment by adsorption. *Ecotoxicol. Environ. Saf.* **2018**, *150*, 1-17.

(193) Shan, D.; Deng, S.; Zhao, T.; Wang, B.; Wang, Y.; Huang, J.; Yu, G.; Winglee, J.; Wiesner, M. R., Preparation of ultrafine magnetic biochar and activated carbon for pharmaceutical adsorption and subsequent degradation by ball milling. *J. Hazard. Mater.* **2016**, *305*, 156-163.

(194) Reguyal, F.; Sarmah, A. K.; Gao, W., Synthesis of magnetic biochar from pine sawdust via oxidative hydrolysis of FeCl2 for the removal sulfamethoxazole from aqueous solution. *J. Hazard. Mater.* **2017**, *321*, 868-878.

(195) Rossner, A.; Snyder, S. A.; Knappe, D. R., Removal of emerging contaminants of concern by alternative adsorbents. *Water Res.* **2009**, *43*, 3787-96.

(196) Sivarajasekar, N.; Balasubramani, K.; Mohanraj, N.; Prakash Maran, J.; Sivamani, S.; Ajmal Koya, P.; Karthik, V., Fixed-bed adsorption of atrazine onto microwave irradiated Aegle marmelos Correa fruit shell: Statistical optimization, process design and breakthrough modeling. *J. Mol. Liq.* **2017**, *241*, 823-830.

(197) Ali, I., Water Treatment by Adsorption Columns: Evaluation at Ground Level. *Sep. Purif. Rev.* **2014**, *43*, 175-205.

(198) Gupta, V. K.; Ali, I., Removal of lead and chromium from wastewater using bagasse fly ash—a sugar industry waste. *J. Colloid Interface Sci.* **2004**, *271*, 321-328.

(199) U.S. Geological Survey USGS, 2014 Minerals Yearbook: Clay and Shale [Advance Release]. U.S. Department of the Interior, 2014.

(200) Ahmed, M. B.; Zhou, J. L.; Ngo, H. H.; Guo, W., Insight into biochar properties and its cost analysis. *Biomass Bioenergy* **2016**, *84*, 76-86.

(201) Gandhi, M. R.; Meenakshi, S., Recent advancement in heavy metal removal onto silica based adsorbents and chitosan composites - a review. In *A Book on Ion Exchange, Adsorption and Solvent Extraction*; Naushad, M.; Al-Othman, Z. A., Eds.; Nova Science Publishers, Inc.: New York, 2013; pp 201-230.

(202) Lin, S.-H.; Juang, R.-S., Adsorption of phenol and its derivatives from water using synthetic resins and low-cost natural adsorbents: A review. *J. Environ. Manage.* **2009**, *90*, 1336-1349.

(203) Thallapally, P. K.; Strachan, D. M. *Initial proof-of-principle for near room temperature Xe and Kr separation from air with MOFs*; PNNL-21452; PNNL, 2012.

(204) Chen, J.; Buege, J.; Cunningham, F.; Northam, J., Scale-up of Column Adsorption Process by Computer Simulation. *Ind. Eng. Chem. Process Des. Dev.* **1968**, *7*, 26-31.

(205) Svedberg, U. G., Simulation and scale-up of adsorption columns. *Comput. Chem. Eng.* **1979**, *3*, 549-551.

(206) Chowdhury, S.; Saha, P. D., Scale-up of a dye adsorption process using chemically modified rice husk: optimization using response surface methodology. *Desalin. Water Treat.* **2012**, *37*, 331-336.

(207) Pratt, C.; Parsons, S. A.; Soares, A.; Martin, B. D., Biologically and chemically mediated adsorption and precipitation of phosphorus from wastewater. *Curr. Opin. Biotechnol.* **2012**, *23*, 890-896.

(208) Crini, G., Recent developments in polysaccharide-based materials used as adsorbents in wastewater treatment. *Prog. Polym. Sci.* **2005**, *30*, 38-70.

(209) Mailler, R.; Gasperi, J.; Coquet, Y.; Deshayes, S.; Zedek, S.; Cren-Olivé, C.; Cartiser, N.; Eudes, V.; Bressy, A.; Caupos, E.; Moilleron, R.; Chebbo, G.; Rocher, V., Study of a large scale powdered activated carbon pilot: Removals of a wide range of emerging and priority micropollutants from wastewater treatment plant effluents. *Water Res.* **2015**, *72*, 315-330.

(210) Kårelid, V.; Larsson, G.; Björlenius, B., Effects of recirculation in a three-tank pilot-scale system for pharmaceutical removal with powdered activated carbon. *J. Environ. Manage.* **2017**, *193*, 163-171.

(211) Benstoem, F.; Nahrstedt, A.; Boehler, M.; Knopp, G.; Montag, D.; Siegrist, H.; Pinnekamp, J., Performance of granular activated carbon to remove micropollutants from municipal wastewater—A meta-analysis of pilot- and large-scale studies. *Chemosphere* **2017**, *185*, 105-118.

(212) Grover, D. P.; Zhou, J. L.; Frickers, P. E.; Readman, J. W., Improved removal of estrogenic and pharmaceutical compounds in sewage effluent by full scale granular activated carbon: Impact on receiving river water. *J. Hazard. Mater.* **2011**, *185*, 1005-1011.

CAPÍTULO 3. Teste de Afinidade de Adsorção de Fármacos com Materiais Argilosos[§]

3.1 Introdução

No Capítulo 2, discorreu-se extensivamente sobre a problemática da contaminação por compostos farmacêuticos e a relevância da adsorção como tratamento avançado. Materiais baseados em argilas, biochar, quitosana, resíduos agrícolas e industriais, e estruturas metal-orgânicas (MOFs) foram detalhados como adsorventes não convencionais e promissores alternativas ao carvão ativado para a remoção efetiva de fármacos de água e efluentes. O uso de argilas desperta grande interesse, considerando o baixo custo, abundância no território brasileiro, variadas propriedades superficiais e estruturais, estabilidade mecânica e facilidade de modificação visando a maiores taxas de adsorção. O grupo de pesquisa no qual o presente trabalho se insere tem vasta experiência em processos de adsorção usando materiais argilosos. Por exemplo, as argilas bentonitas brasileiras Verde-lodo e Fluidgel foram previamente exploradas na forma natural ou modificada no âmbito de dissertações de mestrado para o tratamento de íons metálicos (GALINDO, 2012; CANTUÁRIA, 2014; FREITAS, 2016), hidrocarbonetos aromáticos (BEDIN, 2014) e fármacos (OLIVEIRA, 2018). A argila bentonita organofílica comercial brasileira Spectrogel Tipo-C também foi tema de estudos recentes pelo grupo de pesquisa (STOFELA, 2014; LIMA, 2016; MAIA, 2017).

Neste contexto, as argilas Verde-lodo, Fluidgel e Spectrogel Tipo-C foram eleitas para prosseguimento do presente trabalho com a realização de teste exploratório de afinidade com diferentes compostos farmacêuticos para seleção do sistema com maior potencial de remoção. Os seguintes fármacos de interesse acadêmico e ambiental foram escolhidos para avaliação: losartana potássica (anti-hipertensivo), cloridrato de propranolol (anti-hipertensivo), cloridrato de metformina (antidiabético) e amoxicilina trihidratada (antibiótico).

A losartana e o propranolol são amplamente consumidos como medicamentos anti-hipertensivos. Após serem introduzidos no meio ambiente, tais fármacos são normalmente encontrados dissolvidos na fase aquosa e apresentam baixa adsorção em material particulado, ácido húmico e sedimentos. Ambos são estáveis à hidrólise, sendo que o tempo de meia-vida do propranolol em meio aquático a 25°C é superior a um ano. Considerando a razoável estabilidade e o alto consumo, a losartana e o propranolol têm crescente ocorrência em compartimentos aquáticos (GODOY; KUMMROW e PAMPLIN, 2015). No Brasil, a losartana

[§] Resultados apresentados no trabalho *Adsorção do Fármaco Losartana Potássica em Argila Organofílica Comercial: Teste de Afinidade e Planejamento Experimental* do 12º Encontro sobre Adsorção (EBA 12), Gramado, 2018.

foi quantificada em água marinha da Baia de Santos (São Paulo) com concentração variando entre 0,29 ng/L a 8,70 ng/L (CORTEZ et al., 2018). A presença de propranolol foi detectada em água do rio Monjolinho em São Carlos (São Paulo) com concentração média de 15,2 ng/L (CAMPANHA et al., 2015). A metformina figura como o agente oral mais empregado no tratamento de diabetes tipo 2. Segundo Rena; Pearson e Sakamoto (2013), mais de 100 milhões de pacientes são prescritos com metformina por ano em todo o mundo. Além de seu elevado consumo, a metformina tem absorção limitada no corpo humano e cerca de 80% da dose oral é excretada inalterada em urina e fezes. Por outro lado, nas estações de tratamento de efluentes, a metformina é em sua maior parte (93–97%) microbiologicamente transformada a guanilureia (TRAUTWEIN et al., 2014). Apesar da elevada taxa de remoção, a metformina tem sido detectada em águas superficiais e efluentes devido à alta carga nos influentes (OOSTERHUIS; SACHER e TER LAAK, 2013). A amoxicilina é um dos micropoluentes emergentes mais comumente investigados no Brasil. Segundo levantamento de Montagner et al. (2019), a amoxicilina apresenta concentração média de 8 ng/L em amostras de águas superficiais coletadas entre 2006 e 2015 no estado de São Paulo. Uma das principais preocupações quanto à presença de antibióticos no meio ambiente é o desenvolvimento de resistência antimicrobiana, conforme anunciado pela Organização Mundial da Saúde (2015).

Diante de todo o exposto, estudos sobre a adsorção de contaminantes farmacêuticos emergentes, tais como losartana, propranolol, metformina ou amoxicilina, são de grande interesse para a área ambiental, especialmente quando utilizados adsorventes abundantes como as argilas. No desenvolvimento de processos adsortivos, testes preliminares de afinidade são essenciais para determinar o potencial de aplicação de um dado adsorvente na remoção de certo adsorbato. Neste sentido, esta etapa do trabalho objetiva avaliar as diferentes argilas brasileiras (Verde-lodo, Fluidgel e Spectrogel Tipo-C) em testes de afinidade com os fármacos para definição do sistema (fármaco e argila) a ser estudado de forma aprofundada em etapas subsequentes.

3.2 Metodologia

3.2.1 *Preparo das argilas*

As argilas bentonitas do tipo Verde-lodo (Dolomil) e Fluidgel (Dolomil) foram calcinadas em forno Mufla por 24 h a 500 °C e 750 °C, respectivamente, a fim de aumentar a capacidade de troca iônica e estabilidade. A argila bentonita organofílica Spectrogel – Tipo C (Spectrochem) foi utilizada conforme recebida, sem maiores modificações. Os materiais

argilosos foram moídos, quando necessário, e classificados com peneiras 16 e 24 Mesh Tyler para obtenção de diâmetro médio de partícula de 0,855 mm.

3.2.2 *Preparo do adsorbato*

Soluções sintéticas dos fármacos cloridrato de propranolol (Pharmanostra), cloridrato de metformina (Pharmanostra), losartana potássica (Purifarma) e amoxicilina trihidratada (EMS) foram preparadas utilizando água ultrapura de osmose reversa (modelo OS20LXE, Gehaka, Brasil). As concentrações inicial e final de fármaco na fase aquosa foram determinadas por espectrofotômetro UV-vis (Shimadzu, Uvmini-1240, Brasil) nos seguintes comprimentos de onda: 220 nm (losartana), 232 nm (metformina), 215 nm (propranolol), e 228 nm (amoxicilina).

3.2.3 *Teste de afinidade*

Os testes de afinidade foram realizados em triplicata com 0,5 g de argila (Verde-lodo calcinada, Fluidgel calcinada ou Spectrogel) adicionado a frascos de Erlenmeyer de 125 mL contendo 50 mL de solução de fármaco com concentração inicial de 0,09 mmol/L. Foi feito o branco para cada ensaio contendo água ultrapura (sem fármaco) e adsorvente, nas mesmas quantidades. Os Erlenmeyers foram agitados constantemente a 200 rpm em Shaker incubador e refrigerador (Lab Companion, SI-600R, Coréia do Sul) com temperatura controlada a 30 °C por 24 h.

Por meio das Equações (3.1) e (3.2), foram calculados os parâmetros de quantidade adsorvida de fármaco, (mmol/g), e porcentagem de remoção, (%), respectivamente:

$$q = (C_0 - C_f)V/m \tag{3.1}$$

$$\%R = (C_0 - C_f)/C_0 * 100 \tag{3.2}$$

sendo: C_0 = concentração inicial de fármaco na solução (mmol/L); C_f = concentração após o tempo de contato de 24 h (mmol/L); V = volume de solução de fármaco (L); m = massa de adsorvente (g).

3.3 **Resultados e discussão**

A Tabela 3.1 lista os resultados obtidos pelo teste de afinidade para a quantidade adsorvida, porcentagem de remoção e desvio padrão dos diferentes fármacos utilizando materiais argilosos.

Tabela 3.1. Valores de quantidade adsorvida, $\boldsymbol{q}$, e porcentagem de remoção, $\%\boldsymbol{R}$, obtidos por testes de afinidade em triplicata de diferentes fármacos com argilas Verde-lodo calcinada, Fluidgel calcinada e Spectrogel.

Fármaco	**Verde-lodo calcinada**		**Fluidgel calcinada**		**Spectrogel Tipo-C**	
	$q.10^3$ (mmol/g)	$\%R$ (%)	$q.10^3$ (mmol/g)	$\%R$ (%)	$q.10^3$ (mmol/g)	$\%R$ (%)
Cloridrato de propranolol	–	–	0,93 ± 0,05	10,2 ± 0,5	8,89 ± 0,01	98,0 ± 0,1
Cloridrato de metformina	–	–	1,44 ± 0,07	14,6 ± 0,7	4,02 ± 0,20	40,6 ± 2,1
Losartana potássica	2,56 ± 0,55	29,3 ± 6,2	0,06 ± 0,11	0,7 ± 1,2	8,65 ± 0,03	98,7 ± 0,3
Amoxicilina trihidratada	–	–	3,24 ± 0,68	35,2 ± 7,4	3,12 ± 0,2	33,9 ± 0,2

Os testes de afinidade utilizando a argila Verde-lodo como adsorvente forneceram resultados confiáveis apenas para a losartana, por isso, não são exibidos os dados para os demais fármacos. Esse fato pode ser associado a erros de leitura de concentração no UV-vis, levando em conta que, com a adição da argila Verde-lodo, as soluções aquosas de fármaco apresentam coloração bastante avermelhada, o que pode afetar as medidas, mesmo tomando-se o cuidado de fazer o branco.

Conforme Tabela 3.1, a adsorção de losartana pela argila Fluidgel calcinada foi a menos favorável, sendo que a porcentagem de remoção se limitou a 1%. Por outro lado, elevadas capacidades de adsorção foram verificadas para os fármacos cloridrato de propranolol e losartana potássica quando utilizada a argila organofílica Spectrogel como adsorvente. As porcentagens de remoção nestes casos chegaram a 98% para o propranolol e 99% para a losartana, sendo as maiores obtidas nas condições avaliadas. Isso pode ser relacionado ao fato de que a argila Spectrogel, ao contrário das demais, apresenta caráter organofílico que favorece a remoção dos fármacos (compostos orgânicos).

Com base nos resultados dos testes de afinidade, na continuação do estudo de adsorção de fármacos no presente trabalho será empregada a argila comercial organofílica Spectrogel Tipo-C como material adsorvente para a remoção dos fármacos losartana potássica. Como destacado anteriormente, a losartana potássica é um anti-hipertensivo popularmente usado no mundo todo, e tem tido ocorrência detectada em estações de tratamento de água, efluentes industriais, água marinha e até mesmo água potável (LARSSON; DE PEDRO e PAXEUS, 2007; GROS; RODRÍGUEZ-MOZAZ e BARCELÓ, 2012). Apesar destas condições, tanto

quanto é do conhecimento da autora, estudos sobre a adsorção de losartana potássica não existiam na literatura até o início do presente trabalho, o que motivou ainda mais o seu desenvolvimento.

3.4 Conclusão

O teste de afinidade indicou que, dentre os materiais argilosos testados (Verde-lodo calcinada, Fluidgel calcinada, Spectrogel Tipo-C) e os fármacos examinados (propranolol, metformina, losartana e amoxicilina), o sistema que oferece resultado mais promissor consiste de argila do tipo bentonita organofílica Spectrogel e anti-hipertensivo losartana potássica. Tal sistema apresenta porcentagem de remoção de 99% e capacidade de adsorção de 0,00865 mmol/g nas condições examinadas e foi selecionado para dar continuidade ao estudo aprofundado de adsorção.

Referências

BEDIN, S. **Preparação e caracterização de argila organofílica para adsorção de BTX**. 2014. 168 f. Dissertação (Mestrado em Engenharia Química)−Faculdade de Engenharia Química, Universidade Estadual de Campinas, Campinas, 2014.

CAMPANHA, M. B.; AWAN, A. T.; DE SOUSA, D. N. R.; GROSSELI, G. M.; MOZETO, A. A.; FADINI, P. S. A 3-year study on occurrence of emerging contaminants in an urban stream of São Paulo State of Southeast Brazil. **Environmental Science and Pollution Research**, v. 22, n. 10, p. 7936-7947, 2015.

CANTUÁRIA, M. L. **Recuperação de prata por adsorção em adsorventes alternativos**. 2014. 139 f. Dissertação (Mestrado em Engenharia Química)−Faculdade de Engenharia Química, Universidade Estadual de Campinas, Campinas, 2014.

CORTEZ, F. S.; SOUZA, L. D. S.; GUIMARÃES, L. L.; ALMEIDA, J. E.; PUSCEDDU, F. H.; MARANHO, L. A. et al. Ecotoxicological effects of losartan on the brown mussel Perna perna and its occurrence in seawater from Santos Bay (Brazil). **Science of the Total Environment**, v. 637-638, p. 1363-1371, 2018.

FREITAS, E. D. **Adsorção competitiva de íons prata e cobre em argila bentonítica**. 2016. 133 f. Dissertação (Mestrado em Engenharia Química)−Faculdade de Engenharia Química, Universidade Estadual de Campinas, Campinas, 2016.

GALINDO, L. S. G. **Remoção de íons de chumbo e cádmio em diferentes sistemas de adsorção/troca iônica em argila bentonítica tipo Fluidgel**. 2012. 145 f. Dissertação (Mestrado em Engenharia Química)−Faculdade de Engenharia Química, Universidade Estadual de Campinas, Campinas, 2012.

GODOY, A. A.; KUMMROW, F.; PAMPLIN, P. A. Z. Ecotoxicological evaluation of propranolol hydrochloride and losartan potassium to *Lemna minor* L. (1753) individually and in binary mixtures. **Ecotoxicology**, v. 24, n. 5, p. 1112-1123, 2015.

GROS, M.; RODRÍGUEZ-MOZAZ, S.; BARCELÓ, D. Fast and comprehensive multi-residue analysis of a broad range of human and veterinary pharmaceuticals and some of their metabolites in surface and treated waters by ultra-high-performance liquid chromatography coupled to quadrupole-linear ion trap tandem mass spectrometry. **Journal of Chromatography A**, v. 1248, p. 104-121, 2012.

LARSSON, D. G. J.; DE PEDRO, C.; PAXEUS, N. Effluent from drug manufactures contains extremely high levels of pharmaceuticals. **Journal of Hazardous materials**, v. 148, n. 3, p. 751-755, 2007.

LIMA, L. F. **Adsorção de hidrocarbonetos BTX por argila organofílica em sistema dinâmico de leito fixo**. 2016. 98 f. Dissertação (Mestrado em Engenharia Química)−Faculdade de Engenharia Química, Universidade Estadual de Campinas, Campinas, 2016.

MAIA, G. S. **Adsorção de diclofenaco de sódio em material argiloso**. 2017. 104 f. Dissertação (Mestrado em Engenharia Química)−Faculdade de Engenharia Química, Universidade Estadual de Campinas, Campinas, 2017.

MONTAGNER, C. C.; SODRÉ, F. F.; ACAYABA, R. D.; VIDAL, C.; CAMPESTRINI, I.; LOCATELLI, M. A. et al. Ten Years-Snapshot of the Occurrence of Emerging Contaminants in Drinking, Surface and Ground Waters and Wastewaters from São Paulo State, Brazil. **Journal of the Brazilian Chemical Society**, v. 30, p. 614-632, 2019.

OLIVEIRA, M. F. **Avaliação da argila Verde-lodo calcinada como adsorvente na remoção de cafeína**. 2018. 149 f. Dissertação (Mestrado em Engenharia Química)−Faculdade de Engenharia Química, Universidade Estadual de Campinas, Campinas, 2018.

OOSTERHUIS, M.; SACHER, F.; TER LAAK, T. L. Prediction of concentration levels of metformin and other high consumption pharmaceuticals in wastewater and regional surface water based on sales data. **Science of the Total Environment**, v. 442, p. 380-388, 2013.

ORGANIZAÇÃO MUNDIAL DA SAÚDE - OMS. **Global action plan on antimicrobial resistance**. Geneva, 2015. 28 p. Disponível em: < https://apps.who.int/iris/handle/10665/193736 >. Acesso em: 01 jun. 2020.

RENA, G.; PEARSON, E. R.; SAKAMOTO, K. Molecular mechanism of action of metformin: old or new insights? **Diabetologia**, v. 56, n. 9, p. 1898-1906, 2013.

STOFELA, S. K. F. **Remoção de compostos BTX em argila organofílica por adsorção em fase líquida**. 2014. 195 f. Dissertação (Mestrado em Engenharia Química)−Faculdade de Engenharia Química, Universidade Estadual de Campinas, Campinas, 2014.

TRAUTWEIN, C.; BERSET, J.-D.; WOLSCHKE, H.; KÜMMERER, K. Occurrence of the antidiabetic drug Metformin and its ultimate transformation product Guanylurea in several compartments of the aquatic cycle. **Environment International**, v. 70, p. 203-212, 2014.

CAPÍTULO 4. Adsorção de Losartana Potássica em Banho Finito

Performance of organoclay in adsorptive uptake of antihypertensive losartan potassium: A comparative batch study using micro-grain activated carbon[§]

Julia Resende de Andrade[a], Meuris Gurgel Carlos da Silva[a], Marcelino Luiz Gimenes[b], Melissa Gurgel Adeodato Vieira[a]

[a] *School of Chemical Engineering, University of Campinas (UNICAMP), Cidade Universitária Zeferino Vaz, Campinas, São Paulo, 13083-852, Brazil*

[b] *Chemical Engineering Department, State University of Maringá (UEM), Colombo Avenue, 5790, Maringá, Paraná, 87020-900, Brazil*

Abstract

The antihypertensive losartan potassium is an emerging pharmaceutical contaminant that has been traced in aquatic media; hence, up-to-date water treatment methods are urged. This paper is the first of its kind to examine losartan uptake by adsorption using an organophilic clay, Spectrogel. In comparison, a micro-grain activated carbon (μGAC) was employed. Adsorption kinetics, isotherms and thermodynamics were examined and characterizations were performed. Pseudo-first order, pseudo-second order, external diffusion, surface diffusion and pore diffusion models were adjusted to kinetic data, and Langmuir, Freundlich and Dubinin-Radushkevich models were correlated to isotherms. Adsorption mechanisms were elucidated for surface features and surface chemistry. The latter was unraveled to have a crucial role on losartan removal by Spectrogel. The best adsorbent dosage was stablished as 6 g/L and initial solution pH (2.5–10) had no significant impact on the process. Spectrogel exhibited faster kinetics and superior maximum adsorption capacity (~2200 min, 0.0820 mmol/g) than μGAC (~2600 min, 0.0441 mmol/g). Compared to water or ethanol eluents, methanol showed the highest efficiency as desorption agent (65%). The results indicate that Spectrogel organoclay is a potential non-traditional adsorbent for losartan remediation.

Keywords: adsorption; pharmaceutical; losartan potassium; organoclay; activated carbon; water treatment.

[§] Manuscript published in *Journal of Environmental Chemical Engineering* 8 (2020) 103562. DOI: 10.1016/j.jece.2019.103562. Reprinted with permission from *Journal of Environmental Chemical Engineering*.

4.1 Introduction

Antihypertensive is among the largest globally consumed therapeutic class of pharmaceuticals. In Germany, the usage of this medication by grown-ups augmented from 54% in 1998 to 72% in 2008–2011 [1]. The antihypertensive losartan potassium (referred here as losartan) is a popular angiotensin-II receptor antagonist that is listed as essential medicine by the World Health Organization [2]. In the USA, the consumption of losartan doubled between 2001 and 2011 [3]. In Brazil, it is the primary hypertensive drug supplied in the public health system [4].

Because of expanding consumption, losartan have been introduced into the aquatic environment in high levels and it has been traced with mean concentrations of 0.17–36.5 ng/L in surface water [5], 5 ng/L in drinking water [6], 1–2 μg/L in effluents of wastewater treatment plants (WWTPs), and 4.5 μg/L in raw hospital wastewater [7]. Losartan is anticipated to easily enter aquatic media owing to its great water solubility (>1.1 mmol/L) and hard removal through conventional biological treatments. Losartan is stable to hydrolysis and biodegradation, and has low probability to bind to sludge, since its log octanol water partition coefficient is inferior to 3 ($\log P_{ow}$ = 1.19 at pH 7) [8].

The discharge of effluents from WWTPs is assigned as the major cause of pharmaceutical incidence in the environment. This is particularly triggered by the largely variable efficiencies of conventional treatments in removing such micropollutants. Regarding losartan, its removal in WWTPs oscillate around 33% in Japan [9], below 40% in Colombia [7], and below 20% in Spain [10]. As a consequence, versatile up-to-date methods have been pursued for pharmaceutical remediation, including adsorption and advanced oxidation processes (AOPs). Recently, losartan removal was studied by means of electrochemical oxidation [11] and catalytic oxidation [12]. Although total degradations of losartan were achieved, both processes yielded mineralization rates around 70%, indicating that primary and/or reaction intermediates were generated.

Contrarily to AOPs, adsorption does not potentially form transformation by-products and may offer lower costs [13]. Moreover, adsorption has uncomplicated operation and design, and has been indicated as a propitious process to be incorporated into current WWTPs as advanced treatment [14, 15]. Activated carbons (ACs) are broadly employed adsorbent materials and have well-documented application in pharmaceutical removal [16, 17]. Traditionally, ACs have great surface area (600–2000 m^2/g), well-developed porosity and recognized efficiency for adsorbing organic pollutants in trace levels. Nevertheless, the elevated costs and not-easy regeneration obviate the practical application of ACs [18]. Hence, a massive

interest has been devoted to adsorbents alternative to AC, such as chitosan, clays, and agro-industrial by-products [19].

Montmorillonite is a type of clay that presents high capacities of layer expansion and cation exchange. Its application as adsorbent is advantageous considering low prices, natural plentitude, and facile modification of surface structure and physicochemical properties. Targeting enhanced affinity towards organic contaminants, organic cations have been exchanged into the interlayers of montmorillonite to form the so-called organoclays [20]. This paper proposes the examination of a Brazilian commercial organoclay, Spectrogel–Type C (referred here as Spectrogel), which is a bentonite organoclay synthesized using dialkyl dimethylammonium ions (DMA, $C_{35}H_{74}N^{+}$). Spectrogel has been already verified as adsorbent of volatile organic compounds [21-23] and pharmaceuticals [24]. Maia, et al. [25] recently exploited Spectrogel for adsorbing the anti-inflammatory diclofenac sodium and obtained Langmuir adsorption capacity up to 0.133 mmol/g.

To date, losartan uptake through adsorption process using clay materials has not been researched yet. Aiming to fill this gap, the fundamental purpose of this work is to analyze losartan adsorption onto Spectrogel organoclay. A comprehensive batch study was conducted for kinetics, isotherms and thermodynamics, which knowledge is essential within the fundamentals of adsorption theory. Regeneration tests were performed and Spectrogel was characterized prior and subsequent to adsorption. A commercial coconut shell-based AC was included as a comparative adsorbent to probe the roles of surface features and surface chemistry in adsorption pathways. The relevance and novelty of this paper consists on the inedited examination of losartan uptake employing a non-traditional adsorbent, aiming at consolidating adsorption as advanced treatment for environmental remediation of emerging pharmaceutical contaminants.

4.2 Material and methods

4.2.1 *Adsorbent materials*

Spectrogel was ceded by SpectroChem (Brazil) and coconut shell-based AC was purchased from Dinâmica (Brazil). Both materials were pestle to smaller pieces and sifted with Tyler sieves to get 655 μm mean particle diameter. The AC sample is referred here as micro-grain AC (μGAC), ascribable to particle size between powdered AC (< 100 μm) and granular AC (> 800 μm) [15]. Before use, ultra-fine particulate of μGAC was eliminated by rinsing four times with ultrapure water (250 g/L), followed by drying in continuous flow oven (120 °C, 2 h).

The physicochemical properties of Spectrogel (prior and post losartan uptake) and of μGAC were scrutinized by the techniques outlined in Table 4.1.

Table 4.1. Analyses used to characterize Spectrogel and μGAC

Analysis	Equipment	Parameters
Nitrogen physisorption	Quantachrome/NOVA1200e, Germany Micromeritrics/ASAP 2010, USA	Sample treatment in oven at 50 °C for more than 12 h
Helium picnometry	Micromeritics/AccuPyc II 1340	Helium gas, equilibrium rate 0.05 psig/min
Scanning electron microscope (SEM)	LEO Electron Microscopy/440i, England	Gold coating (200 Å), acceleration voltage 20 kV, beam current 600 pA
X-ray diffraction (XRD)	Philips Analytical X Ray/ X'Pert-MPD, The Netherlands	CuKα radiation (λ = 1.54056 Å), step-scan mode, speed 0.02°/s, voltage 40 kV, range 5–90°, increment 0.02°, current 40 mA
Thermal analysis	Shimadzu/DTG-60, Japan	Alumina pan, range 30–900 °C, rate 10/20 °C/min, nitrogen atmosphere, flux 50 mL/min
Fourier transform infrared spectrometer (FT-IR)	Thermo Scientific/Nicolet 6700, USA	Transmittance mode, scan 32, resolution 4 cm^{-1}, range 4000–400 cm^{-1}
Zeta potential	Anton Paar/SurPASS Electrokinetic	pH Titration, pH range 4–10, $C_2H_7NO_2$ electrolyte (1 mmol/L), HNO_3 (0.5 mol/L), NH_4OH (0.4 mol/L)

4.2.2 *Chemicals and analytic methods*

Losartan potassium (≥ 99%) was supplied by Purifarma (Brazil). Fig. 4.1 depicts the chemical structure of losartan, which molecular formula is $C_{22}H_{22}ClN_6OK$ and chemical name is 1*H*-Imidazole-5-methanol,2-butyl-4-chloro-1-[[2'-(1*H*-tetrazol-5-yl)[1,1'-biphenyl]-4-yl]methyl]-, monopotassium salt. Regarding the main physicochemical characteristics of losartan: molecular weight 461.01 g/mol, ionization constant pK_a=4.9, water solubility > 500 mg/L at 25 °C, log P_{ow}=1.19 at pH 7, vapor pressure < 10^{-7} torr, and melting temperature 183.5–184.5 °C [8, 26, 27].

Figure 4.1. Chemical structure of losartan potassium.

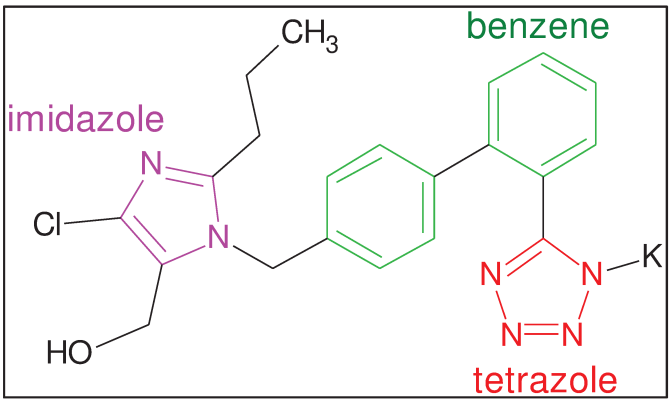

Ultrapure water (OS20LXE, Gehaka, Brazil) was utilized in all the preparations. UV/VIS spectrophotometry (UV-Vis mini 1240, Shimadzu, Brazil) was used at λ=234 nm to measure the quantity of losartan in the samples [28, 29]. Prior to each measurement, aliquots were passed through 0.45 µm polytetrafluoroethylene hydrophilic syringe filters. Working standard solutions between 0.003–0.05 mmol/L were prepared in triplicate to obtain calibration curves with $R^2 \geq 0.99$. Blank controls (ultrapure water and adsorbent) were run in parallel with adsorption tests to avoid interferents.

4.2.3 *Batch adsorption tests*

- Influence of adsorbent dosage and solution pH

Firstly, we probed the effect of adsorbent dosage (2–8 g of Spectrogel per liter of solution) on losartan removal without pH adjustments. The trials were executed in incubated shaker (SI-600R, Lab Companion, South Korea) at 200 rpm and 25 °C for a period of 48 h. The initial concentration of losartan was C_0=0.1 mmol/L.

Secondly, the effects of solution pH were appraised in the same experimental conditions, but with adsorbent dosage fixed at 6 g/L. The starting pH was adjusted between 2.5 to 10 with HCl or NaOH solutions (0.01 mol/L).

All tests were conducted in triplicate and the means were compared by Tukey's test at 5% significance level, using Statistica® 6.0 software. Eq. 4.1 was utilized for the removal efficiency of losartan, Rem (%):

$$Rem = \left(C_0 - C_f\right)/C_0 \cdot 100 \tag{4.1}$$

where: C_0 (mmol/L) = initial concentration; C_f (mmol/L) = final concentration.

- Adsorption kinetics

Adsorption kinetics was examined with adsorbent dosage fixed at 6 g/L, without pH adjustments. In several Erlenmeyer flasks, 0.24 g of Spectrogel was poured into 40 mL of losartan solutions with initial concentration of C_0=0.1, 0.07, 0.04 mmol/L. The flasks were constantly agitated for pre-determined time intervals (0–3240 min) in shaker (25 °C, 200 rpm). The kinetics using μGAC was inspected in the same operational conditions for C_0=0.1 mmol/L. After determining the residual losartan concentration by UV-VIS, the quantity adsorbed at certain time, q_t (mmol/g), was computed by Eq. 4.2:

$$q_t = (V/m)(C_0 - C_t) \tag{4.2}$$

where: V (L) = solution volume; m (g) = adsorbent mass; C_t (mmol/L) = concentration at time t.

- Adsorption equilibrium

For equilibrium study, 6 g/L adsorbent dosage was also adopted and C_0 varied between 0.004–3.00 mmol/L. The flasks were agitated at 200 rpm for 48 hours in shaker at constant temperatures of 15, 25, and 40 °C. A comparative isotherm using μGAC was assessed at 25 °C. The quantity of losartan adsorbed at equilibrium, q_e (mmol/g), was established by Eq. 4.3:

$$q_e = (V/m)(C_0 - C_e) \tag{4.3}$$

where: C_e (mmol/L) = losartan equilibrium concentration in solution.

- Adsorption thermodynamics

Based on equilibrium data, we estimated the thermodynamic parameters of Gibbs energy change ΔG (kJ/mol), enthalpy change ΔH (kJ/mol) and entropy change ΔS (J/mol/K) by Eq. 4.4:

$$\ln K_C = \frac{-\Delta G}{RT} = \frac{\Delta S}{R} - \frac{\Delta H}{RT} \tag{4.4}$$

where: K_C = thermodynamic equilibrium constant (-); R = 8.314 J/mol/K = universal gas constant; T = temperature (K).

Different approaches have been adopted for the calculation of the dimensionless equilibrium constant K_C. Herein, we used the method from Ghosal and Gupta [30] (Eq. 4.5), which is applicable when adsorption isotherms are satisfactorily defined by Freundlich model with q_e in mg/g and C_e in mg/L.

$$K_C = K_F M_W (1000/M_W)^{(1-1/n)} \tag{4.5}$$

where: K_F (mg/g).(L/mg)$^{1/n}$ = Freundlich isotherm constant; n (-) = Freundlich heterogeneity factor; M_W (g/L) = mass of water per liter at given temperature.

- Desorption tests

Three different organic eluents were tested for losartan desorption from Spectrogel organoclay: ultrapure water, ethanol (Dinâmica, Brazil, ≥ 99.5%) and methanol (Êxodo Científica, Brazil, ≥ 99.8%). They were chosen based on previous studies [31, 32].

After achieving adsorption equilibrium, contaminated Spectrogel was separated from losartan solution by filtration and dried at ambient temperature (~25 °C) for 48 h. Desorption assays were run in triplicate inserting 0.3 g of contaminated adsorbent into 50 mL of eluent in shaker (200 rpm, 25 °C, 48 h). The quantity of desorbed losartan was monitored by UV/VIS and desorption efficiency, Des (%), was computed by Eq. 4.6:

$$Des = (C_d V_d)/(q_e m_d) \cdot 100 \tag{4.6}$$

where: C_d (mmol/L) = concentration of losartan after desorption tests; V_d (L) = volume of eluent; q_e (mmol/g) = equilibrium adsorption capacity; m_d (g) = mass of pharmaceutical-loaded adsorbent.

- Mathematical modelling

The kinetic results of losartan adsorption were modelled by the equations of pseudo-first order (PFO) [33], pseudo-second order (PSO) [34], external (film) diffusion [35], surface diffusion (Boyd's model) [36], and pore diffusion [37]. The equilibrium models of Langmuir [38], Freundlich [39] and Dubinin-Radushkevish [40] were chosen to reproduce the isotherms. These equations are detailed in supplementary material (Tables S4.1 and S4.2).

Nonlinear fitting procedure was performed in OriginPro 8 software and the adjustment quality was judged by coefficient of determination, R^2 (Eq. 4.7), and corrected Akaike information criterion, $AICc$ (Eq. 4.8) [41].

$$R^2 = 1 - \left[\sum_{i=1}^{N} \left(Y_i - \hat{Y}_i\right)^2 \Big/ \sum_{i=1}^{N} \left(Y_i - \overline{Y}\right)^2\right] \tag{4.7}$$

$$AICc = N.\ln\left(\sum_{i=1}^{N} (Y_i - \hat{Y}_i)^2/N\right) + 2p + 2p(p+1)/(N-p-1) \tag{4.8}$$

where: N = quantity of experimental observations; Y_i = experimental value; $\hat{Y}_i$ = estimated value; $\overline{Y}$ = average value of experimental results; p = number of parameters +1 (variance component).

4.3 Results

4.3.1 *Adsorbents characterization*

Fig. 4.2 depicts SEM micrographs of Spectrogel in diverse scales. The images of fresh adsorbent (Fig.4.2a) indicate a nonporous solid texture. From Fig. 4.2b, we may infer that losartan adsorption does not cause noticeable textural changes to Spectrogel. SEM images of μGAC (Fig. 4.2c) reveal a well-developed porous structure, which is typical of ACs.

Figure 4.2. SEM micrographs of: (a) fresh Spectrogel; (b) Spectrogel after losartan adsorption; (c) fresh μGAC.

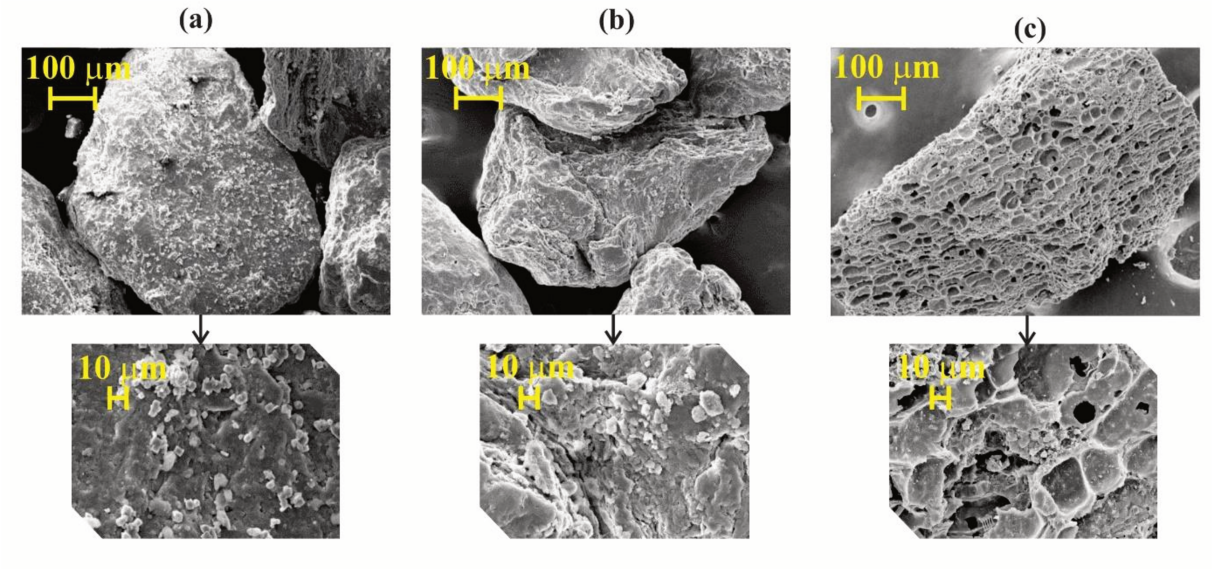

The structural features of the solids were examined by N_2 adsorption/desorption isotherms, which results are summarized in Fig. 4.3a and Table 4.2. N_2 isotherm of fresh Spectrogel is categorized as Type III according to IUPAC, which is usual for nonporous/macroporous materials [42]. From Brunauer-Emmett-Teller method (BET), the specific surface area (SSA) was calculated as 0.14 m²/g (Table 4.2). Subsequent to losartan adsorption, the low SSA was not expressively affected and Spectrogel kept the same shape of N_2 isotherm.

Figure 4.3. (a) N_2 adsorption/desorption isotherms, (b) XRD spectra and (c) FT-IR spectra of fresh Spectrogel, Spectrogel after losartan adsorption and fresh μGAC, (d) influence of pH on zeta potential of fresh Spectrogel.

(a)

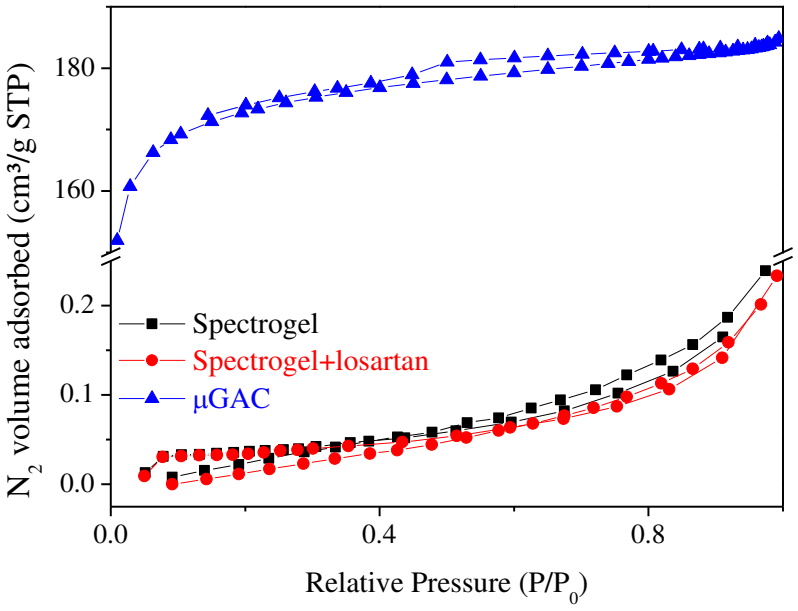

(b)

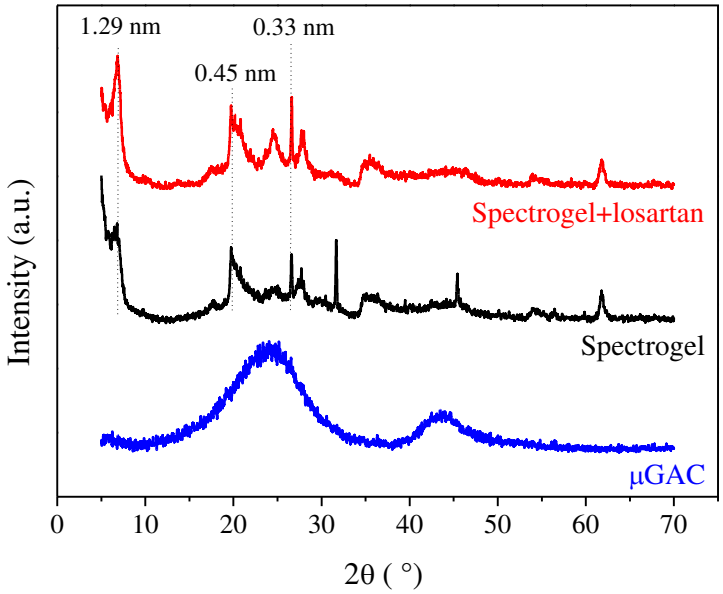

cont. **Fig. 4.3**.

(c)

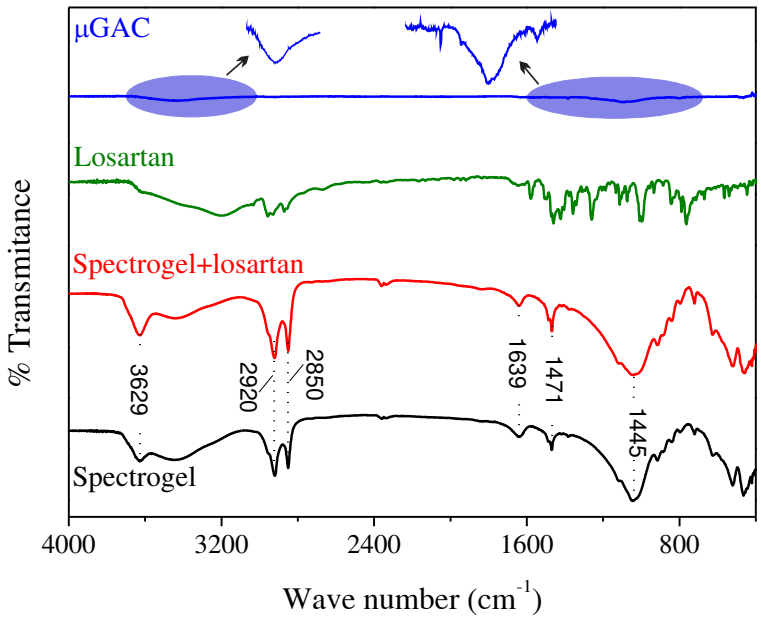

(d)

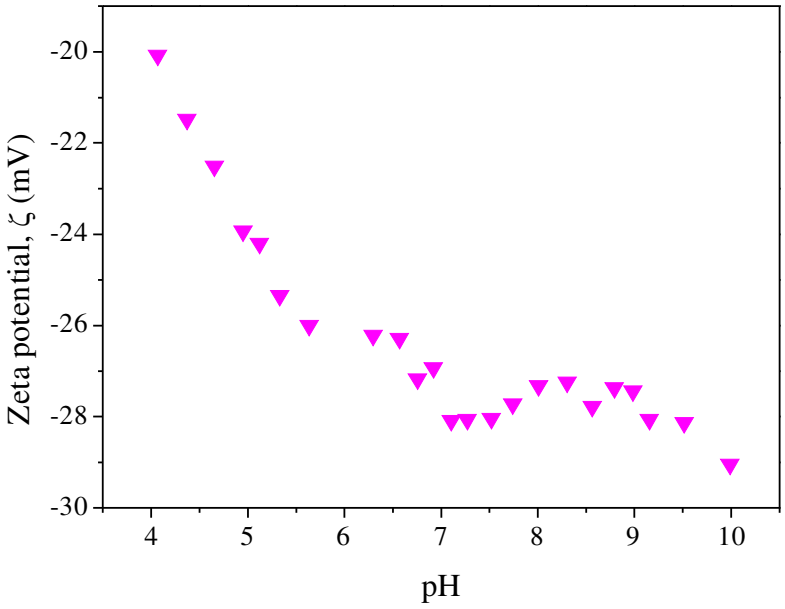

From Fig. 4.3a, μGAC displays type-IV N_2 isotherm with a hysteresis loop in the medium to high relative pressure region, which is characteristic of mesoporous materials. The pore size distribution (Fig. S4.1 in supplementary material) and results from Table 4.2 further reveal that μGAC owns a porous structure rich in meso- and micropores. The SSA of μGAC was estimated as 567.29 m²/g, which is much superior to that of Spectrogel and but relatively inferior to those of other coconut shell-based ACs (717–1194 m²/g) [43].

Table 4.2. Properties of Spectrogel (before and after losartan adsorption) and µGAC.

	Spectrogel	**Spectrogel+Losartan**	**µGAC**
S_{BET} [a] (m²/g)	0.140	0.143	567.290
V_{total} [b] (cm³/g)	--	--	0.284
V_{micro} [c] (g/cm³)	--	--	0.232
V_{meso} [d] (g/cm³)	--	--	0.052
ρ_{true} [e] (g/cm³)	1.644	1.631	2.005
d_{001} [f] (nm)	1.29	1.29	--

[a] Specific surface area by BET method, [b] Total pore volume at P/P_0=0.95, [c] Micropore volume from t-plot report, [d] Mesopore volume estimated by $V_{\text{total}} - V_{\text{meso}}$, [e] True density by helium picnometry, [f] Basal interlayer distance from XRD spectra

From Table 4.2, the true density of Spectrogel was not meaningfully affected by losartan adsorption as it continued as low as ρ_{true}=1.6 g/cm³ after usage. µGAC also presented low ρ_{true} of 1.9989 g/cm³, because of its great total volume induced by high porosity. Other AC prepared from coconut shells presented similar ρ_{true} values [44].

Fig. 4.3b exhibits the XRD patterns. It can be discerned that Spectrogel is predominantly amorphous, which did not change subsequently to losartan adsorption. The basal interlayer distance is 1.29 nm either prior- or post-process (Table 4.2). This d_{001} is close to that expected for bentonite clays, *i.e.*, d_{001}~1.5 nm [45]. Further estimates of crystallinity degree of Spectrogel are hampered by its complexity, triggered by the fact that most details of its synthesis are not supplied by the manufacturer (such as DMA loadings, functionalization method, and degree of impurities).

Concerning µGAC, the XRD spectrum depicts two broad peaks at 23° and 43°, which are ascribable to nanoscale graphite units [43].

Fig. 4.3c depicts FT-IR spectra of µGAC, fresh and contaminated Spectrogel, and pure losartan. The pattern of µGAC presents characteristic peaks of alcoholic or phenolic groups. The strong and broad band at 3442 cm^{-1} may be accredited to the stretching vibration of bonded O−H functional groups, the band around 1090 cm^{-1} may originate from C−O stretching vibration, and the band at 1384 cm^{-1} corresponds to in-plane O−H bend [46]. Characteristic bands of aromatic hydrocarbons could be identified at 1600–1400 cm^{-1} region (skeletal vibrations of C–C stretching) and 900–675 cm^{-1} region (C–H out-of-plane bending). Similar spectra were previously reported for raw coconut shells and derived ACs [47]. The FT-IR spectra of Spectrogel samples exhibit strong absorption band near 3629 cm^{-1}, which is

characteristic of Al-rich montmorillonites. This band designates stretching vibrations of inner OH groups coordinated to octahedral atoms. Corresponding OH bending bands were absorbed in 950–800 cm^{-1} region, which is typical of 2:1-minerals. Si–O stretching vibration can be spotted at 1045 cm^{-1}. The bands in 600–400 cm^{-1} range reflect S–O and Al–O bending vibrations [48, 49]. Provided its organophilic nature, Spectrogel shows distinguished bands of alkylammonium cations. The strong ones at 2920 and 2850 cm^{-1} represent the antisymmetric and symmetric stretching vibrations of C–H bonds, respectively. The N–H bend of ammonium groups is situated at 1639 cm^{-1} and C–H bending vibration is found at 1471 cm^{-1} [46, 50]. Of note, FT-IR spectra of Spectrogel after use is quite similar to that of fresh Spectrogel and absorption bands of pure losartan could not be identified. Thus, we may presume that losartan adsorption does not provoke relevant modifications in the chemical functionalities of the organoclay.

The measurement of zeta potential (ζ) of Spectrogel is disclosed in Fig. 4.3d. The organoclay maintained a negative surface charge under pH conditions between 4 and 10, *i.e.*, Spectrogel does not present a point of zero charge (pH_{PZC}) within the inspected pH range. Of note, the ζ values became increasingly negative as pH increased.

In general, ζ data of organoclays are related to the interactions between surfactant cations used in their synthesis and the clay surface. Organoclays with positive ζ are usually obtained with excess of surfactant concentrations proportional to the cation exchange capacity of the mineral, so that alkyl tails from surfactant shield the negative charges of clay surface [51]. Accordingly, the negative ζ values of Spectrogel suggest that this commercial organoclay is not prepared with excessive loadings of DMA surfactant.

Fig. 4.4 exhibits the thermal behavior of pure losartan and Spectrogel samples. Losartan is thermally stable up to approximately 280 °C, then it starts degrading until 657 °C. The weight loss in this temperature range was about 83%. The first mass-loss of Spectrogel organoclay starts at around 30 °C and proceeds to near 260 °C, what may be ascribed to dehydration/hydroxylation of adsorbed water. Subsequently, a great mass-loss step occurs until 560 °C with maximum degradation at 332 °C, which may relates to releasing DMA surfactant from the organoclay [52]. Considering the resemblance of patterns exhibited by virgin and used Spectrogel, it may be asserted that losartan adsorption did not significantly affect its thermal stability.

Figure 4.4. Thermogravimetric (TG), differential thermogravimetric (DTG), and differential thermal (DTA) analyses for: (a) Spectrogel after losartan adsorption, (b) fresh Spectrogel and (c) pure losartan.

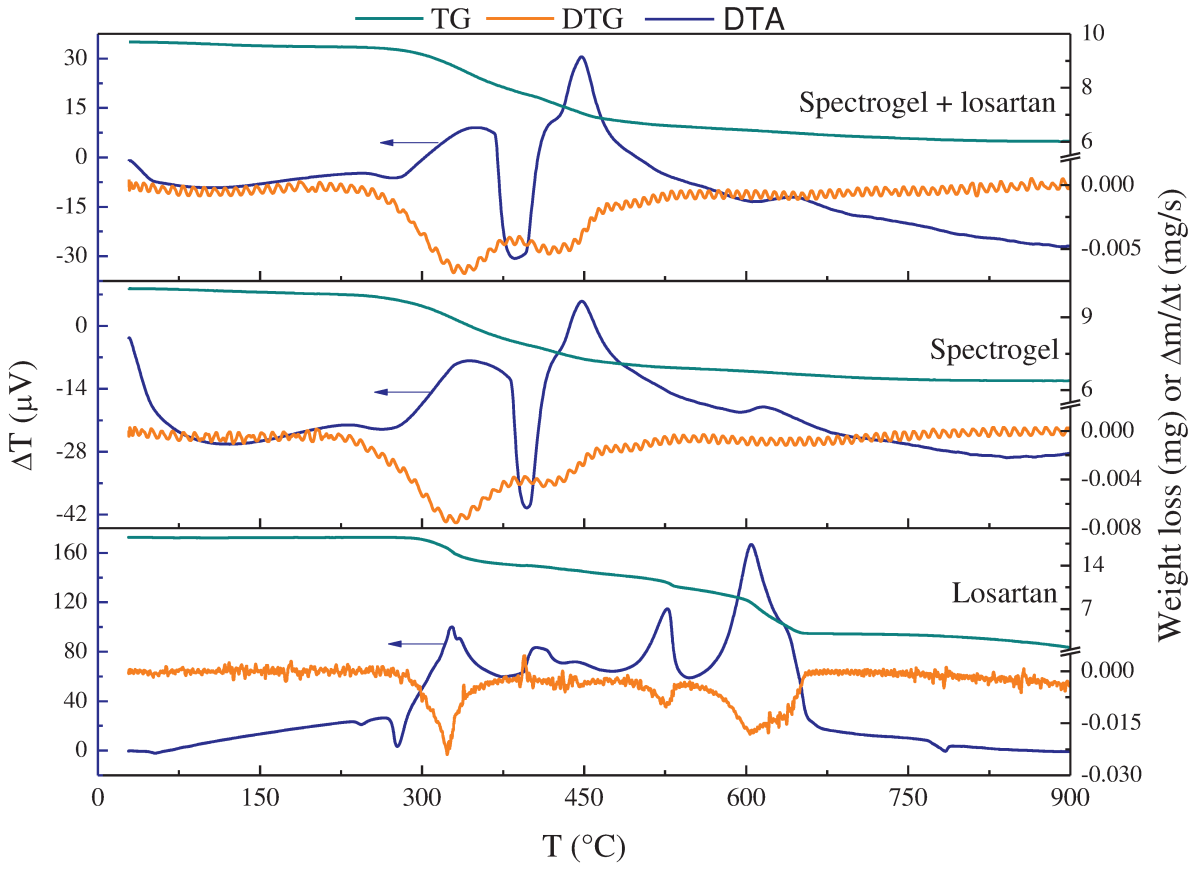

4.3.2 *Influence of adsorbent dosage and solution pH on removal efficiency*

Table 4.3 informs how the quantity of Spectrogel in solution and initial pH impinged on the course of adsorption. Without adjustments in solution pH, it was noticed that losartan removal slightly raised with increasing Spectrogel dosage. However, Tukey's test indicated that using dosages of either 6 or 8 g/L, *Rem* is statistically equivalent at 5% significance level. So, 6 g/L Spectrogel dosage was adopted to the next assays.

For the control test of pH influence, the solution pH was undisturbed, but monitored. We attested that the natural initial pH of losartan solution increased from about pH 5 to pH 7.6 after adding Spectrogel into the system. From Table 4.3, the removal efficiency was maintained around 97% as the initial pH of losartan solution was varied between 2.5–10. The insignificant effect of initial pH may be linked to the highly negative surface charge of Spectrogel, which was verified to be undisturbed under different pH values (Fig. 4.3d). It is inferable that losartan uptake does not rely on electrostatic forces, which will be further discussed in Section 4.3.7.

Table 4.3. Removal efficiency percentage of losartan potassium by Spectrogel at different adsorbent concentrations and initial pH of solution.

Spectrogel dosage (g/L)	Initial solution pH	Rem (%)*
2	Undisturbed (~7.6)	60.37 ± 1.08^{a}
4	Undisturbed (~7.6)	91.37 ± 0.53^{b}
6	Undisturbed (~7.6)	$97.68 \pm 0.13^{c,A}$
8	Undisturbed (~7.6)	98.99 ± 0.12^{c}
6	2.5	97.98 ± 0.16^{A}
6	4	97.49 ± 0.12^{A}
6	5.5	97.58 ± 0.33^{A}
6	7	97.54 ± 0.38^{A}
6	8.5	97.62 ± 0.14^{A}
6	10	97.32 ± 0.32^{A}

* Means with the same letter are statistically equivalent at 5% significance level in Tukey's test (comparison for adsorbent concentration in lower case letters and for solution pH in upper case letters).

4.3.3 *Kinetics of adsorption*

Fig. 4.5a displays adsorption kinetics of losartan using Spectrogel and µGAC. Of note, losartan removal profiles depict a rapid increasing initial step, succeeded by a slow step with asymptotic approximation to the adsorption equilibrium. For initial levels of 0.04, 0.07 and 0.1 mmol/L, equilibrium using Spectrogel was achieved after about 750, 1440 and 2200 min, respectively. Due to enhanced driving force for mass transfer, higher initial concentrations implicated in greater amounts adsorbed at any contact time [53]. The total removal percentage of losartan using Spectrogel remained as approximately 98% in all the cases. Comparatively, µGAC was less efficient than Spectrogel: adsorption process onto µGAC took longer to reach equilibrium (around 2600 min for C_0=0.1 mmol/L) and losartan removal percentage was inferior (Rem=94%).

The shortage of research on losartan adsorption prevents further comparisons with materials other than Spectrogel and µGAC. Recently, Maia, et al. [25] ascertained that 500 min was enough time for attaining the equilibrium of adsorption for diclofenac sodium over Spectrogel. The greater hydrophobicity of diclofenac, represented by $\log P_{ow} = 4.5$ [54], may be ascribed as a promoting factor for its faster uptake in contrast to losartan ($\log P_{ow} = 1.19$). Hence, we may infer that losartan is probably adsorbed onto Spectrogel through a more elaborate process than diclofenac.

Figure 4.5. Experimental adsorption data for losartan onto Spectrogel and μGAC: (a) kinetics at different initial concentrations (scatter) and the fitting of pseudo-second order model (solid line); (b) isotherms at different temperatures (scatter) and the fitting of Freundlich model (solid line).

(a)

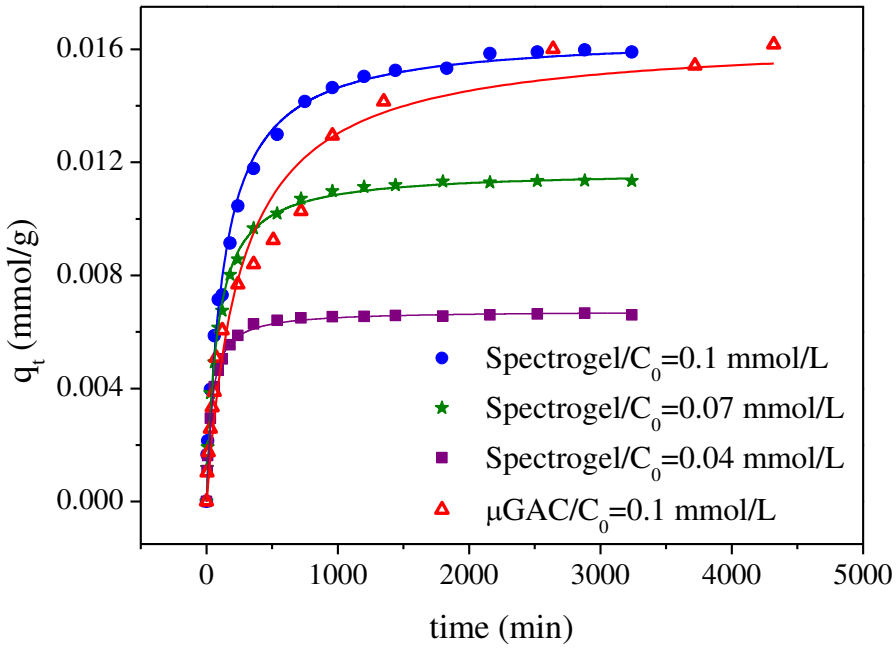

(b)

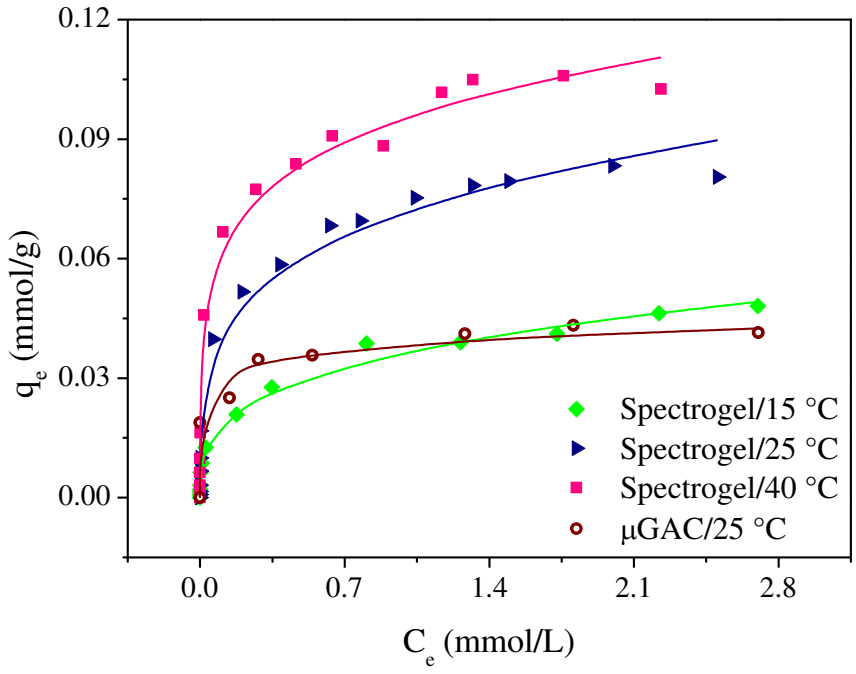

Table 4.4 provides the fittings of the mathematical kinetic models to the experimental data. Initially, we tested the models based on chemical reaction kinetics, *i.e.*, PFO and PSO. As specified by the higher R^2 and lower $AICc$ values, losartan adsorption kinetics onto either Spectrogel or μGAC was better predicted by PSO model than PFO model. The satisfactory adjustment is evidenced in Fig. 4.5a. The reaction rate constant of PSO (k_2) showed a downward trend with increasing initial levels of losartan in solution, as a reflect of the longer contact time necessary to reach adsorption equilibrium. In line with the theoretical approach, the good compliance of experimental data with PSO model suggests that losartan uptake may include a chemisorption mechanism [34, 53].

Table 4.4. Parameters of the kinetic models of pseudo-first order (PFO), pseudo-second order (PSO), film diffusion, surface diffusion and pore diffusion for losartan potassium adsorption onto Spectrogel and μGAC at different initial concentrations ($\boldsymbol{C_0}$ in mmol/L).

Model	**Parameter**		**Spectrogel** C_0=0.04	**Spectrogel** C_0=0.07	**Spectrogel** C_0=0.1	**μGAC** C_0=0.1
PFO	k_1	(min^{-1})	0.016	0.008	0.006	0.003
	q_e	(mmol/g)	0.006	0.011	0.015	0.015
	R^2	(–)	0.98	0.97	0.97	0.93
	$AICc$	(–)	–314.49	–289.71	–271.57	–215.50
PSO	k_2	(g/mmol/min)	3.979	1.098	0.473	0.230
	q_e	(mmol/g)	0.007	0.012	0.017	0.016
	R^2	(–)	1.00	1.00	0.99	0.97
	$AICc$	(–)	–358.06	–323.80	–299.00	–276.19
Film diffusion	K_{FM}	(m/s)	6.5E–07	4.1E–07	4.1E–07	5.9E–11
Surface diffusion	B	(–)	0.002	0.002	0.002	0.001
	D_i	(cm^2/min)	1.7E–07	2.4E–07	1.9E–07	1.2E-07
	R^2	(–)	0.74	0.94	0.96	0.83
Pore diffusion	k_i	(mmol/g/$min^{0.5}$)	0.003	9.5E–05	1.5E–04	2.3E–04
	C	(mmol/g)	1.7E–04	0.008	0.010	0.004
	R^2	(–)	0.97	0.95	0.93	1.00

Apropos of transfer mechanisms, the equations of external, surface and pore diffusions were tested for losartan adsorption. Fig. S4.2 in supplementary material exemplifies the graphical fittings for C_0=0.1 mmol/L. Of note, the mass transfer coefficients of external diffusion model (K_{FM}) were estimated from the initial stage of the kinetic profiles [35]. From

Table 4.4, K_{FM} of Spectrogel exhibited diminished values for higher initial losartan concentrations, ascribed to greater concentration gradients. Comparatively to Spectrogel, μGAC presented lower values of K_{FM} at C_0=0.1 mmol/L, which may be induced by the greater outer surface area of μGAC available for adsorption.

The model from Boyd et al. (1947) was tested for surface diffusion. The linear adjustments of Bt vs. t plots were not satisfactory with R^2 values that did not exceed 0.96 and 0.83 for Spectrogel and μGAC, respectively (Table 4.4). This trend hints that mass transfer in the surface does not restrain the global rate of losartan adsorption onto either Spectrogel or μGAC.

Intraparticle diffusion in the liquid pore was inspected by the model of Weber and Morris [37]. The plots of q_t vs. $t^{0.5}$ were multi-linear, as illustrated in Fig. S4.2c. This implies that yet pore diffusion is relevant in adsorption kinetics, it is the controlling mechanism neither for Spectrogel nor μGAC. Three steps for losartan uptake can be indicated: first the fast adsorption or surface diffusion, second the intraparticle diffusion, and third adsorption equilibrium [55]. The pore diffusion equation was fitted to data set of second step and it was attested that the greater C_0, the higher the magnitude of kinetic parameter C (Table 4.4). This tendency can be entailed by the incremental hindrance to external diffusion at greater concentrations, since C denotes the boundary layer's thickness.

In conclusion, considering the minor effects of both surface and pore diffusion, external mass resistance can be attested as the predominant rate-limiting step of losartan adsorption onto Spectrogel. Similar conclusion can be drawn for μGAC. External resistance was also identified as the foremost controlling step for diclofenac adsorption onto Spectrogel [25]. Increasing agitation speeds might minimize film diffusion effects, but this is restricted in bench tests by equipment limitations.

4.3.4 *Equilibrium of adsorption*

The equilibrium assays were carried out for 2800 min (48 h) to assure equilibrium reaching. Fig. 4.5b discloses the isotherms for losartan adsorption using Spectrogel at 15 °C, 25 °C and 40 °C and μGAC at 25 °C. We may observe that the isotherms present the same shape, which can be distinct as extremely favorable [56]. Remarkably, losartan adsorption capacity by Spectrogel increases with increasing temperatures, *i.e.* the operation is endothermic.

Table 4.5 displays the parameters for the isotherm equations of Langmuir, Freundlich and Dubinin-Radushkevich.

Table 4.5. Parameters of isotherm models fitted to equilibrium data of losartan adsorption onto Spectrogel at 15, 25 and 40 °C and µGAC at 25 °C.

Model	**Parameter**		**Spectrogel** *T*=15 ºC	**Spectrogel** *T*=25 ºC	**Spectrogel** *T*=40 ºC	**µGAC** *T*=25 ºC
Langmuir	q_{max}	(mmol/g)	0.048	0.082	0.099	0.044
	k_L	(L/mmol)	4.903	10.396	27.402	10.165
	R^2	(–)	0.97	0.97	0.97	0.84
	$AICc$	(–)	–161.92	–167.78	–146.91	–68.01
Freundlich	K_F	(mmol/g)(L/mmol)$^{1/n}$	0.037	0.072	0.095	0.038
	n	(–)	3.347	4.090	5.448	9.617
	R^2	(–)	0.99	0.98	0.97	0.96
	$AICc$	(–)	–186.82	–179.44	–164.16	–82.51
Dubinin-Radushkevich	q_m	(mmol/g)	0.043	0.078	0.098	0.043
	K_D	(10^8 mol²/J²)	2.2E–08	1.5E–08	7.9E–09	1.9E–08
	E	(kJ/mol)	4.719	5.805	7.945	5.142
	R^2	(–)	0.95	0.97	0.96	0.74
	$AICc$	(–)	–155.99	–165.86	–98.31	–66.87

On comparing the fittings for Spectrogel, Freundlich model finest correlated the equilibrium information of losartan adsorption onto Spectrogel (higher R^2 and lower $AICc$). This indicates that the phenomenon occurs in multilayer on an energetically non-homogeneous surface. Moreover, the magnitude of n factor in 2–10 range points to the favorable adsorption of losartan onto Spectrogel [57, 58]. The superior adjustment of Freundlich model was also noted for µGAC isotherm.

The efficacy of Spectrogel and µGAC can be compared based on the Freundlich constant K_F, which is an indicative of the relative adsorption capacity. From Table 4.5, K_F of Spectrogel at 25 °C surpassed that of µGAC, ergo the organoclay is best indicated for removing losartan. This is confirmed considering the maximum adsorption capacity from Langmuir equation, q_{max}, which is almost two times greater for Spectrogel than µGAC. An in-depth search of relevant literature did not yield extra equilibrium data for losartan adsorption, what prevents further comparisons. Noteworthy, Genç and Dogan [59] also found improved removal capabilities for bentonite clay than activated carbon in adsorbing ciprofloxacin pharmaceutical.

4.3.5 *Thermodynamics of adsorption*

Thermodynamic parameters are requisite to delineate how feasible is losartan adsorption using Spectrogel. In this article, we computed the following: ΔG (15 °C) = –18.93 kJ/mol; ΔG (25 °C) = –22.07 kJ/mol; ΔG(40 °C) = –24.90 kJ/mol; ΔS = 236.55 J/mol/K; ΔH = 48.95 kJ/mol.

The negative ΔG values support a spontaneous proceeding [35], whilst the increasing trend with temperature suggests that losartan adsorption is favored by higher temperatures. This is corroborated by the positive ΔH value, which reveals endothermicity and suggests the involvement of chemisorption, but it cannot be affirmed that if is the sole phenomena [60]. The positive ΔS value reflects that the organization of losartan molecules at the interface becomes more random with larger degree of freedom during adsorption [61].

4.3.6 *Desorption tests and cost effectiveness considerations*

Desorption studies are important aiming the prolongation of adsorbent's lifetime with reuse within the process, and the consequent reduction in solid waste generation and expenditures with fresh adsorbents. Fig. 4.6 portrays the desorption efficiency of losartan from Spectrogel using ultrapure water, ethanol and methanol as eluents.

Figure 4.6. Desorption efficiency of losartan from Spectrogel using ultrapure water, ethanol and methanol as eluents.

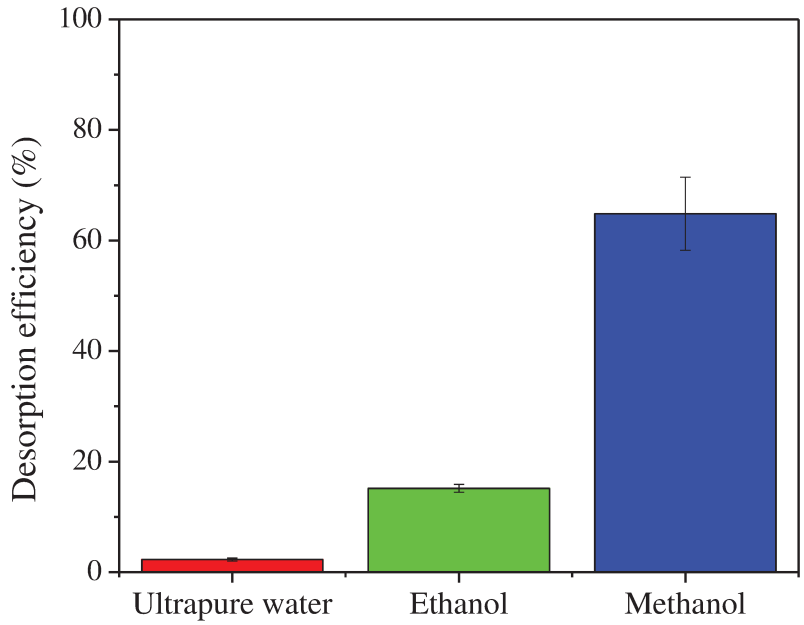

Notably, the maximum desorption efficiency (~65%) was given by methanol, which might be acknowledged to its greater polarity in relation to that of ethanol or water. Kyzas, et

al. [31] found similar result for desorpting atenolol and propranolol from graphene oxide. However, since methanol is extremely toxic, further investigations should be conducted for environmentally friendly solvents or alternative regeneration techniques, such as thermal treatment or desorption with steam. Stability and reusability of Spectrogel in multiple cycles should be inspected in packed bed adsorption columns, which are better intended for large-scale exertions [35].

Under the canopy of reusability, economic aspects have to be pondered since the disposal with landfilling/incineration and the purchase of fresh low-cost adsorbents may be more lucrative than having the materials regenerated [19]. This is especially true for clay materials, which are plentiful in nature and have lower costs comparatively to traditional adsorbents. For exemplifying, the price estimates for bentonite clay and commercial activated carbon are US $0.072/kg and US $20–22/kg, correspondingly [62, 63]. Momina, et al. [64] recently mentioned the better cost effectiveness of clay-based materials. To boost, according to life cycle impact assessments, organoclays can offer lower environmental impacts than granular activated carbons [65]. Therefore, we may say that besides top efficiency in losartan removal, opting for Spectrogel as adsorbent rather than µGAC may be economically and environmentally advantageous.

4.3.7 *Mechanisms of losartan uptake*

In general, adsorbents with well-developed porosity and high surface area are pursued for improved adsorption performance. µGAC has a higher degree of microporosity and a SSA more than 4000 times larger than Spectrogel, which is predominantly macroporous. So, the surface features of µGAC were expected to enhance adsorption potential of losartan via dispersive forces [66]; nevertheless, much more losartan was adsorbed by Spectrogel (q_{max}=0.0820 mmol/g) than µGAC (q_{max}=0.0441 mmol/g). In this respect, molecular sieving might affect adsorption onto µGAC due to the difficult of large losartan molecules, which have great molecular weight, to access the micropores inside the innermost surface of µGAC. Therefore, it may be deduced that surface area and porosity are not primordial in losartan adsorption.

Surface chemistry is a fundamental factor in pharmaceutical adsorption. Regarding surface charge, Spectrogel presents a negative surface as a function of pH (Fig. 4.3d) and commercial AC obtained from coconut shells traditionally has point of zero charge (pH_{PZC}) around 9.5–9.8 [17, 67]. As above-mentioned, losartan solution containing Spectrogel presents pH=7.6, at which losartan should exist in anionic form owing to lower pKa=4.9. Therefore,

charge repulsion between losartan and Spectrogel is expected and electrostatic interactions cannot be assigned as the key adsorption force. Opposingly, the positive charge of μGAC in losartan solution might favor adsorption via electrostatic attractive forces. However, additional specific/chemical interactions cannot be ignored in derivation of adsorption mechanisms [17].

Despite its low hydrophobicity, losartan molecule (Fig. 4.1) presents multiple functional groups, which potentially interacts with polar adsorption sites. μGAC presents some polar mineral phase and surface hydrophobicity owing to graphitic content (Fig. 4.3b) and carbon phase, respectively. Comparatively to carbonaceous adsorbents, Spectrogel not only presents more abundant ionic/polar sites in the mineral surface [68], but also an organic environment formed by the conglomeration of DMA surfactant molecules in the interlayer and clay surface. The mineral surface acts as a traditional adsorbent, whereas the organic phase can behave as a partition medium, *i.e.*, a solvent-type sink for the contaminant.

Partition has been widely acknowledged as the prevailing mechanism of removal of organic compounds by organoclays in the case of linear isotherms obtained over a relatively wide concentration range [20, 21, 69]. In this work, the downward curvature of Spectrogel isotherms (Fig. 4.5b) and values of Freundlich exponents (n) far from unit (Table 4.5) suggest that partition is not the single - nor the dominant - interaction. The preservation of Spectrogel's basal interlayer space after losartan removal (Table 4.2) corroborates that. A dual mode mechanism for losartan uptake over Spectrogel may be proposed: (i) hydrophobic partitioning interactions of molecular losartan in the organic phase and (ii) adsorption onto the mineral surface of the organoclay. Non-covalent interactions (*e.g.* cation-π) may arise between the aromatic moieties of losartan and DMA organic cations, which might favor the greater affinity of losartan to Spectrogel in comparison to μGAC [70].

4.4 Conclusions

This work offers an in-depth analysis of losartan adsorption using Spectrogel organoclay and micro-grain activated carbon for comparison. Kinetics and equilibrium data sets were satisfactorily correlated by pseudo-second order equation and Freundlich isotherm, respectively. External diffusion was identified as the most relevant mass transfer mechanism. Methanol provided a desorption efficiency of 65%, but utilizing Spectrogel as one-way adsorbent might be recommended considering cost effectiveness. Langmuir maximum adsorption capacity was 0.0820 mmol/g for Spectrogel and 0.0441 mmol/g for μGAC. In contrast to Spectrogel, μGAC offered slower kinetics and lower removal efficiency, despite its greater surface area and porosity. Although the governing mechanisms of losartan uptake are

not totally elucidated, this study probed the preeminent role of specific/chemical factors rather than surface features. Losartan removal using Spectrogel is governed by both adsorption and partition interactions. Summing up, the findings from this paper testify that Spectrogel is a propitious non-traditional adsorbent for pharmaceutical remediation. Nonetheless, it is demanding to further exploit the impacts of competitive adsorption and wastewater matrix, and to evaluate continuous adsorption in fixed-bed columns.

Acknowledgements

This study was financed in part by the Coordenação de Aperfeiçoamento de Pessoal de Nível Superior - Brasil (CAPES - Finance Code 001) [Proc. 88882.329686/2018-01], Conselho Nacional de Desenvolvimento Científico e Tecnológico (CNPq) [Proc. 406193/2018-5] and Fundação de Amparo à Pesquisa do Estado de São Paulo – Brasil (FAPESP) [Proc. 2016/05007-1]. We acknowledge SpectroChem for donating Spectrogel organoclay and Purifarma for losartan potassium sample.

Appendix 4.A. Supplementary information

Supplementary material related to this article can be found, in the online version, at doi:https://doi.org/10.1016/j.jece.2019.103562.

Table S4.1. Kinetic models of adsorption.

	Models	Equation		Reference
Kinetic models	Pseudo-first order (PFO)	$\ln(q_e - q_t) = \ln(q_e) - k_1 t$	(S1)	Lagergren [33]
	Pseudo-second order (PSO)	$\frac{1}{q_e - q_t} = \frac{1}{q_e} + k_2 t$	(S2)	Ho and McKay [34]
	Film diffusion	$\frac{dC_t}{dt} = -K_{FM} a_m \frac{m}{V}[C_t - C_S]$	(S3)	Worch [35]
	Surface diffusion (Boyd's model)	$F(t) = \frac{q_t}{q_e}$	(S4)	Boyd, et al. [71]
		$Bt = -0.4977 - \ln(1 - F)$	(S5)	
		$B = \frac{\pi^2 D_i}{r^2}$	(S6)	
	Pore diffusion	$q_t = k_i t^{1/2} + C$	(S7)	Weber and Morris [37]

q_e: concentration in the solid phase at equilibrium (mmol/g); k_1: first order rate constant (min^{-1}); k_2: second order rate constant (g/mmol/min); C_t: concentration in the bulk solution (mmol/L); C_s: concentration at the external surface (mmol/L); K_{FM}: film mass transfer coefficient (m/s); a_m: specific surface area of the adsorbent material by the BET method (m^2/g); m: adsorbent mass (g); V: volume of solution (L); F: fraction of solute adsorbed at time t (-); Bt: mathematical function of F (-); B: time constant (min^{-1}); D_i: internal diffusion coefficient (cm^2/min); r: radius of the adsorbent particles (cm); k_i: intraparticle diffusion constant ($mmol/g/min^{0.5}$); C: parameter of intraparticle diffusion model (mmol/g).

Table S4.2. Isotherm models of adsorption.

Isotherm models	Langmuir	$q_e = \frac{k_L q_{max} C_e}{1 + K_L C_e}$ $R_L = \frac{1}{1 + K_L C_0}$	(S9) (S10)	Langmuir [38]
	Freundlich	$q_e = K_F C_e^{1/n}$	(S11)	Freundlich [39]
	Dubinin-Radushkevich (D-R)	$q_e = q_m \exp(-K_D \varepsilon^2)$ $\varepsilon = RT \ln\left(1 + \frac{1}{C_e}\right)$ $E = (2K_D)^{-0.5}$	(S12) (S13) (S14)	Dubinin [40]
	Redlich-Peterson (R-P)	$q_e = \frac{q_{m,RP} K_{RP} C_e}{1 + (K_{RP} C_e)^{n_{RP}}}$	(S15)	Redlich and Peterson [72]
	Tóth	$q_e = \frac{q_{m,T} K_T C_e}{[1 + (K_{RP} C_e)^{n_T}]^{1/n_T}}$	(S16)	Tóth [73]

q_{max}: Langmuir maximum adsorption capacity (mmol/g); K_L: Langmuir isotherm constant (L/mmol); C_e: concentration in the liquid phase at equilibrium (mmol/L); R_L: separation factor (-); K_F: Freundlich isotherm constant (mmol/g).(L/mmol)$^{1/n}$; n: Freundlich heterogeneity factor (-); q_m: adsorption capacity of D-R isotherm (mmol/g); K_D: D-R isotherm constant (mol^2/J^2); ε: Polanyi potential (J/mol); R: universal gas constant (J/mol/K); T: temperature (K); E: mean free energy of adsorption (J/mol); $q_{m,RP}$: adsorption capacity of R-P isotherm (mmol/g); K_{RP}: R-P isotherm constant (L/mmol); n_{RP}: R-P index of heterogeneity (-);$q_{m,T}$: adsorption capacity of Tóth isotherm (mmol/g); K_T: Tóth isotherm constant (L/mmol); n_T: Tóth index of heterogeneity (-).

Figure S4.1. Pore size distributions of micro-grain activated carbon obtained by Barrett, Joyner and Halenda (BJH) method from N2-desorption isotherm.

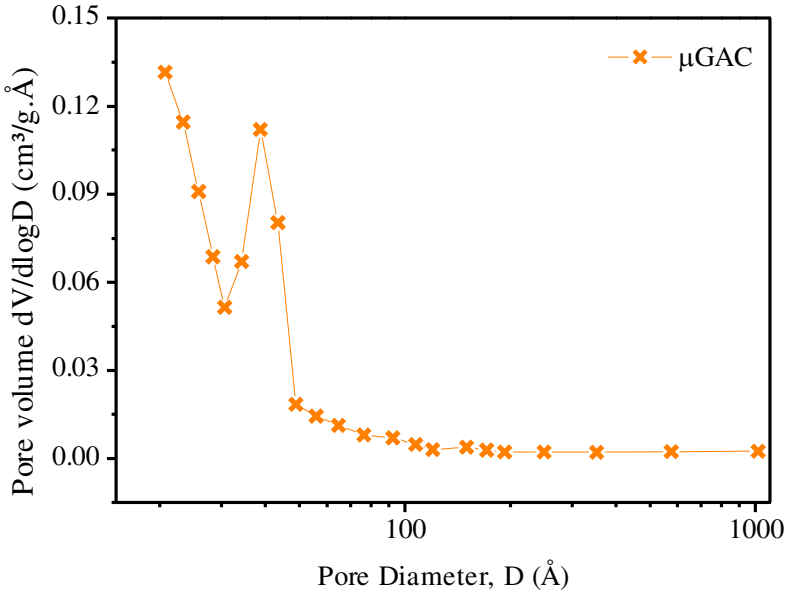

Figure S4.2. Kinetics of losartan adsorption onto Spectrogel and μGAC at C_0=0.1 mmol/L adjusted by the mass transfer models: (a) film diffusion, (b) surface diffusion, and (c) pore diffusion.

(a)

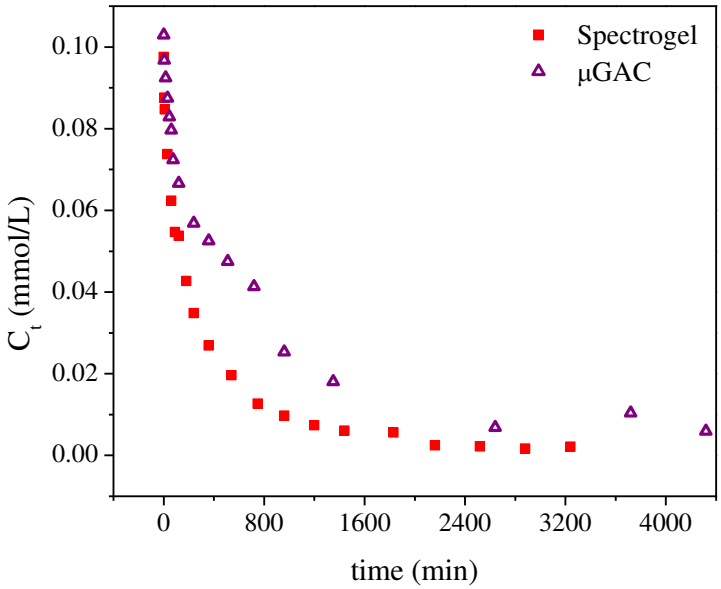

(b)

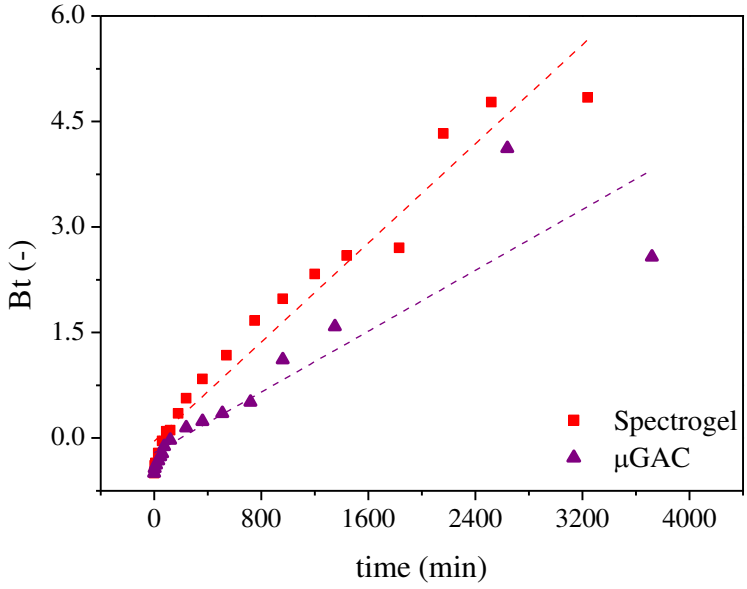

cont. **Fig. S4.2.**

(c)

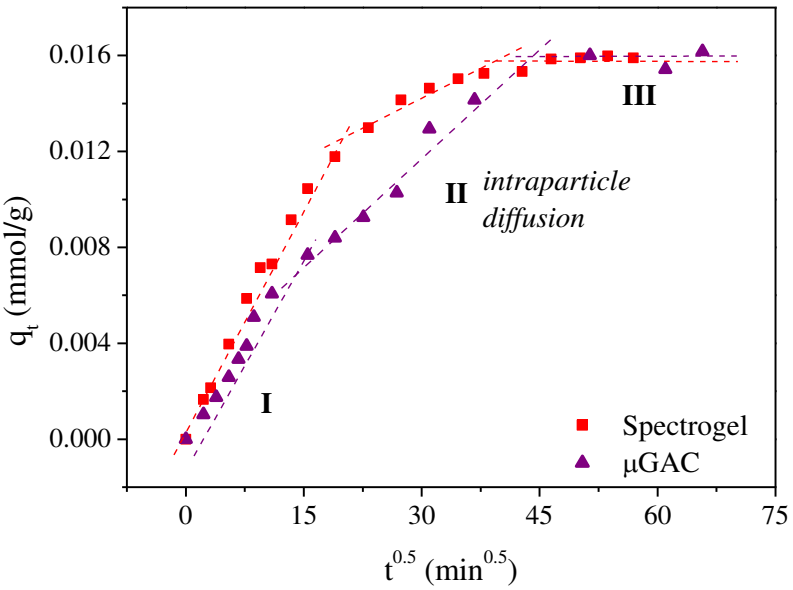

References

[1] G. Sarganas, H. Knopf, D. Grams, H.K. Neuhauser, Trends in Antihypertensive Medication Use and Blood Pressure Control Among Adults With Hypertension in Germany, Am. J. Hypertens. 29 (2016) 104-113.

[2] World Health Organization, WHO Model List of Essential Medicines, World Health Organization, 2017.

[3] Q. Gu, V.L. Burt, C.F. Dillon, S. Yoon, Trends in antihypertensive medication use and blood pressure control among UnitedStates adults with hypertension: the National Health and Nutrition Examination Survey, 2001 to 2010, Circulation 126 (2012) 2105-2114.

[4] R.M.d. Silva, G.C. Chaves, L.A. Chaves, M.R. Campos, V.L. Luiza, A.D. Bertoldi, D. Ross-Degnan, I.C.M. Emmerick, Farmácia Popular Program: pharmaceutical market analysis of antihypertensive acting on the renin-angiotensin system medicines, Ciência & Saúde Coletiva 22 (2017) 2501-2512.

[5] V. Osorio, A. Larrañaga, J. Aceña, S. Pérez, D. Barceló, Concentration and risk of pharmaceuticals in freshwater systems are related to the population density and the livestock units in Iberian Rivers, Sci. Total Environ. 540 (2016) 267-277.

[6] M. Gros, S. Rodríguez-Mozaz, D. Barceló, Fast and comprehensive multi-residue analysis of a broad range of human and veterinary pharmaceuticals and some of their metabolites in surface and treated waters by ultra-high-performance liquid chromatography coupled to quadrupole-linear ion trap tandem mass spectrometry, J. Chromatogr. 1248 (2012) 104-121.

[7] A.M. Botero-Coy, D. Martínez-Pachón, C. Boix, R.J. Rincón, N. Castillo, L.P. Arias-Marín, L. Manrique-Losada, R. Torres-Palma, A. Moncayo-Lasso, F. Hernández, 'An investigation into the occurrence and removal of pharmaceuticals in Colombian wastewater', Sci. Total Environ. 642 (2018) 842-853.

[8] Food and Drug Administration, Review of Environmental Assessment for Cozaar Tablets (50 and 100 mg Losartan Potassium), Center for Drug Evaluation and Research (Ed.), FDA, 2002.

[9] H. Matsuo, H. Sakamoto, K. Arizono, R. Shinohara, Behavior of pharmaceuticals in waste water treatment plant in Japan, Bull. Environ. Contam. Toxicol. 87 (2011) 31-35.

[10] N. Collado, S. Rodriguez-Mozaz, M. Gros, A. Rubirola, D. Barceló, J. Comas, I. Rodriguez-Roda, G. Buttiglieri, Pharmaceuticals occurrence in a WWTP with significant industrial contribution and its input into the river system, Environ. Pollut. 185 (2014) 202-212.

[11] C. Salazar, N. Contreras, H.D. Mansilla, J. Yáñez, R. Salazar, Electrochemical degradation of the antihypertensive losartan in aqueous medium by electro-oxidation with boron-doped diamond electrode, J. Hazard. Mater. 319 (2016) 84-92.

[12] J.R. de Andrade, M.G.A. Vieira, M.G.C. da Silva, S. Wang, Oxidative degradation of pharmaceutical losartan potassium with N-doped hierarchical porous carbon and peroxymonosulfate, Chem. Eng. J. (2019) 122971.

[13] M. Grassi, G. Kaykioglu, V. Belgiorno, G. Lofrano, Removal of emerging contaminants from Water and Wastewater by adsorption process, in: G. Lofrano (Ed.) Emerging Compounds Removal from Wastewater, Springer, Netherlands, 2012, pp. 15-37.

[14] J. Margot, C. Kienle, A. Magnet, M. Weil, L. Rossi, L.F. de Alencastro, C. Abegglen, D. Thonney, N. Chèvre, M. Schärer, D.A. Barry, Treatment of micropollutants in municipal wastewater: Ozone or powdered activated carbon? Sci. Total Environ. 461-462 (2013) 480-498.

[15] R. Mailler, J. Gasperi, Y. Coquet, A. Buleté, E. Vulliet, S. Deshayes, S. Zedek, C. Mirande-Bret, V. Eudes, A. Bressy, E. Caupos, R. Moilleron, G. Chebbo, V. Rocher, Removal of a wide range of emerging pollutants from wastewater treatment plant discharges by micro-grain activated carbon in fluidized bed as tertiary treatment at large pilot scale, Sci. Total Environ. 542 (2016) 983-996.

[16] S.N.F. Ali, E.I. El-Shafey, S. Al-Busafi, H.A.J. Al-Lawati, Adsorption of chlorpheniramine and ibuprofen on surface functionalized activated carbons from deionized water and spiked hospital wastewater, J. Environ. Chem. Eng. 7 (2019) 102860.

[17] L. Nielsen, M.J. Biggs, W. Skinner, T.J. Bandosz, The effects of activated carbon surface features on the reactive adsorption of carbamazepine and sulfamethoxazole, Carbon 80 (2014) 419-432.

[18] A. Bhatnagar, M. Sillanpää, Utilization of agro-industrial and municipal waste materials as potential adsorbents for water treatment—A review, Chem. Eng. J. 157 (2010) 277-296.

[19] J.R. de Andrade, M.F. Oliveira, M.G.C. da Silva, M.G.A. Vieira, Adsorption of pharmaceuticals from water and wastewater using nonconventional low-cost materials: A review, Ind. Eng. Chem. Res. 57 (2018) 3103-3127.

[20] R. Zhu, Q. Chen, Q. Zhou, Y. Xi, J. Zhu, H. He, Adsorbents based on montmorillonite for contaminant removal from water: a review, Appl. Clay Sci. 123 (2016) 239-258.

[21] L.F. Lima, J.R. de Andrade, M.G.C. da Silva, M.G.A. Vieira, Fixed bed adsorption of benzene, toluene, and xylene (BTX) contaminants from Monocomponent and multicomponent solutions using a commercial organoclay, Ind. Eng. Chem. Res. 56 (2017) 6326-6336.

[22] S.K.F. Stofela, J.R. de Andrade, M.G.A. Vieira, Adsorption of benzene, toluene, and xylene (BTX) from binary aqueous solutions using commercial organoclay, Can. J. Chem. Eng. 95 (2017) 1034-1044.

[23] S.K.F. Stofela, A.F. de Almeida Neto, M.L. Gimenes, M.G.A. Vieira, Adsorption of toluene into commercial organoclay in liquid phase: kinetics, equilibrium and thermodynamics, Can. J. Chem. Eng. 93 (2015) 998-1008.

[24] G.S. Maia, J.R. Andrade, M.F. Oliveira, M.G.A. Vieira, M.G.C. Silva, Affinity studies between drugs and clays as adsorbent material, Chem. Eng. Trans. 57 (2017) 583 - 588.

[25] G.S. Maia, J.R. de Andrade, M.G.C. da Silva, M.G.A. Vieira, Adsorption of diclofenac sodium onto commercial organoclay: kinetic, equilibrium and thermodynamic study, Powder Technol. 345 (2019) 140-150.

[26] A.-R.A. Al-Majed, E. Assiri, N.Y. Khalil, H.A. Abdel-Aziz, Losartan, in: H.G. Brittain (Ed.) Profiles of Drug Substances, Excipients and Related Methodology, Academic Press2015, 159-194.

[27] R.C. Williams, M.S. Alasandro, V.L. Fasone, R.J. Boucher, J.F. Edwards, Comparison of liquid chromatography, capillary electrophoresis and super-critical fluid chromatography in the determination of Losartan Potassium drug substance in Cozaar® tablets, J. Pharm. Biomed. Anal. 14 (1996) 1539-1546.

[28] O.C. Lastra, I.G. Lemus, H.J. Sánchez, R.F. Pérez, Development and validation of an UV derivative spectrophotometric determination of Losartan potassium in tablets, J. Pharm. Biomed. Anal. 33 (2003) 175-180.

[29] S. Naveed, Analytical Method for Estimation of losartan by using uv – spectrophotometer, global journal of medical research: B pharma, drug discovery, Toxicol. Forensic Med. – Open J. 14 (2014) 14-18.

[30] P.S. Ghosal, A.K. Gupta, An insight into thermodynamics of adsorptive removal of fluoride by calcined Ca-Al-(NO3) layered double hydroxide, RSC Adv. 5 (2015) 105889-105900.

[31] G.Z. Kyzas, A. Koltsakidou, S.G. Nanaki, D.N. Bikiaris, D.A. Lambropoulou, Removal of beta-blockers from aqueous media by adsorption onto graphene oxide, Sci. Total Environ. 537 (2015) 411-420.

[32] C. Ding, J. He, M. Xu, C. Wang, Fabrication of β-cyclodextrin modified mesostructured silica coated multi-walled carbon nanotubes composites and application for paraben removal, Water Sci. Technol. 78 (2018) 1001-1009.

[33] S. Lagergren, Zur theorie der sogenannten adsorption gelöster stoffe, Kungliga Svenska Vetenskapsakademiens., Handlingar 24 (1898) 1-39.

[34] Y.S. Ho, G. McKay, A comparison of chemisorption kinetic models applied to pollutant removal on various sorbents, Process Saf. Environ. Prot. 76 (1998) 332-340.

[35] E. Worch, Adsorption Technology in Water Treatment: Fundamentals, Processes, and Modeling, De Gruyter, Berlim, 2012.

[36] G.E. Boyd, A.W. Adamson, L.S. Myers, The exchange adsorption of ions from aqueous solutions by organic zeolites. II. Kinetics1, J. Am. Chem. Soc. 69 (1947) 2836-2848.

[37] W.J. Weber, J.C. Morris, Kinetics of adsorption on carbon from solution, J. Sanit. Eng. Div. 89 (1963) 31-60.

[38] I. Langmuir, The adsorption of gases on plane surfaces of glass, mica and platinum, J. Am. Chem. Soc. 40 (1918) 1361-1403.

[39] H.M.F. Freundlich, Over the adsorption in solution, J. Phys. Chem. 57 (1906) 385–470.

[40] M.M. Dubinin, The potential theory of adsorption of gases and vapors for adsorbents with energetically nonuniform surfaces, Chem. Rev. 60 (1960) 235-241.

[41] P.L. Bonate, Pharmacokinetic-Pharmacodynamic Modeling and Simulation, 2nd ed., Springer, New York, 2011.

[42] M. Thommes, K. Kaneko, A.V. Neimark, J.P. Olivier, F. Rodriguez-Reinoso, J. Rouquerol, K.S.W. Sing, Physisorption of gases, with special reference to the evaluation of surface area and pore size distribution (IUPAC Technical Report), Pure Appl. Chem. 87 (2015).

[43] K. Sun, C.-y. Leng, J.-c. Jiang, Q. Bu, G.-f. Lin, X.-c. Lu, G.-z. Zhu, Microporous activated carbons from coconut shells produced by self-activation using the pyrolysis gases produced from them, that have an excellent electric double layer performance, New Carbon Mater. 32 (2017) 451-459.

[44] J. Laine, S. Yunes, Effect of the preparation method on the pore size distribution of activated carbon from coconut shell, Carbon 30 (1992) 601-604.

[45] P.S. Santos, Tecnologia De Argilas Aplicada Às Argilas Brasileiras: Aplicações, Edgard Blücher, São Paulo, 1975.

[46] R.M. Silverstein, F.X. Webster, D.J. Kiemle, Spectrometric Identification of Organic Compounds, John Wiley & Sons, U.S.A., 2005.

[47] A.L. Cazetta, A.M.M. Vargas, E.M. Nogami, M.H. Kunita, M.R. Guilherme, A.C. Martins, T.L. Silva, J.C.G. Moraes, V.C. Almeida, NaOH-activated carbon of high surface area produced from coconut shell: kinetics and equilibrium studies from the methylene blue adsorption, Chem. Eng. J. 174 (2011) 117-125.

[48] J. Madejová, FTIR techniques in clay mineral studies, Vib. Spectrosc. 31 (2003) 1-10.

[49] Z. Navrátilová, L. Vaculíková, Electrodeposition of mercury film on electrodes modified with clay minerals, Chem. Pap. 60 (2006) 348-352.

[50] M. Kozak, L. Domka, Adsorption of the quaternary ammonium salts on montmorillonite, J. Phys. Chem. Solids 65 (2004) 441-445.

[51] B. Sarkar, M. Megharaj, Y. Xi, R. Naidu, Surface charge characteristics of organo-palygorskites and adsorption of p-nitrophenol in flow-through reactor system, Chem. Eng. J. 185-186 (2012) 35-43.

[52] Y. Xi, Z. Ding, H. He, R.L. Frost, Structure of organoclays—an X-ray diffraction and thermogravimetric analysis study, J. Colloid Interface Sci. 277 (2004) 116-120.

[53] Y.S. Ho, G. McKay, The kinetics of sorption of divalent metal ions onto sphagnum moss peat, Water Res. 34 (2000) 735-742.

[54] L.J. Carter, E. Harris, M. Williams, J.J. Ryan, R.S. Kookana, A.B.A. Boxall, Fate and uptake of pharmaceuticals in soil-plant systems, J. Agric. Food Chem. 62 (2014) 816-825.

[55] R. Baccar, P. Blánquez, J. Bouzid, M. Feki, M. Sarrà, Equilibrium, thermodynamic and kinetic studies on adsorption of commercial dye by activated carbon derived from olive-waste cakes, Chem. Eng. J. 165 (2010) 457-464.

[56] W. McCabe, J. Smith, P. Harriott, Unit Operations of Chemical Engineering, 7th ed., McGraw-Hill, New York, 2005.

[57] R.E. Treybal, Mass-Transfer Operations, McGraw-Hill, Singapore, (1981).

[58] F. Rouquerol, J. Rouquerol, K. Sing, CHAPTER 1 - Introduction, Adsorption by Powders and Porous Solids, Academic Press, London, 1999, pp. 1-26.

[59] N. Genç, E.C. Dogan, Adsorption kinetics of the antibiotic ciprofloxacin on bentonite, activated carbon, zeolite, and pumice, Desalin. Water Treat. 53 (2015) 785-793.

[60] C.G. Hill, An Introduction to Chemical Engineering Kinetics and Reactor Design, 1st ed., John Wiley & Sons, USA, 1977.

[61] H.N. Tran, S.-J. You, H.-P. Chao, Thermodynamic parameters of cadmium adsorption onto orange peel calculated from various methods: a comparison study, J. Environ. Chem. Eng. 4 (2016) 2671-2682.

[62] D.M. Flanagan, Minerals Yearbook: Clay and Shale–2014 [Advance Release], U.S. Geological Survey - U.S. Department of the Interior, 2017.

[63] S. Babel, T.A. Kurniawan, Low-cost adsorbents for heavy metals uptake from contaminated water: a review, J. Hazard. Mater. 97 (2003) 219-243.

[64] Momina, M. Shahadat, S. Isamil, Regeneration performance of clay-based adsorbents for the removal of industrial dyes: a review, RSC Adv. 8 (2018) 24571-24587.

[65] N. Vlasopoulos, F.A. Memon, D. Butler, R. Murphy, Life cycle assessment of wastewater treatment technologies treating petroleum process waters, Sci. Total Environ. 367 (2006) 58-70.

[66] C.O. Ania, T.J. Bandosz, Importance of Structural and Chemical Heterogeneity of Activated Carbon Surfaces for Adsorption of Dibenzothiophene, Langmuir 21 (2005) 7752-7759.

[67] A. Behnamfard, M.M. Salarirad, Characterization of coconut shell-based activated carbon and its application in the removal of Zn(II) from its aqueous solution by adsorption, Desalin. Water Treat. 52 (2014) 7180-7195.

[68] L. Ji, W. Chen, L. Duan, D. Zhu, Mechanisms for strong adsorption of tetracycline to carbon nanotubes: a comparative study using activated carbon and graphite as adsorbents, Environ. Sci. Technol. 43 (2009) 2322-2327.

[69] Z. Rawajfih, N. Nsour, Characteristics of phenol and chlorinated phenols sorption onto surfactant-modified bentonite, J. Colloid Interface Sci. 298 (2006) 39-49.

[70] R. Zhu, Q. Zhou, J. Zhu, Y. Xi, H. He, Organo-Clays As sorbents of hydrophobic organic contaminants: sorptive characteristics and approaches to enhancing sorption capacity, Clays Clay Miner. 63 (2015) 199-221.

[71] G.E. Boyd, A.E. Adamson, L.S. Meyers, The exchange of adsorption ions from aqueous solutions by organic zeolites. Part II. Kinetics, J. Am. Chem. Soc. 69 (1947) 2836-2848.

[72] O. Redlich, D.L. Peterson, A Useful Adsorption Isotherm, J. Phys. Chem. 63 (1959) 1024-1024.

[73] J. Tóth, State equation of the solid-gas interface layers, Acta Chim. Acad. Sci. Hung. 69 (1971) 311-328.

CAPÍTULO 5. Adsorção de Losartana em Leito

Comparative adsorption of diclofenac sodium and losartan potassium in organophilic clay-packed fixed-bed: X-ray photoelectron spectroscopy characterization, experimental tests and theoretical study on DFT-based chemical descriptors[§]

Julia Resende de Andrade[1], Maria Fernanda Oliveira[1], Rafael Luan Sehn Canevesi[2], Richard Landers[3], Meuris Gurgel Carlos da Silva[1], Melissa Gurgel Adeodato Vieira[1]

[1] *School of Chemical Engineering, University of Campinas, Cidade Universitária Zeferino Vaz, 13083-970, Campinas, São Paulo, Brazil*

[2] *Institut Jean Lamour, UMR CNRS-Université de Lorraine n°7198, ENSTIB, 27 rue Philippe Seguin, BP 21042 - 88051 EPINAL Cedex 9, France*

[3] *Institute of Physics Gleb Wataghin, University of Campinas, Cidade Universitária Zeferino Vaz, 13083-970, Campinas, São Paulo, Brazil*

Abstract

Diclofenac sodium (DS) and losartan potassium (LP) are pharmaceuticals extensively used worldwide and contaminants of emerging concern. This work aims to examine the monocomponent continuous adsorption of DS and LP in fixed-beds packed with the organophilic clay, Spectrogel. The external surface of Spectrogel was studied by X-ray photoelectron spectroscopy (XPS) prior and post application as adsorbent. Continuous tests were conducted for the effects of flow rate (0.4–1.0 mL/min) and inlet concentration (0.05–0.15 mmol/L). Both DS- and LP-systems best operated at 0.4 mL/min and 0.15 mmol/L condition, which provided the highest breakthrough adsorption capacities (0.0047 mmol/g for DS and 0.0013 mmol/g for LP) and the lowest mass transfer zones (4.3 cm for DS and 4.4 cm for LP). Five different models were applied to describe the breakthrough curves and Dual site diffusion approach showed high suitability (R^2> 0.97). The DS adsorption performance by Spectrogel was contrasted with other materials. Density functional theory (DFT) computations were combined with experimental findings to clarify the particularities of DS and LP adsorption. Greater hydrophobicity, lower water solubility, reduced steric hindrance effects and greater chemical molecular

[§] Manuscript published in *Journal of Molecular Liquids* 312 (2020) 113427. DOI: 10.1016/j.molliq.2020.113427. Reprinted with permission from *Journal of Molecular Liquids*. Copyright 2020 Elsevier (*Anexo A*).

reactivity were some of the factors attributed to the enhanced DS adsorption onto Spectrogel compared to LP.

Keywords: diclofenac sodium; losartan potassium; continuous adsorption; pharmaceutical contaminants; organoclay; DFT-based descriptors

5.1 Introduction

Diclofenac sodium (DS) is a non-steroidal anti-inflammatory drug (NSAID) selected for pain relief [1], and losartan potassium (LP) is an angiotensin II receptor antagonist employed for controlling high blood pressure [2]. After their consumption, most of the non-metabolized drugs is excreted through urine and feces [1, 2]. Domestic wastes, along with effluents from pharmaceutical industries and hospitals, contribute to increasing pharmaceutical loads in wastewaters [3]. Pharmaceuticals, as organic micropollutants, generally present low biodegradability and are recalcitrant to conventional physical and chemical treatments of wastewater treatment plants (WWTPs), which are usually designed for removing bulk pollutants [4, 5]. Consequently, trace levels of DS [6-8] and LP [6, 9-11] have been encountered in WWTP effluents worldwide. The presence of DS and LP in water compartments is of environmental concern as both drugs can pose acute toxicity to bacteria, algae, invertebrates and fishes [12-14].

Aiming the remediation of emerging pharmaceutical contaminants, advanced oxidation processes (AOPs) and adsorption are pointed as preeminent technologies. Some recent papers examine the oxidative degradation of DS [15] and of LP [16]. Nevertheless, the introduction of unknown subproducts to the solution is a limiting factor of AOPs. Alternatively, adsorption does not add adverse byproducts and presents low energy consumption, simplicity of design and mild operation in comparison to other technologies, *e.g.*, oxidative processes, membrane separation, nanofiltration, reverse osmosis [17, 18]. Yet some research interest has been devoted to DS adsorption [4, 19-21], studies about LP adsorption are relatively rare [22]. Moreover, research about pharmaceutical adsorption is mostly restricted to batch mode, which is ideally advantageous for treating low volumes or for seasonal applications. Batch systems entail further separation steps to withdraw the loaded adsorbent and have removal capability limited by adsorption-desorption equilibrium. In case of engineered processes for continuous treatment of large contaminated volumes, fixed-bed columns are preferred, as

they guarantee low outlet concentrations until the breakthrough, demand lower adsorbent amounts for a target treatment goal and do not require the separation of the packed adsorbent, which can also be regenerated and recycled [23]. To boot, fixed-bed adsorption systems can be easily scaled up from lab to industrial scale. Ahmed and Hameed [24] conducted an extensive review about pharmaceutical adsorption in continuous-flow systems with adsorbents like activated carbon, zeolite, silica and biochar. Comparatively to such traditional adsorbents, eco-friendly and natural materials have been less explored in fixed-bed applications, and still demand research to gather information about adsorption capacity, fluidynamics and column breakthrough.

When it comes to the choice of the adsorbent, clay minerals stand out as naturally materials abundantly encountered in the environment. According to Awad, et al. [25], there is a growing research interest about clay-based adsorption of organic pollutants. Some studies claim that clays are able to adsorb certain pharmaceuticals more efficiently than activated carbon [17, 18], with the advantages of costing up to 20 times less than the traditional material and having better environmental disposal [25]. In addition, clays can be easily modified for improved properties and adsorption performance by, for example, calcination [26] and introduction of organic molecules [27].

Spectrogel - Type C (denoted as Spectrogel) is a Brazilian commercial bentonite clay, which is chemically functionalized by the intercalation of dialkyl dimethylammonium cations (DMA) to generate an organophilic clay with joint characteristics of an inorganic layered clay and the hydrophobic medium. Spectrogel has already been successfully used for the uptake of benzene, toluene, xylene and other petroleum hydrocarbons [28-31], and had adsorption affinity checked for a multitude of pharmaceutical contaminants [32]. More recently, Spectrogel was tested in batch adsorption of DS [19] and LP [22] for kinetic, equilibrium and thermodynamic aspects. The organoclay showed outstanding performance in removing such compounds, surpassing even activated carbon. In this context, the inspection of DS and LP adsorption onto Spectrogel in fixed-bed mode is a promising and next fundamental step to support future industrial applications. To the best of the authors' knowledge, the continuous adsorption of LP molecules has not yet been explored in the literature.

Hence, this work objects examining the continuous-flow adsorption on organophilic clay as advanced treatment approach for the remediation of two mostly consumed pharmaceuticals, DS and LP. Single adsorption tests were conducted in lab-scale fixed-bed columns packed with Spectrogel, which is a commercial organoclay with

adsorption potential previously consolidated in batch mode. This paper's outcomes show that the dynamic adsorption performance depends not only on operational conditions and adsorbent features, but also on the characteristics of the target contaminants.

In this paper, the experimental breakthrough curves were correlated by the well-known models of Thomas [33], Yoon and Nelson [34], and Yan, et al. [35] (Modified dose-response model, MDR), and by alternative phenomenological models, like Instantaneous Local Equilibrium (ILE) and Dual Site Diffusion (DualSD). As supplement to experimental tests, quantum chemical calculations were performed to obtain reactivity descriptors of DS and LP molecules based on density functional theory (DFT), aiming at molecular-level insights about the adsorption processes. Moreover, the external surface of Spectrogel was detailed by X-ray photoelectron spectroscopy (XPS) to disclose interface-dominated interactions. Combining experimental data, theoretical calculations and characterization observations, this paper attempts to comprehensively elucidate the particularities of DS and LP molecules in fixed-bed adsorption using Spectrogel clay.

5.2 **Experimental**

5.2.1 *Spectrogel adsorbent*

The Spectrogel – Type C was kindly provided by SpectroChem Company (Brazil). It consists of an organophilic clay of bentonite type, which is prepared by the introduction of dialkyl dimethylammonium cations (DMA, $C_{35}H_{74}N^{+}$) to change its condition from hydrophilic to hydrophobic. The provider does not inform further details about the synthesis of Spectrogel. Before use in the adsorption tests, the as-received material was ground and 24 and 28 Tyler mesh sieves were used to obtain 655 μm mean particle size.

5.2.2 *Pharmaceutical solutions*

High purity diclofenac sodium (DS) (≥100%) and losartan potassium (LP) (≥99%) were supplied by Geolab (Brazil) and Purifarma (Brazil), respectively. Ultrapure water from reverse osmosis purification system (Gehaka, OS20LXE) was used to obtain solutions of each of the pharmaceutical at concentrations of 0.15; 0.10 and 0.05 mmol/L.

The solutions were used without pH adjustment, *i.e.*, natural pH in ultrapure water, which was appraised as approximately 5 for both pharmaceuticals. As shown in the speciation diagram of DS in Fig. 5.1a, at pH values greater than the pK_a of 4.2, the predominant species of DS are anionic [36, 37]. At pH values lower than 4.2, DS assumes its neutral form and has decreased solubility in water (1.2–3.6 mg/L) [38]. Regarding LP,

it presents two pK_a values due to the prevalent dissociation of imidazole ring (pK_{a1} = 2.95) and tetrazole ring (pK_{a2} = 4.25). According to the ionization profile of Fig. 5.1b, LP exists mainly in cationic form at pH lower than 2.95, as zwitterionic and neutral forms at pH between 2.95 and 4.25 and as anionic form at pH higher than 4.25 [39].

Figure 5.1. Speciation diagram of (a) diclofenac sodium (DS) and (b) losartan potassium (LP) as a function of pH.

(a)

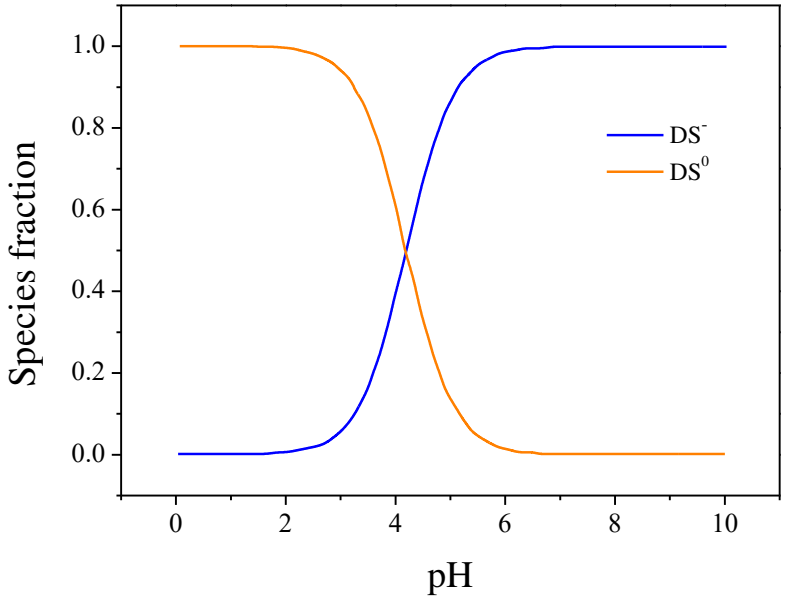

(b)

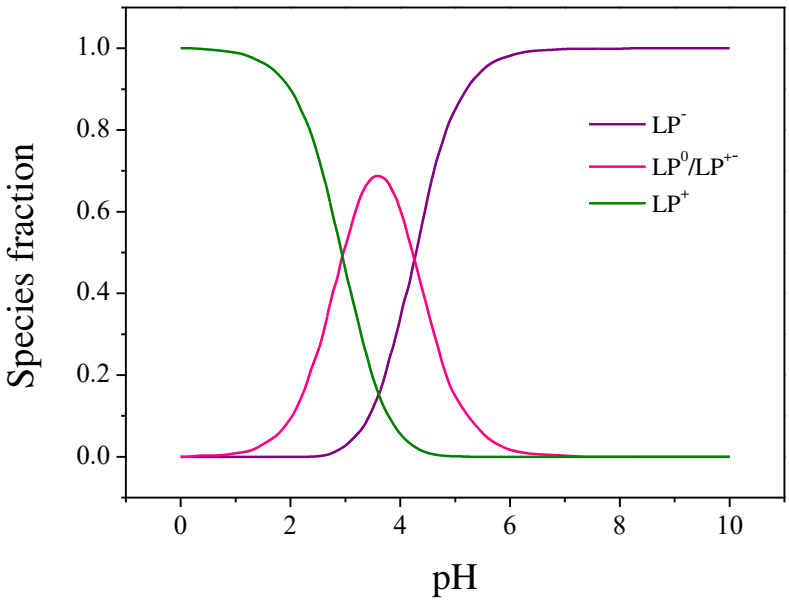

The pharmaceutical concentrations were analyzed by ultraviolet–visible spectrophotometry (UV–Vis mini 1240, Shimadzu). The corresponding characteristic wavelength of DS (λ=276 nm) and LP (λ=234 nm) were adopted. Standard curves were obtained with standard solutions within the linear range of 0.01–0.10 mmol/L of DS and 0.003–0.052 mmol/L of LP.

5.2.3 *X-ray photoelectron spectroscopy*

X-ray photoelectron spectrometer (XPS) is a surface-sensitive apparatus that provides quantitative elemental constitution, and chemical, electronic and binding states of elements in the outermost surface layers [40]. In this work, XPS analysis was performed for Spectrogel prior and post-adsorption of DS and LP. The XPS tests were conducted using a VSW HA100 spherical energy analyzer with an AlKα X-Ray source (hv = 1486.6 eV). Small amounts of powdered samples were placed to the stainless-steel holder with double-sided adhesive carbon tape and analyzed without further preparation. The system was evacuated to pressure bellow 6×10^{-8} mbar, which was maintained throughout the analysis. The X-ray bombardment at the sample surface causes the emission of photoelectrons with elemental characteristic binding energies (BE). Survey scans were measured from 0 to 1090 eV with steady pass energy of 44 eV, which yields a full width at half-maximum as 1.6 eV for Au (4f7/2) line. High resolution spectra were also recorded at 44 eV with 100 meV energy steps. Surface charging was calibrated based on the C 1s line due to adventitious carbon fixed at 284.6 eV. Curve adjustments were conducted applying Gaussian shape lines and Shirley background was deduced from the baseline.

5.2.4 *Fixed-bed adsorption experiments*

The continuous adsorption trials were conducted in a fixed-bed system illustrated in Fig. S5.1 in supplementary material. The glass column employed had internal diameter of 0.6 cm and was filled with Spectrogel organoclay until reaching a bed height of 6 cm, which corresponds to 1.33 ± 0.04 g of Spectrogel. A layer of glass wool was packed at the top of the bed, ensuring a close packed arrangement without losses of adsorbent. The column was positioned vertically to avoid poor distribution of the flow, which was upward and controlled by a peristaltic pump (7523-80, Cole-Parmer, USA). Although down-flow mode can offer lower energy consumption, the upward flow was selected because it prevents the formation of preferred pathways and promotes greater solid-liquid contact [41]. Previous hydration and expansion tests attested the hydrophobic condition

of the Spectrogel organoclay, which displays expansion inferior to 2 mL/g in water, *i.e.*, non-swelling behavior [31]. This information allowed the adsorbent in the column to be rinsed with ultrapure water for at least 2 h prior to the start of each test to eliminate any fine particulate. Then, pharmaceutical solution of known concentration was passed through the fixed-bed for mass transference. At pre-determined time intervals, an automatic fraction collector (FC203, Gilson) collected aliquots, which concentration was measured by UV–Vis. The assays were conducted at room temperature (~25 °C) and the column kept in operation until the pharmaceutical concentration stabilization at the exit.

Two sets of tests were run. First, we kept constant the inlet concentration of DS or LP at C_{in} = 0.15 mmol/L, and varied the volumetric flow rates at Q = 1; 0.7 and 0.4 mL/min, which correspond to superficial velocities of u_0 = 3.54; 2.48 and 1.41 cm/min. After identifying the best flow rate condition, we examined the influence of inlet concentration at C_{in} = 0.15; 0.10 and 0.05 mmol/L. The experimental data of continuous adsorption of DS and LP onto Spectrogel was plotted as breakthrough curves (BTCs), which relate the outlet-to-inlet concentration with time (C/C_{in} vs. t). In this paper, the breakthrough point (t_b, min) is settled as the instant at which the exit concentration attains 5% of the inlet concentration (C/C_{in} = 0.05) and the exhaustion point (t_e, min) as the instant at which no significant changes on the outlet concentration was verified. The processes were evaluated based on efficiency parameters: breakthrough adsorption capacity (q_b, mmol/g), exhaustion adsorption capacity (q_e, mmol/g), length of mass transfer zone (h_{MTZ}, cm), breakthrough removal percentage (REM_b, %), and exhaustion removal percentage (REM_e, %), which are described by Eqs. 5.1–5.5, respectively [42]:

$$q_b = \frac{C_{in}Q}{m}\int_0^{t_b}\left(1-\frac{C}{C_{in}}\right)dt \tag{5.1}$$

$$q_e = \frac{C_{in}Q}{m}\int_0^{t_e}\left(1-\frac{C}{C_{in}}\right)dt \tag{5.2}$$

$$h_{ZTM} = \left(1-\frac{q_b}{q_e}\right)H_L \tag{5.3}$$

$$REM_b = 100\left(\frac{q_b m}{C_{in}Q t_b}\right) \tag{5.4}$$

$$REM_e = 100\left(\frac{q_e m}{C_{in}Q t_e}\right) \tag{5.5}$$

where: H_L (cm) = bed height; C_{in} (mmol/L) = inlet concentration; Q (L/min) = volumetric flow rate; m (g) = adsorbent amount; C (mmol/L) = outlet concentration.

5.2.5 *Mathematical modelling and error analysis*

In the present work, five mathematical models were used to adjust the experimental BTCs obtained for the adsorption of DS and LP onto Spectrogel. The first three models applied were developed by Thomas [33], Yoon and Nelson [34], and Yan, et al. [35], respectively, and are some of the most common models used to examine breakthrough data in the literature. The other two models applied to describe the dynamic behaviors are based on mass conservation law. One of them was recently proposed by Georgin, et al. [43], whereas the other was elaborated by the authors of this study.

Thomas model is frequently selected to represent fixed-bed column performance [20, 44]. It assumes that diffusion processes in the column are negligible and that the rate driving force for adsorption obeys reversible second order kinetic profiles, which reduces to Langmuir isotherm at equilibrium. Eq. 5.6 expresses the analytic solution of Thomas model:

$$\frac{C}{C_{in}} = \frac{1}{1 + \exp\left(\frac{K_{Th}.q_{Th}.m}{Q} - K_{Th}.C_{in}.t\right)} \tag{5.6}$$

where: C (mmol/L) = outlet adsorbate concentration at time t; C_{in} (mmol/L) = inlet adsorbate concentration; K_{Th} (L/(mmol.min)) = Thomas rate constant; q_{Th} (mmol/g) = theoretical saturated adsorption capacity from Thomas model; m (g) = adsorbent mass and Q (L/min) = volumetric flow rate.

Yoon-Nelson model proposes that the reducing rate of adsorption probability is proportional to the probability of adsorbate adsorption and adsorbate breakthrough on adsorbent [45]. From Eq. 5.7, Yoon-Nelson model is concise and does not depend on features of the adsorbent or the adsorbate, nor on the physical features of the fixed-bed.

$$\frac{C}{C_{in}} = \frac{1}{1 + \exp\left[K_{YN}(\tau - t)\right]} \tag{5.7}$$

where: K_{YN} (min^{-1}) = rate constant from Yoon-Nelson model; τ (min) = time needed for 50% adsorbate breakthrough (at $t = \tau$, $C/C_{in} = 0.5$).

Despite being widely used for analysis of adsorption column data, Thomas model counteracts reality by presenting constant values of normalized concentration C/C_{in} at time t=0. The empirical model introduced by Yan, et al. [35], well-known as Modified dose-response model (MDR), minimizes the errors from Thomas model, particularly at very low and high operation times [35]. Eq. 5.8 expresses the MDR model:

$$\frac{C}{C_{in}} = 1 - \frac{1}{1 + \left(\frac{C_{in}Q}{q_y m}.t\right)^{A_Y}} \tag{5.8}$$

where: q_y (mmol/g) = quantity of solute adsorbed and A_Y (dimensionless) = constant of Modified dose-response model.

The model developed by Georgin, et al. [43] is called Instantaneous local equilibrium (ILE), and the one proposed in this work is referred as Dual site diffusion (DualSD). Both of these models are based on mass conservation law, and consider the following assumptions: thermodynamic equilibrium between the adsorbent and the liquid phase; isobaric and isothermal process; properties of the liquid and solid phases remain constant. Hence, the material balance can be mathematically represented by Eq. 5.9:

$$\frac{\partial C}{\partial t} = D_a \frac{\partial^2 C}{\partial z^2} - u_0 \frac{\partial C}{\partial z} - \frac{\rho_B}{\varepsilon} \frac{\partial q}{\partial t} \tag{5.9}$$

where: C (mmol/L) = concentration of pollutant in the liquid phase; q (mmol/g) = amount of pollutant at the adsorbent; D_a (cm²/min) = axial dispersion coefficient; u_0 (cm/min) = interstitial velocity; ρ_B (g/L) = fixed bed density and ε (dimensionless) = void fraction.

The main assumption of ILE model is that that the mass transfer between the phases is quick and the local solid-liquid equilibrium is always ensured within all elements of the fixed-bed [43]. Thus, the adsorption rate ($\partial q/\partial t$ term in Eq. 5.9) can be written as a function of the liquid phase-concentration considering the Langmuir isotherm equation, as shown in Eq. 5.10. Further details of ILE model are provided by [43].

$$\frac{\partial q}{\partial t} = \frac{\partial}{\partial t}\left(\frac{q_{max} K_L C}{1 + K_L C}\right) \tag{5.10}$$

where: q_{max} (mmol/g) and K_L (L/mmol) are the Langmuir isotherm parameters.

The previous studies on batch adsorption of DS and LP onto Spectrogel revealed that different kinetic rates control the overall process [19, 22]. Thereby, a phenomenological model that takes into account this behavior should be applied to describe the fixed-bed adsorption of these systems. The novel DualSD approach proposed in this work derives from the application of linear driving force (LDF) models [46, 47] and assumes that two types of adsorption sites exist at the surface of the adsorbent with different kinetic behaviors due to textural or chemical conditions. The two parallel mass transfer resistance components were mathematically combined, so that $\partial q/\partial t$ term in Eq. 5.9 can be substituted by the following equations:

$$\frac{\partial q}{\partial t} = \frac{\partial q_1}{\partial t} + \frac{\partial q_2}{\partial t} \tag{5.11}$$

$$\frac{\partial q_1}{\partial t} = K_{S1}\left(\alpha\left(\frac{q_{max}K_L C}{1+K_L C}\right) - q_1\right) \tag{5.12}$$

$$\frac{\partial q_2}{\partial t} = K_{S2}\left((1-\alpha)\left(\frac{q_{max}K_L C}{1+K_L C}\right) - q_2\right) \tag{5.13}$$

where: q_1 (mmol/g) = amounts adsorbed at type-1 sites; q_2 (mmol/g) = amounts adsorbed at type-2 sites; K_{S1} (min^{-1}) = mass transfer coefficient at type-1 sites; K_{S2} (min^{-1}) = mass transfer coefficient at type-2 sites; α (dimensionless) = contribution fraction of type-1 sites on the total amount adsorbed.

While the axial dispersion coefficient in ILE model is a parameter estimated through the fittings to the experimental data, in DualSD it is calculated by the following correlation [48]:

$$D_a = u_0 d_p\left(\frac{20}{\varepsilon}\frac{D_m}{u_0 d_p} + \frac{1}{2}\right) \tag{5.14}$$

where: d_p (cm) = adsorbent particle diameter and D_m (cm²/min) = molecular diffusivity calculated by Stokes-Einstein equation [49].

The standard models of Thomas, Yoon-Nelson and MDR were adjusted to experimental BTCs through non-linear fitting procedure. The resolution of ILE and DualSD models was done by using Maple 17. The finite volume method with 30 divisions was used, the resulting ordinary differential equations (ODEs) were solved by the implicit Rosenbrock method [50], and SIMPLEX as the optimization method [51]. The quality of fit of the models was evaluated using coefficient of determination R^2 (Eq. 5.15) and corrected Akaike information criterion $AICc$ (Eq. 5.16). High R^2 values and low $AICc$ values characterize the best fitting models [52].

$$R^2 = 1 - \frac{\sum_{i=1}^{N}\left(Y_i - \hat{Y}_i\right)^2}{\sum_{i=1}^{N}\left(Y_i - \overline{Y}\right)^2} \tag{5.15}$$

$$AICc = N.\ln\left(\sum_{i=1}^{N}\frac{(Y_i - \hat{Y}_i)^2}{N}\right) + 2p + \frac{2p(p+1)}{N-p-1} \tag{5.16}$$

where N = number of experimental points, Y_i = observed value, $\hat{Y}_i$ = predicted value, $\overline{Y}$ = mean of observed values, p = total number of estimable model parameters + 1 (variance).

5.2.6 *Molecular simulation*

Molecular modelling uses theoretical models to represent and manipulate chemical structures and to stablish quantitative relations with the physico-chemical

properties of molecules (QSPR). In the present study, density functional theory (DFT) computations were carried out to detail geometric properties and to compute quantum chemical molecular descriptors of DS and LP, including highest occupied molecular orbital energy (HOMO energy, E_H), lowest unoccupied molecular orbital energy (LUMO, E_L) and chemical energy gap (Δ_{H-L}). Based on E_H and E_L values, electronic chemical potential (μ), global chemical hardness (η) and overall electrophilicity index (ω) can be estimated by corresponding Eqs. 5.17, 5.18 and 5.19 [53, 54]. Such DFT-based reactivity descriptors contribute to gain an insight into the chemical reactivity and interactions of DS and LP molecules to be adsorbed onto Spectrogel.

$$\mu = -(E_H + E_L)/2 \tag{5.17}$$

$$\eta = (-E_H + E_L)/2 \tag{5.18}$$

$$\omega = \mu^2/2\,\eta \tag{5.19}$$

The chemical structures of DS and LP were designed in ChemSketch program; the three-dimensional (3D) molecular structures were obtained with Avogadro software. The minimum energy geometry and quantum chemical descriptors of DS and LP molecules were analyzed by DFT calculations implemented in Gaussian 09 program package [55] using the 'Becke, 3-parameter, Lee–Yang–Parr' (B3LYP) level of theory, which is extensively applied for intermediate sized molecules and delivers satisfactory outcomes within fairly short computational times [56]. In turn, two variations of 6-31G basis set were tested for lower molecular energies: 6-31G(d,p), supplemented only by polarization functions, and 6-31G(d,p)$^{++}$, supplemented by both polarization and diffuse functions.

5.3 Results and discussion

5.3.1 *Characterization of Spectrogel*

Previous characterizations revealed that Spectrogel is a non-porous/microporous organoclay with specific surface area (N_2 physisorption-BET method) and true density (helium picnometry) around 0.14 m²/g and 1.6 g/cm^3, respectively. The basal interlayer space of Spectrogel is d_{001} = 1.29 nm (X-ray diffraction) and the following main vibrational bands (infrared spectroscopy with Fourier transform): –OH stretching (3629 cm^{-1}), asymmetric and symmetric C–H stretching (2920 and 2850 cm^{-1}), N–H and C–H bending (1639 and 1471 cm^{-1}), Si–O stretching (1045 cm^{-1}), –OH bending (950–800 cm^{-1}), and Si–O–Al and Si–O–Si bending (600–400 cm^{-1}). The surface of the organoclay is negatively charged within pH range 4–10 (zeta potential analysis) [22].

Although much of structural and physicochemical characteristics of Spectrogel have already been disclosed [19, 28-30], XPS analysis has not yet been performed.

In the present work, XPS was used to stablish the elemental composition of Spectrogel prior- and post-adsorption of DS and LP. The survey scans are portrayed in Fig. S5.2 in supplementary material.

The surface chemical composition of virgin Spectrogel is comparable to that of other organoclays detailed in literature [57]. Spectrogel derives from a natural bentonite clay, which is an aluminum phyllosilicate consisting mostly of montmorillonite mineral. Montmorillonite presents light cations, like Na^{+} and Ca^{2+}, preferably in the interlayer space to balance the negative 2:1 charge [58]. During the organophilization process, such cations are exchanged by the organic cations of DMA surfactant to form Spectrogel. The wide survey scan of virgin Spectrogel reveals the absence of Ca element and trace levels of Na. This may be related to the naturally low incidence of such elements on the outer surface of the sample where XPS signal is sensitive, but it may also indicate that Spectrogel's external surface had these cations replaced in some extent by DMA cations [40]. The occurrence of Mg was confirmed by Mg 1 s scan (Fig. S5.3 in supplementary material) and the corresponding Mg KLL Auger peak was recorded in the survey scans around 305 eV. The trace amounts of Mg in Spectrogel plausibly originate from the montmorillonite structure. Conversely, the intercalated DMA surfactant molecules are responsible for the peaks of N (~402 eV) and C (~286.5 eV) [57].

XPS spectrum of fresh Spectrogel has noticeable peaks of C, Al and Si. The C/Si ratio, derived from elemental atomic concentrations, was estimated as 3.31. This value is comparable to those previously reported for organoclays synthesized using hexadecyltrimethylammonium bromide (HDTMA). For instance, ratios of C/Si = 3.41 and C/Si < 3.35 were obtained for organoclays with HDTMA concentrations of 1.5 and 2.0 times the cation exchange capacity (CEC) of montmorillonite, respectively [57, 59]. After use as adsorbent of DS and LP, Spectrogel had the C/Si ratio reduced to 2.59 and 3.12, respectively. These variations demonstrate changes in the clay structure during the processes, and the more pronounced decreasing in C/Si ratio after DS adsorption suggests that this pharmaceutical has greater interactions with Spectrogel than LP. This will be further reinforced by the higher adsorption capacity of DS in comparison to LP in Spectrogel-packed fixed-beds.

Fig. 5.2 depicts high resolution XPS spectra for C 1s, Si 2p and Al 2p of Spectrogel prior and post adsorption of DS and LP. The fluctuation of binding energies among Spectrogel samples corroborates the structural changes after the processes.

In the XPS C 1s scan (Fig. 5.2a), the spectrum of fresh Spectrogel was resolved to three peaks centered at around 282.2, 284.6 and 286.2 eV, which correspond to metal carbide, C–C bond in the long chain and C–N bond, respectively [59]. While C–C bond was not expressively changed, the metal carbide peak was displaced to 281.3 eV after LP adsorption and was no longer observed after DS adsorption. The spectra corresponding to C–N slightly increased from 286.2 eV to 286.5 eV for DS-contaminated Spectrogel and to 286.3 eV for LP-contaminated Spectrogel, indicating that groups containing N take part in adsorption. The more expressive changes in C 1s peaks of Spectrogel after DS uptake supports the idea of higher affinity of the organoclay in retaining DS in comparison to LP. The metal carbide peak in LP-loaded Spectrogel can be specifically assigned to SiC, which occurrence is supported by the transition centered at 101.5 eV in the Si 2p scan (Fig. 5.2b).

The Si 2p scan of LP-loaded Spectrogel also presents peaks ascribable to pure Si element (~99.7 eV) and aluminosilicate (~102.5 eV), which are encountered in the Si 2p scans of fresh and DS-contaminated Spectrogel as well. Aluminosilicate was further verified in Al 2p spectra (Fig. 5.2c) with a peak centered at 74.4 eV for fresh Spectrogel and at slightly modified binding energies for samples contaminated with DS (74.6 eV) and LP (73.8 eV). The variation in the binding energy of Si 2p and Al 2p points to alterations in the structure of the organoclay intercalated with surfactant molecules [57]. However, it is important to stress that both Si and Al are majorly located in the interlayer space and, therefore, have highly sensitive detection by XPS signal, which collects information mainly from the first monolayers [40].

Fig. 5.2d presents O1s spectra, which interpretation is not clear-cut, because the O1s binding energy of multiple compounds and species overlap and so cannot be clearly distinguished. However, the main peak at about 531.6 eV in O 1s scan of fresh Spectrogel can be assigned to O(OH) in clay structural sheets [59]. Observably, pharmaceutical uptake is accompanied by changes in O binding, since the main O peak was shifted by 0.5 eV and 0.7 eV after DS and LP adsorption, respectively. So, it can be inferred that O groups participate in the processes.

Figure 5.2. XPS high-resolution spectra of C 1s (a), Si 2p (b), Al 2p (c) and O 1s (d) for virgin Spectrogel, Spectrogel after DS adsorption and Spectrogel after LP adsorption.

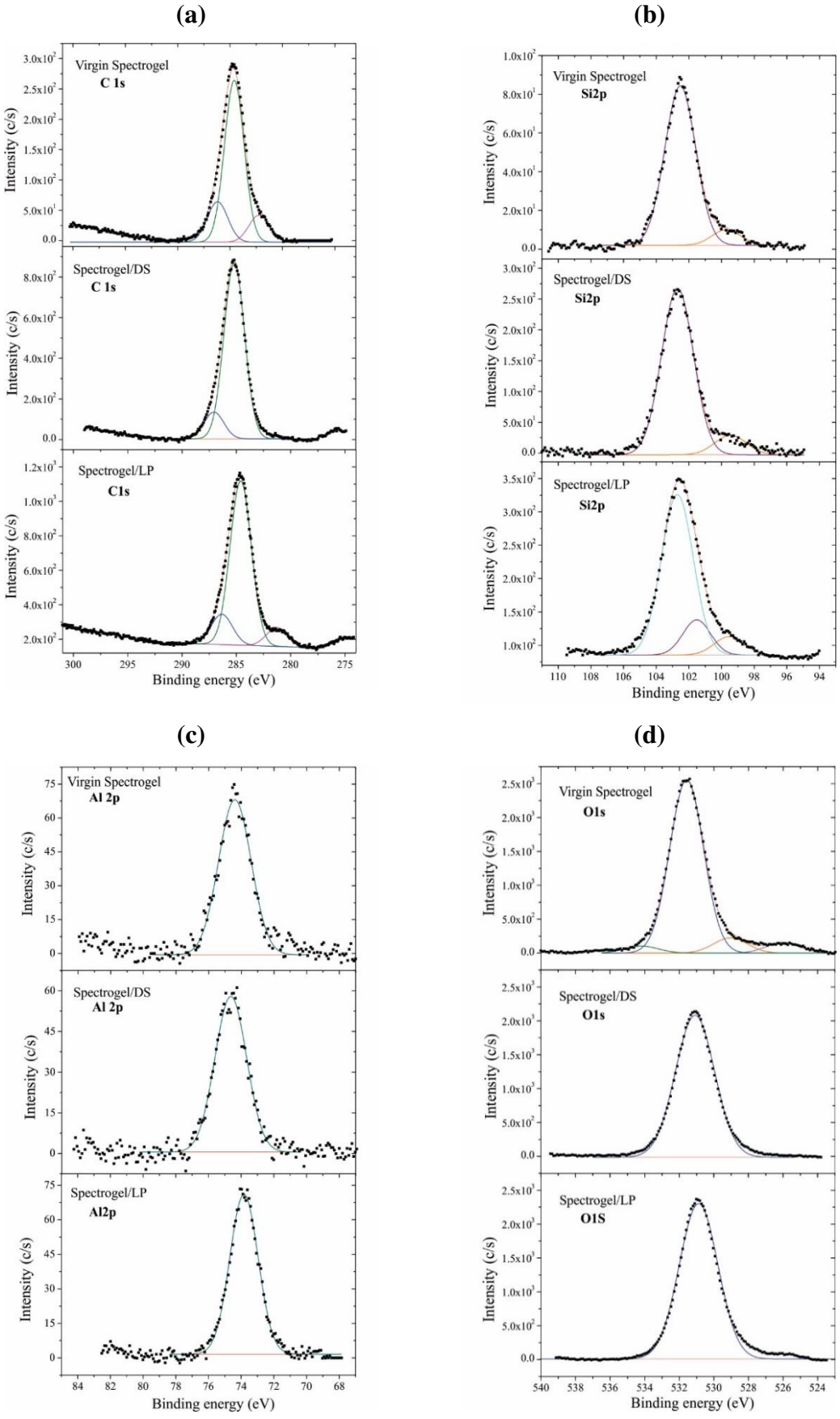

Regarding N element, there is significant difference between its peaks before and after pharmaceutical adsorption. Fresh Spectrogel and DS-loaded Spectrogel presented signals of N in such low intensity that prevented the examination in high-resolution. Conversely, from Fig.S5.3b of supplementary material, the deconvolution of N 1s core energy level for LP-loaded Spectrogel reveals the presence of C–NH_2 (400.3 eV) besides NSi_2O (402.9 eV). Such peaks can be attributed to interactions between the organoclay and LP molecules, which have higher N atomic content than DS molecules.

5.3.2 *Fixed-bed column experiments*

Fig. 5.3 displays the breakthrough curves (BTCs) attained for DS and LP adsorption in continuous-flow mode. It can be noticed that none of the BTCs present classical S-shape profile. Besides that, except for the case of LP at 1.0 mL/min flow rate and 0.15 mmol/L inlet concentration, the fixed-bed systems do not become totally saturated at the examined conditions range, that is, they do not reach the bed maximum saturation level of C/C_{in}=1. The exhaustion saturation for DS varied from 52% up to 89%, and for LP had a minimum value of 90%. The same behavior was previously reported for BTCs of diclofenac on granular activated carbon [60], and BTCs of benzene, toluene and xylene on Spectrogel in single- and multi-component systems [30]. The phenomenon of not reaching higher levels of saturation was attributed to very slow adsorption rates in certain regions of the bed, which lead to extremely large time periods required to reach 100% of saturation. Table 5.1 lists the efficiency parameters of the fixed-bed systems at distinct flow rates and inlet concentrations.

Noticeably, the estimates of mass transfer zone, h_{MTZ}, are close to the total height of the beds (6 cm). This fact indicates that the adsorption of DS and LP takes part in almost all bed extension with great resistance to mass transfer, which dispels such systems from ideality and justifies the long saturation times obtained [61]. Noteworthy, lower mass transfer zones and fully developed BTCs could be favored if used longer bed heights (greater adsorbent mass) [62], and/or jacketed beds at higher temperatures, considering that increasing temperatures were previously demonstrated to have positive effects in both DS and LP adsorption on Spectrogel due to their endothermic character [19, 22].

Figure 5.3. Breakthrough curves obtained for DS and LP adsorption using Spectrogel in fixed bed column as function of: (a, b) flow rate; and (c, d) inlet concentration.

(a)

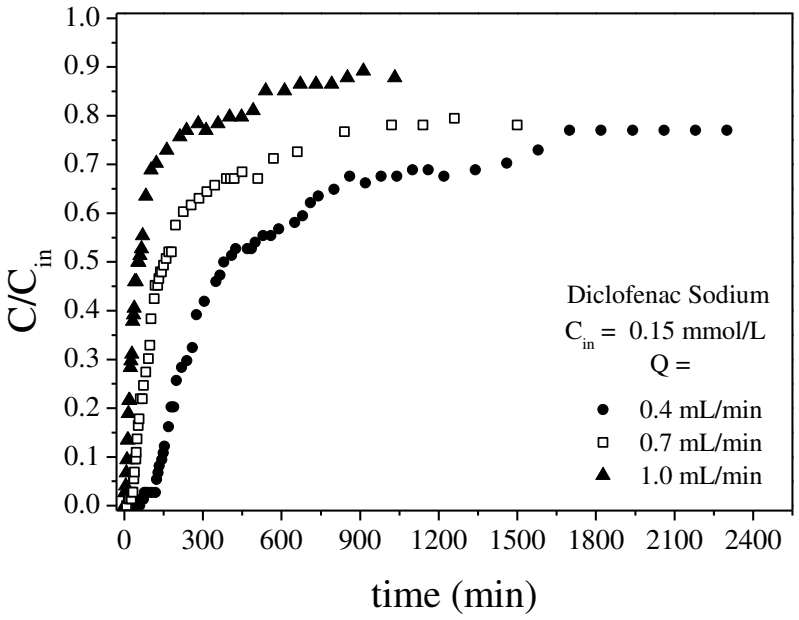

(b)

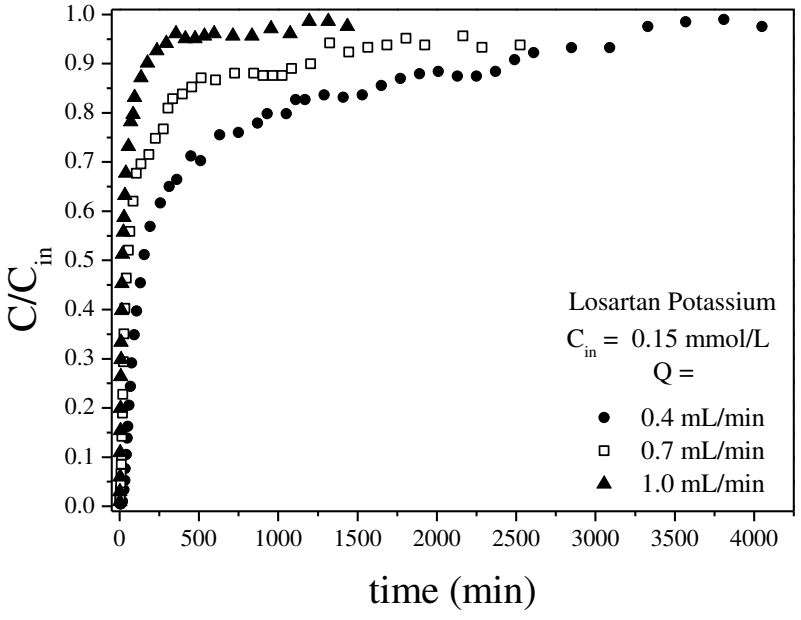

cont. **Fig. 5.3**.

(c)

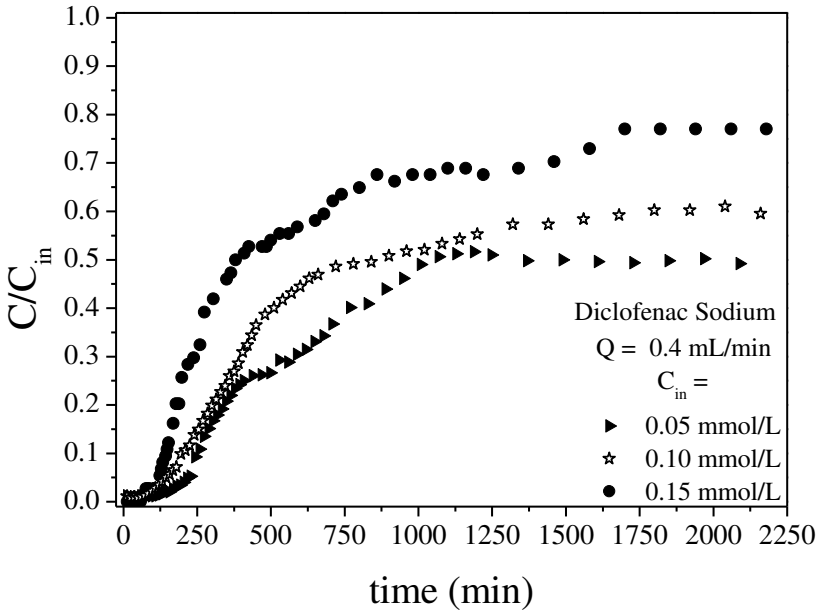

(d)

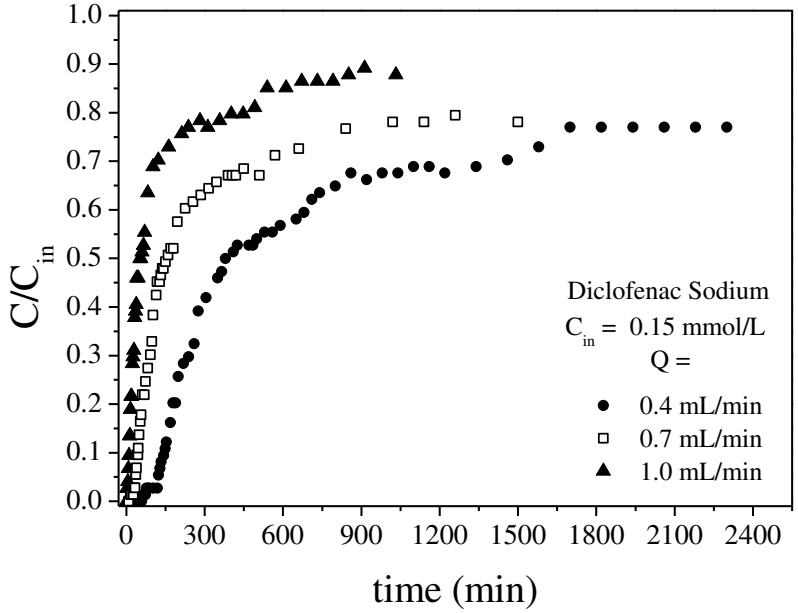

Table 5.1. Breakthrough parameters obtained for the adsorption of diclofenac sodium (DS) and losartan potassium (LP) using Spectrogel in fixed-bed systems.

	Q (mL/min)	1.0	0.7	0.4	0.4	0.4
	u_0 (cm/min)	3.54	2.48	1.41	1.41	1.41
	C_{in}(mmol/L)	0.15	0.15	0.15	0.10	0.05
DS	t_b (min)	7	35	123	143	221
	q_b (mmol/g)	0.0006	0.0020	0.0047	0.0036	0.0029
	REM_b	82%	73%	88%	90%	93%
	t_e (min)	852	1020	1700	1920	1188
	q_e (mmol/g)	0.0222	0.0292	0.0322	0.0300	0.0120
	REM_e	23%	36%	43%	55%	70%
	h_{MTZ} (cm)	5.1	4.6	4.3	4.7	4.4
LP	t_b (min)	3	8	32	38	85
	q_b (mmol/g)	0.0002	0.0005	0.0013	0.0010	0.0011
	REM_b	61%	78%	89%	82%	84%
	t_e (min)	1195	2165	3810	4782	6960
	q_e (mmol/g)	0.0104	0.0267	0.0288	0.0326	0.0267
	REM_e	7%	15%	16%	22%	25%
	h_{MTZ} (cm)	5.2	5.0	4.4	4.7	5.0

Fig. 5.3a and b show the effects of flow rates for fixed inlet concentrations of 0.15 mmol/L. Distinctly, the lower the flow rate through the bed, the flatter the BTCs with elongated exhaustion profiles. This is because lower flow rates increase the solution residence time in the system and, consequently, the contact time between the Spectrogel and the pharmaceuticals [63]. So, reduced flow rates are expected to have favorable impacts on the adsorption processes. From Table 5.1, the lower the flow rate, the higher the breakthrough time, t_b, and the exhaustion time, t_e. For both DS and LP molecules, at constant inlet concentration of 0.15 mmol/L, the lowest flow rate of 0.4 mL/min led to the smallest values of mass transfer zone (h_{MTZ} = 4.3 cm for DS and h_{MTZ} = 4.4 cm for LP) and to the highest values of t_b, q_b, REM_b. Thus, it is accurate to posit that 0.4 mL/min flow rate provided enhanced adsorption performances of DS and LP and so was selected for the subsequent trials.

Fixing the flow rate at 0.4 mL/min, the influence of inlet concentration on the removal of DS and LP was inspected, as depicted in Fig. 5.3c and d. From Table 5.1, it is noted that shorter breakthrough times t_b were obtained for both pharmaceuticals at higher inlet concentrations. This is ascribable to increased driving forces for mass transfer happening during adsorption at greater concentrations, which reflect in the lowest values of mass transfer zones (h_{MTZ}) and the highest breakthrough adsorption capacities (q_b) [64]. It is seen that reducing the inlet concentration of DS caused considerably greater exhaustion times (t_e) and slightly higher total removal percentages (REM_b). On the other

hand, the effects of altering the LP inlet concentration were not so obvious, and a tendency could not be established.

According to Table 5.1, the removal percentage until breakthrough reached $REM_b = 93\%$ and $REM_b = 89\%$ for DS and LP, respectively. This fact suggests that Spectrogel is a promising adsorbent to be applied in scaled-up fixed-bed systems for pharmaceutical remediation. Moreover, as the inlet concentration diminished from 0.15 to 0.05 mmol/L, the values of breakthrough adsorption capacity (q_b) slightly decreased for DS (<0.002 mmol/g), but did not significantly vary for LP. So, it can be speculated that DS and LP fixed-bed adsorption using Spectrogel could be evaluated at even lower initial concentrations, closer to that of real wastewaters or superficial waters. Besides that, the satisfactory results point that future studies may include the application of Spectrogel in multicomponent systems for simultaneous adsorption of DS and LP, as well as other pharmaceutical molecules.

On examining the trends of the adsorbed pharmaceutical amounts, Fig. 5.3 shows that LP reaches higher levels of saturation ($C/C_{in} = 1$) than DS ($C/C_{in} = 0.89$). In spite of that, the efficiency parameters from Table 5.1 reveal that much more DS than LP could be adsorbed onto Spectrogel. For example, at 0.4 mL/min and 0.15 mmol/L condition, the adsorption capacity at breakthrough point was $q_b = 0.0047$ mmol/g for DS and $q_b = 0.0013$ mmol/g for LP. This behavior agrees with previous outcomes from adsorption studies in batch mode using Spectrogel, which showed that Langmuir's maximum adsorption capacity at 15 °C is higher for DS, 0.086 mmol/g, than LP, 0.048 mmol/g. Furthermore, while the equilibration time for DS was 500 min, LP required at least 750 min [19, 22]. Taking the above into account, it plausible that LP adsorption process onto Spectrogel is more complex than that of DS. The roles of specific features on the distinct adsorption rates of DS and LP are comprehensively discussed in Section 5.3.5.

5.3.3 *Mathematical modelling*

The standard dynamic models from Thomas [33], Yoon and Nelson [34], Yan, et al. [35] (MDR), as well as the phenomenological models developed by Georgin, et al. [43] (ILE) and by the present work (DualSD) were applied to describe the experimental BTCs of DS and LP adsorption onto Spectrogel. Table 5.2 shows the model parameters and correlation coefficients, and Fig. 5.4 illustrates the graphical adjustments for the operational condition of 0.4 mL/min flow rate and 0.15 mmol/L inlet concentration.

Table 5.2. Adjusted parameters of Thomas, Yoon-Nelson, Modified dose-response (MDR), Instantaneous local equilibrium (ILE) and Dual site diffusion (DualSD) models calculated for diclofenac sodium (DS) and losartan potassium (LP) adsorption breakthrough curves

	Model	Q (mL/min)	1.0	0.7	0.4	0.4	0.4
		C_{in}(mmol/L)	0.15	0.15	0.15	0.10	0.05
DS	Thomas	K_{Th} (L/mmol/min)	0.184	0.046	0.018	0.013	0.028
		q_{Th} (mmol/g)	0.007	0.019	0.028	0.036	0.021
		R^2	0.81	0.74	0.76	0.70	0.72
		$AICc$	–172	–195	–223	–244	–250
	Yoon-Nelson	K_{YN} (min^{-1})	0.028	0.007	0.003	0.001	0.001
		τ (min)	64	238	649	1266	1439
		R^2	0.81	0.74	0.76	0.70	0.72
		$AICc$	–172	–195	–223	–244	–250
	MDR	A_Y (–)	0.9	1.1	1.2	1.0	1.1
		q_Y (mmol/g)	0.007	0.015	0.023	0.029	0.019
		R^2	0.98	0.95	0.95	0.94	0.93
		$AICc$	–271	–277	–318	–337	–330
	ILE	D_a (cm^2/min)	2.18×10^{9}	7.51×10^{9}	1.45×10^{9}	1.11×10^{9}	4.58×10^{9}
		R^2	–1.95	–1.41	–1.25	–1.22	–1.01
		$AICc$	–56	–86	–98	–130	–145
	DualSD	D_a (cm^2/min)	0.540	0.367	0.256	0.282	0.264
		α (–)	0.047	0.065	0.092	0.068	0.053
		$K_{S,1}$ (min^{-1})	2.47×10^{-2}	1.52×10^{-2}	6.69×10^{-3}	6.46×10^{-3}	6.20×10^{-3}
		$K_{S,2}$ (min^{-1})	2.54×10^{-4}	3.15×10^{-4}	1.94×10^{-4}	1.76×10^{-4}	1.19×10^{-4}
		$q_{e,pred}$ (mmol/g)	0.023	0.031	0.033	0.031	0.012
		R^2	0.99	0.99	0.99	1.00	0.98
		$AICc$	–298	–391	–429	–533	–409

cont. **Table 5.2**.

	Model	Q (mL/min)	1.0	0.7	0.4	0.4	0.4
		C_{in}(mmol/L)	0.15	0.15	0.15	0.10	0.05
LP	Thomas	K_{Th} (L/mmol/min)	0.404	0.153	0.042	0.014	0.019
		q_{Th} (mmol/g)	0.003	0.006	0.012	0.022	0.020
		R^2	0.93	0.87	0.86	0.78	0.87
		$AICc$	–164	–178	–190	–162	–249
	Yoon-Nelson	K_{YN} (min^{-1})	0.061	0.023	0.006	0.001	0.001
		τ (min)	26	76	268	706	1283
		R^2	0.93	0.87	0.86	0.78	0.87
		$AICc$	–164	–178	–190	–162	–249
	MDR	A_Y (–)	1.1	0.9	1.0	0.8	1.0
		q_Y (mmol/g)	0.002	0.005	0.009	0.010	0.011
		R^2	1.00	0.98	0.98	0.97	0.99
		$AICc$	–263	–272	–295	–246	–375
	ILE	D_a (cm^2/min)	8.46×10^8	1.21×10^9	5.07×10^8	7.63×10^9	2.27×10^8
		R^2	–0.69	0.06	0.43	0.45	0.83
		$AICc$	–56	–95	–127	–127	–238
	DualSD	D_a (cm^2/min)	0.484	0.361	0.221	0.216	0.213
		α (–)	0.056	0.071	0.099	0.081	0.096
		$K_{S,1}$ (min^{-1})	6.42×10^{-2}	4.17×10^{-2}	2.01×10^{-2}	3.15×10^{-2}	3.41×10^{-2}
		$K_{S,2}$ (min^{-1})	2.37×10^{-4}	4.06×10^{-4}	3.44×10^{-4}	4.22×10^{-4}	5.02×10^{-4}
		$q_{e,pred}$ (mmol/g)	0.013	0.028	0.035	0.033	0.025
		R^2	0.97	0.98	0.99	1.00	0.99
		$AICc$	–201	–268	–303	–368	–393

Figure 5.4. Adjustments of Thomas, Yoon-Nelson, Modified dose-response (MDR) Instantaneous local equilibrium (ILE) and Dual site diffusion (DualSD) models for breakthrough curve obtained at 0.4 mL/min and 0.15 mmol/L for DS (a) and LP (b)

(a)

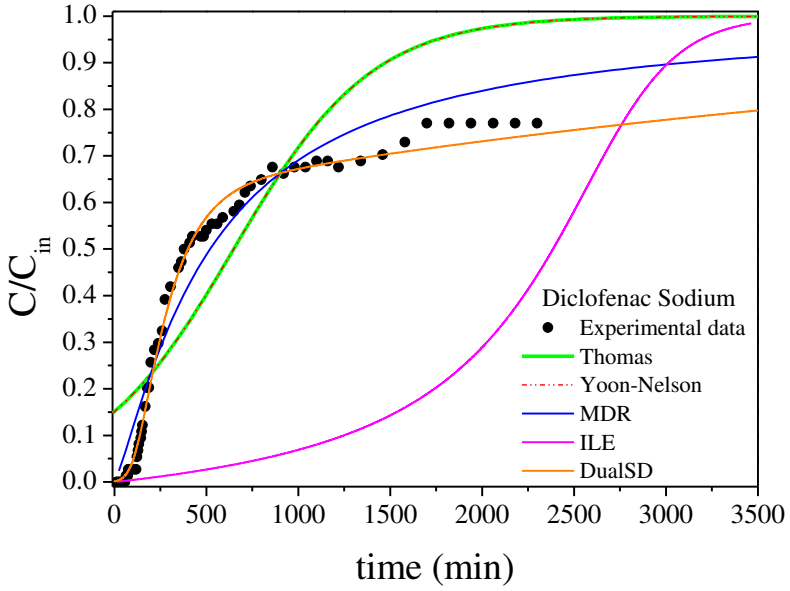

(b)

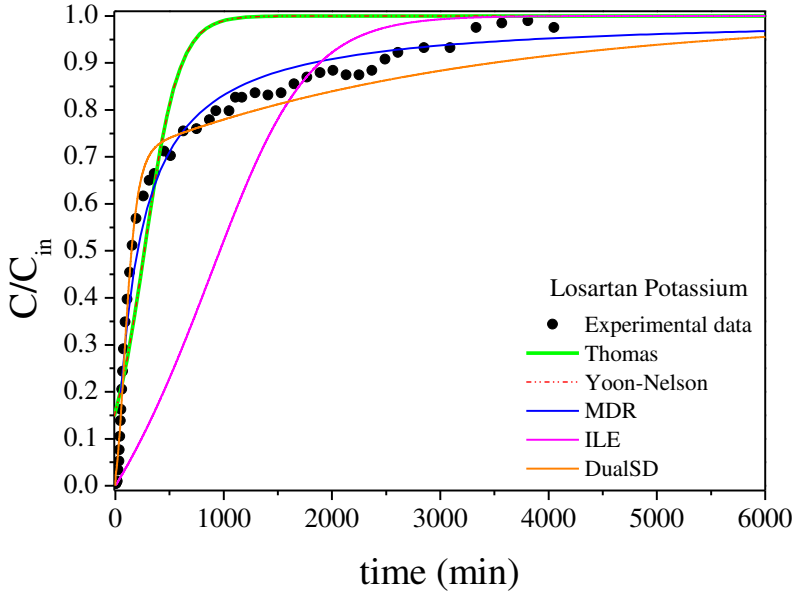

It is noticeable that the models of Thomas and of Yoon-Nelson have equal fittings to the BTCs with the same values of R^2 and $AICc$, what occurs due to the mathematical equivalence between these models [65]. As it can be noted in Fig. 5.4, the models of Thomas and Yoon-Nelson overestimate the values of C/C_{in}, especially in times below 125 min and over 750 min. Considering the fact that the present fixed-bed systems packed with Spectrogel take very long times to reach adsorptive saturation, especially for DS molecules, the errors associated with Thomas and Yoon-Nelson models were also high.

The MDR model presents relatively high values of R^2 (>0.93) accompanied by low values of $AICc$, and so reasonably describes the continuous adsorption data of both DS and LP onto Spectrogel. The MDR model was proposed to minimize the errors of Thomas' model at low and high times of the breakthrough curves [35]. Even so, under certain conditions, Thomas model predicted the amount adsorbed by the Spectrogel-packed bed better than MDR model. That is, some q_{Th} estimates from Thomas model are closer to the experimental values (q_e of Table 5.1) than the q_Y estimates from MDR model. This suggests that the parameters from Thomas model could be used for the design and scale-up of DS- and LP-adsorption systems using Spectrogel aiming at large-scale applications.

In the application of the ILE and DualSD models, the Langmuir isotherm data (q_{max}, K_L) were retrieved from [19, 22]. From Table 5.2, ILE model does not describe satisfactorily any of the BTCs and presents R^2 as low as –1.95. The negative R^2 values indicate that ILE model deviations can be greater than the variance of the experimental data. A main reason for the poor fitting of ILE model is that it assumes insignificant mass transfer resistance through the adsorbent, *i.e.*, null mass transfer zones within the column, which is a condition exactly opposite to that of our systems. As previously discussed, the Spectrogel-packed beds have great diffusion resistance and so elevated mass transfer zones relatively to the total length of the beds. Thereby, the axial diffusion coefficients (D_a) provided by ILE model are unrealistic, because the hypotheses on which this model is based do not correspond to the reality of the systems examined in this work.

Comparatively to ILE model, the DualSD model proposed in this work offers much better performance in describing the experimental curves. The improved fittings may be related to the fact that DualSD model considers not just one diffusion rate, but two, each of which showing effects at different times of the breakthrough profiles. According to Table 5.2, DualSD approach best correlates all DS curves, and most LP

curves, especially those obtained at the lowest flow rate condition. Moreover, DualSD model predicted the amounts adsorbed in exhaustion, $q_{e,pred}$, with relatively high precision. Upcoming studies should explore the multi-site approach of DualSD model in describing adsorption equilibrium behavior in batch tests, for example.

5.3.4 *Comparison of Spectrogel with other adsorbents from the literature in fixed-bed adsorption*

Thomas equation has been widely used to predict breakthrough data for pharmaceutical adsorption in fixed-bed systems. Table 5.3 summarizes Thomas rate constants (K_{Th}) and adsorption capacities (q_{Th}) reported for continuous adsorption of DS on different adsorbents. It was not possible to obtain comparative data for LP, since the present work is the first in literature to examine its continuous fixed-bed adsorption.

Thanhmingliana and Tiwari [21] tested the adsorption of DS using a commercial bentonite clay and an Indian local clay, which were organo-modified by cations of hexadecyltrimethyl ammonium bromide (HDTMA). The authors also prepared inorgano-organo-modified clays, which were pillared with aluminum (Al) prior to HDTMA modification. BTCs were obtained at flow rate of 1 mL/min, inlet concentration of 0.031 mmol/L (10 mg/L) and 0.5 g of adsorbent. The breakthrough profiles were well-correlated by Thomas equation. From Table 5.3, the maximum amounts of DS loaded on the prepared clays from [21] are higher than on the DMA-modified bentonite clay Spectrogel from the present paper, whereas the saturation times are comparatively shorter even using lower inlet concentrations and lesser adsorbent masses.

Tiwari, et al. [4] obtained BTCs for DS adsorption on Al pillared sericite clay, which was further modified with organic cations HDTMA or AMBA (alkyldimethylbenzyl ammonium chloride). Similarly to [21], it was used 1 mL/min flow rate and 0.5 g adsorbent mass, but almost halved inlet concentration of 0.016 mmol/L (5 mg/L). Contrarily to the expected at much lower concentrations, the columns rapidly achieved saturation after 2.8 h and 1.8 h for Al pillared HDTMA-sericite and Al-pillared AMBA sericite, respectively. As a consequence of insufficient contact time, low removal capacities for DS were obtained on both of the Al pillared organo-modified sericite clays.

Table 5.3. Comparative theoretical rate constants ($\boldsymbol{K_{Th}}$) and adsorption capacities ($\boldsymbol{q_{Th}}$) of Thomas model, and breakthrough time ($\boldsymbol{t_b}$) and saturation time ($\boldsymbol{t_e}$) reported for fixed-bed adsorption of diclofenac sodium on different adsorbent materials (conditions: $\boldsymbol{D_i}$=column diameter; $\boldsymbol{C_{in}}$=inlet concentration; $\boldsymbol{Q}$=flow rate; $\boldsymbol{u}$=superficial velocity; $\boldsymbol{H}$=bed height; $\boldsymbol{m}$=mass of adsorbent).

Adsorbent	D_i	C_{in}	Q	u	H	m	t_b	t_e	q_{Th}	K_{Th}	Error [a]	Reference
	cm	mmol/L	mL/min	cm/min	cm	g	min	h	mmol/g	L/mmol/min	-	
DMA modified-bentonite. Spectrogel [b]	0.6	0.15	1	3.537	6	1.4	7	14.2	0.007	0.184	R^2 = 0.81	This work
	0.6	0.15	0.7	2.476	6	1.4	35	17	0.019	0.046	R^2 = 0.74	
	0.6	0.15	0.4	1.415	6	1.3	123	28.3	0.028	0.018	R^2 = 0.76	
	0.6	0.10	0.4	1.415	6	1.3	143	32	0.036	0.013	R^2 = 0.70	
	0.6	0.05	0.4	1.415	6	1.3	221	19.8	0.021	0.028	R^2 = 0.72	
HDTMA-modified bentonite [c]	1	0.031	1	1.273	–	0.5	–	26	0.060	0.162	s^2 = 3.2	[21]
Al pillared HDTMA-modified bentonite [c]	1	0.031	1	1.273	–	0.5	–	22	0.044	0.180	s^2 = 5.6	[21]
HDTMA-modified local clay [c]	1	0.031	1	1.273	–	0.5	–	10.3	0.025	0.379	s^2 = 0.99	[21]
Al pillared HDTMA-modified local clay [c]	1	0.031	1	1.273	–	0.5	–	8.5	0.017	0.499	s^2 = 3.5	[21]
Al pillared HDMA-modified sericite clay [c]	1	0.016	1	1.273	–	0.5	–	2.8	0.003	2.061	s^2 = 0.18	[4]
Al pillared AMBA-modified sericite clay [d]	1	0.016	1	1.273	–	0.5	–	1.8	0.002	3.976	s^2 = 0.04	[4]
Granular activated carbon	1.2	0.063	3	2.653	–	0.5	13	–	0.009	2.994	R^2 = 0.96	[20]
	1.2	0.063	5	4.421	–	0.5	8	–	0.008	5.758	R^2 = 0.96	
	1.2	0.063	3	2.653	–	1.5	10.7	–	0.003	2.503	R^2 = 0.96	
	1.2	0.314	5	4.421	–	0.5	7.2	–	0.037	1.191	R^2 = 0.97	

[a] Error analysis based on coefficient of determination (R^2) or least square sum (s^2); [b] DMA=dialkyl dimethylammonium; [c] HDTMA=hexadecyltrimethyl ammonium bromide; [d] AMBA=alkyldimethylbenzyl ammonium chloride.

Commercial granular activated carbon (GAC) was employed by de Franco, et al. [20] for DS adsorption in fixed-bed systems. The effects of initial concentration (10–20 mg/L), adsorbent mass (0.5–1.5 g) and volumetric flow rate (3–5 mL/min) on DS adsorption were explored by a two-level full factorial design. Analogous to the present work, the model from Yan, et al. [35] (MDR) well-described the BTCs of DS with average R^2 = 0.98. It was shown that decreasing flow rates, increasing concentrations and/or increasing GAC dosages caused increasing saturation times and consequently lower Thomas kinetic constants K_{Th} due to broader mass transfer zones. Under distinct experimental conditions, the breakthrough times at C/C_{in} = 0.05 for GAC-packed columns varied from 7.2 to 14.6 min, whereas for Spectrogel-packed columns were in 7–221 min range. Moreover, the DS loading capacities on GAC were comparatively lower than on all the organo-modified clays listed in Table 5.3. Hence, it can be speculated that clay-based materials can offer better prospects than GAC for the continuous adsorption of pharmaceuticals like DS. Previously, Sotelo, et al. [60] also verified that GAC was not an efficient adsorbent for DS molecules in fixed-bed systems due to steric hindrance effects.

In sum, the comparison of DS adsorption capacity by Spectrogel organophilic clay and other materials is not straightforward, since it is highly influenced by fixed-bed adsorption conditions, including flow rate, inlet concentrations and bed heights (adsorbent mass). The analysis of Table 5.3 hints that the Spectrogel organoclay possesses removal capacity for DS relatively lower than some other modified clays from the literature, but higher than the traditional material GAC. This corroborates dynamic adsorption using modified clays as advantageous approach for enhanced remediation of pharmaceutical contaminants. Future research should focus on exploring, for example, the combination of inorgano-, organo- and thermal treatments to obtain advanced clay-based materials.

The reuse of adsorbents is a crucial factor in the techno-economic assessment of an adsorption process, but it is rarely explored in literature for spent clays [25]. For instance, none of the clay adsorbents listed in Table 5.3 had regeneration tested. Regarding Spectrogel, previous studies verified that chemical treatment with methanol provides desorption efficiency of LP up to 65% [22]. However, methanol has controversial application due to high toxicity. On the other hand, thermal regeneration methods are prohibitive for Spectrogel systems considering the thermal degradation profiles of the organoclay and of the loaded pharmaceuticals. Remarkably, the degradation peak of Spectrogel occurs at a relatively low temperature of 329 °C, which is close to that of LP at 323 °C [22]. In this scenario, future studies should explore more complex regeneration methods to allow the reuse of spent clays,

such as supercritical extraction, oxidative degradation or biological degradation [66]. Nevertheless, for naturally abundant and relatively low-cost adsorbents, such as clay-based materials, the final disposal by landfilling or incineration and the purchase fresh adsorbents may be a more suitable and economical approach than investing in sophisticated regeneration techniques [18].

5.3.5 *Mechanisms of adsorption*

The experimental results in fixed-bed systems indicate that Spectrogel organoclay shows distinct adsorption affinities for DS and LP. It is noticeable that DS was more efficiently adsorbed than LP under all the examined conditions. Elucidating the uptake mechanisms of these pharmaceutical molecules is not a trivial task, since adsorption can be governed by various interactions between the adsorbent and the adsorbate [67]. However, valuable insights can be obtained from the physico-chemical properties and electronic molecular features of DS and LP.

- Physico-chemical properties

Table 5.4 exposes the unique physico-chemical properties of DS and LP.

Contaminant molecules can interact with Spectrogel through electrostatic attractive or repulsive forces, subject to the chemical/physical characteristics of the system. The dissociation constant in solution (pK_a) is of great value in elucidating the behavior of DS and LP in solution, since this parameter measures how strong a base or acid is. LP is a weakly acidic model pharmaceutical [73], which contains a basic group (imidazole) and an acidic group (tetrazole). Such groups can be connected to the two pK_a values of LP molecule [39]. Concerning DS, it is a salt of a weak acid with $pK_a = 4.2$. DS is part of to the NSAID group of acetic acid derivatives and presents a phenyl acetic group, a secondary amino group and a phenyl ring with dual ortho chloro groups [74]. As comprehensively discussed in Section 5.2.2, the tests were conducted in ultrapure water without adjusting the pH with initial values around 5 for both pharmaceuticals. At this condition, DS and LP molecules are present in solution mainly as negatively charged species. Considering that Spectrogel has been characterized to keep a negatively charged surface over pH ranging from 4 to 10 [22], it can be anticipated that repulsive electrostatic interactions can occur between both pharmaceuticals and the organoclay's surface. Therefore, it is inferable neither DS and LP are majorly adsorbed through electrostatic interactions.

Table 5.4. Physico-chemical properties of diclofenac sodium and losartan potassium

	Diclofenac sodium	Losartan potassium
Systemic Chemical name [68]	Sodium [*o*-(2,6-dichloroanilino)phenyl]acetate	2-Butyl-4-chloro-1-[*p*-(*o*-l*H*-tetrazol-5-ylphenyl)benzyl] imidazole-5-methanol, monopotassium salt
Therapeutic category	Non-steroidal anti-inflammatory agent	Cardiovascular agent
Molecular structure [68]	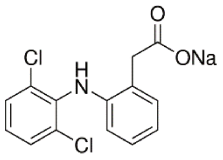	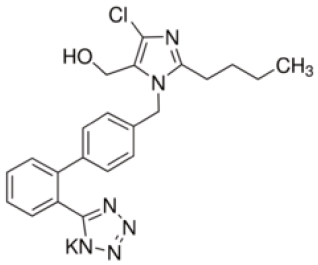
Molecular formula [68]	$C_{14}H_{10}Cl_2NNaO_2$	$C_{22}H_{22}ClKN_6O$
Molecular weight [68]	318.13 g/mol	461.01 g/mol
Melting point [69, 70]	275–277 °C	183.5–184.5 °C
Ionization constant, pK_a [36, 39]	4.2	2.95; 4.25
Octanol-water partition coefficient, $logK_{OW}$ [71, 72]	4.51	1.19
Dipole Moment [a]	5.5 debye	16.1 debye

[a] Estimated using the chemical modelling software, Gaussian 09 [55]

In most cases, the hydrophobicity of the compound is directly related to the adsorption rates. The $logK_{O/W}$ (partition coefficient of the molecule in octanol/water system) is employed to assess hydrophobicity, being acknowledged in literature that compounds with $logK_{O/W}$ superior to 2 or 2.5 are hydrophobic [75]. From Table 5.4, $logK_{O/W}$ of LP is much lower than that of DS, *i.e.*, LP is less hydrophobic than DS. In general, compounds with more pronounced hydrophobic nature have fewer polar groups and so are less solvated [75]. Accordingly, the water solubility of LP is substantially higher than that of DS. In the literature, while the solubility values reported for DS vary between 1113 and 20670 mg/L [76, 77], those for LP

reach up to 97,058 mg/L [78]. This means that LP molecules have higher affinity with aqueous phase and so would adsorb onto Spectrogel surface with greater difficult in comparison to DS molecules.

However, it is important to mention that molecular polarity can also yield specific interactions and so expressively impact the adsorption performance. Some authors speculate that the dipole of polar molecules can point to the counter-charged surface of the adsorbent, promoting higher adsorption rates [79]. This does not apply to the present work, since although the dipole moment of LP (16.1 debye) is much higher than that of DS (5.5 debye), the latter was shown to be more easily adsorbed onto the organoclay. Hence, it is inferable that other factors interfere with the overall uptake processes of DS and LP.

- DFT-based reactivity descriptors calculations

Striving at greater clarity about the reasons for the distinguished behaviors of DS and LP adsorption onto Spectrogel, DFT theoretical calculations were implemented focusing on the molecular and electronic properties of the isolated adsorbate molecules.

The geometry of a molecule consists on the three-dimensional organization of its atoms and is controlled by the quantum mechanical behavior of electrons [80]. In this paper, geometry optimization of isolated DS and LP molecules was tested by B3LYP method using both 6-31G(d,p) standard basis set and 6-31G(d,p)$^{++}$ diffuse basis set. According to Fig. S5.4 of Supplementary material, the latter provided lower molecular energies and thereby more stable conformers. The same was previously verified for LP by Mizera, et al. [56]. Stability calculations and vibrational analyzes were undertaken to assure that the obtained structures are stable and correspondent to the configurations of minimum energy. Fig. 5.5 illustrates the final optimized geometries of DS and LP molecules obtained by B3LYP/6-31G(d,p)$^{++}$ method. It is noticeable that the aromatic rings in both pharmaceuticals are twisted with respect to each other as a consequence of repulsion interactions. Table S5.1 of supplementary material lists the optimized bond lengths, which quantify the average distance between the centers of two bonded atoms. The values obtained agree well with experimental and theoretical bond lengths from literature [56, 81].

Figure 5.5. Optimized molecular structures of DS and LP calculated at B3LYP/6-31G(d,p)$^{++}$ level of theory.

(a)

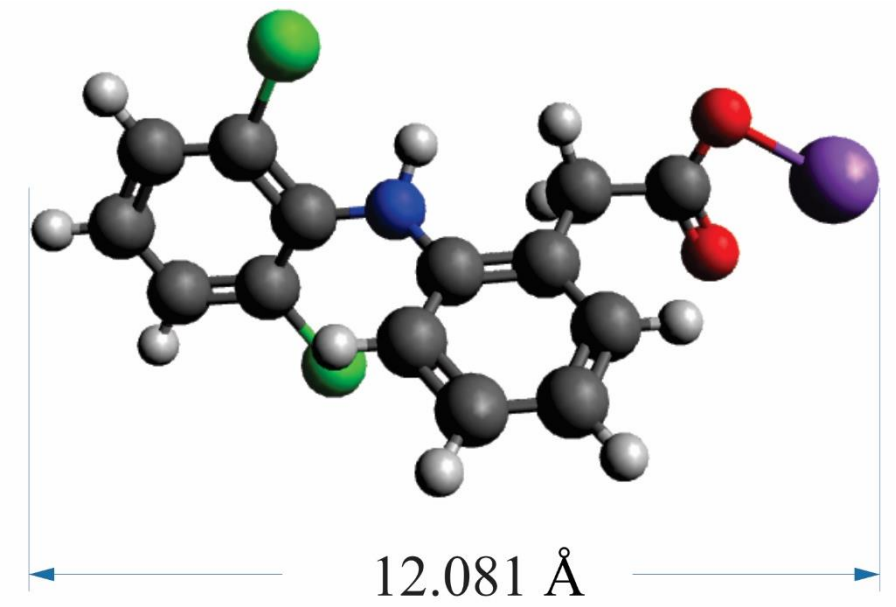

(b)

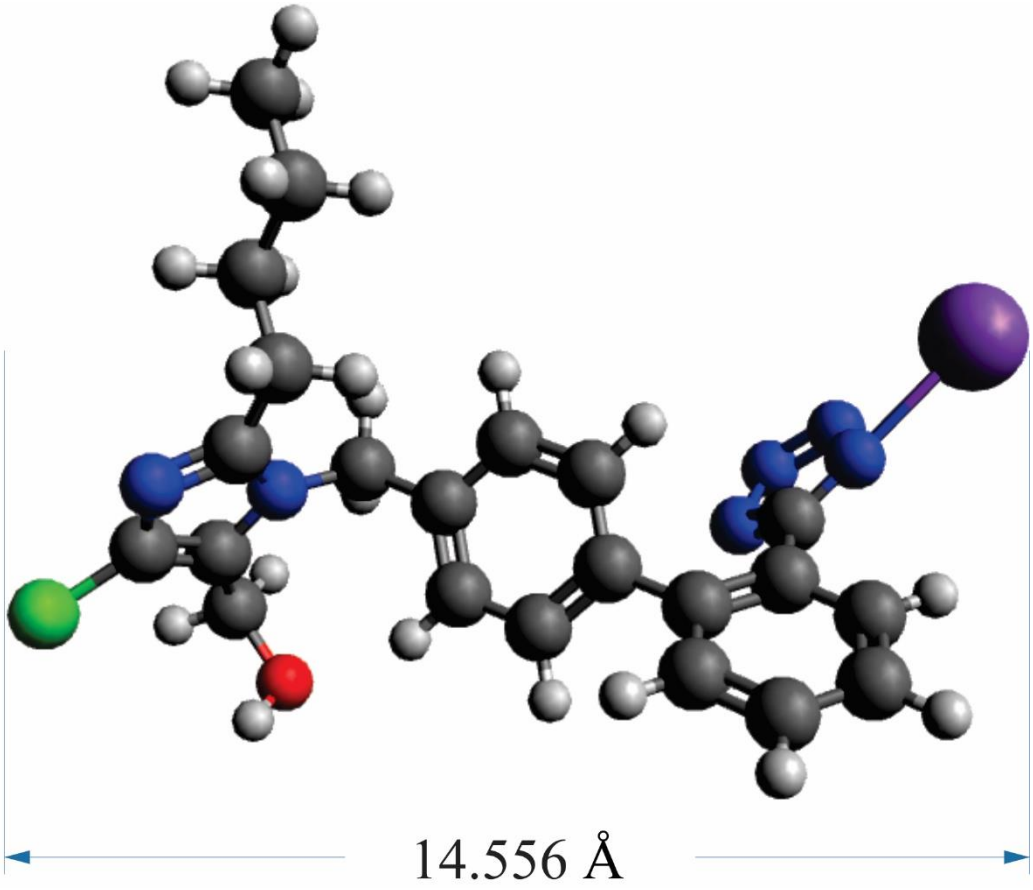

It is noteworthy that the molecular size and shape of the organic contaminants can impair the accessibility to the adsorption sites of the surface of the adsorbent and, therefore, the overall adsorption performance [67]. Steric hindrance occurs when a molecule of significant size covers adjoining adsorption sites, preventing them from binding [5]. According to Table 5.4 and Fig. 5.5, LP has greater length (14.556 Å) and higher molecular weight (461.01 g/mol) than DS (12.081 Å and 318.13 g/mol). Hence, in comparison to DS, LP molecules may cause a relatively greater steric hindrance, so that some of the adsorption sites of the Spectrogel surface become unable to effectively bind to other molecules. This factor can be related to the greater difficult of the organoclay in adsorbing LP in relation to DS molecules.

Table 5.5 lists the DFT-based reactivity descriptors obtained for the pharmaceuticals.

Table 5.5. Calculated quantum chemical parameters of diclofenac sodium and losartan potassium by B3LYP/6-31G(d,p)$^{++}$ approach

Quantum chemical parameter	Diclofenac sodium	Losartan potassium
HOMO energy (E_H, eV)	–5.52	–5.81
LUMO energy (E_L, eV)	–1.61	–1.89
Energy gap (Δ_{H-L}, eV)	3.91	3.92
Chemical potential (μ, eV)	3.56	3.85
Chemical hardness (η, eV)	1.95	1.96
Electrophilicity index (ω, eV)	3.25	3.79

The molecular frontier orbitals HOMO and LUMO are useful quantum chemical descriptors, which provide information about charge transfer that occurs within the molecule. HOMO represents the utmost orbital holding electrons and LUMO denotes the inmost orbital having available sites to accommodate electrons. Hence, HOMO and LUMO energies (E_H and E_L) measure the electron donating and accepting abilities of molecules, respectively [80]. From these concepts, the higher the E_H value, the easier to donate electrons, whereas the lower the E_L value, the easier to gain electrons. From Table 5.5, DS presents both E_H and E_L values almost 0.3 eV greater than LP does. So, it is inferable that DS has higher facility to donate electrons, but greater resistance to gain electrons [82].

Fig. 5.6 presents the 3D contours of HOMO (electron rich sites) and LUMO (electron deficient sites) of DS and LP molecules.

Figure 5.6. 3-D plots of HOMO and LUMO of (a) DS and (b) LP (Green color: negative phase; pink color: positive phase)

(a)

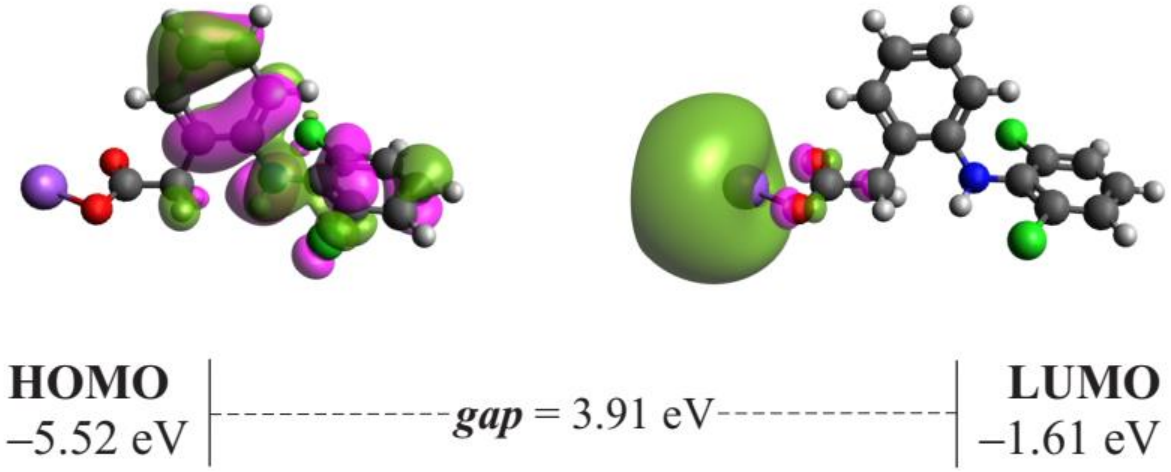

(b)

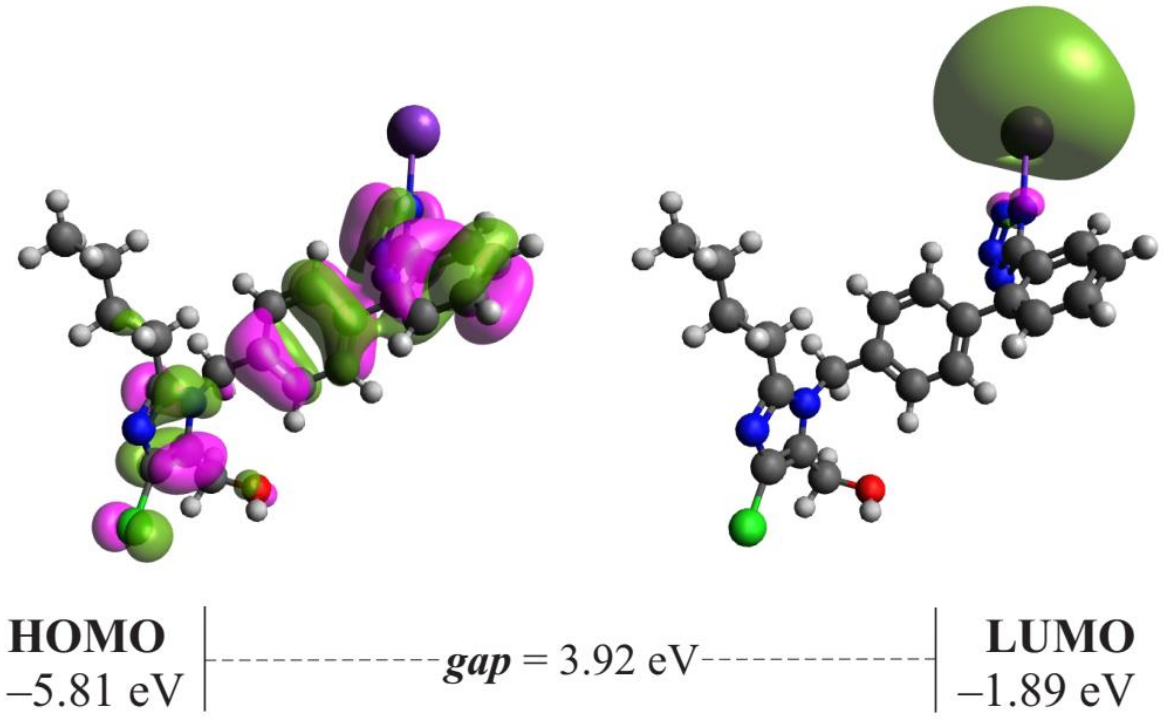

In DS molecule, HOMO is mainly localized in the two aromatic rings and the amino group (the linkage) and LUMO concentrates over the Na atom. In LP molecule, HOMO ranges over the regions of imidazole, benzoic and tetrazole rings, while LUMO is mostly located around the Na atom. The HOMO-LUMO energy gap (Δ_{H-L}) describes the relative reactivity of a molecule. The higher the Δ_{H-L} value, the lower the reactivity of a molecule and the other way around [53]. In this work, Δ_{H-L} was estimated as 3.91 eV for DS and 3.92 eV for LP, which indicates that DS is a slightly more reactive pharmaceutical.

Besides characterizing the molecular reactivity, the values of E_H and E_L also commonly correlate with other chemical indices as defined in Eq 11–13 (Section 5.2.6). The global chemical hardness (η) measures the resistance of a molecule to have electron density modified and so is useful to describe molecular stability and reactivity [83]. From DFT theory, the chemical potential (μ) is the negative of electronegativity and thereby measures the escaping tendency of electrons from equilibrium system [84]. The electrophilicity index (ω) measures the energy lowering of a ligand due to maximum electron flow between donor and acceptor and so is a indicative of electron accepting ability [85].

The values of η, μ and ω obtained for DS and LP molecules are listed in Table 5.5. Comparatively to LP, DS presents higher chemical potential μ, indicating a lower electron holding ability. Nevertheless, DS has lower value of electrophilicity index ω and so lower propensity to accept electrons. The chemical hardness η of DS is around 0.01 eV lower than that of LP; hence DS can be considered slightly "softer". It means that DS owns lower excitation energies and is relatively more reactive than LP. This indicative of molecular reactivity (DS > LP) agrees with the order of HOMO-LUMO energy gap obtained for the pharmaceutical molecules. In sum, the theoretical study of DTF-based chemical descriptors revealed that DS is more reactive than LP molecules, which corroborates the experimental findings of fixed-bed adsorption that showed that DS is more easily removed from solution than LP.

5.4 Conclusions

The present paper establishes the potential use of Spectrogel organoclay as adsorbent of DS and LP pharmaceuticals in fixed-bed monocomponent systems. The characterization analysis by XPS revealed modifications in surface chemical composition of Spectrogel after the adsorption processes. The experimental results showed BTCs mostly not fully developed under the examined conditions, *i.e.*, do not reach saturation level (C/C_{in} = 1). Despite the great diffusion resistance, the adsorption processes proved to be efficient with high values of removal percentage and adsorption capacity at the breakthrough time (corresponding to C/C_{in} = 0.05).

The adsorption systems exhibited the lowest heights of mass transfer zone at the condition of higher inlet concentration (0.15 mmol/L) and lower flow rate (0.4 mL/min), and the proposed Dual site diffusion approach best correlated most of the experimental BTCs. In general terms, the DS adsorption capacity of Spectrogel in fixed-bed is relatively worse than other organo-modified clays from literature, but better than granular activated carbon. The more favorable continuous adsorption of DS compared to LP agrees with its hydrophobic nature, low water solubility and better stereo-selective fit. Moreover, DFT theoretical calculations showed that DS owns higher chemical reactivity than LP due to lower values of HOMO-LUMO energy gap and molecular hardness. The present work endorses further studies regarding the fixed-bed adsorption of DS, LP and other pharmaceuticals by clay-based materials with the examination of synthetic solutions at even lower concentrations, multi-component mixtures, real samples of water/effluent, regeneration by advanced methods and applicability in large-scale.

Acknowledgments

This research was developed with the support of CENAPAD SP and was financed in part by the Coordenação de Aperfeiçoamento de Pessoal de Nível Superior - Brasil (CAPES) - Finance Code 001 [Proc. 88882.329686/2018-01], Conselho Nacional de Desenvolvimento Científico e Tecnológico - Brasil (CNPq) [Proc. 406193/2018-5], and Fundação de Amparo à Pesquisa do Estado de São Paulo - Brasil (FAPESP) [Proc. 2016/05007-1].

Appendix 5.A. Supplementary information

Figure S5.1. Column system used for the adsorption of diclofenac sodium (DS) or losartan potassium (LP) by Spectrogel organoclay

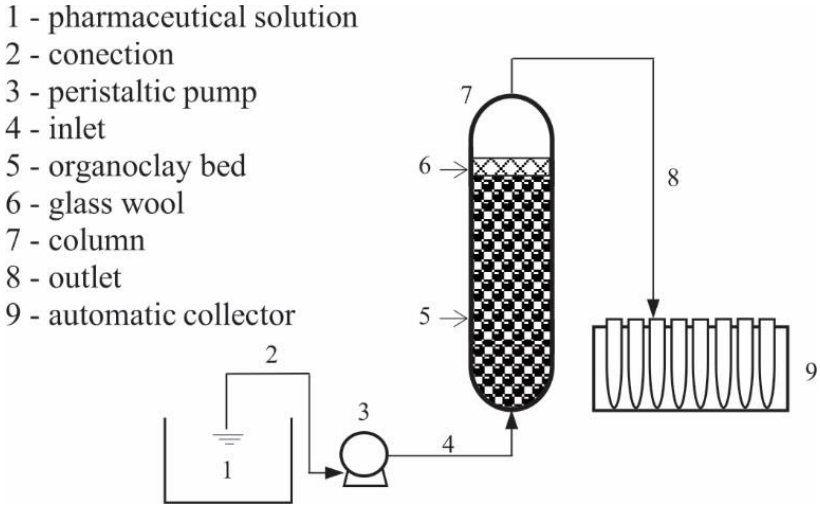

Figure S5.2. Wide survey XPS spectra of Spectrogel organoclay: (a) virgin; (b) after DS adsorption and (c) after LP adsorption

(a)

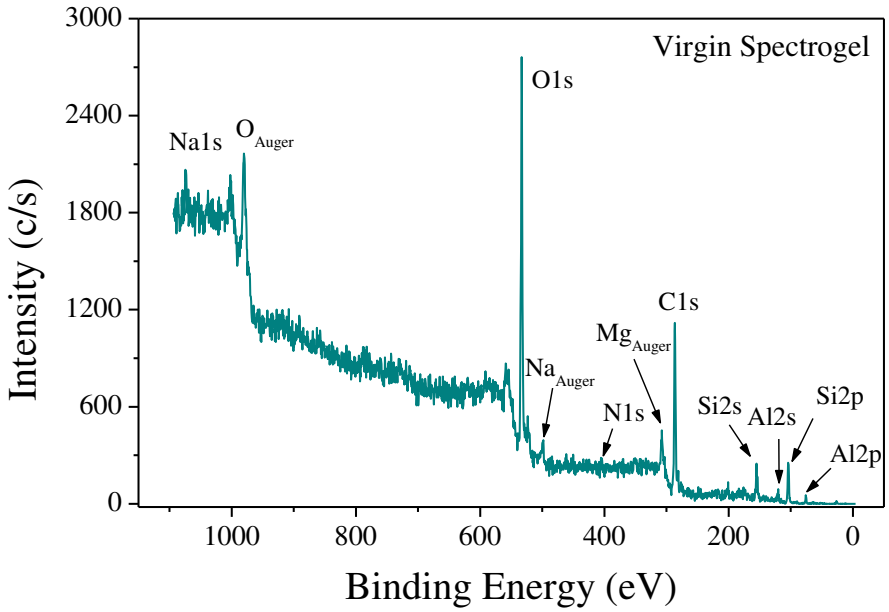

cont. **Fig. S5.2.**

(b)

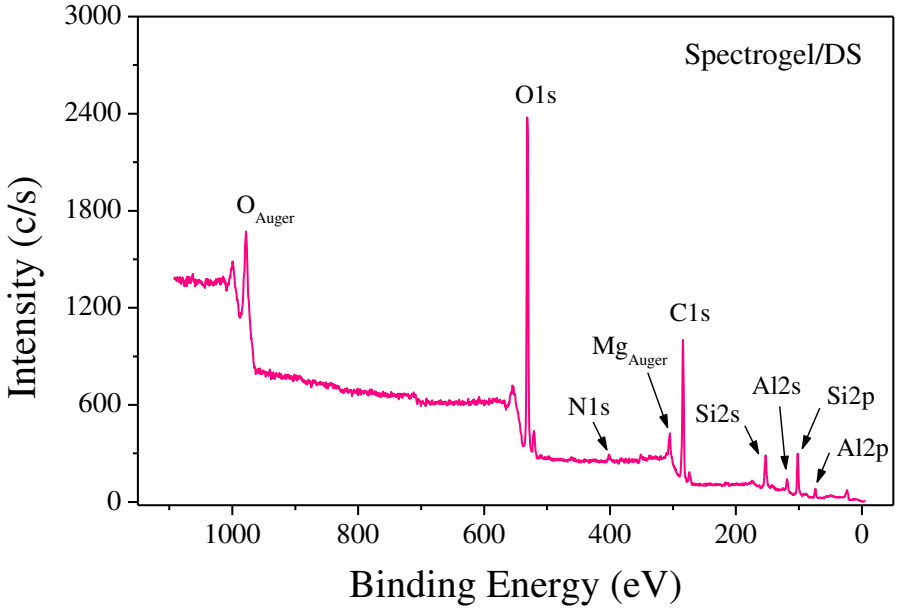

(c)

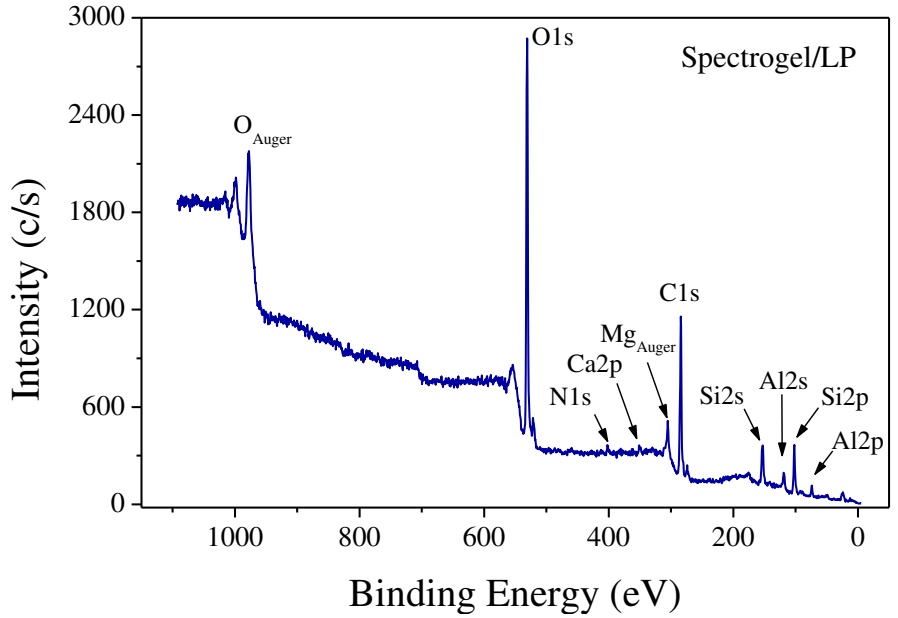

Figure S5.3. High resolution XPS: (a) Mg 1s scan of Spectrogel before use; (b) N 1s scan of Spectrogel after LP adsorption

(a)

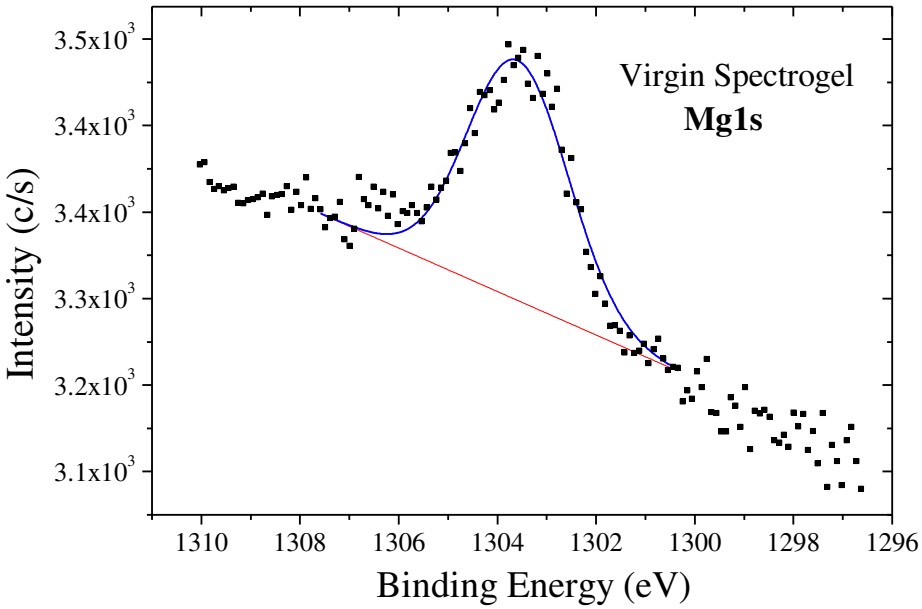

(b)

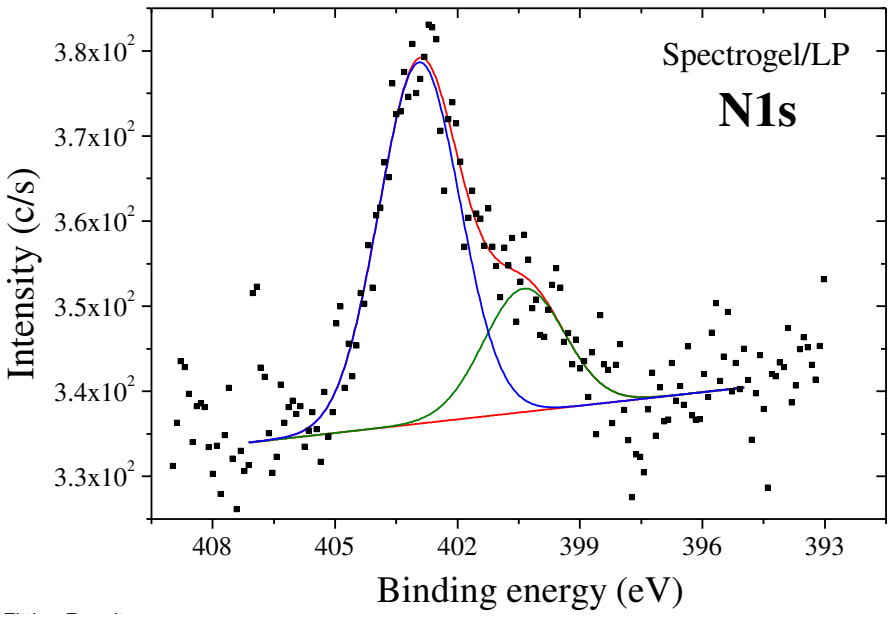

Figure S5.4. Molecular energies of DS and LP obtained from geometry optimizations by B3LYP method with 6-31G(d,p) basis set and 6-31G(d,p)$^{++}$ basis set.

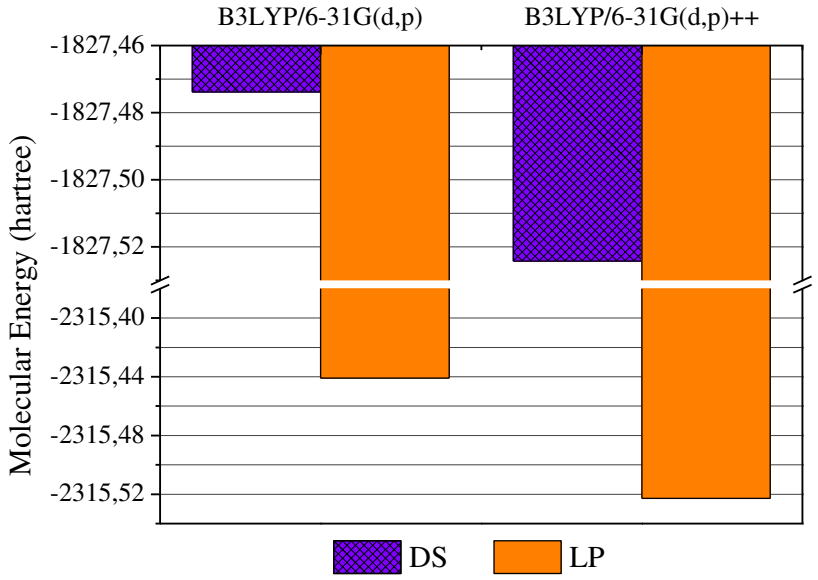

Table S5.1. Bond lengths (Å) of DS and LP with optimized geometries obtained with B3LYP/6-31G(d,p)$^{++}$

Diclofenac Sodium		**Losartan Potassium**			
Atoms	Bond Lenghts	Atoms	Bond Lenghts	Atoms	Bond Lenghts
C1–C2	1.3943	Cl1–C1	1.7425	C13–C14	1.3942
C1–C6	1.3922	C1–C2	1.3786	C13–H14	1.0855
C1–H1	1.0841	C1–N2	1.3543	C14–H15	1.0878
C2–C3	1.3948	C2–C3	1.4899	C15–C16	1.4063
C2–H2	1.085	C2–N1	1.3979	C15–C20	1.4166
C3–C4	1.3937	C3–O1	1.4396	C16–C17	1.3943
C3–H3	1.0842	C3–H1	1.0961	C16–H16	1.0862
C4–C5	1.4146	C3–H2	1.0933	C17–C18	1.3965
C4–Cl2	1.7517	O1–H3	0.9673	C17–H17	1.0863
C5–C6	1.4137	N1–C4	1.3719	C18–C19	1.3934
C5–N1	1.3961	N1–C8	1.473	C18–H18	1.0864
C6–Cl1	1.7627	C4–N2	1.3284	C19–C20	1.4063
N1–C7	1.4225	C4–C5	1.498	C19–H19	1.0854
N1–H4	1.0123	C5–C6	1.5442	C20–C21	1.4764
C7–C8	1.4003	C5–H4	1.0949	C21–N4	1.3459
C7–C10	1.4142	C5–H5	1.0948	C21–N5	1.345
C8–C9	1.3947	C6–C7	1.5339	N4–N6	1.3358
C8–H5	1.0851	C6–H6	1.0972	N5–N7	1.3596
C9–C12	1.3947	C6–H7	1.0993	N5–K1	2.6123
C9–H7	1.0863	C7–C22	1.533	N6–N7	1.3162
C10–C11	1.3983	C7–H8	1.0991	N7–K1	2.5732
C10–C13	1.5191	C7–H9	1.0985	C22–H20	1.0966
C11–C12	1.3976	C8–C9	1.5185	C22–H21	1.0954
C11–H6	1.0841	C8–H10	1.0936	C22–H22	1.0962
C12–H8	1.086	C8–H11	1.0924		
C13–C14	1.5296	C9–C10	1.4009		
C13–H9	1.0968	C9–C14	1.4003		
C13–H10	1.0985	C10–C11	1.3944		
C14–O1	1.2725	C10–H12	1.0866		
C14–Na1	2.4985	C11–C12	1.4044		
C14–O2	1.2728	C11–H13	1.0862		
O1–Na1	2.2023	C12–C13	1.4019		
Na1–O2	2.2012	C12–C15	1.4912		

References

[1] P.A. Todd, E.M. Sorkin, Drugs 35 (1988) 244.
[2] K.L. Goa, A.J. Wagstaff, Drugs 51 (1996) 820.
[3] J. Rivera-Utrilla, M. Sánchez-Polo, M.Á. Ferro-García, G. Prados-Joya, R. Ocampo-Pérez, Chemosphere 93 (2013) 1268.
[4] D. Tiwari, C. Lalhriatpuia, S.-M. Lee, J. Ind. Eng. Chem. 30 (2015) 167.
[5] A.V. Dordio, S. Miranda, J.P. Prates Ramalho, A.J.P. Carvalho, J. Hazard. Mater. 323 (2017) 575.
[6] N. Collado, S. Rodriguez-Mozaz, M. Gros, A. Rubirola, D. Barceló, J. Comas, I. Rodriguez-Roda, G. Buttiglieri, Environ. Pollut. 185 (2014) 202.
[7] T. Heberer, Toxicol. Lett. 131 (2002) 5.
[8] Y. Zhang, S.-U. Geißen, C. Gal, Chemosphere 73 (2008) 1151.
[9] A. Bayer, R. Asner, W. Schüssler, W. Kopf, K. Weiß, M. Sengl, M. Letzel, Environ. Sci. Pollut. Res. 21 (2014) 10830.
[10] Q. Sun, M. Lv, A. Hu, X. Yang, C.-P. Yu, J. Hazard. Mater. 277 (2014) 69.
[11] D.G.J. Larsson, C. de Pedro, N. Paxeus, J. Hazard. Mater. 148 (2007) 751.
[12] B.t. Ferrari, N. Paxéus, R.L. Giudice, A. Pollio, J. Garric, Ecotoxicol. Environ. Saf. 55 (2003) 359.
[13] J.M. Brausch, K.A. Connors, B.W. Brooks, G.M. Rand, in: D.M. Whitacre (Ed.) Reviews of Environmental Contamination and Toxicology Volume 218, Springer US, Boston, MA, 2012, p. 1-99.
[14] A.A. Godoy, F. Kummrow, P.A.Z. Pamplin, Ecotoxicology 24 (2015) 1112.
[15] M. Irandost, R. Akbarzadeh, M. Pirsaheb, A. Asadi, P. Mohammadi, M. Sillanpää, J. Mol. Liq. 291 (2019) 111342.
[16] J.R. de Andrade, M.G.A. Vieira, M.G.C. da Silva, S. Wang, Chem. Eng. J. 382 (2019) 122971.
[17] M. Grassi, G. Kaykioglu, V. Belgiorno, G. Lofrano, in: G. Lofrano (Ed.) Emerging Compounds Removal from Wastewater, Springer Netherlands, 2012, p. 15-37.
[18] J.R. de Andrade, M.F. Oliveira, M.G.C. da Silva, M.G.A. Vieira, Ind. Eng. Chem. Res. 57 (2018) 3103.
[19] G.S. Maia, J.R. de Andrade, M.G.C. da Silva, M.G.A. Vieira, Powder Technol. 345 (2019) 140.
[20] M.A.E. de Franco, C.B. de Carvalho, M.M. Bonetto, R. de Pelegrini Soares, L.A. Féris, J. Clean. Prod. 181 (2018) 145.
[21] Thanhmingliana, D. Tiwari, Chem. Eng. J. 263 (2015) 364.
[22] J.R. de Andrade, M.G.C. da Silva, M.L. Gimenes, M.G.A. Vieira, J. Environ. Chem. Eng. (2019) 103562.
[23] E. Worch, Adsorption Technology in Water Treatment: Fundamentals, Processes, and Modeling. De Gruyter, Berlim, 2012.
[24] M.J. Ahmed, B.H. Hameed, Ecotoxicol. Environ. Saf. 149 (2018) 257.
[25] A.M. Awad, S.M.R. Shaikh, R. Jalab, M.H. Gulied, M.S. Nasser, A. Benamor, S. Adham, Sep. Purif. Technol. 228 (2019) 115719.
[26] M.F. Oliveira, M.G.C. da Silva, M.G.A. Vieira, Appl. Clay Sci. 168 (2019) 366.
[27] F.M. De Souza, O.A.A. Dos Santos, M.G.A. Vieira, Environ. Sci. Pollut. Res. 26 (2019) 18329.
[28] S.K.F. Stofela, J.R. de Andrade, M.G.A. Vieira, Can. J. Chem. Eng. 95 (2017) 1034.
[29] S.K.F. Stofela, A.F. de Almeida Neto, M.L. Gimenes, M.G.A. Vieira, Can. J. Chem. Eng. 93 (2015) 998.
[30] L.F. Lima, J.R. de Andrade, M.G.C. da Silva, M.G.A. Vieira, Ind. Eng. Chem. Res. 56 (2017) 6326.

[31] D.D.C.A. Speridião, O.A.A. Santos, A.F. Almeida Neto, M.G.A. Vieira, Mater. Sci. Forum 798-799 (2014) 558.
[32] G.S. Maia, J.R. Andrade, M.F. Oliveira, M.G.A. Vieira, M.G.C. Silva, Chem. Eng. Trans. 57 (2017) 583
[33] H.C. Thomas, J. Am. Chem. Soc. 66 (1944) 1664.
[34] Y.H. Yoon, J.H. Nelson, Am. Ind. Hyg. Assoc. J. 45 (1984) 509.
[35] G. Yan, T. Viraraghavan, M. Chen, Adsorpt. Sci. Technol. 19 (2001) 25.
[36] H. Cheng, D. Song, H. Liu, J. Qu, Chemosphere 136 (2015) 297.
[37] M. Antunes, V.I. Esteves, R. Guégan, J.S. Crespo, A.N. Fernandes, M. Giovanela, Chem. Eng. J. 192 (2012) 114.
[38] S.K. Bajpai, M. Bhowmik, J. Appl. Polym. Sci. 117 (2010) 3615.
[39] P. Tosco, B. Rolando, R. Fruttero, Y. Henchoz, S. Martel, P.-A. Carrupt, A. Gasco, Helv. Chim. Acta 91 (2008) 468.
[40] B. Schampera, R. Solc, S.K. Woche, R. Mikutta, S. Dultz, G. Guggenberger, D. Tunega, Clay Miner. 50 (2015) 353.
[41] W.J. Thomas, B.D. Crittenden, Adsorption Technology and Design. Butterworth-Heinemann, Lymington, 1998.
[42] C.J. Geankoplis, Transport and Unit Operations. 3 edn. Prentice-Hall International Editions, New Jersey, 1993.
[43] J. Georgin, D. Franco, F.C. Drumm, P. Grassi, M.S. Netto, D. Allasia, G.L. Dotto, Powder Technol. 364 (2020) 584.
[44] P.R. Rout, P. Bhunia, R.R. Dash, Journal of Water Process Engineering 17 (2017) 168.
[45] S. Ayoob, A.K. Gupta, Chem. Eng. J. 133 (2007) 273.
[46] M.G. Sausen, F.B. Scheufele, H.J. Alves, M.G.A. Vieira, M.G.C. da Silva, F.H. Borba, C.E. Borba, Sep. Purif. Technol. 207 (2018) 477.
[47] J. Staudt, F.B. Scheufele, C. Ribeiro, T.Y. Sato, R. Canevesi, C.E. Borba, Sep. Purif. Technol. 230 (2020) 115857.
[48] D.M. Ruthven, Principles of Adsorption and Adsorption Processes. John Wiley & Sons, New York, 1984.
[49] J.T. Edward, J. Chem. Educ. 47 (1970) 261.
[50] L.F. Shampine, R.M. Corless, J. Comput. Appl. Math. 125 (2000) 31.
[51] J.A. Nelder, R. Mead, Comput. J. 7 (1965) 308.
[52] P.L. Bonate, Pharmacokinetic-Pharmacodynamic Modeling and Simulation. 2 edn. Springer, New York, 2011.
[53] C. Verma, L.O. Olasunkanmi, I. Bahadur, H. Lgaz, M.A. Quraishi, J. Haque, E.-S.M. Sherif, E.E. Ebenso, J. Mol. Liq. 273 (2019) 1.
[54] T.N.V. de Souza, S.M.L. de Carvalho, M.G.A. Vieira, M.G.C. da Silva, D.d.S.B. Brasil, Appl. Surf. Sci. 448 (2018) 662.
[55] M.J. Frisch, G.W. Trucks, H.B. Schlegel, G.E. Scuseria, M.A. Robb, J.R. Cheeseman, G. Scalmani, V. Barone, G.A. Petersson, H. Nakatsuji, X. Li, M. Caricato, A. Marenich, J. Bloino, B.G. Janesko, R. Gomperts, B. Mennucci, H.P. Hratchian, J.V. Ortiz, A.F. Izmaylov, J.L. Sonnenberg, D. Williams-Young, F. Ding, F. Lipparini, F. Egidi, J. Goings, B. Peng, A. Petrone, T. Henderson, D. Ranasinghe, V.G. Zakrzewski, N.R. J. Gao, G. Zheng, W. Liang, M. Hada, M. Ehara, K. Toyota, R. Fukuda, J. Hasegawa, M. Ishida, T. Nakajima, Y. Honda, O. Kitao, H. Nakai, T. Vreven, K. Throssell, J.A.M. Jr., J.E. Peralta, F. Ogliaro, M. Bearpark, J.J. Heyd, E. Brothers, K.N. Kudin, V.N. Staroverov, T. Keith, R. Kobayashi, J. Normand, K. Raghavachari, A. Rendell, J.C. Burant, S.S. Iyengar, J. Tomasi, M. Cossi, J.M. Millam, M. Klene, C. Adamo, R. Cammi, J.W. Ochterski, R.L. Martin, K. Morokuma, O. Farkas, J.B. Foresman, D.J. Fox, Gaussian 09. Gaussian, Inc., Wallingford, 2009.

[56] M. Mizera, K. Lewadowska, A. Talaczyńska, J. Cielecka-Piontek, Spectrochim. Acta A Mol. Biomol. Spectrosc. 137 (2015) 1029.
[57] Y. Park, G.A. Ayoko, E. Horváth, R. Kurdi, J. Kristof, R.L. Frost, J. Colloid Interface Sci. 393 (2013) 319.
[58] M.F. Brigatti, E. Galan, B.K.G. Theng, in: F. Bergaya, B.K.G. Theng, G. Lagaly (Eds.), Developments in Clay Science, Elsevier, 2006, p. 19-86.
[59] H. He, Q. Zhou, R.L. Frost, B.J. Wood, L.V. Duong, J.T. Kloprogge, Spectrochim. Acta A Mol. Biomol. Spectrosc. 66 (2007) 1180.
[60] J.L. Sotelo, A. Rodríguez, S. Álvarez, J. García, Chem. Eng. Res. Des. 90 (2012) 967.
[61] W. McCabe, J. Smith, P. Harriott, Unit Operations of Chemical Engineering. 7 edn. McGraw-Hill, New York, 2005.
[62] W.L. McCabe, J.C. Smith, P. Harriott, Unit Operations of Chemical Engineering. 5 edn. McGraw-Hill, New York, 1993.
[63] A.A. Ahmad, B.H. Hameed, J. Hazard. Mater. 175 (2010) 298.
[64] A.H. Sulaymon, K.W. Ahmed, Environ. Sci. Technol. 42 (2008) 392.
[65] M.F. Oliveira, V.M. de Souza, M.G.C. da Silva, M.G.A. Vieira, Ind. Eng. Chem. Res. 57 (2018) 17480.
[66] Momina, M. Shahadat, S. Isamil, RSC Adv. 8 (2018) 24571.
[67] A. Gil, N. Taoufik, A.M. García, S.A. Korili, Environ. Technol. 40 (2019) 3017.
[68] U.S.Pharmacopeia, The United States Pharmacopeia. 31 edn. United States Pharmacopoeial Convention, Rockville, 2008.
[69] A.-R.A. Al-Majed, E. Assiri, N.Y. Khalil, H.A. Abdel-Aziz, in: H.G. Brittain (Ed.) Profiles of Drug Substances, Excipients and Related Methodology, Academic Press, 2015, p. 159-194.
[70] M. Kaur, M. Datta, Adsorpt. Sci. Technol. 32 (2014) 365.
[71] L.J. Carter, E. Harris, M. Williams, J.J. Ryan, R.S. Kookana, A.B.A. Boxall, J. Agric. Food Chem. 62 (2014) 816.
[72] Food and Drug Administration, in: Center for Drug Evaluation and Research (Ed.), FDA, 2002.
[73] H.T.T. Tran, J.B. Park, K.-H. Hong, H.-G. Choi, H.-K. Han, J. Lee, K.T. Oh, B.-J. Lee, Int. J. Pharm. 415 (2011) 83.
[74] F. Hafeez, A.F. Zahoor, S. Ahmad, M. Ahmad, S. Faiz, Synth. Commun. 49 (2019) 325.
[75] D. Dolar, N. Drašinac, K. Košutić, I. Škorić, D. Ašperger, J. Appl. Polym. Sci. 134 (2017).
[76] A. Llinàs, J.C. Burley, K.J. Box, R.C. Glen, J.M. Goodman, J. Med. Chem. 50 (2007) 979.
[77] A.A. Saei, F. Jabbaribar, M.A.A. Fakhree, W.E. Acree, A. Jouyban, J. Drug Deliv. Sci. Technol. 18 (2008) 149.
[78] H.A. Pawar, K.G. Lalitha, Chromatography Research International 2014 (2014).
[79] A.M. Comerton, R.C. Andrews, D.M. Bagley, P. Yang, J. Membr. Sci. 303 (2007) 267.
[80] B. Latha, S. Gunasekaran, S. Srinivasan, G.R. Ramkumaar, Spectrochim. Acta A Mol. Biomol. Spectrosc. 132 (2014) 375.
[81] M. Baia, S. Astilean, T. Iliescu, in: M. Baia, S. Astilean, T. Iliescu (Eds.), Raman and SERS Investigations of Pharmaceuticals, Springer, Berlin, 2008.
[82] F. Chiter, C. Lacaze-Dufaure, H. Tang, N. Pébère, Phys. Chem. Chem. Phys. 17 (2015) 22243.
[83] R.G. Parr, R.G. Pearson, J. Am. Chem. Soc. 105 (1983) 7512.
[84] P. Geerlings, F. De Proft, W. Langenaeker, Chem. Rev. 103 (2003) 1793.
[85] R.G. Parr, L.v. Szentpály, S. Liu, J. Am. Chem. Soc. 121 (1999) 1922.

CAPÍTULO 6. Degradação Oxidativa de Losartana Potássica

Oxidative degradation of pharmaceutical losartan potassium with N-doped hierarchical porous carbon and peroxymonosulfate[§]

Julia Resende de Andrade[a], Melissa Gurgel Adeodato Vieira[a], Meuris Gurgel Carlos da Silva[a], Shaobin Wang[b,c]

[a] *School of Chemical Engineering, University of Campinas, Albert Einstein Avenue, 500, 13083-852, Campinas, São Paulo, Brazil*

[b] *Department of Chemical Engineering, Curtin University, GPO Box U1987, WA, 6845, Australia*

[c] *School of Chemical Engineering, The University of Adelaide, Adelaide, SA, 5005, Australia*

Abstract

Losartan potassium (LOS) is a most globally consumed antihypertensive and emerging pharmaceutical contaminant of concern due to increasingly ubiquity in water and wastewater. For its effective environmental remediation, we propose the catalytic oxidation of losartan via peroxymonosulfate (PMS) activation using a metal-free N-doped hierarchically porous carbon (N-PC). We found out that N-PC exhibits both excellent adsorption capacity and catalytic oxidation efficiency with 100% LOS uptake within 240 min at 0.026 g/L of the N-PC. Fresh and used N-PC were scrutinized for textural properties and surface chemistry. The effects of PMS dose, temperature, pH, organic matter and coexisting anions on losartan decomposition were examined. Moreover, total organic removal was obtained and the catalyst was tested in three consecutive runs. Electron paramagnetic resonance and quenching assays revealed that the nonradical oxidation pathway plays a major role in LOS degradation by N-PC/PMS.

Keywords: Advanced oxidation process; Adsorption; Porous carbon; Losartan potassium; Water treatment; Pharmaceutical contaminant.

[§] Manuscript published in *Chemical Engineering Journal* 382 (2020) 122971. DOI: 10.1016/j.cej.2019.122971. Reprinted with permission from *Chemical Engineering Journal*. Copyright 2020 Elsevier (*Anexo A*).

6.1 Introduction

With the expansion and ageing of population, the number of adults with high blood pressure in the world has augmented 90% between 1975 and 2015 [1]. As a result, antihypertensive medications, such as losartan potassium, have been increasingly consumed. Table 6.1 depicts the main characteristics of losartan potassium (LOS).

Table 6.1. Physical and chemical properties of losartan potassium [2, 3].

Molecular Formula	$C_{22}H_{22}ClKN_6O$
Molecular weight	461.01 g/mol
Chemical structure	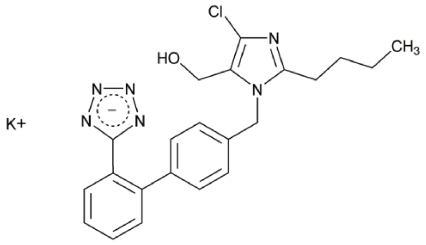
Antihypertensive class	Angiotensin-II receptor antagonist
Ionization constant (pK_a)	4.9
Solubility	>500 mg/L (25 °C)

Although LOS poses an acceptable ecological risk for freshwater species, it is classified as hazardous to aquatic environment [4] and is highly stable to hydrolysis and biodegradation [2].

Due to elevated consumption and high degree of persistence, LOS has been widespread detected in the aquatic environment [5, 6]. The frequent presence of LOS in water can also be blamed on its incomplete removal in wastewater treatment plants by conventional activated-sludge processes [7]. Therefore, we have witnessed an urge for effective environmental remediation technologies. Although adsorption has been extensively explored for the uptake of pharmaceuticals [8-12], this method entails a post-treatment for complete abatement of the pollutants and may present limited capability at ultralow concentrations [13]. Advanced oxidation processes (AOPs) have been promisingly examined to treat emerging pharmaceutical contaminants and previous studies report the efficient removal of LOS using AOPs mediated by hydroxyl radicals (•OH) [14, 15].

Alternatively to classical •OH-based AOPs, AOPs involving sulfate radicals ($SO_4^{\bullet-}$) have attracted massive attention recently, because $SO_4^{\bullet-}$ manifests equal or greater oxidative potential (E_0=2.5–3.1 V) at a prolonged life span (30–40 μs) in relation to •OH (E_0=1.9–2.7 V with half-

life of 20 ns) [16-18]. $SO_4^{\bullet-}$ is commonly generated from activating the peroxymonosulfate (HSO_5^-, PMS) by heterogeneous catalysis. Different metal-free carbon-sourced catalysts have been ultimately exploited for PMS-mediated AOPs in order to overcome the eco-unfriendly nature of traditional metal-based catalysts. Carbon catalysts with tailored features and enhanced activation performance have been obtained by inserting heteroatoms (*e.g.*, nitrogen) into the carbon matrix. A myriad of papers reports the improved catalytic degradation of pharmaceuticals using N-doped metal-free carbocatalysts, such as graphene [19, 20], carbon nanotubes [21, 22] and porous carbons (PC) [23].

Recently, Tian, et al. [24] proposed a facile and scalable method to obtain a super high-surface area and N-doped hierarchically porous carbon. The authors employed a one-pot mild direct pyrolysis with low-cost and sustainable precursors: wheat flour as a low-cost biomass carbon source, dicyandiamide as a source of N atoms, and a mixture of K_2CO_3, Na_2CO_3 and $NaHCO_3$ as green activation agents. The functionalized porous nanocarbon displayed outstanding PMS activation performance for efficient degradation of two persistent organic pollutants: p-hydroxybenzoic acid (HBA) and phenol. Nevertheless, both of these pollutants contain only one benzene ring as an aromatic moiety and their oxidation has been already widely explored in the literature [25-29]. Besides phenol and HBA [24], most recent reports on N-doped hierarchically porous carbons to activate PMS focus on the degradation of dyes as model organic pollutants [30, 31]. The catalytic oxidation of contaminants of emerging concern, such as pharmaceuticals, still requires more investigations.

In the present work, we used the N-doped hierarchically porous carbon (N-PC) for environmental remediation of the pharmaceutical LOS, which molecule contains imidazole, tetrazole, and benzene rings (Table 6.1). As far as we are concerned, LOS has not been previously treated using environmental benign metal-free carbocatalysts for PMS activation. Besides degrading LOS in the presence of PMS, N-PC itself is expected to adsorb LOS molecules. Therefore, we propose a novel approach for removing pharmaceuticals in low levels: a system with both strong catalytic oxidation ability and high adsorption ability.

Herein, the individual/synergistic effects between adsorption and catalysis for LOS removal in N-PC/PMS system were examined. Kinetic assays were performed to investigate the influences of PMS dose, reaction temperature, pH, and coexisting ions and organic matter in solution on LOS removal. PMS activation and pharmaceutical oxidation were examined by electron paramagnetic resonance and radical quenching tests. The total mineralization rate was assessed. The stability and reusability of N-PC were also inspected and various characterization analyses were used to assess the effects of the process on the properties of the catalyst.

6.2 Material and methods

6.2.1 *Chemicals*

The chemicals were analytical grade or superior. Sodium bicarbonate (≥ 99.5%), potassium hydroxide (85%), dicyandiamide (99%), potassium peroxymonosulfate (Oxone®, $KHSO_5 \cdot 0.5KHSO_4 \cdot 0.5K_2SO_4$, > 99%), losartan potassium (LOS, 100%), ethanol (EtOH, 99.5%), methanol (≥ 99.9%), 5,5-dimethyl-1-pyrroline-*N*-oxide (DMPO, ≥ 97.0%), 2,2,6,6-tetramethyl-4-piperidinol (TMP, 98%), sodium azide (NaN_3, 99.5%), *tert*-butyl alcohol (TBA, 100%), acetonitrile (HPLC grade), humic acid sodium salt (HA, 100%), phosphoric acid (≥ 85%) were procured from Sigma-Aldrich. Plain wheat flour was purchased from White Wings brand (Australia). Ultra-pure water was employed for solution preparation.

6.2.2 *Catalyst synthesis*

N-PC was prepared following the procedure from Tian, et al. [24]. Firstly, 2 g wheat flour was dissolved in 40 mL deionized (DI) water by magnetic agitation. A solution (50 mL) containing sodium bicarbonate (40 g/L) and potassium hydroxide (24 g/L) was added to 30 mL dicyandiamide solution (66.67 g/L). The two solutions were mixed under magnetic agitation for 24 h on a hot plate at 90 °C, and then dried in an oven at 100 °C overnight. The material was grounded and subjected to pyrolysis at 800 °C for 2 h in a tube furnace, with a ramp rate of 5 °C/min under a N_2 flow of 60 mL/min. The carbon sample was ground to powder using the mortar, washed three times with DI water and ethanol to eliminate remaining inorganic salts, and dried at 60 °C.

6.2.3 *Characterizations*

The alterations in surface chemistry and structure of N-PC were assessed before and after PMS-mediated AOP. The following characterization techniques were used: scanning electron microscopy with an energy dispersive spectroscopy (SEM/EDS) by FEI Verios XHR 460; transmission electron microscopy (TEM) by JEOL 2100; high angle annular dark field scanning TEM (HAADF-STEM) and correspondent energy-dispersive X-ray spectroscopy (EDX) elemental mapping by FEI Titan G2 80-200; X-ray photoelectron spectroscopy (XPS) by Kratos AXIS Ultra DLD; Fourier transform infrared spectroscopy (FT-IR) by Perkin Elmer 100-FT-IR; N_2 adsorption/desorption (-196 °C) using Micromertics Tristar 3000. Additional information about these characterizations is available in Text S6.1 in supplementary material. The point of zero charge (pH_{pzc}) of N-PC was inspected by inserting 0.1 g of carbon into 5 mL ultrapure water at 25 °C. The suspension was shaken for 48 h for the stabilization of pH [32].

In-situ electron paramagnetic resonance (EPR) by Bruker EMS-plus instrument and Xeon software (Bruker) was utilized to inspect active radical species with DMPO and TMP as spin trapping agents. The operation of the EPR analyzer is detailed in Text S6.1 in supplementary material.

6.2.4 *Experimental procedures*

All the tests were conducted at 25 °C, except as mentioned. The adsorption of N-PC was examined without the introduction of PMS. Using a water bath apparatus, N-PC (0.026 g/L) was added to a LOS solution of 150 mL (0.04 mmol/L) under constant stirring. Aliquots were collected throughout the course of time and filtered with 0.22 μm membrane.

In a typical catalytic degradation test, PMS (3.5 mmol/L) and N-PC (0.026 g/L) were simultaneously added to 100 mL LOS solution (0.04 mmol/L). At pre-determined times, 1 mL sample was removed, filtered and immediately added into vials with 0.5 mL methanol to quench PMS-induced oxidation.

The effects of PMS dosage (0; 0.5; 3.5; 6.5 mmol/L) and reaction solution temperature (25, 35, 45 °C) were examined. The roles of coexisting ions and natural organic matter on LOS degradation were researched using $NaHCO_3$ (5 mmol/L), NaCl (5 mmol/L), and humic acid (20 mg/L).

LOS removal efficiency in PMS/N-PC system was determined by Eq. 6.1 and rate constant of degradation was calculated by pseudo-first order kinetic model (Eq. 6.2).

$$\%D = (C_0 - C_f)/C_0 \times 100 \quad (6.1)$$

$$\ln C/C_0 = -kt \quad (6.2)$$

where: $\%D$=LOS degradation efficiency (%), C_0=starting LOS concentration (mmol/L), C_f=final LOS concentration (mmol/L), C=residual LOS concentration at t (mmol/L), k=pseudo-first order rate constant (min^{-1}) and t=reaction time (min).

Stability tests of N-PC/PMS were carried out using the same methodology of the oxidation tests for up to three cycles. After completing each run, N-PC was gathered by vacuum filtration, washed with DI water and ethanol (3 times) and dried in an oven at 60 °C for at least 6 h. As there might be losses during the collection because of extremely low catalyst dosage (0.026 g/L), the initial run was performed using 300 mL solution volume and the subsequent ones using lower volumes (200 mL and 100 mL), but always keeping the same catalyst and oxidant proportions.

Quenching experiments were carried out using sodium azide (NaN_3, 20 mmol/L) as a scavenger for $^1O_2$, *tert*-butyl alcohol (TBA, 1.75 mol/L) as a scavenger for •OH, and ethanol

(EtOH, 3.5 mol/L) as a scavenger for both •OH and $SO_4^{\bullet-}$. The concentrations of quenching agents were determined according to previous papers [19, 26].

6.2.5 *Analytical procedures*

Residual LOS concentration was measured by ultra-high performance liquid chromatography (UHPLC) (UltiMate 300, Thermo Fisher Scientific) equipped with an Acclaim® Organic Acid column (150 mm × 4 mm i.d., 5 µm, Thermo Fisher Scientific) and UV-Vis detector at λ=254 nm. The mobile phase contained 0.1% solution of phosphoric acid and acetonitrile (60:40, v/v), the flow rate was set as 1.0 mL/min, column temperature as 35 °C and injection volume as 10 µL [15]. Alternatively, the ultra-fast liquid chromatography (UFLC, Shimadzu) with a Restek Raptor C18 column was used.

The mineralization rate for a chosen system was assessed by a total organic carbon analyzer (TOC-$L_{CSH/CSN}$, Shimadzu). For each assessment, 10 mL aliquot was extracted at pre-determined time using syringe, promptly filtered by filter with 0.22 µm Millipore films, and diluted into a vial containing 10 mL sodium nitrite solution (0.3 mol/L) to quench the reaction [21].

6.3 **Results and discussion**

6.3.1 *Cost analysis*

Table 6.2 details the price (chemical reagents-based) and consumption of the raw materials for preparing N-PC. Ignoring the costs of DI water and power, and considering 2.75% product yield, the production cost of N-PC is estimated to be about AU$17.15/g (~US$12.03/g), which is comparable to sulfur-doped porous carbons derived from 2-thiophenemethanol (¥113~AU$23.72/g~US$16.63) and thiophene (¥79~AU$16.58/g~US$11.63) [33]. It is noteworthy that in large-scale applications the expenditures with raw materials to prepare N-PC would be lower in final price.

Table 6.2. Cost and consumption of raw materials in the preparation of N-PC catalyst.

Material item	Wheat flour	Sodium Bicarbonate	Potassium hydroxide	Dicyandiamide	Yield, wt.%
Unit Price	AU$2.45/kg	AU$106/kg	AU$82.50/kg	AU$69.50/kg	2.75
Consumption	2 kg	2 kg	1.4 kg	2 kg	
Total price	(2.45×2+2×106+1.4×82.50+2×69.50)/0.0275= AU$17,145.45/kg				

6.3.2 *Characterizations of N-PC before and after the oxidative tests*

The fabrication process of N-PC involves a combination of physical and chemical activations of the interlinked precursors, which take place concomitantly with pyrolysis at 800 °C. This strategy generates a carbon structure with high porosity suitable for adsorption and catalytic processes [24]. Although some surface features and surface chemistry of fresh N-PC have been already inspected [24], we provide additional ones for proper examination of oxidation mechanism of LOS.

SEM and TEM images were obtained in order to examine the microstructural morphology of N-PC before and after one cycle of catalytic degradation of LOS (Fig. 6.1). The porous structure of the as-prepared N-PC was confirmed with numerous micro- and mesopores (Fig. 6.1a and 6.1b). The porous texture essentially persists after the AOP, but the surface is comparatively rougher (Fig. 6.1e and 6.1f).

High resolution TEM images reveal a turbostratic structure with a random stacking of short graphene layers (Fig. 6.1c and 6.1d). The spotted interlayer distance of 0.34 nm is close to the (0 0 2) plane of ideal crystalline graphite (d_{002}=0.3354 nm) [34], pointing to some sp^2 hybridization of carbon network. N-PC after the use presents a lattice distance of 0.23 nm, which indicates the (1 0 0) facet of graphene [35] (Fig. 6.1h). This result suggests that some extent of crystal phase is transferred into amorphous phase.

XPS spectra were recorded to assess the chemistry at the surface of N-PC. Four characteristic peaks are identified in the survey spectrum of the virgin catalyst (Fig. S6.1 in supplementary material): carbon (C 1s, 284.55 eV), nitrogen (N 1s, 397.55 eV), oxygen (O 1s, 531.55 eV) and sodium (Na 1s, 1070 eV). The corresponding atomic levels of these elements were 80.89, 6.52, 12.42 and 0.18%. Noticeably, the nitrogen content of N-PC is consistent with the 7.33% previously achieved by Tian et al. (2018), which verifies dicyandiamide as an effective nitrogen precursor. The N-doping level is higher than that of other N-doped carbon materials [36, 37]. The post-process spectrum does not present significant amounts of Na, but C, N and O were observed with atomic concentrations of 79.07, 3.03 and 17.90%, respectively. The elemental mapping analysis by HAADF-STEM (Fig. 6.1i and 6.1j) attested that C, N, and O are uniformly spread within the pore structure of N-PC either pre- or post-process.

Figure 6.1. (a, b) SEM and (c, d) TEM images of fresh N-PC. (e, f) SEM and (g, h) TEM images of N-PC after losartan AOP. (i) and (j) HAADF-STEM images of N-PC with EDX elemental mapping images of N-PC before and after use, respectively.

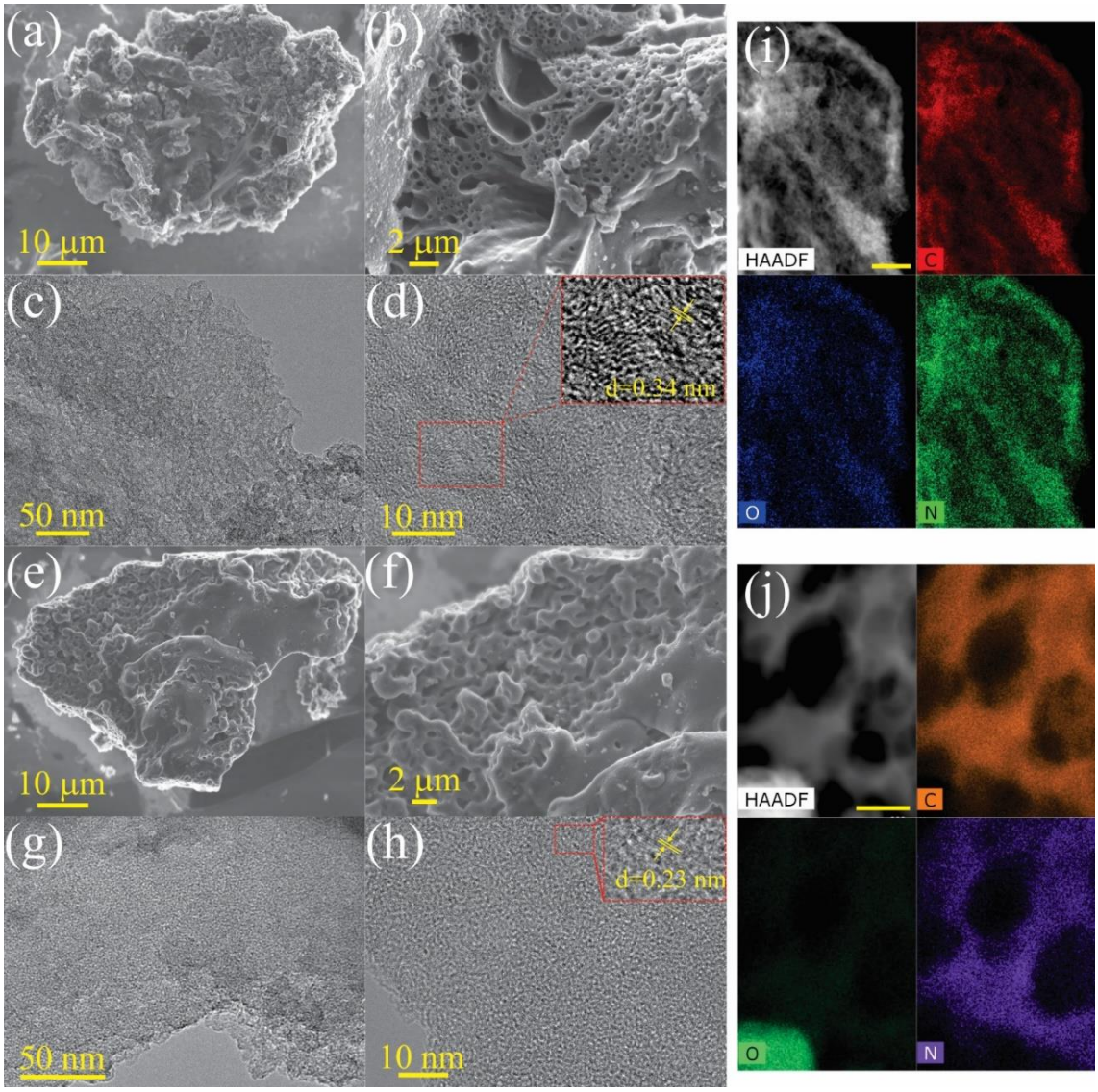

XPS spectrum of C1s core level (Fig. 6.2a) can be decomposed into four regions with binding energies around 284.5, 285.3, 286.3 and 288.6 eV, corresponding to sp^2 graphitic carbon, sp^2 carbon bonded to heteroatoms (C–O and/or C–N), carbonyl/quinine groups (C=O), and carboxyl or ester groups (O–C=O) [33, 38, 39]. Yet the sp^2-hybridized carbon remains dominant after the reaction, its ratio reduces in 5%, which verifies the decreasing of graphitization and further C bonding.

The magnified N 1s spectrum of fresh N-PC (Fig. 6.2b) shows the predominance of three nitrogen functionalities: pyridinic N (398 eV), pyrrolic N (400 eV), and quaternary N (401 eV). It contains primarily pyridinic N (>50%), which dangling bond has been assigned to enhanced catalytic performance due to the establishment of localized sites of higher charge

densities (pyridine-like defects) in the carbon structure [40, 41]. The N 1s spectrum of N-PC after reaction contains an extra peak at 405 eV, correspondent to nitrogen-oxides (405 eV), in addition to pyridinic N, pyrrolic N and quaternary N.

Figure 6.2. (a) High resolution XPS C 1s scan and (b) high resolution XPS N 1s scan of N-PC before and after use.

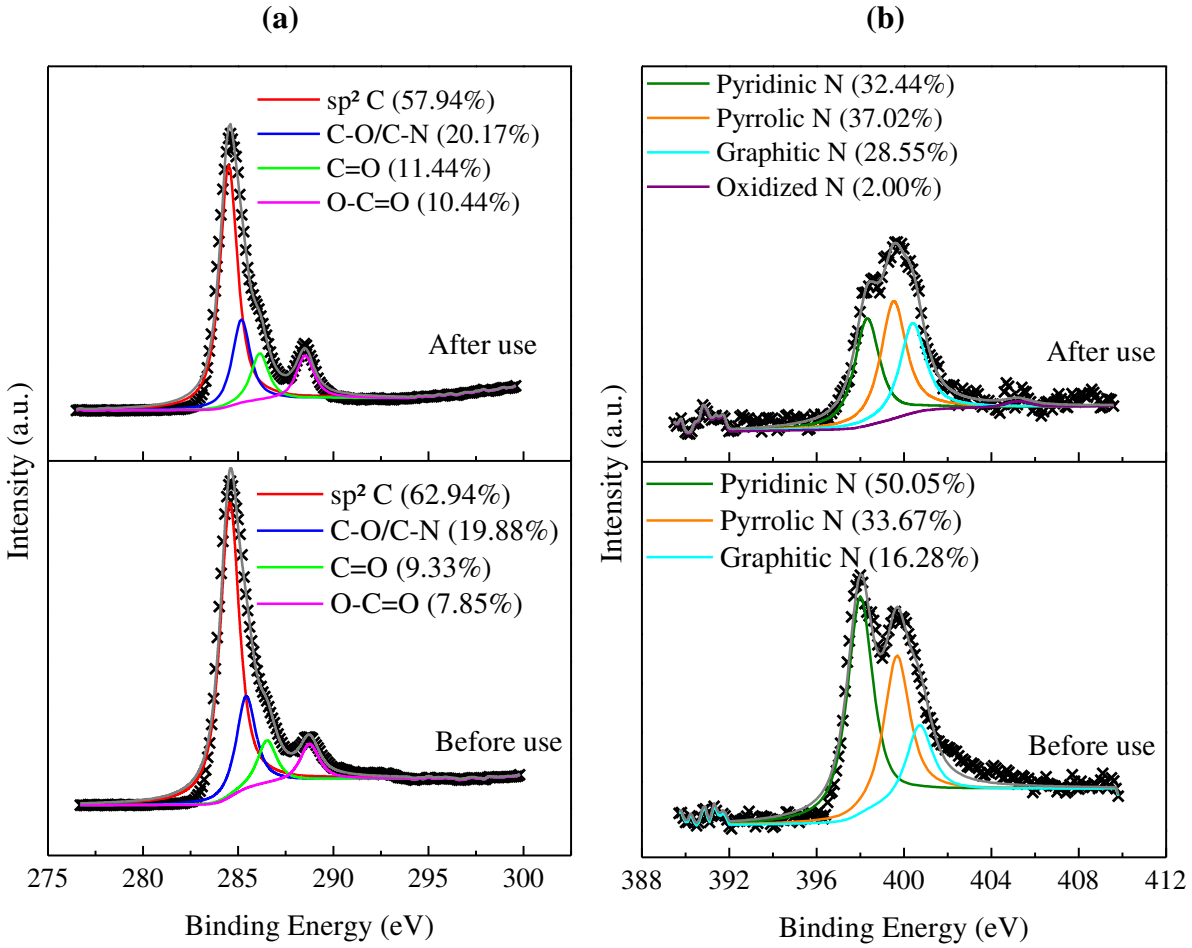

The characteristic chemical bonding structure of N-PC was also determined by FTIR spectra (Fig. 6.3a). Although low intensity IR signals were obtained, the as-prepared catalyst presents peaks between 3100 and 2800 cm^{-1}, corresponding to C–H stretches. The signal around 2350 cm^{-1} represents C≡N symmetrical stretching vibration and the peaks between 2100 and 1900 cm^{-1} can be accredited to C=C=C or C=C=N groups. The peaks in the 1150–1000 cm^{-1} region confirm the presence of oxygen in groups such as C–O or C–O–C [33, 37, 42]. The absorption of C=C stretching slighted shifted from 1557 cm^{-1} to 1582 cm^{-1} at FTIR spectrum of N-PC after LOS degradation [33]. According to the literature, the bonding of N heteroatoms into the sp²-hybridized C network can be verified between 1200 and 1600 cm^{-1}. Noteworthy,

major changes in FTIR spectra of N-PC after the process are observed in this region, with the identification of peaks at 1216 and 1516 cm^{-1} attributed to C–N and N–O stretching vibrations, respectively [42, 43]. This observation corroborates N-doped heteroatoms as important participants of the catalytic process.

Figure 6.3. (a) FTIR spectra of N-PC before and after use in losartan degradation. (b) Nitrogen sorption isotherm and pore size distribution (inset) of fresh N-PC.

(a)

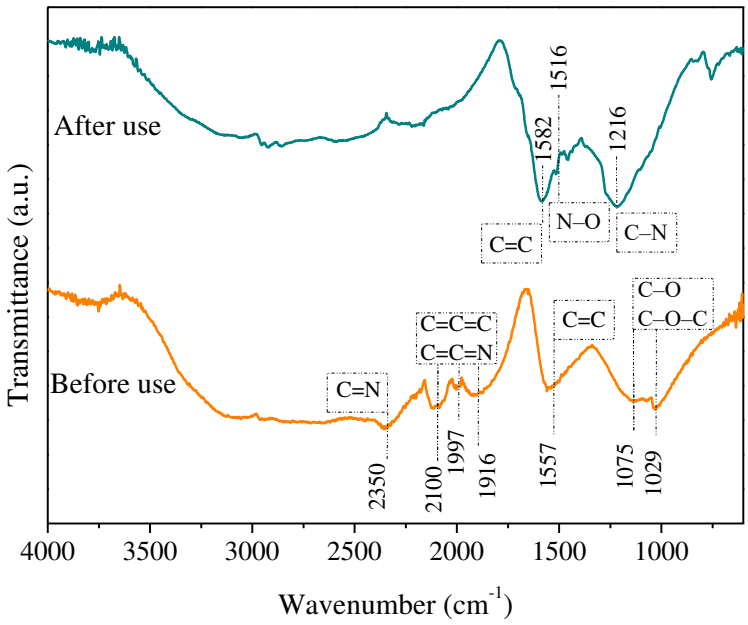

(b)

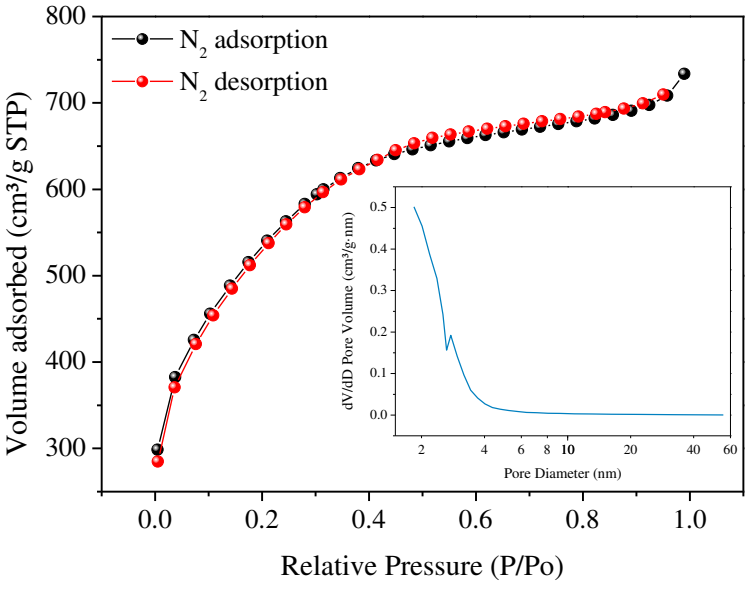

Fig. 6.3b shows N_2 sorption isotherm of the as-prepared N-PC. The type IV shape indicates a hierarchical structure rich in mesopores (widths between 2 and 50 nm) and micropore (widths < 2 nm) [44]. As expected, N-PC presented an elevated BET surface area of 1791 m^2/g, yet much lower than N-doped porous carbon (3041 m^2/g) that was previously prepared in the same experimental conditions [24]. Comparatively, the total pore volume obtained for N-PC (1.09 cm^3/g) is also inferior to that formerly reported (1.90 cm^3/g) [24]. This may indicate that in the present work the N-precursor dicyandiamide was not so well decomposed for enhanced surface area and abundant porosities. N-PC possesses a micropore volume based on the t-plot method of 0.11 cm^3/g and a mesopore volume of 0.98 cm^3/g, which was considered by deducting micropore volume from total volume. From the pore distribution of N-PC, the peak at 2.8 nm verifies the predominance of mesopores and micropores in the hierarchical architecture of N-PC.

The pH_{pzc} of the fresh N-PC was appraised as 9.2. This basic character may be ascribable to the chemical treatment (N-doping) and thermal treatment (800 °C pyrolysis), which cause the dropping of acidic active sites and rising of basic active sites. It has been shown that, apart from having electron withdrawing capacity, acidic functionalities occupy electron donating active sites of the carbon materials. So, a positive relation between basicity of carbon materials and enhanced catalytic activities has been reported [33, 45, 46]. Herein, we may infer that the basicity of N-PC would favor oxidant activation through electron transfer from the catalyst surface to PMS molecules. Moreover, electrostatic attractive forces might enhance LOS adsorption onto N-PC surface prior to PMS introduction, since LOS molecules are predominantly anionic (pK_a=4.9) in solution with natural pH of about 5.2 (discussed later in Section 6.3.6).

6.3.3 *Adsorption and catalytic oxidation of losartan*

Fig. 6.4a depicts the removal profiles of LOS by adsorption, PMS self-oxidation and catalytic degradation over N-PC. The adsorptive removal of LOS over N-PC was about 52% and the adsorption capacity was calculated as 265.2 mg/g. Previous work using similar N-PC, but in higher dosage of 0.1 g/L, reported a 39% adsorptive removal efficiency for HBA, which was also preferably adsorbed over phenol molecules (negligible uptake) [24].

Figure 6.4. (a) LOS removal by adsorption and AOP over N-PC, (b) Effect of PMS dose on LOS degradation by N-PC/PMS. Experimental conditions: $[LOS]_0$=0.04 mM, [N-PC]=0.026 g/L, [PMS]=6.5 mM, T=25 °C.

(a)

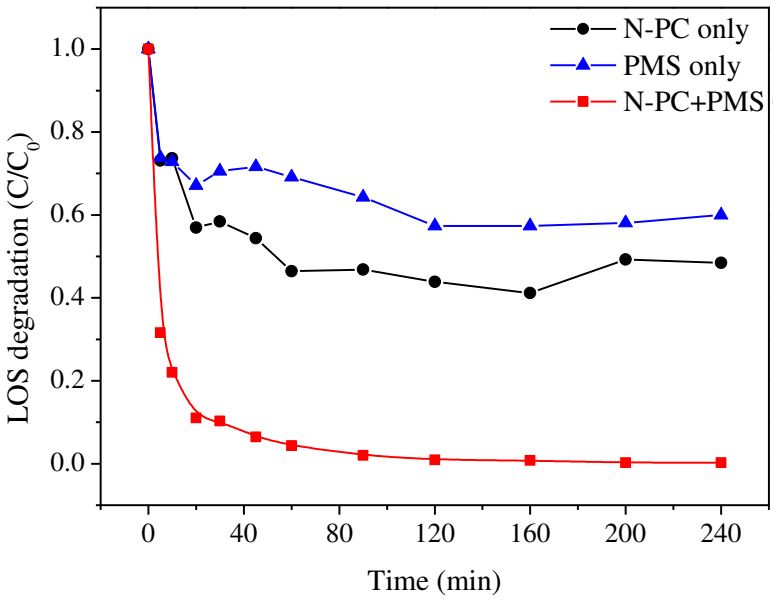

(b)

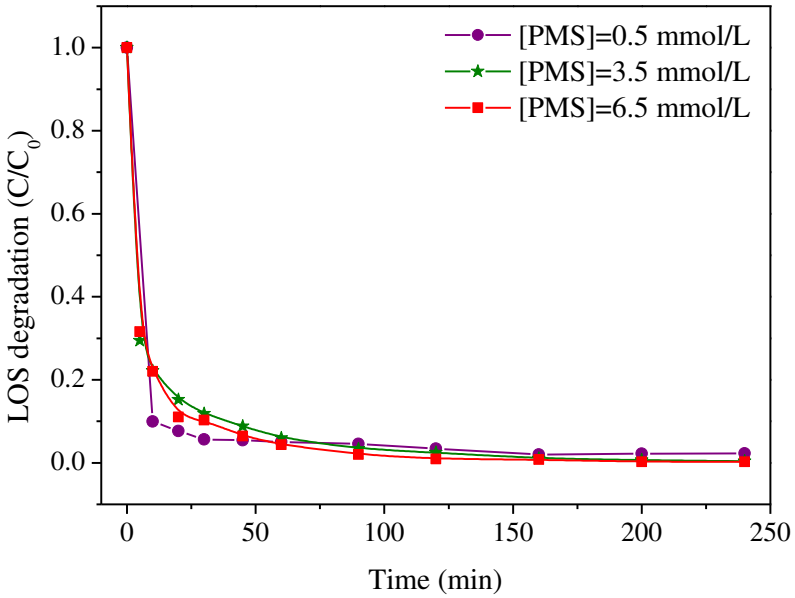

The adsorptive performance of carbons is highly dependent on textural parameters and surface chemistry. The latter has been shown to provide specific adsorption forces based on several interactions, such as π-π, H-bonding and intermolecular acid-base interactions. It has been verified that the smaller the organic pollutant, the greater the influence of surface

chemistry. Concerning phenolic compounds, functional groups in carbon surface were found to hamper adsorption. Conversely, the adsorption of other polar organics is boosted by the O- or N-containing groups [39]. Herein, the basic N-functionalities in N-PC favorably interact with acid moieties of LOS. Presumably, this acid-base interaction is stronger for LOS than for HBA or phenol, corroborating the higher adsorptive efficiencies obtained for the former contaminant in the present work. Remarkably, the graphitic degree of N-PC enables the interactions among sp^2-hybridized C and delocalized π-bond of LOS, which is recognized as a pivotal adsorptive force [23].

From Fig. 6.4a, only 36% of LOS was eliminated when PMS was applied alone. Yet PMS is a powerful oxidant (redox potential=1.82 V), it reacts slowly with the vast majority of organic pollutants and external activation is typically needed [16]. In fact, with the introduction of the N-PC catalyst, the ability of PMS to remove LOS is significantly enhanced to 100% within 240 min, which might be credited to the origination of more active radical species, *e.g.* sulfate and hydroxyl, as well as to adsorptive phenomenon on N-PC surface. As shown in Fig. S6.2, LOS degradation profile could obey the pseudo-first order kinetics (Eq. 6.2) and the apparent rate constant was 0.021 min^{-1} (R^2>0 .95) in N-PC/PMS system. The results show that even a small amount of N-PC (0.026 g/L) was sufficient to activate PMS to achieve the total degradation of LOS, proving the catalytic role of N-PC.

6.3.4 *Influence of oxidant dosage*

The outcome of PMS dosage on LOS decomposition by N-PC/PMS is illustrated in Fig. 6.4b. As PMS concentration lessened from 6.5 to 3.5 or 0.5 mmol/L, LOS degradation efficiency remained in 100–97% range after 240 min reaction time. This almost invariant performance indicates that PMS is not a restraining factor for LOS decomposition, but rather the fixed dosage of catalyst (0.026 g/L), which determines the quantity of active sites and thereby might control not only radical yields from PMS, but also N-PC adsorption capability.

Of note, 0.5 mmol/L of PMS offered the most accelerated initial LOS degradation. This is because excessive PMS loading can act as radical quencher for •OH and $SO_4^{\bullet-}$ producing $SO_5^{\bullet-}$ with relatively less reactivity (E_0=1.1 V), according to Eq. 6.3–6.7 [17, 47]:

$$HSO_5^- + {}^{\bullet}OH \rightarrow SO_5^{\bullet-} + H_2O \qquad k=1.7\times10^7 \qquad (6.3)$$

$$SO_5^{2-} + {}^{\bullet}OH \rightarrow SO_5^{\bullet-} + {}^{-}OH \qquad k=2.1\times10^9 \qquad (6.4)$$

$$HSO_5^- + SO_4^{\bullet-} + \rightarrow SO_5^{\bullet-} + HSO_4^- \qquad k<10^5 \qquad (6.5)$$

$$SO_5^{\bullet-} + SO_5^{\bullet-} \rightarrow S_2O_8^{2-} + O_2 \qquad k=1\times10^8 \qquad (6.6)$$

$$SO_5^{\bullet-} + SO_5^{\bullet-} \rightarrow SO_4^{\bullet-} + SO_4^{\bullet-} + O_2 \qquad k=1\times10^8 \qquad (6.7)$$

In this paper, the in-between PMS dosage of 3.5 mmol/L was preferred for the subsequent trials for good activation performance and to avoid an excess of PMS (6.5 mmol/L).

6.3.5 *Influence of reaction temperature*

The LOS removal profile over N-PC/PMS was examined at three solution temperatures (25, 35, and 45 °C). According to the literature, PMS alone is hardly activated under this temperature range [48, 49]. From Fig. 6.5a, LOS degradation is practically the same at 25 or 35 °C, but has a relatively faster onset at 45 °C. Broadly speaking, the reaction temperature range inspected had no major impact on system's performance. From Fig. S6.3, apparent first-order reaction rates do not follow a linear trend, which prevents the accurate estimation of activation energy of PMS over N-PC from Arrhenius correlation. Previously, the activation energy for HBA decomposition using the same catalyst was accounted as E_a=26.3 kJ/mol [24].

Figure 6.5. LOS degradation by N-PC/PMS system: (a) Effect of reaction temperature. (b) Influence of solution pH. (c) Variation of pH solution during reaction at different starting pH. (d) Effect of humic acid (20 mg/L), bicarbonate ion (5 mM) and chloride ion (5 mM) on LOS removal efficiency. Experimental conditions: $[LOS]_0$=0.04 mM, [N-PC]=0.026 g/L, [PMS]=3.5 mM, T=25 °C.

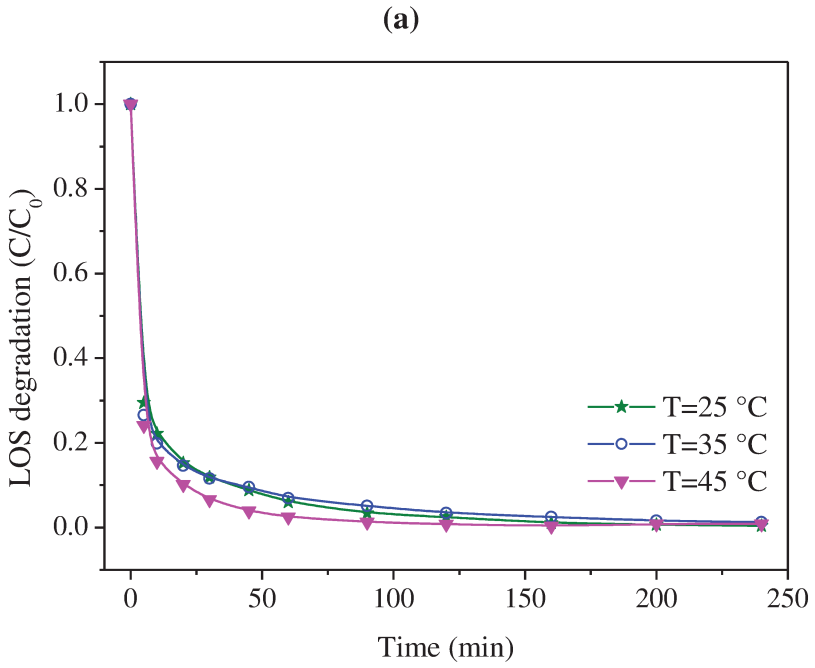

cont. **Fig. 6.5.**

(b)

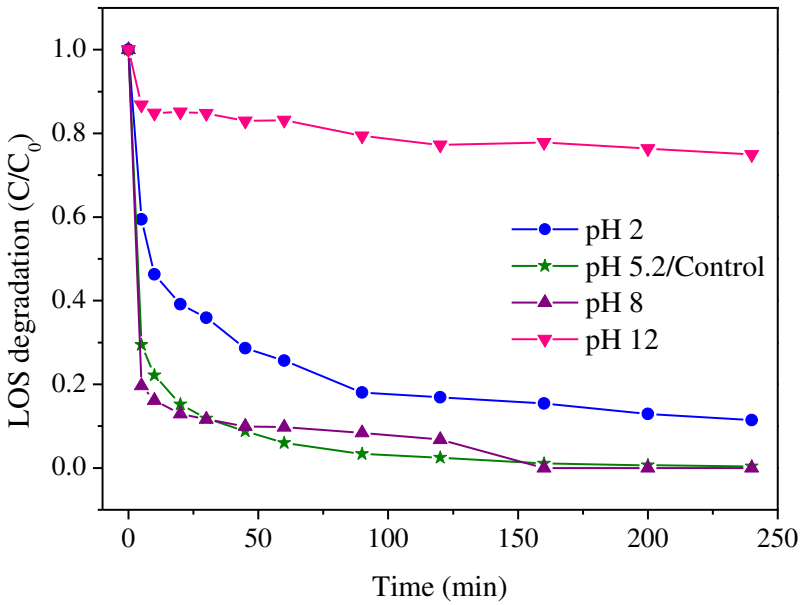

(c)

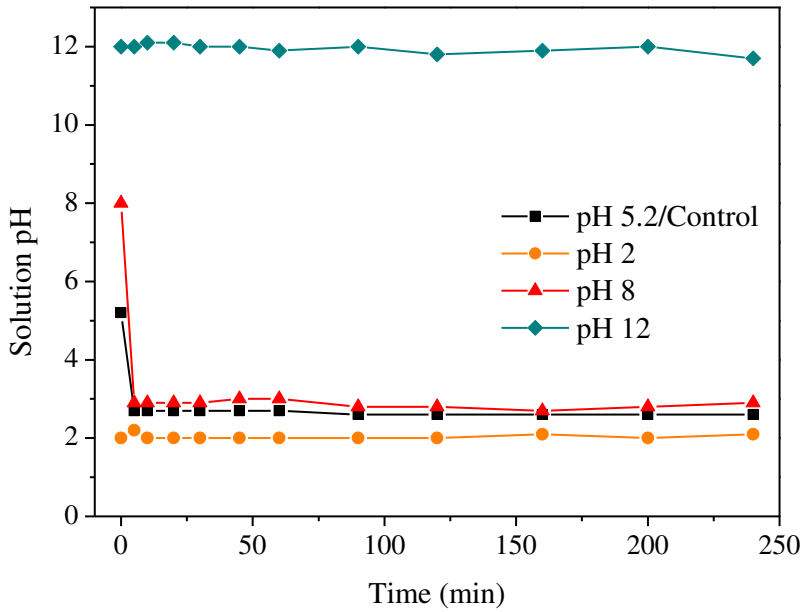

cont. **Fig. 6.5.**

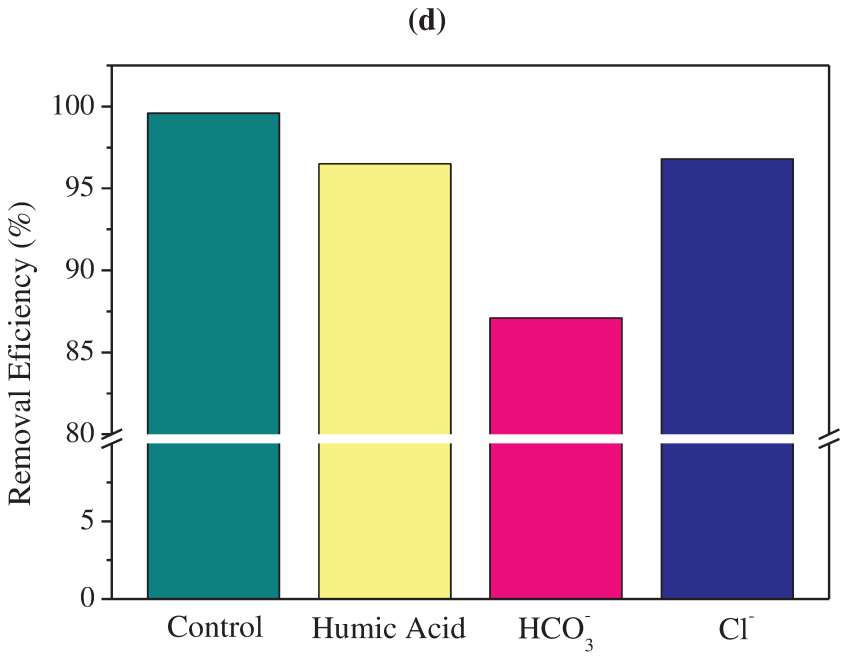

6.3.6 *Effect of initial pH*

Fig. 6.5b depicts the influence of solution pH on the LOS removal performance in N-PC/PMS system. Sulfuric acid and sodium hydroxide were used for regulating starting solution pH, and no further adjustments were made during the process. The changes in reaction solution pH were checked in the course of time, as shown in Fig. 6.5c.

LOS solution presented an initial pH 5.2, which abruptly decreased to 2.7 within 5 min of reaction. Likewise, the reaction solution was also acidified to pH 2.8 when the initial pH was pre-adjusted as 8. This is ascribable to the catalyzed PMS decomposition, which makes solution pH drop with producing protons [17]. Congruently, the LOS degradation profiles witnessed for initial pH 5.2 or 8 are similar, which can be linked to attractive interactions between the solid and the oxidant molecules. As the pH_{pzc} of N-PC is 9.2 and the second ionization constant of PMS's parent acid (H_2SO_5) is pK_{a2}=9.4, it is inferable that, at solution pH 2.8, the catalyst's surface is positively charged and HSO_5^- is the main PMS species [50].

However, at alkaline conditions, N-PC has a more negative charge and PMS exists mainly as divalent SO_5^{2-}, which might hinder PMS activation on the catalyst surface. This is accountable to the negligible change in pH solution and minimum LOS oxidation for initial pH 12. At pH 2, the solution pH was also not greatly altered during the process, which might have been prejudiced by the excess of anions in solution. The strong H-bonding between H^+ and the O–O group of HSO_5^- might impair the attractive interactions among N-PC surface and PMS

species. Analogous finding was conveyed for acetaminophen oxidation in a Fe_3O_4/PMS system [47].

Acidic or alkaline conditions also affect the distribution of LOS species in solution. With pK_a=4.9, LOS is preponderantly anionic at pH> 4.9 and cationic at pH< 4.9. At solution pH 2, LOS molecules are positively charged, as the same to the surface of N-PC. Whilst, both LOS molecules and catalyst's surface are negatively charged at pH 12. The resulting repulsive electrostatic forces at these pH conditions may hinder the interactions of LOS species and N-PC and thus jeopardize adsorption and oxidation processes.

6.3.7 *Influence of organic matter and coexisting ions*

Natural water elements, *e.g.*, natural organic matter (NOM) and inorganic anions, are reported to have either positive or detrimental influence on PMS-mediated AOPs [51, 52]. In this work, humic acid (HA), HCO_3^- and Cl^- were selected as representative water matrix constituents and their impacts on LOS elimination are shown in Fig. 6.5d. Given the decrease in removal efficiency, it is noticeable that HA dosage weakened LOS degradation over N-PC in comparison to the control test. The inhibition effect of HA may be ascribed to two factors: (i) HA owns free radical scavenging properties due to electron-rich moieties, specially phenolic groups, which may act as antioxidants [53]; (ii) HA may be adsorbed onto catalyst surface, leading to reduced availability of reactive sites for PMS activation and hindered LOS adsorption [54, 55]. Conversely, HA was previously verified to also incite PMS activation to form sulfate radicals, causing enhanced organic oxidation [56]. In this work, the detrimental impact of HA at 20 mg/L level outweighed its promotive effect for LOS degradation in PMS/N-PC system.

From Fig. 6.5d, drug removal efficiency in the presence of bicarbonate ions decreased from 99.6% to 87.1%. This may be accredited to the double action of HCO_3^- in the process: (i) scavenging hydroxyl and sulfate radicals and (ii) producing carbonate radicals, according to Eqs. 6.8 and 6.9 [57, 58]. $CO_3^{\bullet-}$ is expected in this deprotonated form, as its conjugate $HCO_3^{\bullet}$ is a strong acid with pK_a< 0 [57]. Herein, the inferior reduction potential (E_0=1.59 V) [59] of $CO_3^{\bullet-}$ oxidant in comparison to that of •OH or $SO_4^{\bullet-}$ undermined LOS degradation. Besides, HCO_3^- presence might also inflate the pH role because of buffering effect (Eq. 6.10). According to Section 6.6, increasing solution pH could contribute to drop down LOS oxidation. Similarly to the present case, detrimental influence of high levels of bicarbonate (>4 mmol/L) was also verified for atrazine degradation by $CuFe_2O_4$/PMS system [54].

$$^{\bullet}OH + HCO_3^- \rightarrow H_2O + CO_3^{\bullet-} \qquad k=8.5\times10^6\ M^{-1}s^{-1} \qquad (6.8)$$

$$SO_4^{\bullet-} + HCO_3^- \rightarrow SO_4^{2-} + H^+ + CO_3^{\bullet-} \qquad k=9.1\times10^6\ M^{-1}s^{-1} \qquad (6.9)$$

$$H_2CO_3(aq) \rightleftharpoons H^+ + HCO_3^- \qquad pK_a=6.37 \qquad (6.10)$$

$$^{\bullet}OH + Cl^- \rightleftharpoons ClOH^{\bullet-} \qquad k_f=4.3\times10^9\ M^{-1}s^{-1};\ k_r=6.1\times10^9\ s^{-1} \qquad (6.11)$$

$$SO_4^{\bullet-} + Cl^- \rightleftharpoons SO_4^{2-} + Cl^{\bullet} \qquad k_f=2.7\times10^8\ M^{-1}s^{-1};\ k_r=2.5\times10^8\ M^{-1}s^{-1} \qquad (6.12)$$

$$2Cl^- + HSO_5^- + H^+ \rightarrow SO_4^{2-} + Cl_2 + H_2O \qquad (6.13)$$

$$Cl^- + HSO_5^- \rightarrow SO_4^{2-} + HOCl \qquad (6.14)$$

Chloride ions have contrasting roles in N-PC/PMS system. On one hand, LOS degradation might be impaired due to scavenging potential of Cl^- for both •OH and $SO_4^{\bullet-}$ radicals (Eq. 6.11 and 6.12) [19, 60, 61]. On the other hand, reactive halogens (Cl_2 and OHCl) can be produced by the direct oxidation of Cl^- by PMS through nonradical pathways (Eq. 6.13 and 6.14). This can favor LOS decomposition, though a myriad of halogenated organic compounds may be formed during oxidation course [62, 63]. Given the overall decrease in LOS degradation efficiency, we may say that the negative impact of Cl^- somehow overwhelmed the positive one. The increased complexity of the reaction system in the presence of Cl^- manifested in the poor fit of pseudo-first order model (R^2= 0.10, Fig. S6.4).

6.3.8 *TOC results*

Besides degradation of the target pharmaceutical pollutant, its mineralization is a crucial factor in water/wastewater treatment perspective. Fig. 6.6a shows the removal rate of TOC under 3.5 mmol/L PMS with 0.026 g/L N-PC at 25 °C. It can be observed a major TOC removal trend in the first 75 min of the process, which agrees with the corresponding LOS removal rates from HPLC results under identical conditions (Fig. 6.4b). Within 240 min reaction time, approximately 70% of TOC removal was obtained, while LOS was completely removed from solution. Hence, it can be inferred that most of LOS and its oxidation products are not resistant to the N-PC/PMS treatment and could be partially adsorbed and/or decomposed into innocuous substances, *e.g.*, carbon dioxide and water.

Figure 6.6. Changes of TOC removal rate during LOS oxidation over N-PC/PMS. (b) Reusability of N-PC for PMS-mediated AOP of LOS. Experimental conditions: $[LOS]_0$=0.04 mM, [N-PC]=0.026 g/L, [PMS]=3.5 mM, T=25 °C.

(a)

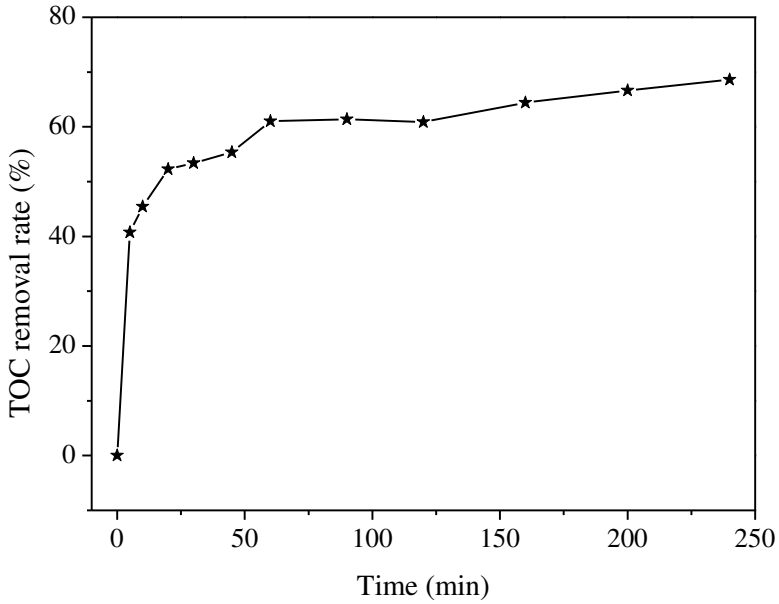

(b)

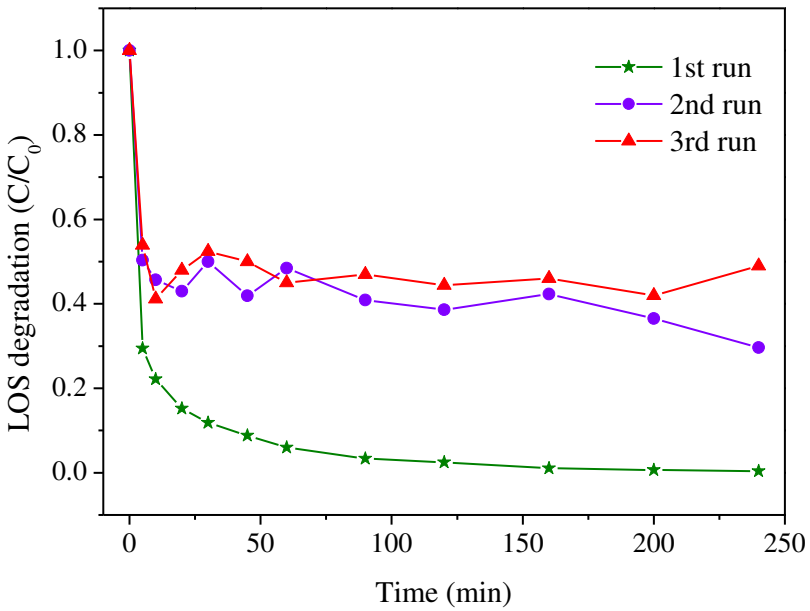

6.4 Stability tests

Fig. 6.6b reveals the stability and reusability of N-PC. LOS was totally degraded by the as-prepared catalyst within 240 min. Nevertheless, LOS removal rates dropped to 70% and 51% in the second and third cycles, accordingly. This can be related to alterations in surface chemistry and porosity of N-PC, which is bifunctional for LOS adsorption and PMS catalytic activation. As characterized in Section 6.3.2, LOS degradation modifies the pore structure, graphitic degree and N-functionalities of N-PC. These properties have remarkable effects on adsorptive interactions between N-PC and LOS molecules, as well as on catalytic active sites for PMS activation, as further disclosed here. It is also important to mention that, due to strong adsorption ability of N-PC, the washing with ethanol and water may not be sufficient for effective release of preoccupied sites on N-PC surface. This way, new adsorption of LOS in solution is refrained causing reduced reactivity for the second and third runs.

6.4.1 *EPR and scavenger quenching tests*

It is well accepted in literature that •OH and $SO_4^{\bullet-}$ radicals are intricated in PMS-mediated AOP using metal-free catalysts [19, 22, 64]. In this work, the generation and evolution of •OH and $SO_4^{\bullet-}$ during LOS degradation was examined by *in situ* EPR employing DMPO as a spin trapping agent [49, 65].

Fig. 6.7a shows both DMPO/•OH and DMPO/$SO_4^{\bullet-}$ adducts when PMS was used alone, suggesting that •OH and $SO_4^{\bullet-}$ participate in PMS-only oxidation process. It is possible to note that the introduction of N-PC effectively promoted continuous PMS activation to yield more •OH and $SO_4^{\bullet-}$. With the course of reaction time from 5 to 120 min, the peak intensities of the radicals receded due to the consumption by LOS oxidation. Furthermore, DMPO/•OH presents characteristic peaks much stronger than DMPO/$SO_4^{\bullet-}$. The relatively lower amounts of $SO_4^{\bullet-}$ can be attributed to its reaction with PMS and ^-OH to produce •OH via Eq. 6.15–6.17 [19].

$$HSO_5^- + e^- \rightarrow {}^{\bullet}OH + SO_4^{2-} \quad (6.15)$$

$$HSO_5^- + e^- \rightarrow {}^-OH + SO_4^{\bullet-} \quad (6.16)$$

$$SO_4^{\bullet-} + {}^-OH \rightarrow SO_4^{2-} + {}^{\bullet}OH \quad (6.17)$$

$$HSO_5^- + SO_5^{2-} \rightarrow HSO_4^- + SO_4^{2-} + {}^1O_2 \quad (6.18)$$

Figure 6.7. (a) EPR spectra of PMS-only system (20 min) and N-PC/PMS system at different reaction times of losartan degradation using DMPO as spin trapping agent (▼DMPO/•**OH**, ▪ DMPO/$\mathbf{SO_4^{\bullet-}}$,× HDMPO/**OH**); (b) EPR spectra of PMS-only system (30 min) and N-PC/PMS system at different reaction times of losartan degradation using TMP as spin trapping agent. Reaction conditions: $[LOS]_0$=0.04 mM, [N-PC]=0.026 g/L, [PMS]=3.5 mM, [DMPO]=80 mM, [TMP]=10 mM, T=25 °C.

(a)

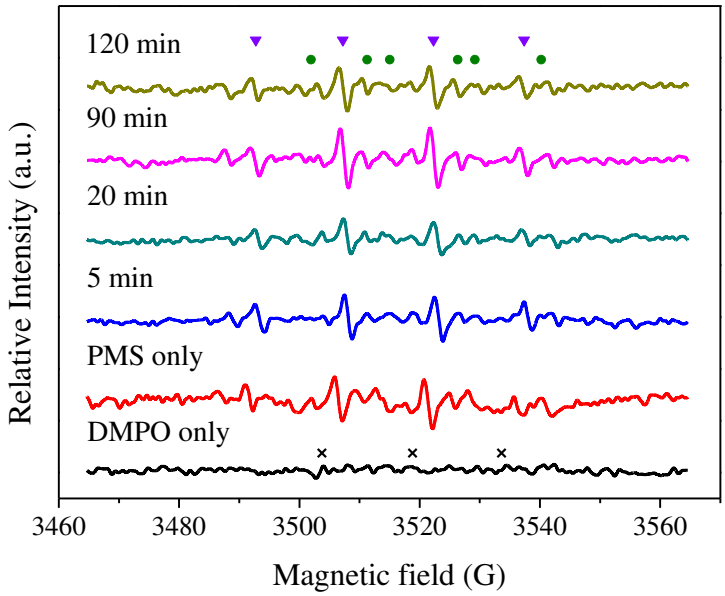

(b)

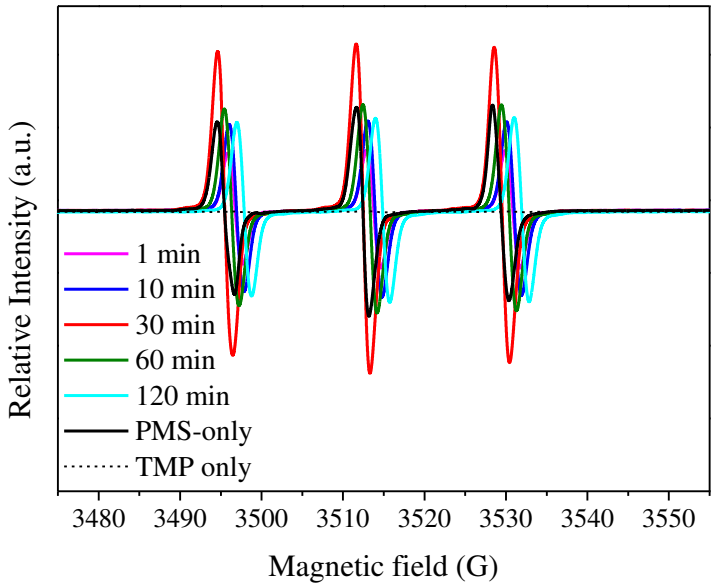

According to Eq. 6.18, the self-decomposition of PMS may generate singlet oxygen ($^1O_2$), which can work together with the free radicals •OH and $SO_4^{\bullet-}$ for enhanced degradation efficiency of PMS-mediated AOPs. Moreover, N-doped carbocatalysts have been verified to enhance PMS activation to produce further $^1O_2$ [26, 66]. In the present paper, ERP tests using TMP as a spin trapping agent were conducted to detect $^1O_2$. Fig. 6.7b exhibits no peaks for TMP alone, but the characteristic 1:1:1 triplet signal (α_N=16.9 G) can be observed when only PMS (without N-PC) was introduced into LOS solution. This spectrum may result from the production of TMP- $^1O_2$ adducts, but may also be due to the interaction between PMS and TMP, which generates analogous peaks. Nevertheless, we have noticed that adding N-PC into LOS/PMS solution led to stronger TMP triplet-peaks, indicating that greater amounts of $^1O_2$ are generated. This finding verifies that N-PC improved PMS activation and that $^1O_2$ contributes to LOS degradation. Fig. 6.7b also shows that the intensity of $^1O_2$ signals for N-PC/PMS system is utmost at 30 min, which is consistent with LOS decomposition profile that has its maximum during the first 30 min (Fig. 6.4b).

The contributions of •OH, $SO_4^{\bullet-}$ radicals, as well as $^1O_2$, were supplementally disclosed by competitive radical tests using ethanol, *tert*-butanol and sodium azide, as shown in Fig. 6.8. While EtOH is an effective scavenger of both •OH ($k_{\bullet OH}$=1.2–2.8×10^9 M^{-1}s^{-1}) and $SO_4^{\bullet-}$ ($k_{SO_4^{\bullet-}}$=1.6–7.7×10^7 M^{-1}s^{-1}), TBA has a much high scavenging effect for •OH ($k_{\bullet OH}$=3.8–7.6×10^8 M^{-1}s^{-1}) than for $SO_4^{\bullet-}$ ($k_{SO_4^{\bullet-}}$=4.0–9.1×10^5 M^{-1}s^{-1}). NaN_3 is an effective scavenger of $^1O_2$ ($k_{^1O_2}$=2×10^9 M^{-1}s^{-1}) [17].

The presence of either EtOH or TBA radical scavengers stalled LOS degradation. Notably, EtOH triggered greater inhibitory effect than TBA, pointing out that, although both •OH and $SO_4^{\bullet-}$ took part in LOS oxidation, the last reactive radical had a more preeminent role. Fig. 6.8 further reveals that, despite the lowered LOS decomposition efficiency after adding EtOH, a high LOS removal of 95% was still obtained within 240 min reaction time. Thus, it can be deduced that other oxidative pathway, which was not dependent on free radicals, dominated the pharmaceutical degradation. It was noted that NaN_3 had a quenching effect much more significant than EtOH and TBA, confirming that the nonradical oxidation by $^1O_2$ plays a major role in LOS removal. Of note, reaction temperature was found not to have a crucial impact on LOS degradation (Fig. 6.5a). This can be related to the greater effect of nonradical approach on the catalytic performance of N-PC, keeping in mind that temperature generally only controls electron transfer by typical radical-based processes [67].

Figure 6.8. LOS degradation efficiency without and with the radical scavengers ethanol, tert-butanol and sodium azide. Reaction conditions: $[LOS]_0$=0.04 mM, [N-PC]=0.026 g/L, [PMS]=3.5 mM, [EtOH]=3.5 M, [TBA]=1.75 M, $[NaN_3]$=20 mM, T=25 °C

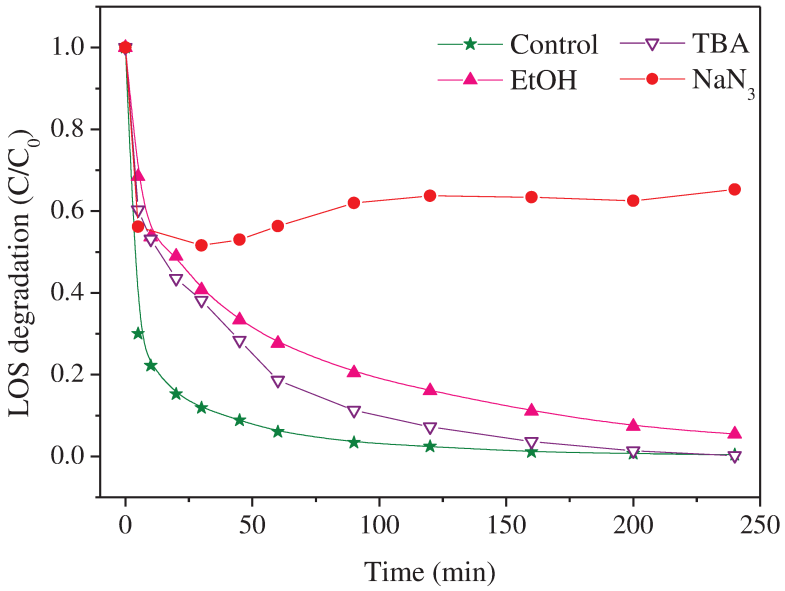

6.4.2 *Mechanistic insights to losartan degradation*

The findings of this paper reveal that N-PC performed as a bifunctional material with both a high adsorption capacity for LOS and catalytic ability for PMS activation. As a result, the complete degradation of LOS results from synergistic effects of adsorption and multi-reaction oxidation, but clarifying their individual roles in the whole process is not straightforward. Moreover, PMS self-oxidation performance for LOS degradation (36%) cannot be neglected. From EPR results, $^1O_2$ was identified to co-exist with •OH and $SO_4^{\bullet-}$ free radicals in PMS-only system. Noteworthy, PMS direct oxidation has been recently admitted to participate together with PMS decomposition to $^1O_2$ in nonradical pathways for organics degradation [68]. Therefore, PMS self-oxidation performance can be inferred as a miscellany of radical (•OH and $SO_4^{\bullet-}$) and nonradical processes ($^1O_2$ and direct oxidation).

From quenching and EPR detection tests, N-PC was verified to boost PMS activation for greater amounts of •OH and $SO_4^{\bullet-}$. These free radicals are produced through electron transport from N-PC to PMS, which has O_3SO–OH bond to be activated. This redox process is mainly induced by the free-flowing electrons of sp^2-hybridized C and unpaired electrons of defect sites in N- PC. Moreover, the carbonyl groups at the boundary sites of N-PC can mediate PMS activation to evolve $^1O_2$ reactive species, which were verified to have a major role in LOS decomposition. Complementarily, PMS can be activated/bounded on N-PC surface

without prompt liberating free radicals, generating surface confined radicals (activated complex) that co-occur with $^1O_2$ as nonradical pathways of LOS degradation [66, 69].

Subsequent to its discovery by Duan, et al. [67], the nonradical processes upon N-doping in carbocatalysts for PMS-mediate oxidation systems have been widely acknowledged [19, 26, 66]. It has been shown that N-doping intrinsically changes the electron states of the carbon network, since the electronegativity of nitrogen is superior to that of carbon (χN = 3.04 vs χC = 2.55). Doped N (especially quaternary N) attracts electrons from adjacent carbon atoms creating a positively charged carbon domain, which interacts with PMS molecules to constitute the reactive complex (surface- attached radical) for organic degradation through intramolecular electron transfer [69]. Additionally, this nonradical pathway as a surface confined reaction was reported to foster greater attractions between organic pollutants and catalyst surface [70]. In this study, adsorption can be indicated as a key step for the *in-situ* degradation of LOS by adjacent surface-attached radicals due to the elevated LOS adsorption potential onto N-PC (52%). We may infer that N doping provided N-PC not only with good adsorption sites for LOS but also with active sites for PMS activation, producing reactive complexes. Thus, N-PC and PMS constitute a complex heterogenous system, which could synergistically and effectively adsorb and oxidize LOS.

6.5 Conclusions

In summary, N-doped porous carbon was successfully replicated by the simple, cheap and available method. The textural parameters (high porosity and elevated surface area) and surface chemistry (N-functionalities) of N-PC promoted adsorptive removal of LOS (52%). LOS was totally degraded in 240 min reaction time using 0.026 g/L N-PC and 3.5 mmol/L PMS. It was verified that enhanced catalytic activity occurred at starting pH close to neutrality. Higher reaction temperature had a minor impact on the process. Humic acid, bicarbonate ion and chloride ion could weaken LOS decomposition efficiency. The 70% mineralization rate verified that the majority of LOS and intermediates are effectively degraded in N-PC/PMS system. The catalytic activity of N-PC significantly reduced after consecutive cycles, ascribable to the inherent changes in porosity, elemental composition, graphitization degree, and functional groups. N-PC was shown to activate PMS through multi-reaction pathways, but dominated by the nonradical mechanism comprising the yield of reactive complex and/or singlet oxygen.

Acknowledgments

This study was financed in part by the Coordenação de Aperfeiçoamento de Pessoal de Nível Superior - Brasil (CAPES) - Finance Code 001 [Proc. 88882.329686/2018-01; 88881.188856/2018-01, 88881.310551/2018-01], Fundação de Amparo à Pesquisa do Estado de São Paulo (FAPESP) and Conselho Nacional de Desenvolvimento Científico e Tecnológico (CNPq) [Proc. 406193/2018-5].

Appendix 6.A. Supplementary information

Supplementary data to this article can be found online at https://doi.org/10.1016/j.cej.2019.122971.

Text S6.1. Analytical Procedures

Fourier transform infrared spectrometer (FT-IR)

FT-IR spectra were recorded from 650 to 4000 cm^{-1} with a 4 cm^{-1} resolution under force gauge of 80 in attenuated total reflectance (ATR) mode using the 100-FT-IR Spectrometer (Perkin Elmer).

Scanning electron microscope with an energy dispersive spectrometer (SEM/EDS)

For SEM analysis, the samples were prepared by cleaning them with ethanol (100%) and mounting on specimen stubs. The SEM micrographs were obtained by FEI Verios XHR 460 equipment under electron high tension EHT=5.00 kV, InLens signal detector, aperture size=60 µm, working distance WD=2 mm.

Transmission electron microscope (TEM)

The TEM samples were prepared by diluting the material with ethanol (100%) under sonication, before dropping into copper grid. TEM micrographs were obtained on a JEOL 2100 equipment.

High angle annular dark field scanning transmission electron microscopy (HAADF-STEM) and energy-dispersive X-ray spectroscopy (EDX) elemental mapping

The samples were prepared in a similar way to TEM analysis. The equipment FEI Titan G2 80-200 TEM/STEM was used under high tension of 200 kV.

X-ray photoelectron spectroscopy (XPS)

XPS tests were performed on a VG Multi lab 2000 spectrometer (Kratos AXIS Ultra DLD) under ultra-high vacuum conditions. A monochromatic Al-Kα X-ray source (1486.6 eV) was used at an operating power of 225 W. Survey spectra were measured at constant pass energy of 160 eV with 1.0 eV energy step and high-resolution spectra were acquired at constant pass energy of 40 eV with 0.1 eV energy step. The binding energies were calibrated based on the C 1s line at 284.6 eV. Shirley-type background was deducted from the data and core-level spectra were decomposed into their components with mixed Gaussian–Lorentzian (20:80) shape lines employing CasaXPS software.

Nitrogen adsorption/desorption

A Micromertics TriStar 3000 was used for N_2 adsorption/desorption analysis at -196 °C. The samples were degassed at 130 °C for 4 h before the tests.

The specific surface area was calculated by the Brunauer-Emmett-Teller (BET) model. The total pore volume was computed as the volume adsorbed at a relative pressure of 0.99. The method from the Barrett, Joyner, and Halenda (BJH) was applied to determine the pore size distribution.

Paramagnetic resonance (EPR)

A Bruker EMS-plus instrument and Xeon software (Bruker) were used to obtain EPR spectra at the following conditions: room temperature, center field 3514.7 G, sweep width 150G, sweep time 30 s, modulation amplitude 1.0 G, receiver gain 30 dB, microwave power of 0.01156 mW.

The spin trapping agent, 5,5-dimethyl-1-pyrroline-*N*-oxide (DMPO, 0.08 mol/L), was used for the detection of hydroxyl (•OH) and sulfate radicals ($SO_4^{\bullet-}$). The EPR spectra were analyzed considering the hyperfine coupling constants of the adducts: α_N=α_H =14.9 G (DMPO/•OH); α_N=13.2 G, α_H=9.6 G, α_H=1.48 G, α_H=0.78 G (DMPO/$SO_4^{\bullet-}$); α_N=14.7 G, α_H=1.1 G (HDMPO/OH) [49, 65]. HDMPO/OH is produced from DMPO by oxidizing species in the system.

The spin trapping agent, 2,2,6,6-tetramethyl-4-piperidinol (TMP, 0.01 mol/L), was employed to capture EPR signals of singlet oxygen ($^1O_2$). $^1O_2$ can oxidize TMP into 2,2,6,6-tetramethyl-4-piperidinol-N-oxyl radical, which can be detected by the characteristic EPR spectrum with 1:1:1 triplet signal (α_N=16.9 G, *g*=2.0054) [26].

Regarding the experimental procedure, at determined times, 40 µL of reaction solution was collected, mixed with 40 µL DMPO or TMP in a vial and agitated for 15 s. Then, the sample was transferred to a 100 µL capillary tube for EPR analysis.

Figure S6.1. Wide survey XPS spectra of N-PC before and after use in losartan degradation.

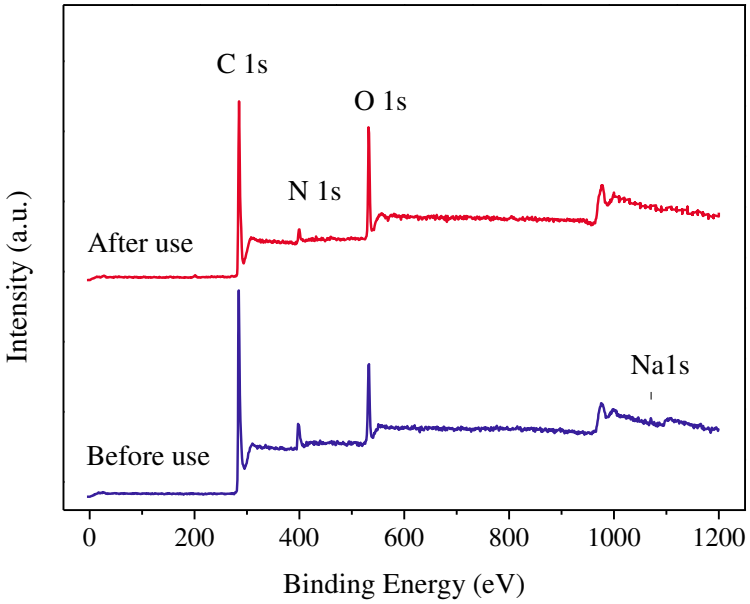

Figure S6.2. Effect of PMS dosage on pseudo-first order rate constant, k, for LOS degradation. Experimental conditions: [LOS]0=0.04 mM, [N-PC]=0.026 g/L, T=25 °C. Note: result at 0 min was not adjusted since the mixture is not homogeneous in the early stage of reaction.

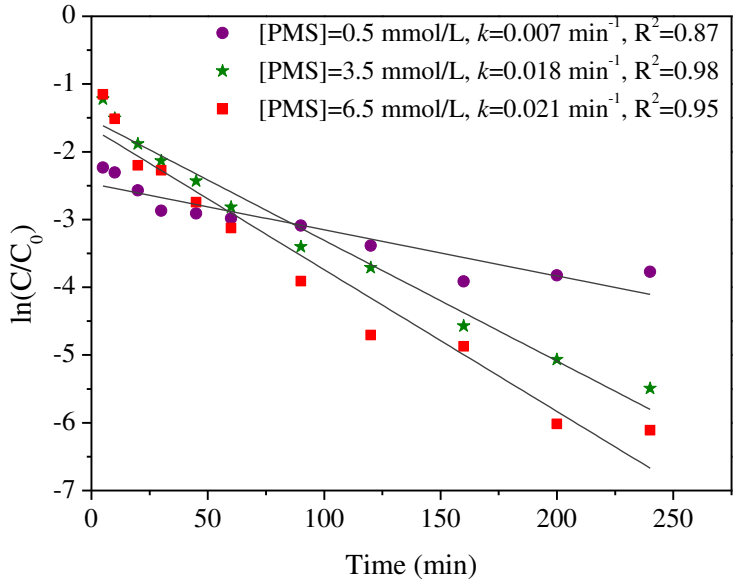

LOS degradation using 3.5 mmol/L and 6.5 mmol/L of PMS follows a pseudo-first-order kinetic pattern (R^2>0.98). However, the adjustment is not satisfactory at 0.5 mmol/L PMS concentration (R^2=0.87), what can be associated to the distinct behavior observed at this condition with more accelerated initial degradation of LOS in N-PC/PMS system. This indicates that at 0.5 mmol/L PMS, the process is more complex and cannot be represented by pseudo-first-order model.

Figure S6.3. (a) Effect of temperature on pseudo-first order rate constant, *k*, for LOS degradation. (b) Plot of rate constant versus inverse temperature. Experimental conditions: $[LOS]_0$=0.04 mM, [PMS]=3.5 mM, [N-PC]=0.026 g/L. Note: result at 0 min was not adjusted since the mixture is not homogeneous in the early stage of reaction.

(a)

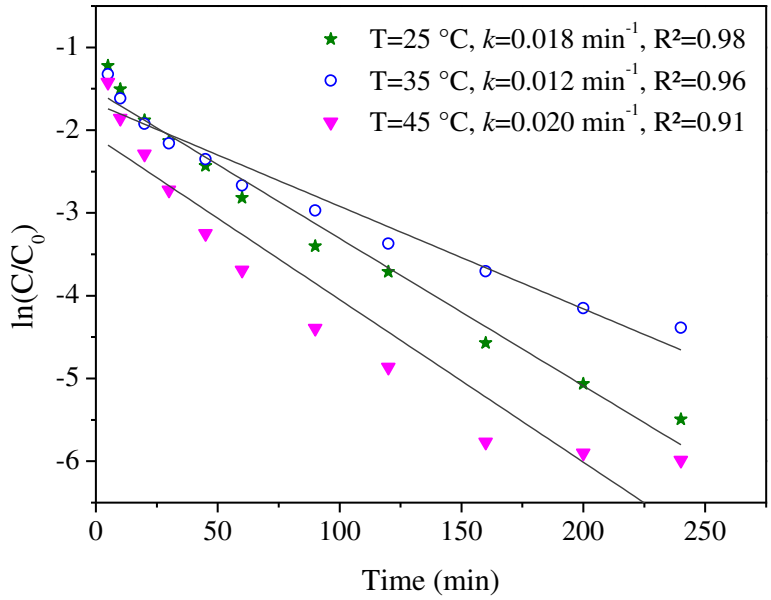

(b)

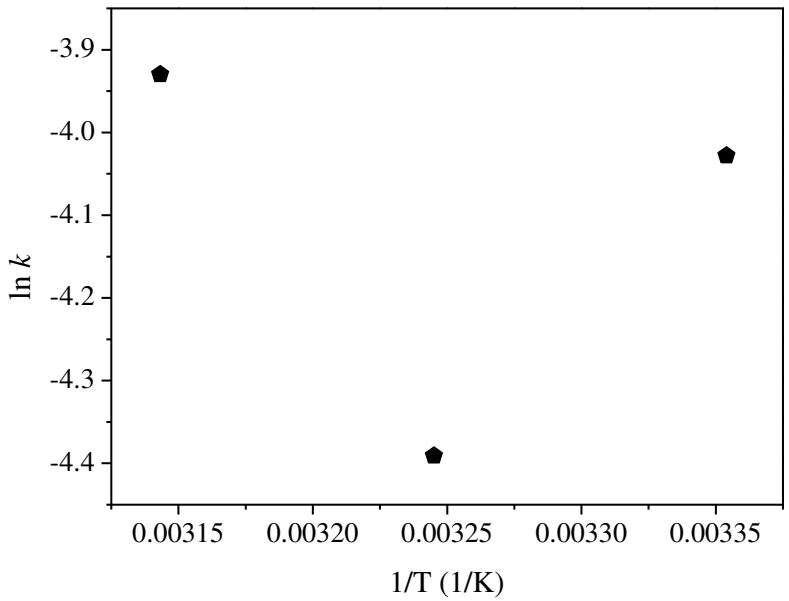

Fig. S6.3a shows the fittings of pseudo-first order kinetics to LOS degradation at different temperatures. The rate constants obtained are very close to each other, what evidences the relative scant impact of temperature on the process.

From Fig. S6.3b, $\ln k$ *vs.* $1/T$ plot does not follow a linear trend. This fact impairs the accurate calculation of activation energy from Arrhenius equation, which presupposes the following linear relation:

$$\ln k = \ln A - E_a/RT \quad \text{(S1)}$$

where: k=rate constant, A=pre-exponential factor, R=universal gas constant (8.314 J/(mol K)), T=temperature (K).

Figure S6.4. Effect of humic acid (HA) (20 mg/L), HCO_3^- (5 mM) and Cl^- (5 mM) on pseudo-first order rate constant, k, for LOS degradation. Experimental conditions: [LOS]0=0.04 mM, [PMS]=3.5 mM, [N-PC]=0.026 g/L, T=25 °C. Note: result at 0 min was not adjusted since the mixture is not homogeneous in the early stage of reaction.

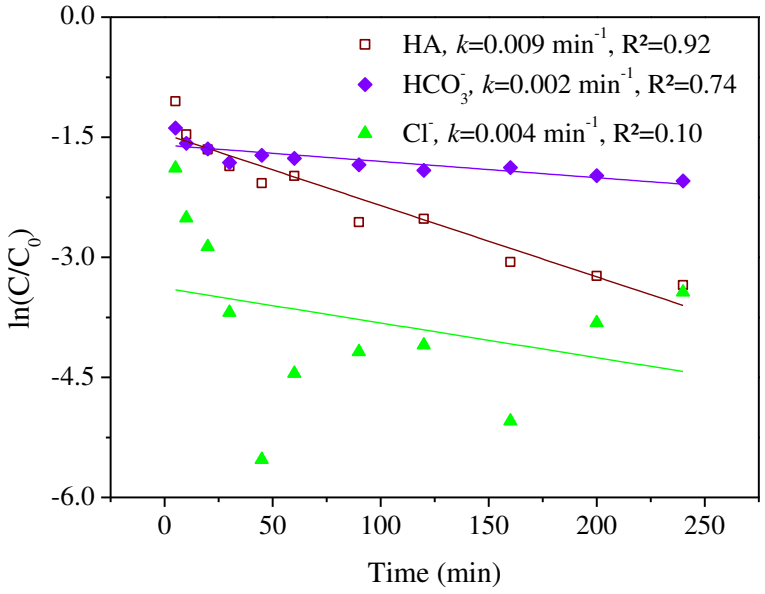

The detrimental effect of HA addition on LOS removal is evidenced by the reduction of the pseudo-first rate constant from k=0.018 min^{-1} (control test) to k=0.009 min^{-1}. The poor fittings of pseudo-first order kinetics to LOS degradation profile in the presence of HCO_3^- or Cl^- indicate increased complexity of reaction systems, but no further conclusions can be drawn.

References

[1] NCD Risk Factor Collaboration (NCD-RisC), Worldwide trends in blood pressure from 1975 to 2015: a pooled analysis of 1479 population-based measurement studies with 19.1 million participants, Lancet 389 (2017) 37-55.

[2] Food and Drug Administration, Review of Environmental Assessment for Cozaar Tablets (50 and 100 mg Losartan Potassium), Center for Drug Evaluation and Research, FDA, 2002.

[3] R.C. Williams, M.S. Alasandro, V.L. Fasone, R.J. Boucher, J.F. Edwards, Comparison of liquid chromatography, capillary electrophoresis and super-critical fluid chromatography in the determination of Losartan Potassium drug substance in Cozaar® tablets, J. Pharm. Biomed. Anal. 14 (1996) 1539-1546.

[4] A.A. Godoy, F. Kummrow, P.A.Z. Pamplin, Ecotoxicological evaluation of propranolol hydrochloride and losartan potassium to *Lemna minor* L. (1753) individually and in binary mixtures, Ecotoxicology 24 (2015) 1112-1123.

[5] M.B. Campanha, A.T. Awan, D.N.R. de Sousa, G.M. Grosseli, A.A. Mozeto, P.S. Fadini, A 3-year study on occurrence of emerging contaminants in an urban stream of São Paulo State of Southeast Brazil, Environ. Sci. Pollut. Res. 22 (2015) 7936-7947.

[6] V. Osorio, A. Larrañaga, J. Aceña, S. Pérez, D. Barceló, Concentration and risk of pharmaceuticals in freshwater systems are related to the population density and the livestock units in Iberian Rivers, Sci. Total Environ. 540 (2016) 267-277.

[7] A.A. Godoy, F. Kummrow, P.A.Z. Pamplin, Occurrence, ecotoxicological effects and risk assessment of antihypertensive pharmaceutical residues in the aquatic environment - a review, Chemosphere 138 (2015) 281-291.

[8] G.Z. Kyzas, A. Koltsakidou, S.G. Nanaki, D.N. Bikiaris, D.A. Lambropoulou, Removal of beta-blockers from aqueous media by adsorption onto graphene oxide, Sci. Total Environ. 537 (2015) 411-420.

[9] G.S. Maia, J.R. de Andrade, M.G.C. da Silva, M.G.A. Vieira, Adsorption of diclofenac sodium onto commercial organoclay: Kinetic, equilibrium and thermodynamic study, Powder Technol. 345 (2019) 140-150.

[10] M.F. Oliveira, M.G.C. da Silva, M.G.A. Vieira, Equilibrium and kinetic studies of caffeine adsorption from aqueous solutions on thermally modified Verde-lodo bentonite, Appl. Clay Sci. 168 (2019) 366-373.

[11] M.F. Oliveira, V.M. de Souza, M.G.C. da Silva, M.G.A. Vieira, Fixed-bed adsorption of caffeine onto thermally modified Verde-lodo bentonite, Ind. Eng. Chem. Res. 57 (2018) 17480-17487.

[12] G.S. Maia, J.R. Andrade, M.F. Oliveira, M.G.A. Vieira, M.G.C. Silva, Affinity studies between drugs and clays as adsorbent material, Chem. Eng. Trans. 57 (2017) 583-588.

[13] J.R. de Andrade, M.F. Oliveira, M.G.C. da Silva, M.G.A. Vieira, Adsorption of pharmaceuticals from water and wastewater using nonconventional low-cost materials: a review, Ind. Eng. Chem. Res. 57 (2018) 3103-3127.

[14] M.A. Sousa, C. Gonçalves, V.J.P. Vilar, R.A.R. Boaventura, M.F. Alpendurada, Suspended TiO_2-assisted photocatalytic degradation of emerging contaminants in a municipal WWTP effluent using a solar pilot plant with CPCs, Chem. Eng. J. 198-199 (2012) 301-309.

[15] C. Salazar, N. Contreras, H.D. Mansilla, J. Yáñez, R. Salazar, Electrochemical degradation of the antihypertensive losartan in aqueous medium by electro-oxidation with boron-doped diamond electrode, J. Hazard. Mater. 319 (2016) 84-92.

[16] J. Wang, S. Wang, Activation of persulfate (PS) and peroxymonosulfate (PMS) and application for the degradation of emerging contaminants, Chem. Eng. J. 334 (2018) 1502-1517.

[17] F. Ghanbari, M. Moradi, Application of peroxymonosulfate and its activation methods for degradation of environmental organic pollutants: review, Chem. Eng. J. 310 (2017) 41-62.

[18] P. Hu, M. Long, Cobalt-catalyzed sulfate radical-based advanced oxidation: a review on heterogeneous catalysts and applications, Appl. Catal. B 181 (2016) 103-117.

[19] J. Kang, L. Zhou, X. Duan, H. Sun, S. Wang, Catalytic degradation of antibiotics by metal-free catalysis over nitrogen-doped graphene, Catal. Today (2018), https://

doi.org/10.1016/j.cattod.2018.12.002.

[20] X. Chen, W.-D. Oh, Z.-T. Hu, Y.-M. Sun, R.D. Webster, S.-Z. Li, T.-T. Lim, Enhancing sulfacetamide degradation by peroxymonosulfate activation with N-doped graphene produced through delicately-controlled nitrogen functionalization via tweaking thermal annealing processes, Appl. Catal. B 225 (2018) 243-257.

[21] J. Kang, X. Duan, C. Wang, H. Sun, X. Tan, M.O. Tade, S. Wang, Nitrogen-doped bamboo-like carbon nanotubes with Ni encapsulation for persulfate activation to remove emerging contaminants with excellent catalytic stability, Chem. Eng. J. 332 (2018) 398-408.

[22] T.D. Minh, M.C. Ncibi, V. Srivastava, S.K. Thangaraj, J. Jänis, M. Sillanpää, Gingerbread ingredient-derived carbons-assembled CNT foam for the efficient peroxymonosulfate-mediated degradation of emerging pharmaceutical contaminants, Appl. Catal. B 244 (2019) 367-384.

[23] W. Tian, H. Zhang, H. Sun, M.O. Tadé, S. Wang, Template-free synthesis of N-doped carbon with pillared-layered pores as bifunctional materials for supercapacitor and environmental applications, Carbon 118 (2017) 98-105.

[24] W. Tian, H. Zhang, H. Sun, M.O. Tadé, S. Wang, One-step synthesis of flour-derived functional nanocarbons with hierarchical pores for versatile environmental applications, Chem. Eng. J. 347 (2018) 432-439.

[25] H. Sun, Y. Wang, S. Liu, L. Ge, L. Wang, Z. Zhu, S. Wang, Facile synthesis of nitrogen doped reduced graphene oxide as a superior metal-free catalyst for oxidation, Chem. Commun. 49 (2013) 9914-9916.

[26] P. Liang, C. Zhang, X. Duan, H. Sun, S. Liu, M.O. Tade, S. Wang, An insight into metal organic framework derived N-doped graphene for the oxidative degradation of persistent contaminants: formation mechanism and generation of singlet oxygen from peroxymonosulfate, Environ. Sci. Nano 4 (2017) 315-324.

[27] G. Wang, S. Chen, X. Quan, H. Yu, Y. Zhang, Enhanced activation of peroxymonosulfate by nitrogen doped porous carbon for effective removal of organic pollutants, Carbon 115 (2017) 730-739.

[28] X. Duan, Z. Ao, D. Li, H. Sun, L. Zhou, A. Suvorova, M. Saunders, G. Wang, S. Wang, Surface-tailored nanodiamonds as excellent metal-free catalysts for organic oxidation, Carbon 103 (2016) 404-411.

[29] P. Liang, C. Zhang, X. Duan, H. Sun, S. Liu, M.O. Tade, S. Wang, N-Doped graphene from metal–organic frameworks for catalytic oxidation of p-hydroxylbenzoic acid: N-functionality and mechanism, ACS Sustainable Chem. Eng. 5 (2017) 2693-2701.

[30] Y. Long, S. Bu, Y. Huang, Y. Shao, L. Xiao, X. Shi, N-doped hierarchically porous carbon for highly efficient metal-free catalytic activation of peroxymonosulfate in water: A non-radical mechanism, Chemosphere 216 (2019) 545-555.

[31] Z. Zhu, J. Ma, C. Ji, Y. Liu, W. Wang, F. Cui, Nitrogen doped hierarchically structured porous carbon fibers with an ultrahigh specific surface area for removal of organic dyes, RSC Adv. 8 (2018) 19116-19124.

[32] L. Nielsen, M.J. Biggs, W. Skinner, T.J. Bandosz, The effects of activated carbon surface features on the reactive adsorption of carbamazepine and sulfamethoxazole, Carbon 80 (2014) 419-432.

[33] Y. Guo, Z. Zeng, Y. Zhu, Z. Huang, Y. Cui, J. Yang, Catalytic oxidation of aqueous organic contaminants by persulfate activated with sulfur-doped hierarchically porous carbon derived from thiophene, Appl. Catal. B 220 (2018) 635-644.

[34] Y. Saito, T. Yoshikawa, S. Bandow, M. Tomita, T. Hayashi, Interlayer spacings in carbon nanotubes, Phys. Rev. B 48 (1993) 1907-1909.

[35] J. Lu, J.-x. Yang, J. Wang, A. Lim, S. Wang, K.P. Loh, One-pot synthesis of fluorescent carbon nanoribbons, nanoparticles, and graphene by the exfoliation of graphite in ionic liquids, ACS Nano 3 (2009) 2367-2375.

[36] J. Wang, H. Liu, X. Gu, H. Wang, D.S. Su, Synthesis of nitrogen-containing ordered mesoporous carbon as a metal-free catalyst for selective oxidation of ethylbenzene, Chem. Commun. 50 (2014) 9182-9184.

[37] A. Zahoor, M. Christy, Y.J. Hwang, Y.R. Lim, P. Kim, K.S. Nahm, Improved electrocatalytic activity of carbon materials by nitrogen doping, Appl. Catal. B 147 (2014) 633-641.

[38] A. Ganguly, S. Sharma, P. Papakonstantinou, J. Hamilton, Probing the thermal deoxygenation of graphene oxide using high-resolution in situ X-ray-based spectroscopies, J. Phys. Chem. C 115 (2011) 17009-17019.

[39] T.J. Bandosz, C.O. Ania, Chapter 4 Surface chemistry of activated carbons and its characterization, in: T.J. Bandosz (Ed.), Interface Science and Technology, Elsevier, 2006, pp. 159-229.

[40] S. Shang, W. Dai, L. Wang, Y. Lv, S. Gao, Metal-free catalysis of nitrogen-doped nanocarbons for the ammoxidation of alcohols to nitriles, Chem. Commun. 53 (2017) 1048-1051.

[41] X.-F. Li, K.-Y. Lian, L. Liu, Y. Wu, Q. Qiu, J. Jiang, M. Deng, Y. Luo, Unraveling the formation mechanism of graphitic nitrogen-doping in thermally treated graphene with ammonia, Sci. Rep. 6 (2016) 23495.

[42] V. Ţucureanu, A. Matei, A.M. Avram, FTIR Spectroscopy for carbon family study, Crit. Rev. Anal. Chem. 46 (2016) 502-520.

[43] A. Misra, P.K. Tyagi, M.K. Singh, D.S. Misra, FTIR studies of nitrogen doped carbon nanotubes, Diamond Relat. Mater. 15 (2006) 385-388.

[44] M. Thommes, K. Kaneko, A.V. Neimark, J.P. Olivier, F. Rodriguez-Reinoso, J. Rouquerol, K.S.W. Sing, Physisorption of gases, with special reference to the evaluation of

surface area and pore size distribution (IUPAC Technical Report), Pure Appl. Chem. 87 (2015) 1051-1069.

[45] R.S. Ribeiro, A.M.T. Silva, J.L. Figueiredo, J.L. Faria, H.T. Gomes, The influence of structure and surface chemistry of carbon materials on the decomposition of hydrogen peroxide, Carbon 62 (2013) 97-108.

[46] P. Serp, J.L. Figueiredo, Carbon Materials for Catalysis, John Wiley & Sons, Hoboken, NJ, 2009.

[47] C. Tan, N. Gao, Y. Deng, J. Deng, S. Zhou, J. Li, X. Xin, Radical induced degradation of acetaminophen with Fe_3O_4 magnetic nanoparticles as heterogeneous activator of peroxymonosulfate, J. Hazard. Mater. 276 (2014) 452-460.

[48] S. Yang, P. Wang, X. Yang, L. Shan, W. Zhang, X. Shao, R. Niu, Degradation efficiencies of azo dye Acid Orange 7 by the interaction of heat, UV and anions with common oxidants: persulfate, peroxymonosulfate and hydrogen peroxide, J. Hazard. Mater. 179 (2010) 552-558.

[49] J. Cui, L. Zhang, B. Xi, J. Zhang, X. Mao, Chemical oxidation of benzene and trichloroethylene by a combination of peroxymonosulfate and permanganate linked by in-situ generated colloidal/amorphous MnO_2, Chem. Eng. J. 313 (2017) 815-825.

[50] D.L. Ball, J.O. Edwards, The kinetics and mechanism of the decomposition of Caro's Acid. I, JACS 78 (1956) 1125-1129.

[51] W.-D. Oh, S.-K. Lua, Z. Dong, T.-T. Lim, Performance of magnetic activated carbon composite as peroxymonosulfate activator and regenerable adsorbent via sulfate radical-mediated oxidation processes, J. Hazard. Mater. 284 (2015) 1-9.

[52] Z. Zhao, J. Zhao, C. Yang, Efficient removal of ciprofloxacin by peroxymonosulfate/Mn_3O_4-MnO_2 catalytic oxidation system, Chem. Eng. J. 327 (2017) 481-489.

[53] M.V. Zykova, I.A. Schepetkin, M.V. Belousov, S.V. Krivoshchekov, L.A. Logvinova, K.A. Bratishko, M.S. Yusubov, S.V. Romanenko, M.T. Quinn, Physicochemical Characterization and Antioxidant Activity of Humic Acids Isolated from Peat of Various Origins, Molecules 23 (2018) 753.

[54] Y.-H. Guan, J. Ma, Y.-M. Ren, Y.-L. Liu, J.-Y. Xiao, L.-q. Lin, C. Zhang, Efficient degradation of atrazine by magnetic porous copper ferrite catalyzed peroxymonosulfate oxidation via the formation of hydroxyl and sulfate radicals, Water Res. 47 (2013) 5431-5438.

[55] J. Kang, H. Zhang, X. Duan, H. Sun, X. Tan, S. Wang, Nickel in hierarchically structured nitrogen-doped graphene for robust and promoted degradation of antibiotics, J. Cleaner Prod. 218 (2019) 202-211.

[56] Y. Pang, Z.-h. Tong, L. Tang, Y.-n. Liu, K. Luo, Effect of humic acid on the degradation of methylene blue by peroxymonosulfate, Open Chemistry 16 (2018) 401-406.

[57] G. Czapski, S.V. Lymar, H.A. Schwarz, Acidity of the carbonate radical, J. Phys. Chem. A 103 (1999) 3447-3450.

[58] L. Dogliotti, E. Hayon, Flash photolysis of per[oxydi]sulfate ions in aqueous solutions. The sulfate and ozonide radical anions, J. Phys. Chem. 71 (1967) 2511-2516.

[59] R.E. Huie, C.L. Clifton, P. Neta, Electron transfer reaction rates and equilibria of the carbonate and sulfate radical anions, Int. J. Radiat. Appl. Instrum., Part C: Radiat. Phys. Chem. 38 (1991) 477-481.

[60] H.V. Lutze, N. Kerlin, T.C. Schmidt, Sulfate radical-based water treatment in presence of chloride: Formation of chlorate, inter-conversion of sulfate radicals into hydroxyl radicals and influence of bicarbonate, Water Res. 72 (2015) 349-360.

[61] G.L. Truong, J.D. Laat, B. Legube, Effects of chloride and sulfate on the rate of oxidation of ferrous ion by H_2O_2, Water Res. 38 (2004) 2384-2394.

[62] S. Qu, C. Li, X. Sun, J. Wang, H. Luo, S. Wang, J. Ta, D. Li, Enhancement of peroxymonosulfate activation and utilization efficiency via iron oxychloride nanosheets in visible light, Sep. Purif. Technol. 224 (2019) 132-141.

[63] Z. Wang, R. Yuan, Y. Guo, L. Xu, J. Liu, Effects of chloride ions on bleaching of azo dyes by Co^{2+}/oxone regent: kinetic analysis, J. Hazard. Mater. 190 (2011) 1083-1087.

[64] Y. Wang, Z. Ao, H. Sun, X. Duan, S. Wang, Activation of peroxymonosulfate by carbonaceous oxygen groups: experimental and density functional theory calculations, Appl. Catal. B 198 (2016) 295-302.

[65] E. Finkelstein, G.M. Rosen, E.J. Rauckman, Spin trapping of superoxide and hydroxyl radical: practical aspects, Arch. Biochem. Biophys. 200 (1980) 1-16.

[66] D. Li, X. Duan, H. Sun, J. Kang, H. Zhang, M.O. Tade, S. Wang, Facile synthesis of nitrogen-doped graphene via low-temperature pyrolysis: the effects of precursors and annealing ambience on metal-free catalytic oxidation, Carbon 115 (2017) 649-658.

[67] X. Duan, H. Sun, Y. Wang, J. Kang, S. Wang, N-doping-induced nonradical reaction on single-walled carbon nanotubes for catalytic phenol oxidation, ACS Catal. 5 (2015) 553-559.

[68] R. Yin, W. Guo, H. Wang, J. Du, X. Zhou, Q. Wu, H. Zheng, J. Chang, N. Ren, Selective degradation of sulfonamide antibiotics by peroxymonosulfate alone: direct oxidation and nonradical mechanisms, Chem. Eng. J. 334 (2018) 2539-2546.

[69] X. Duan, H. Sun, Z. Shao, S. Wang, Nonradical reactions in environmental remediation processes: uncertainty and challenges, Appl. Catal. B 224 (2018) 973-982.

[70] X. Wang, Y. Qin, L. Zhu, H. Tang, Nitrogen-Doped Reduced Graphene Oxide as a Bifunctional Material for Removing Bisphenols: synergistic Effect between Adsorption and Catalysis, Environ. Sci. Technol. 49 (2015) 6855-6864.

CAPÍTULO 7. Discussão Geral

Considerando os impactos dos contaminantes farmacêuticos emergentes na saúde humana e no meio ambiente, há um consenso sobre a necessidade de estudos sobre tecnologias avançadas de tratamento terciário ou de polimento para remoção efetiva de fármacos de água e efluentes. A losartana potássica é um contaminante farmacêutico emergente preocupante, pois é um dos anti-hipertensivos mais consumidos mundialmente e tem crescente presença detectada em água e efluentes. Desta forma, o presente trabalho de doutorado foi desenvolvido com a intenção de avaliar o processo de adsorção e o processo de oxidação catalítica como duas tecnologias promissoras para a remoção de losartana de solução aquosa.

No que se refere ao processo adsortivo, a seleção do material adsorvente é um dos fatores primordiais, já que está essencialmente vinculada à capacidade de remoção de contaminantes bem como aos custos de operação. Neste sentido, há crescente interesse pela comunidade científica em adsorventes substitutos ao carvão ativado comercial, cujo alto custo relativo restringe o emprego em larga escala. No presente trabalho de doutorado, propôs-se a avaliação da argila Spectrogel Tipo-C como adsorvente não convencional e de baixo custo para a remoção de losartana. A argila Spectrogel é uma argila brasileira do tipo bentonita organofílica, cuja potencialidade adsortiva vem sendo consolidada em variados estudos conduzidos pelo grupo de pesquisa no qual a autora do presente trabalho se insere. O teste preliminar de afinidade, discutido no Capítulo 3 e com resultados sumarizados na Fig. 7.1, confirmou a Spectrogel como material argiloso eminente para a adsorção de losartana potássica com remoção de até 99% nas condições avaliadas.

Figura 7.1. Porcentagem de remoção de cloridrato de propranolol (PRO), cloridrato de metformina (MET), losartana potássica (LOS) e amoxicilina trihidratada (AMO) por argilas.

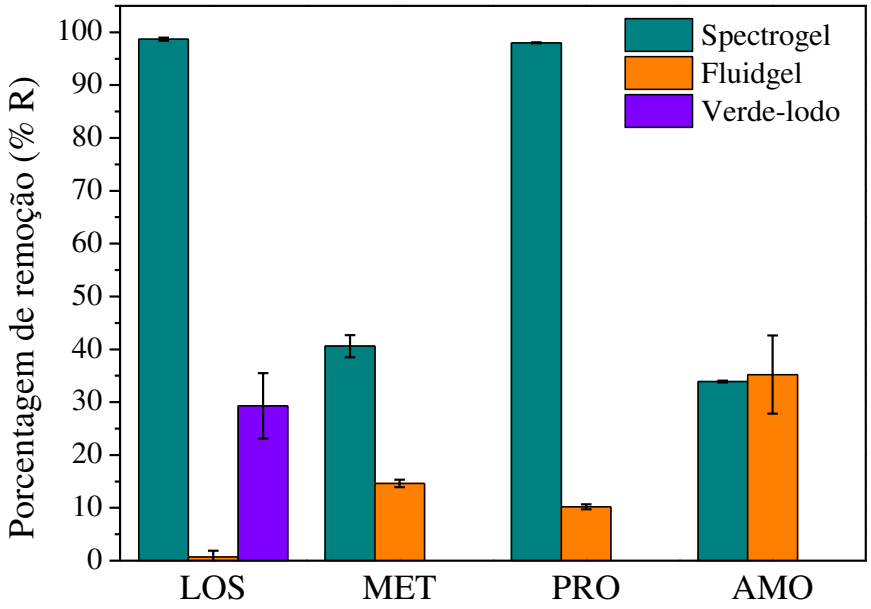

Os estudos aprofundados de adsorção em banho finito demonstraram que a argila Spectrogel apresenta melhor performance de remoção de losartana do que um carvão ativado comercial derivado de casca de coco, que foi referenciado como µGAC. Conforme sintetizado na Tabela 7.1 e amplamente discutido no Capítulo 4, a Spectrogel apresenta cinética de adsorção mais rápida, maior valor de constante cinética e maior porcentagem de remoção do que µGAC nas mesmas condições experimentais. Com relação ao equilíbrio de adsorção, a capacidade máxima de adsorção de losartana estimada pela isoterma de Langmuir foi quase o dobro para a Spectrogel em comparação com o µGAC.

Dentre outras tantas características avaliadas no Capítulo 4, o µGAC sendo um carvão ativado distingue-se por uma estrutura com alto teor de micro- e mesoporos, e área específica de cerca de SSA=567 m²/g. Por outro lado, a Spectrogel é majoritariamente não porosa com baixa área específica de SSA=0,14 m²/g. Desta forma, os resultados de melhor desempenho adsortivo da Spectrogel em relação ao µGAC estão associados aos grupos funcionais na superfície da argila.

Tabela 7.1. Comparação de cinética e equilíbrio de adsorção de losartana potássica usando argila organofílica, Spectrogel, e carvão ativado comercial derivado de casca de coco, µGAC.

	Spectrogel	**µGAC**
Tempo para atingir o equilíbrio de adsorção[a]	2200 min	2600 min
Constante cinética do modelo de pseudossegunda ordem[a]	0,017 g/(mol.min)	0,016 g/(mol.min)
Porcentagem de remoção total[a]	98%	94%
Comportamento isoterma de adsorção[b]	Extremamente favorável	Extremamente favorável
Capacidade máxima de adsorção de Langmuir[b]	0,082 mmol/g	0,044 mmol/g
Capacidade de adsorção normalizados pela área específica	0,59 mmol/m²	$7{,}8\times10^{-5}$ mmol/m²

[a] Dados do estudo cinético de adsorção conduzido nas condições de: [adsorvente] = 6 g/L; [losartana] = 0,1 mmol/L; 0-3240 min; 25 °C; 200 rpm.

[b] Dados do estudo de equilíbrio de adsorção conduzido nas condições de: [adsorvente] = 6 g/L; [losartana] = 0,004-3,00 mmol/L; 25 °C; 200 rpm; 48 horas.

Dados de capacidade de adsorção normalizados pela área específica (q_{max}/SSA) da Tabela 7.1 revelam que a argila Spectrogel tem maior superfície disponível para a adsorção, enquanto que o µGAC tem elevada microporosidade e consequentemente menor superfície acessível para moléculas de losartana. Em outras palavras, µGAC oferece efeitos de peneiramento molecular mais pronunciados do que a argila Spectrogel. Conforme estudo de otimização de geometria molecular do Capítulo 5, a losartana tem dimensão máxima de aproximadamente 1,46 nm. Este valor é muito próximo do limítrofe de classificação de microporos da IUPAC, *i.e.*, diâmetro de poros menor que 2 nm (THOMMES et al., 2015).

A química de superfície também pode ser invocada para elucidar a maior afinidade das moléculas de losartana pela Spectrogel, pois materiais argilosos são caracteristicamente mais ricos em sítios carregados/polares do que materiais a base de carbono como o carvão ativado. De fato, espectros de FT-IR (Figura 4.3c do Capítulo 4) expõem a maior abundância de grupos funcionais na argila Spectrogel do que no µGAC. Neste sentido, infere-se que os grupos funcionais da molécula de losartana podem interagir com os grupos funcionais da Spectrogel. Por exemplo, ligações não covalentes do tipo cátion-π podem ocorrer. Com relação a interações eletrostáticas, pode-se dizer que estas não têm papel determinante na remoção de losartana pela Spectrogel, pois na condição natural de pH da solução de aproximadamente 7.6 a superfície da argila apresenta-se majoritariamente negativa, bem como a molécula de fármaco que tem

pka=4.9. Além do processo de adsorção em si, o mecanismo de partição na fase orgânica da Spectrogel pode contribuir para a remoção da losartana de solução. O bom ajuste do modelo de pseudossegunda ordem reforça a ocorrência do mecanismo de adsorção química da losartana em Spectrogel, enquanto que a elevada correspondência da isoterma de Freundlich aos dados de equilíbrio é indicativo de processo multicamadas em superfície adsortiva energeticamente heterogênea.

A possibilidade de regeneração e reuso dos adsorventes é aspecto fundamental na avaliação técnico-econômica de um processo de adsorção. Com relação à Spectrogel, estudos de regeneração térmica mostram-se proibitivos considerando o perfil de degradação deste material e da losartana adsorvida. Conforme Figura 4.4 do Capítulo 4, o pico de degradação da losartana em ~323 °C é muito próximo ao da Spectrogel em ~329 °C. No caso da regeneração química, o metanol mostrou eficiência de dessorção de 65%, mas tem aplicação controversa devido à elevada toxicidade. Neste cenário, a abordagem de disposição final da Spectrogel saturada com aterramento ou incineração seria a mais indicada. Isso não torna a Spectrogel menos atraente, pois no caso de adsorventes naturalmente abundantes e de relativo baixo custo como argilas, pode ser economicamente mais vantajoso adquirir novos adsorventes frescos do que investir em métodos de regeneração mais sofisticados, como extração supercrítica, degradação oxidativa ou degradação biológica.

Até o presente momento, tanto quanto é do conhecimento da autora, não há na literatura outros estudos sobre a temática de adsorção de losartana potássica. Por isso, o desempenho de adsorção de losartana não pôde ser contrastado com adsorventes que não a argila Spectrogel e o carvão ativado μGAC, que foram adotados neste projeto de doutorado. Contudo, no que tange à argila Spectrogel, sua elevada potencialidade como adsorvente de fármacos foi estabelecida não somente para a losartana, mas também para o anti-inflamatório diclofenaco de sódio conforme estudo prévio desenvolvido pelo grupo de pesquisa (MAIA, 2017; MAIA et al., 2019). Comparativamente, nota-se que ambos os processos de adsorção de losartana e de diclofenaco em Spectrogel são termodinamicamente espontâneos e endotérmicos. Já os testes de equilíbrio de adsorção realizados a 15 °C, que foi a temperatura em comum avaliada nos trabalhos, forneceram capacidade máxima de adsorção de Langmuir de q_{max} = 0,048 mmol/g para a losartana e de q_{max} = 0,086 mmol/g para o diclofenaco. A capacidade de adsorção mais elevada do diclofenaco indica que a Spectrogel tem maior afinidade por este fármaco do que losartana. Para melhor avaliar tal comportamento, foram realizados testes em modo contínuo usando colunas de leito fixo empacotadas com Spectrogel para a adsorção monocomponente de

losartana, que é o contaminante farmacêutico foco deste trabalho, bem como de diclofenaco para fins comparativos.

Conforme discutido no Capítulo 5, dentro das faixas avaliadas de concentração inicial (0,05−0,15 mmol/L) e de vazão volumétrica de alimentação (0,4−1,0 mL/min), a condição de 0,15 mmol/L e 0,4 mL/min foi a mais eficiente, levando em consideração os menores valores de altura de zona de transferência de massa no leito fixo empacotado com Spectrogel. Os principais parâmetros de eficiência de adsorção obtidos nesta condição de operação contínua são compilados na Tabela 7.2.

Tabela 7.2. Parâmetros experimentais das curvas de ruptura de adsorção de losartana potássica e de diclofenaco de sódio em Spectrogel na condição de concentração de entrada de 0,15 mmol/L e vazão de alimentação de 0,4 mL/min.

	Losartana	**Diclofenaco**
Tempo de ruptura, t_b	32 min	123 min
Quantidade útil removida até o ponto de ruptura, q_b	0,0013 mmol/g	0,0047 mmol/g
Remoção até o ponto de ruptura, REM_b	89%	88%
Tempo de exaustão, t_e	3810 min	1700 min
Quantidade total removida, q_e	0,0288 mmol/g	0,0322 mmol/g
Altura da zona de transferência de massa, h_{MTZ}	4,4 cm	4,3 cm

A elevada porcentagem de remoção até o ponto de ruptura obtida para ambos os fármacos consolida a Spectrogel como adsorvente promissor a ser empregado em larga escala no tratamento de soluções com concentração de fármacos ainda mais baixas e próximas daquelas encontradas em amostras reais de água e efluentes, bem como misturas complexa multicomponentes. Contudo, destacamos que os sistemas contínuos avaliados apresentaram grande resistência difusional com perfis de curva de ruptura alongados e zonas de transferência de massa elevadas em relação ao comprimento total dos leitos empacotados com Spectrogel. Por conseguinte, o modelo fenomenológico proposto de difusão de dois sítios, referenciado como DualSD (do inglês, *Dual site diffusion*), apresentou elevada correlação aos resultados experimentais. Isso porque o modelo assume que existe não apenas uma taxa de difusão, mas duas, cada qual atuando em momentos distintos durante a operação dos leitos empacotados.

Conforme a Tabela 7.2, o diclofenaco foi mais eficientemente adsorvido do que a losartana pela Spectrogel nas mesmas condições experimentais de operação em modo contínuo. Destacadamente, o sistema contendo diclofenaco apresenta tempo de ruptura mais longo e

maiores quantidades útil e total removidas até o ponto de ruptura e exaustão, respectivamente. Estes resultados corroboram aqueles obtidos nos estudos de adsorção descontínua em banho finito. O melhor desempenho da Spectrogel na remoção de diclofenaco do que de losartana pode ser relativamente elucidada invocando as propriedades físico-químicas e os parâmetros de reatividade química das moléculas de fármaco. Destacadamente, a molécula de losartana é menos hidrofóbica e mais solúvel em água do que a molécula de diclofenaco. Consequentemente, a losartana tem maior afinidade com a fase líquida e deve adsorver na superfície da Spectrogel com maior dificuldade do que o diclofenaco. Ademais, a losartana tem maior peso molecular de 461,01 g/mol do que o diclofenaco, que tem 318,13 g/mol. De acordo com cálculos de geometria otimizada, as moléculas de losartana e de diclofenaco tem dimensões máximas de cerca de 1,5 nm e 1,2 nm, respectivamente. Com isso, a losartana pode causar efeitos de impedimento estérico mais pronunciados, de forma que as moléculas de fármaco podem cobrir sítios adjacentes da superfície da Spectrogel, impedindo-os de se ligarem efetivamente a novas moléculas. Por fim, descritores moleculares das estruturas otimizadas mostram que a molécula de diclofenaco tem maior reatividade química, *e.g.*, menor energia gap entre os orbitais HOMO e LUMO e menor dureza química, o que pode vir a favorecer sua adsorção pela Spectrogel.

Em suma, os testes de adsorção demonstraram o potencial da argila Spectrogel como adsorvente não convencional de contaminante farmacêutico emergente. Porém, apesar de simples e eficaz, o processo de adsorção apresentou desafios relacionados especialmente à grande resistência difusional no leito fixo e à regeneração e disposição do adsorvente saturado. Neste sentido, este projeto de doutorado traz a avaliação de outro método avançado de tratamento terciário, nomeadamente um POA que visa à degradação eficiente de fármaco de solução, mas que tem como limitação a geração de subprodutos. Somando estudos em adsorção e estudos em POA, a tese oferece maior complexidade, abrangência e relevância na área ambiental.

O POA avaliado, mais especificamente o processo de oxidação catalítica heterogênea usando carbono poroso e peroximonossulfato (HSO_5^-, PMS), oferece diversos diferenciais. Primeiro, essa abordagem promove a geração não somente de radicais livres hidroxila •OH e sulfato $SO_4^{\bullet-}$, mas também de oxigênio singlete $^1O_2$. Segundo, o catalisador selecionado de carbono com estrutura hierarquicamente porosa dopado com nitrogênio (N-PC) é inovador, ambientalmente amigável e tem síntese simples, inspirada na fabricação de pães utilizando farinha de trigo como fonte de carbono e bicarbonato de sódio como agente de inchamento, além de diciandiamida como fonte de átomos N e hidróxido de potássio como agente ativador

químico. O grupo de pesquisa da *Curtin University*, onde a autora desta tese realizou estágio de pesquisa, verificou preliminarmente que o catalisador N-PC oferece alta ativação de PMS para a degradação eficiente de moléculas orgânicas simples, *e.g.*, fenol e ácido p-hidroxibenzoico (TIAN et al., 2018b). Isso incentivou a avaliação do sistema N-PC/PMS na oxidação catalítica do contaminante farmacêutico losartana potássica.

A Fig. 7.2 mostra a porcentagem de remoção de losartana obtida usando exclusivamente N-PC (adsorção), PMS sozinho (oxidação) e N-PC juntamente com PMS (oxidação catalítica).

Figura 7.2. Porcentagens de remoção de losartana potássica por adsorção usando N-PC, e por oxidação usando PMS ou N-PC e PMS. Condições experimentais de: [N-PC] = 0,026 g/L; [losartana] = 0,04 mmol/L; [PMS] = 6,5 mmol/L; 25 °C; 240 min.

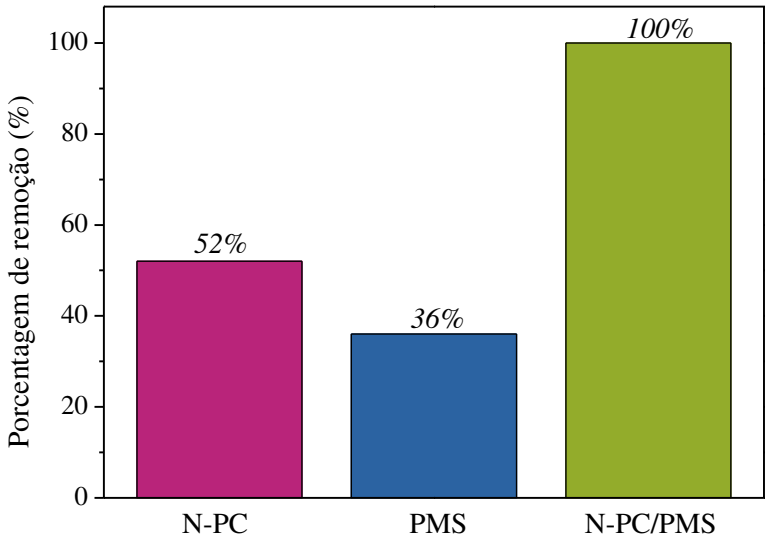

Notavelmente, o N-PC apresenta um elevado potencial adsorção de losartana, o que pode ser associado à sua elevada área específica, que é aproximadamente 1.791 m²/g, e aos grupos funcionais da superfície contendo nitrogênio, em especial nitrogênio piridínico. O PMS é um oxidante forte e quando aplicado sozinho forneceu remoção de losartana de 36%. Contudo, a performance de remoção aumentou significantemente para 100% com a adição de N-PC ao sistema. Desta forma, ficou clara a relevância do N-PC como material bifuncional que atua não somente na adsorção de losartana, mas também na ativação catalítica de PMS para geração aprimorada de espécies reativas. O papel determinante do N-PC fica ainda mais evidente ao considerar que a diminuição da concentração de PMS no sistema de 6,5 para 0,5 mmol/L não causa impacto expressivo na eliminação da losartana. Em suma, a remoção de losartana no sistema N-PC/PMS ocorreu por processos sinérgicos de adsorção e degradação.

A degradação de losartana pode ocorrer via mecanismos envolvendo radicais livres ou não, conforme ilustrado na Fig. 7.3. No primeiro caso, o PMS é ativado por transferência de elétrons do N-PC com geração dos radicais livres •OH e $SO_4^{\bullet-}$. Por outro lado, o mecanismo sem radicais envolve a espécie altamente reativa oxigênio singlete $^1O_2$, bem como a oxidação direta por PMS por meio de complexo reativo. Testes de ressonância paramagnética eletrônica e testes de inibição revelaram que, apesar de •OH e $SO_4^{\bullet-}$ participarem do processo, o mecanismo oxidativo que não depende dos radicais livres é que tem o papel predominante na degradação de losartana no sistema N-PC/PMS.

Figura 7.3. Ilustração das diferentes vias de reação de ativação de PMS para a degradação de losartana potássica em carbono poroso dopado com nitrogênio.

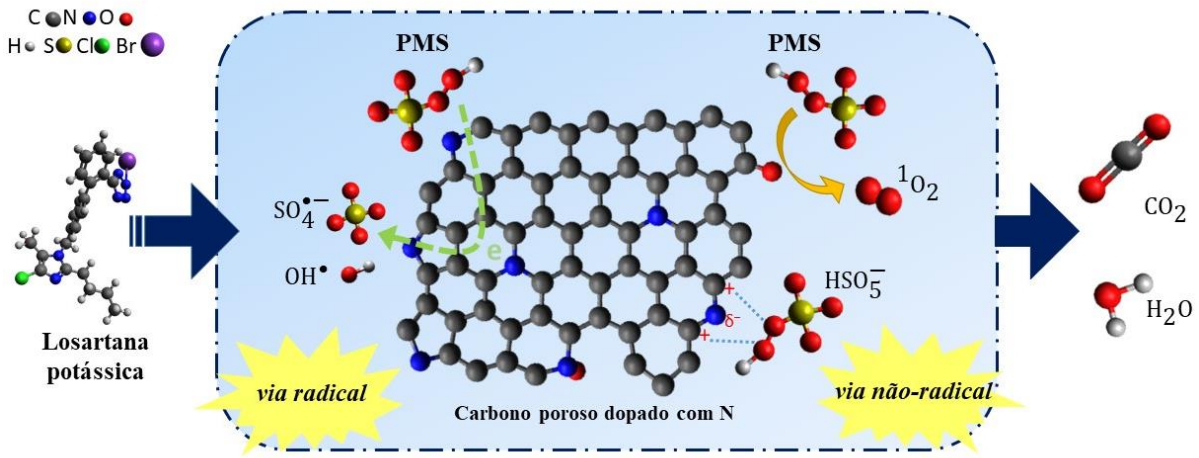

FONTE: adaptado de DE ANDRADE et al., 2020.

As características químicas aprimoradas do catalisador N-PC são essenciais na sua atividade catalítica. Destacadamente, a hibridização sp^2 do carbono introduz elétrons livres para ativação de PMS, gerando •OH e $SO_4^{\bullet-}$; os grupos funcionais contendo oxigênio, como carbonila, mediam a ativação de PMS liberando $^1O_2$; e a dopagem com nitrogênio modifica o estado eletrônico da rede de carbono, criando regiões positivamente carregadas que interagem com o PMS criando complexos ativados que reagem diretamente com as moléculas de losartana.

A avaliação da taxa de mineralização e da estabilidade do catalisador é fundamental no estudo de POAs. No caso do sistema N-PC/PMS, testes de carbono orgânico total revelaram que cerca de 70% da losartana e de seus intermediários de reação foram efetivamente adsorvidos ou degradados a substâncias inócuas, como dióxido de carbono e água. Os 30%

restantes representam os subprodutos de reação, cuja identificação foi impossibilitada por limitações de equipamentos e reagentes. Além disso, testes de estabilidade mostraram que o N-PC tem capacidade de adsorção e atividade catalítica reduzidas significativamente de 100% para 51% após uso em três ciclos consecutivos, o que pode ser atribuído às mudanças inerentes na porosidade, composição elementar, grau de grafitização e grupos funcionais.

A geração de subprodutos desconhecidos, a baixa estabilidade, e o reduzido potencial de reuso do N-PC são certamente fatores limitantes do processo de oxidativo avançado usando N-PC e PMS para a degradação total de losartana potássica. Ademais, é importante mencionar que o N-PC preparado é um pó extremamente fino e leve, cuja retirada de solução após o uso exige processos adicionais de separação como filtração ou centrifugação. Neste sentido, uma alternativa é a introdução de propriedades magnéticas ao catalisador; porém, o custo final do material bem como o potencial de contaminação secundária por lixiviação de metais durante o processo são certamente barreiras. Portanto, maiores pesquisas são requeridas visando ao desenvolvimento de adsorventes/catalisadores com bom custo-benefício, alta estabilidade durante o tratamento e fácil separação de solução.

Concluindo, o presente trabalho de doutorado demonstrou que as tecnologias de adsorção e de oxidação catalítica são promissoras para a remediação de contaminantes farmacêuticos emergentes, mas com desafios e limitações inerentes sob a perspectiva de eficiência, custos, sustentabilidade, poluição secundária, entre outros.

CAPÍTULO 8. Conclusões Gerais e Sugestões

A presente tese de doutorado demonstrou que o processo de adsorção e processo oxidativo avançado são duas tecnologias promissoras para a remoção do contaminante farmacêutico emergente losartana potássica de solução aquosa. O processo de adsorção foi conduzido utilizando uma argila brasileira do tipo bentonita organofílica, Spectrogel-Tipo C. Por outro lado, o processo de oxidação catalítica utilizou catalisador inovador e sustentável a base de carbono com estrutura porosa e dopado com nitrogênio, o N-PC, para ativação de peroximonossulfato (PMS). De modo geral, foi possível contribuir para a elucidação dos mecanismos de adsorção ou degradação de losartana potássica de soluções sintéticas e atestar os principais desafios e limitações de cada uma das técnicas com relação à eficiência, custos e sustentabilidade. Destacadamente, o processo de adsorção em argila Spectrogel oferece elevada resistência difusional que se traduz em elevados tempos de saturação em leito fixo e a regeneração ou disposição final do adsorvente saturado merece atenção. Em contrapartida, a geração de subprodutos e a perda de atividade catalítica do catalisador N-PC no processo oxidativo avançado são dificuldades a serem contornadas. Isso posto, os achados deste trabalho poderão embasar futuros estudos sobre a remoção de contaminantes farmacêuticos emergentes por adsorventes ou catalisadores não convencionais.

Diante dos resultados obtidos, as principais conclusões deste trabalho são:

- A argila do tipo bentonita organofílica Spectrogel tem elevada afinidade e potencial de remoção de 99% de losartana em determinadas condições experimentais, o que encoraja sua aplicação como adsorvente;
- A melhor dosagem de Spectrogel foi estabelecida como 6 g/L e o pH inicial da solução na faixa entre 2,5 e 10 não teve impacto significativo no processo descontínuo de adsorção de losartana usando Spectrogel;
- Os dados de cinética e de equilíbrio de adsorção em banho finito de losartana em Spectrogel foram bem ajustados pela equação de pseudossegunda ordem e pela isoterma de Freundlich, respectivamente. A difusão externa foi identificada como o mecanismo de transferência de massa mais relevante. Termodinamicamente, o processo de adsorção de losartana pela Spectrogel é endotérmico e espontâneo;
- Em comparação à argila Spectrogel (2200 min, 0,082 mmol/g), o carvão ativado de casca de coco (μGAC) apresentou cinética mais lenta (2600 min) e menor capacidade máxima de adsorção de losartana (0,044 mmol/g);

- Análises de caracterização mostraram que a química de superfície é mais importante que as propriedades texturais, como porosidade e área específica, na remoção de losartana por Spectrogel e por μGAC;
- O metanol forneceu uma eficiência de dessorção de 65% da losartana; porém aplicar a argila Spectrogel uma única vez, sem regeneração, pode ser recomendado considerando aspectos econômicos e ambientais;
- A adsorção contínua de losartana em coluna de leito fixo empacotada com Spectrogel teve melhor desempenho, considerando menores alturas de zona de transferência de massa, na condição de maior concentração de alimentação (0,15 mmol/L) e menor vazão (0,4 mmol/L). O modelo desenvolvido neste trabalho, *Dual site diffusion* (DualSD), apresentou melhor ajuste às curvas de ruptura se comparado aos modelos convencionais de Thomas, Yoon-Nelson e Yan e colaboradores (*Modified dose-response,* MDR) ou o modelo fenomenológico proposto por Georgin e colaboradores (*Instantaneous local equilibrium*, ILE);
- A análise de espectroscopia de fotoelétrons de raios X (XPS) revelou modificações na composição química da superfície de Spectrogel após o processo de adsorção contínua de losartana;
- Nas mesmas condições de operação da coluna de leito fixo empacotada com Spectrogel, o fármaco diclofenaco de sódio foi mais eficientemente adsorvido do que a losartana. A capacidade de adsorção no ponto de saturação foi 0,020 mmol/g para losartana e 0,032 mmol/g para diclofenaco;
- O maior potencial de remoção da Spectrogel pelo diclofenaco em comparação a losartana foi associado às propriedades físico-químicas e aos descritores de reatividade molecular destes fármacos. O diclofenaco tem maior hidrofobicidade, menor solubilidade em água, melhor ajuste estéreo-seletivo, e maior reatividade molecular, devido aos valores mais baixos de energia gap dos orbitais HOMO e LUMO e dureza molecular;
- O catalisador N-PC foi preparado com sucesso seguindo um método simples, barato e disponível;
- O N-PC foi caracterizado antes e após a degradação de losartana e verificou-se alterações na sua estrutura porosa, composição elementar, grau de grafitização e grupos funcionais;

- Considerando um rendimento de aproximadamente 2,75 %(m/m), o custo de produção do catalisador foi estimado em US$12,03/g;
- O N-PC quando aplicado sozinho propiciou 52% de remoção de losartana por adsorção. O PMS isoladamente promoveu 36% de degradação de losartana. No sistema contendo N-PC e PMS, a losartana foi totalmente degradada após 240 minutos de tempo de reação;
- Verificou-se uma maior atividade catalítica em pH inicial próximo da neutralidade; a elevação da temperatura de reação teve impacto ínfimo no processo, e a presença de ácido húmico, íon bicarbonato ou íon cloreto prejudicou a decomposição de losartana;
- A taxa de mineralização de 70% confirmou que a maior parte da losartana e de seus intermediários foram efetivamente degradados no sistema N-PC/PMS;
- O N-PC apresentou baixa estabilidade e potencial de reuso em ciclos consecutivos e a remoção de losartana se limitou a 51% ao final do terceiro ciclo;
- Demonstrou-se que o catalisador N-PC ativa o PMS através de múltiplas vias, mas com domínio do mecanismo de oxidação sem radicais, que envolve a produção de complexo reativo ou oxigênio singlete.

Para dar continuidade às pesquisas relacionadas ao tratamento avançado de contaminantes farmacêuticos, sugere-se:

- Testes de adsorção contínua em coluna de leito fixo encamisada para controle da temperatura, visando à maiores quantidades adsorvidas e maior produtividade;
- Combinação de modificações orgânicas, inorgânicas ou tratamentos térmicos para obtenção de argilas com maiores capacidades de adsorção e estabilidade para reuso;
- Devido à coexistência de contaminantes em águas residuais reais, são necessários estudos para investigar o desempenho da argila Spectrogel na presença simultânea de íons e matéria-orgânica, por exemplo;
- Testes de adsorção e de oxidação utilizando soluções sintéticas com concentrações mais próximas às naturalmente verificadas em matrizes aquáticas contaminadas com losartana;
- Testes de adsorção e de oxidação em sistemas sintéticos multicomponente, com a presença de outros contaminantes farmacêuticos emergentes;

- Avaliação da performance da adsorção e da oxidação catalítica para o tratamento de efluentes reais provenientes, por exemplo, de indústrias farmacêuticas;
- Modificação do catalisador a base de carbono para maior eficiência de ativação de PMS e estabilidade para reuso em ciclos;
- Avaliação do ciclo de vida do adsorvente e do catalisador propostos;
- Estudos em combinação de tecnologias avançadas, como por exemplo, PMS ativado e ozonização.

CAPÍTULO 9. Produção Científica Gerada no Período

Publicações em periódicos internacionais indexados

Comparative adsorption of diclofenac sodium and losartan potassium in organophilic clay-packed fixed-bed: X-ray photoelectron spectroscopy characterization, experimental tests and theoretical study on DFT-based chemical descriptors
Autores: Julia R. de Andrade, Maria F. Oliveira, Rafael L. S. Canevesi, Richard Landers, Meuris G. C. da Silva, Melissa G. A. Vieira
Journal of Molecular Liquids, v.312, p.113427, 2020.
DOI: 10.1016/j.molliq.2020.113427

Performance of organoclay in adsorptive uptake of antihypertensive losartan potassium: a comparative batch study using micro-grain activated carbon
Autores: Julia R. de Andrade, Meuris G. C. da Silva, Marcelino L. Gimenes, Melissa G. A. Vieira
Journal of Environmental Chemical Engineering, v.8, p.103562, 2020.
DOI: 10.1016/j.jece.2019.103562

Removal of toxic metals from water using chitosan-based magnetic adsorbents: a review
Autores: Giani V. Brião, Julia R. de Andrade, Meuris G. C. da Silva, Melissa G. A. Vieira
Environmental Chemistry Letters, v.18, p.1145-1168, 2020.
DOI: 10.1007/s10311-020-01003-y

Removal of propranolol hydrochloride by batch biosorption using remaining biomass of alginate extraction from *Sargassum filipendula* algae
Autores: Caroline M. Coelho, Julia R. de Andrade, Meuris G. C. da Silva, Melissa G. A. Vieira
Environmental Science and Pollution Research, v.27, p.16599-16611, 2020.
DOI: 10.1007/s11356-020-08109-4

Oxidative degradation of pharmaceutical losartan potassium with N-doped hierarchical porous carbon and peroxymonosulfate.
Autores: Julia R. de Andrade, Meuris G. C. da Silva, Melissa G. A. Vieira, Shaobin Wang
Chemical Engineering Journal, v.382, p.122971, 2020.
DOI: 10.1016/j.cej.2019.122971

Adsorption of diclofenac sodium onto commercial organoclay: kinetic, equilibrium and thermodynamic study.
Autores: Gabriella S. Maia, Julia R. de Andrade, Meuris G. C. da Silva, Melissa G. A. Vieira
Powder Technology, v.345, p.140-150, 2019.
DOI: 10.1016/j.powtec.2018.12.097

Adsorption of pharmaceuticals from water and wastewater using nonconventional low-cost materials: a review.
Autores: Julia R. de Andrade, Maria F. Oliveira, Meuris G. C. da Silva, Melissa G. A. Vieira
Industrial & Engineering Chemistry Research, v.57, p.3103-3127, 2018.
DOI:10.1021/acs.iecr.7b05137

Affinity studies between drugs and clays as adsorbent material
Autores: Gabriella S. Maia, Julia R. de Andrade, Maria F. Oliveira, Melissa G. A. Vieira, Meuris G. C. da Silva
Chemical Engineering Transactions, v.57, p.583-588, 2017.
DOI: 10.3303/CET1757098

Artigos completos publicados em anais de congresso

Adsorção do fármaco losartana potássica em argila organofílica comercial: teste de afinidade e planejamento experimental
Autores: Julia R. de Andrade, Franco T. Sbragia, Meuris G. C. da Silva, Marcelino L. Gimenes, Melissa G. A. Vieira
In: Encontro Brasileiro sobre Adsorção, 12., 2018, Gramado. **Anais eletrônicos...** Gramado: UFSM, 2018.

Artigo completo submetido a congresso

Adsorption and peroxymonosulfate catalytic oxidation of anti-hypertensive pharmaceutical using porous structure with embedded N, S-codoped core-shell Co@C nanoparticles
Autores: Julia R. de Andrade, Wenjie Tian, Meuris G. C. da Silva, Melissa G. A. Vieira, Shaobin Wang
In: Encontro Brasileiro sobre Adsorção, 13., 2020, Fortaleza. (trabalho aprovado).

Capítulo de livro submetido

Removal of Emerging Pollutants using Magnetic Adsorbents
Autores: Julia R. de Andrade, Giani V. Brião, Meuris G. C. da Silva, Melissa G. A. Vieira
In: *Advanced Magnetic Adsorbents for Water Treatment*. Environmental Chemistry for a Sustainable World, Springer Nature (submetido).

CAPÍTULO 10. Referências

AGÊNCIA NACIONAL DE ÁGUAS - ANA (BRASIL). Ministério do Meio Ambiente. **Conjuntura dos recursos hídricos no Brasil 2019: informe anual**. Brasília, 2019. 100 p.

AHAMAD, T.; NAUSHAD, M.; RUKSANA; ALHABARAH, A. N.; ALSHEHRI, S. M. N/S doped highly porous magnetic carbon aerogel derived from sugarcane bagasse cellulose for the removal of bisphenol-A. **International Journal of Biological Macromolecules**, v. 132, p. 1031-1038, 2019.

AHMED, M. B.; ZHOU, J. L.; NGO, H. H.; GUO, W. Adsorptive removal of antibiotics from water and wastewater: Progress and challenges. **Science of the Total Environment**, v. 532, p. 112-26, 2015.

ASSEMBLEIA GERAL DAS NAÇÕES UNIDAS. **Transforming our world: the 2030 Agenda for Sustainable Development A/RES/70/1**, 2015. 41 p. Disponível em: < https://sustainabledevelopment.un.org/post2015/transformingourworld >. Acesso em: 01 jun. 2020.

BABEL, S.; KURNIAWAN, T. A. Low-cost adsorbents for heavy metals uptake from contaminated water: a review. **Journal of Hazardous materials**, v. 97, n. 1, p. 219-243, 2003.

BOURGIN, M.; BECK, B.; BOEHLER, M.; BOROWSKA, E.; FLEINER, J.; SALHI, E. et al. Evaluation of a full-scale wastewater treatment plant upgraded with ozonation and biological post-treatments: Abatement of micropollutants, formation of transformation products and oxidation by-products. **Water Research**, v. 129, p. 486-498, 2018.

BRASIL. Ministério da Saúde. **Portaria nº 2.914, de 12 de dezembro de 2011 que dispõe sobre os procedimentos de controle e de vigilância da qualidade da água para consumo humano e seu padrão de potabilidade**. Brasília, 2011.

BRASIL. Ministério das Cidades. Secretaria Nacional de Saneamento Ambiental. **Sistema Nacional de Informações sobre Saneamento: Diagnóstico dos Serviços de Água e Esgotos – 2018**. Brasília, 2019a. 180 p.

BRASIL. Ministério da Saúde. Secretaria de Vigilância em Saúde. Departamento de Análise em Saúde e Vigilância de Doenças não Transmissíveis. **Vigitel Brasil 2018: vigilância de fatores de risco e proteção para doenças crônicas por inquérito telefônico: estimativas sobre frequência e distribuição sociodemográfica de fatores de risco e proteção para doenças crônicas nas capitais dos 26 estados brasileiros e no Distrito Federal em 2018**. Brasília, 2019b. 131 p.

CAMPANHA, M. B.; AWAN, A. T.; DE SOUSA, D. N. R.; GROSSELI, G. M.; MOZETO, A. A.; FADINI, P. S. A 3-year study on occurrence of emerging contaminants in an urban stream of São Paulo State of Southeast Brazil. **Environmental Science and Pollution Research**, v. 22, n. 10, p. 7936-7947, 2015.

CONSELHO NACIONAL DO MEIO AMBIENTE (BRASIL). Ministério do Meio Ambiente. **Resolução CONAMA nº 357, de 17 de Março de 2005**. Brasília, 2005.

CONSELHO NACIONAL DO MEIO AMBIENTE (BRASIL). Ministério do Meio Ambiente. **Resolução CONAMA nº 396, de 3 de Abril de 2008**. Brasília, 2008.

CONSELHO NACIONAL DO MEIO AMBIENTE (BRASIL). Ministério do Meio Ambiente. **Resolução CONAMA nº 430, de 13 de Maio de 2011**. Brasília, 2011.

EBELE, A. J.; ABOU-ELWAFA ABDALLAH, M.; HARRAD, S. Pharmaceuticals and personal care products (PPCPs) in the freshwater aquatic environment. **Emerging Contaminants**, v. 3, n. 1, p. 1-16, 2017.

FENT, K.; WESTON, A. A.; CAMINADA, D. Ecotoxicology of human pharmaceuticals. **Aquatic Toxicology**, v. 76, n. 2, p. 122-159, 2006.

FRANCISCO, L. F. V.; DO AMARAL CRISPIM, B.; SPÓSITO, J. C. V.; SOLÓRZANO, J. C. J.; MARAN, N. H.; KUMMROW, F. et al. Metals and emerging contaminants in groundwater and human health risk assessment. **Environmental Science and Pollution Research**, v. 26, n. 24, p. 24581-24594, 2019.

KANG, J.; ZHANG, H.; DUAN, X.; SUN, H.; TAN, X.; LIU, S.; WANG, S. Magnetic Ni-Co alloy encapsulated N-doped carbon nanotubes for catalytic membrane degradation of emerging contaminants. **Chemical Engineering Journal**, v. 362, p. 251-261, 2019.

MACHADO, K. C.; GRASSI, M. T.; VIDAL, C.; PESCARA, I. C.; JARDIM, W. F.; FERNANDES, A. N. et al. A preliminary nationwide survey of the presence of emerging contaminants in drinking and source waters in Brazil. **Science of the Total Environment**, v. 572, p. 138-146, 2016.

MAIA, G. S. **Adsorção de diclofenaco de sódio em material argiloso**. 2017. 104 f. Dissertação (Mestrado em Engenharia Química)−Faculdade de Engenharia Química, Universidade Estadual de Campinas, Campinas, 2017.

MAIA, G. S.; DE ANDRADE, J. R.; DA SILVA, M. G. C.; VIEIRA, M. G. A. Adsorption of diclofenac sodium onto commercial organoclay: Kinetic, equilibrium and thermodynamic study. **Powder Technology**, v. 345, p. 140-150, 2019.

MENGUE, S. S.; BERTOLDI, A. D.; RAMOS, L. R.; FARIAS, M. R.; OLIVEIRA, M. A.; TAVARES, N. U. L.; ARRAIS, P. S. D.; LUIZA, V. L.; PIZZOL, T. D. S. D. Acesso e uso de medicamentos para hipertensão arterial no Brasil. **Revista de Saúde Pública**, v. 50(supl 2), p. 8s, 2016.

MONTAGNER, C. C.; SODRÉ, F. F.; ACAYABA, R. D.; VIDAL, C.; CAMPESTRINI, I.; LOCATELLI, M. A. et al. Ten Years-Snapshot of the Occurrence of Emerging Contaminants in Drinking, Surface and Ground Waters and Wastewaters from São Paulo State, Brazil. **Journal of the Brazilian Chemical Society**, v. 30, p. 614-632, 2019.

MONTAGNER, C. C.; VIDAL, C.; ACAYABA, R. D. Contaminantes emergentes em matrizes aquáticas do Brasil: cenário atual e aspectos analíticos, ecotoxicológicos e regulatórios. **Quimica Nova**, v. 40, p. 1094-1110, 2017.

NETWORK, N. Network of reference laboratories, research centres and related organisations for monitoring of emerging environmental substances. **List of Emerging Substances**, 2016. Disponível em: < www.normannetwork.com >. Acesso em: 20 abr. 2020.

PEÑA-GUZMÁN, C.; ULLOA-SÁNCHEZ, S.; MORA, K.; HELENA-BUSTOS, R.; LOPEZ-BARRERA, E.; ALVAREZ, J.; RODRIGUEZ-PINZÓN, M. Emerging pollutants in the urban water cycle in Latin America: A review of the current literature. **Journal of Environmental Management**, v. 237, p. 408-423, 2019.

PENG, G.; ZHANG, M.; DENG, S.; SHAN, D.; HE, Q.; YU, G. Adsorption and catalytic oxidation of pharmaceuticals by nitrogen-doped reduced graphene oxide/Fe3O4 nanocomposite. **Chemical Engineering Journal**, v. 341, p. 361-370, 2018.

PUTRA, E. K.; PRANOWO, R.; SUNARSO, J.; INDRASWATI, N.; ISMADJI, S. Performance of activated carbon and bentonite for adsorption of amoxicillin from wastewater: Mechanisms, isotherms and kinetics. **Water Research**, v. 43, n. 9, p. 2419-2430, 2009.

SEO, P. W.; BHADRA, B. N.; AHMED, I.; KHAN, N. A.; JHUNG, S. H. Adsorptive Removal of Pharmaceuticals and Personal Care Products from Water with Functionalized Metal-organic Frameworks: Remarkable Adsorbents with Hydrogen-bonding Abilities. **Scientific Reports**, v. 6, p. 34462, 2016.

SING, K. S. W.; EVERETT, D. H.; HAUL, R. A. W.; MOSCOU, L.; PIEROTTI, R. A.; ROUQUÉROL, J.; SIEMIENIEWSKA, T. Reporting physisorption data for gas/solid systems with special reference to the determination of surface area and porosity (Recommendations 1984). **Pure and Applied Chemistry**, v. 57, p. 603-619, 1985.

SPOSITO, J. C. V.; MONTAGNER, C. C.; CASADO, M.; NAVARRO-MARTÍN, L.; JUT SOLÓRZANO, J. C.; PIÑA, B.; GRISOLIA, A. B. Emerging contaminants in Brazilian rivers: Occurrence and effects on gene expression in zebrafish (*Danio rerio*) embryos. **Chemosphere**, v. 209, p. 696-704, 2018.

STUMPF, M.; TERNES, T. A.; WILKEN, R.-D.; SILVANA VIANNA, R.; BAUMANN, W. Polar drug residues in sewage and natural waters in the state of Rio de Janeiro, Brazil. **Science of the Total Environment**, v. 225, n. 1–2, p. 135-141, 1999.

TERNES, T. A.; STUMPF, M.; MUELLER, J.; HABERER, K.; WILKEN, R. D.; SERVOS, M. Behavior and occurrence of estrogens in municipal sewage treatment plants — I. Investigations in Germany, Canada and Brazil. **Science of the Total Environment**, v. 225, n. 1–2, p. 81-90, 1999.

THOMMES, M.; KANEKO, K.; NEIMARK, A. V.; OLIVIER, J. P.; RODRIGUEZ-REINOSO, F.; ROUQUEROL, J.; SING, K. S. W. Physisorption of gases, with special reference to the evaluation of surface area and pore size distribution (IUPAC Technical Report). **Pure and Applied Chemistry**, v. 87, n. 9-10, p. 1051-1069, 2015.

TIAN, W.; ZHANG, H.; QIAN, Z.; OUYANG, T.; SUN, H.; QIN, J.; TADÉ, M. O.; WANG, S. Bread-making synthesis of hierarchically Co@C nanoarchitecture in heteroatom doped porous carbons for oxidative degradation of emerging contaminants. **Applied Catalysis B: Environmental**, v. 225, p. 76-83, 2018a.

TIAN, W.; ZHANG, H.; SUN, H.; TADÉ, M. O.; WANG, S. One-step synthesis of flour-derived functional nanocarbons with hierarchical pores for versatile environmental applications. **Chemical Engineering Journal**, v. 347, p. 432-439, 2018b.

TRAN, H. N.; YOU, S.-J.; CHAO, H.-P. Thermodynamic parameters of cadmium adsorption onto orange peel calculated from various methods: A comparison study. **Journal of Environmental Chemical Engineering**, v. 4, n. 3, p. 2671-2682, 2016.

UNIÃO EUROPEIA. **Directive 2008/105/EC of the European Parliament and of the Council of 16 December 2008**. [S.l.], 2008. 84-97 p.

UNIÃO EUROPEIA. **Directive 2013/39/EU of the European Parliament and of the Council of 12 August 2013 amending Directives 2000/60/EC and 2008/105/EC as regards priority substances in the field of water policy**. [S.l.], 2013. 17 p.

UNIÃO EUROPEIA. **Directive 2000/60/EC of the European Parliament and of the Council of 23 October 2000**. [S.l.], 2014. 73 p. Disponível em: < http://data.europa.eu/eli/dir/2000/60/2014-11-20 >. Acesso em: 20 maio 2020.

UNIÃO EUROPEIA. **Communication from the commission to the European parliament, the council and the European economic and social committee - European Union Strategic Approach to Pharmaceuticals in the Environment**. Brussels, 2019. 12 p. Disponível em: < https://ec.europa.eu/environment/water/water-dangersub/pdf/strategic_approach_pharmaceuticals_env.PDF >. Acesso em: 02 jun. 2020.

UNITED NATIONS WORLD WATER ASSESSMENT PROGRAMME - UNESCO/WWAP. **The United Nations World Water Development Report 2017. Wastewater: The untapped resource**. Paris: UNESCO, 2017. 198 p. ISBN 978-92-3-100201-4.

UNITED NATIONS WORLD WATER ASSESSMENT PROGRAMME - UNESCO/WWAP. **The United Nations World Water Development Report 2019: Leaving no one behind**. Paris: UNESCO, 2019. 186 p. ISBN 978-92-3-100309-7.

UNITED STATES ENVIRONMENTAL PROTECTION AGENCY - U.S. EPA. **Contaminant Candidate List 4**. Washington, DC, 2016. 81099-81114 p.

VASQUEZ, M. I.; LAMBRIANIDES, A.; SCHNEIDER, M.; KÜMMERER, K.; FATTA-KASSINOS, D. Environmental side effects of pharmaceutical cocktails: What we know and what we should know. **Journal of Hazardous materials**, v. 279, p. 169-189, 2014.

WANG, Q.; LI, L.; LUO, L.; YANG, Y.; YANG, Z.; LI, H.; ZHOU, Y. Activation of persulfate with dual-doped reduced graphene oxide for degradation of alkylphenols. **Chemical Engineering Journal**, v. 379, 2019.

ZHANG, X.; GUO, W.; NGO, H. H.; WEN, H.; LI, N.; WU, W. Performance evaluation of powdered activated carbon for removing 28 types of antibiotics from water. **Journal of Environmental Management**, v. 172, p. 193-200, 2016.

ANEXO A. Licenças de publicação de artigos na tese

Autorizações da *American Chemical Society* para a inclusão do artigo publicado em *Industrial & Engineering Chemistry Research* no Capítulo 2 desta tese de doutorado.

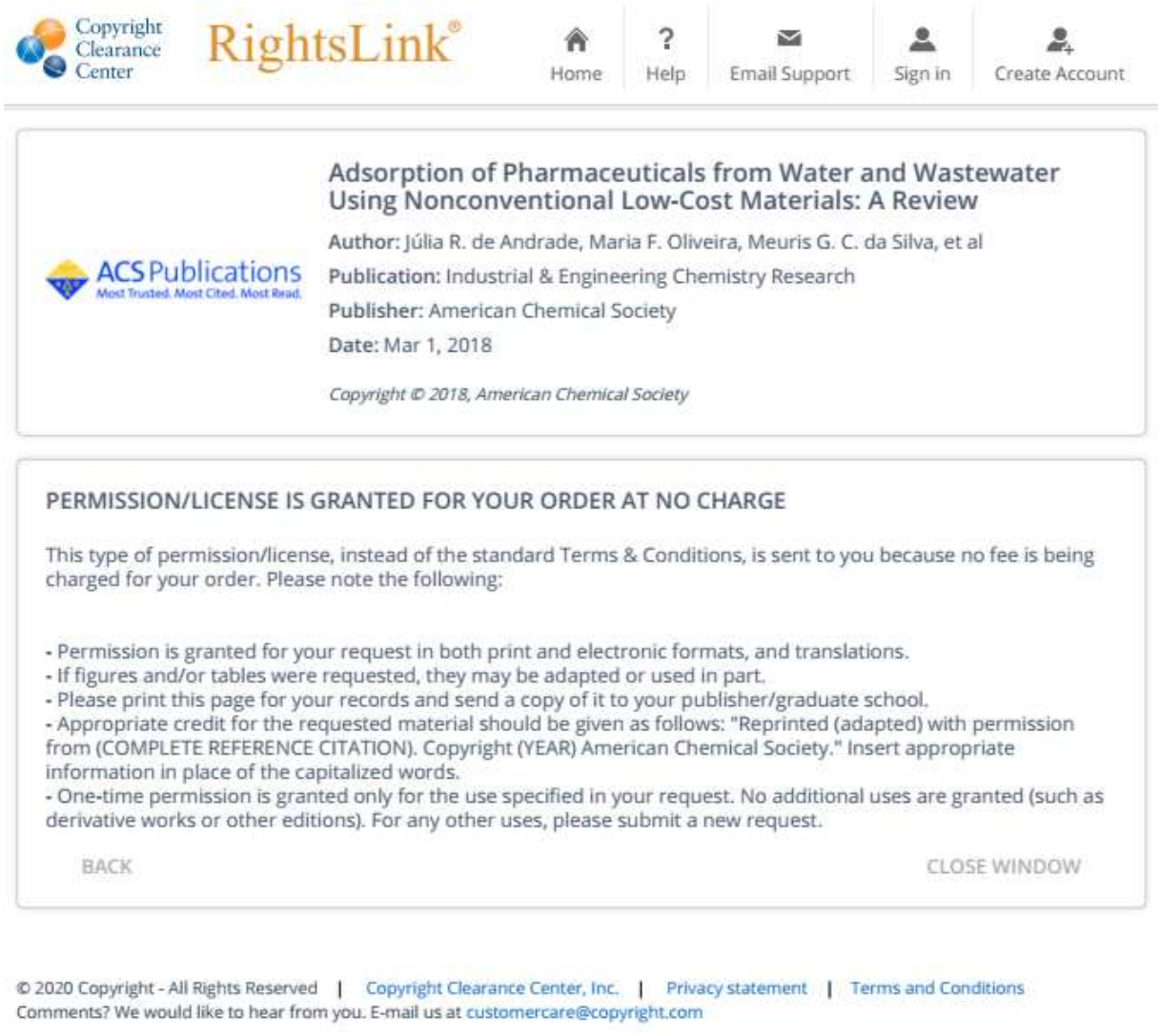

Copyright Clearance Center RightsLink®

Home | Help | Email Support | Sign in | Create Account

ACS Publications
Most Trusted. Most Cited. Most Read.

Adsorption of Pharmaceuticals from Water and Wastewater Using Nonconventional Low-Cost Materials: A Review

Author: Júlia R. de Andrade, Maria F. Oliveira, Meuris G. C. da Silva, et al

Publication: Industrial & Engineering Chemistry Research

Publisher: American Chemical Society

Date: Mar 1, 2018

Copyright © 2018, American Chemical Society

PERMISSION/LICENSE IS GRANTED FOR YOUR ORDER AT NO CHARGE

This type of permission/license, instead of the standard Terms & Conditions, is sent to you because no fee is being charged for your order. Please note the following:

- Permission is granted for your request in both print and electronic formats, and translations.
- If figures and/or tables were requested, they may be adapted or used in part.
- Please print this page for your records and send a copy of it to your publisher/graduate school.
- Appropriate credit for the requested material should be given as follows: "Reprinted (adapted) with permission from (COMPLETE REFERENCE CITATION). Copyright (YEAR) American Chemical Society." Insert appropriate information in place of the capitalized words.
- One-time permission is granted only for the use specified in your request. No additional uses are granted (such as derivative works or other editions). For any other uses, please submit a new request.

BACK CLOSE WINDOW

Autorizações da *Elsevier* para a inclusão do artigo publicado em *Journal of Environmental Chemical Engineering* no Capítulo 4 desta tese de doutorado.

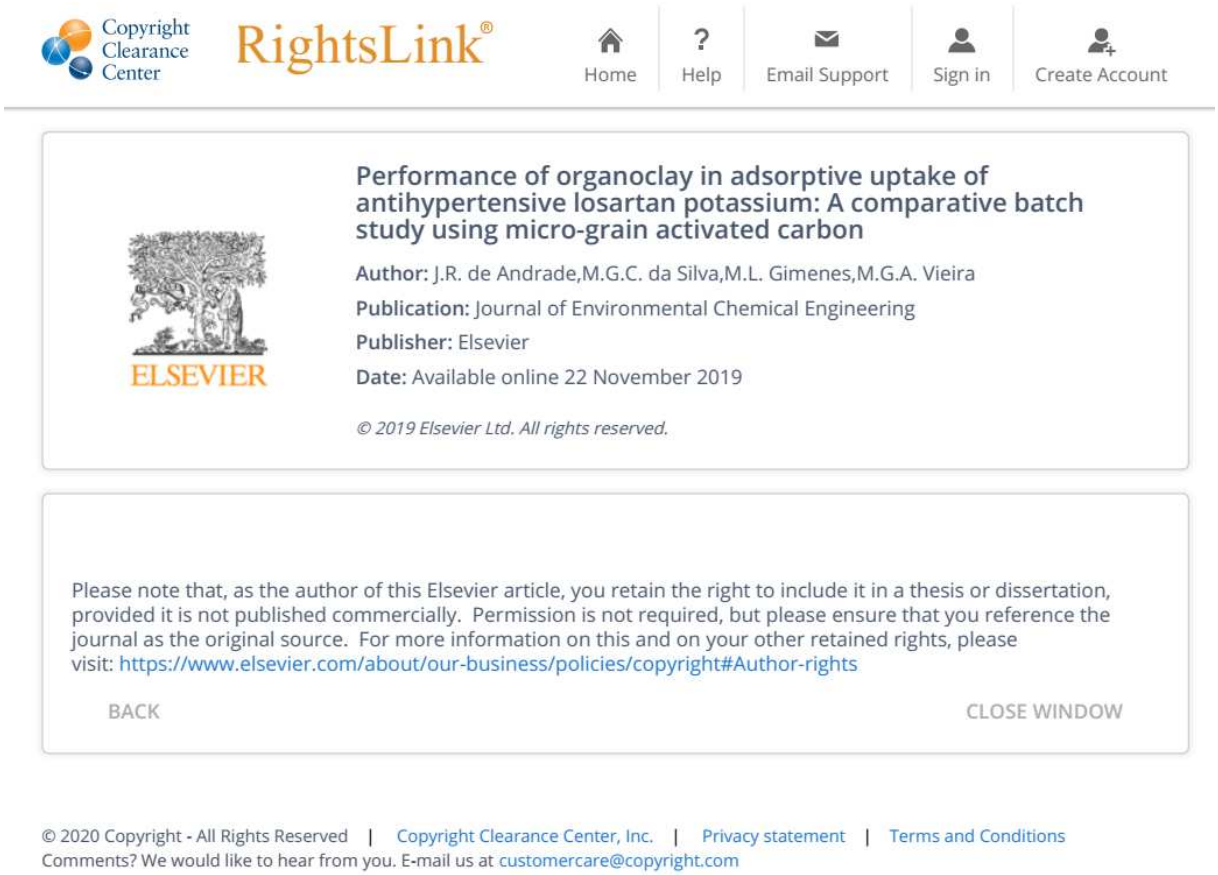

Autorizações da *Elsevier* para a inclusão do artigo publicado em *Journal of Molecular Liquids* no Capítulo 5 desta tese de doutorado.

Autorizações da *Elsevier* para a inclusão do artigo publicado em *Chemical Engineering Journal* no Capítulo 6 desta tese de doutorado.